Dissertation

submitted to the

Combined Faculties for the Natural Sciences and for Mathematics
of the Ruperto-Carola University of Heidelberg, Germany

for the degree of

Doctor of Natural Sciences

presented by

Andrés-Miguel Miguélez-Morán, Lic. Pharm.

born in Esplugues de Llobregat, Spain

Oral-examination: 30th April 2009

ROLLER COMPACTION OF PHARMACEUTICAL INGREDIENTS

ON THE UNDERSTANDING OF THE COMPACTION AND THE USE OF KNOWLEDGE BASED APPLICATIONS IN THE FORMULATION OF TABLETS

Referees: Prof. Dr. Gert Fricker
Priv. Doz. Dr. Ulrich Massing

The following work has been carried out at the Dept. of Pharmaceutical Technology and Biopharmacy of the Institute of Pharmacy and Molecular Biotechnology of the University of Heidelberg (Germany), and at the School of Chemical Engineering of the University of Birmingham.

First of all, I would like to thank Prof. Dr. Fricker for accepting me as a doctorate student at the institute, for allowing me to perform the major part of the experimental of this work, and for agreeing to be my supervisor and my referee. I also would like to express my thanks Dr. Massing, for kindly agreeing to be my second referee. Moreover, I would like to acknowledge Prof. Dr. Hilgenfeldt and Prof. Dr. Reichling, for being part of the committee in this viva examination.

I would like to thank Dr. Martin Bultmann, firstly, for opening the door and offering me the possibility to start my project under his guidance and supervision without hesitation, and for giving me the opportunity for conducting my PhD studies at the University of Heidelberg. I also thank him the support and the effort that he has made at arranging the funding of my stay at the department during the last year and a half. I appreciate enormously his encouragement and his understanding anytime that I made a decision and the freedom of choice that he has always given to me, allowing me the development of all projects that I had in mind, and firing my enthusiasm for the research. I would also like to thank him for the time and patience that he has devoted to me during this time, and recently to the correction of the work. Finally, I would like to acknowledge his advices, which have been essential for the improvement of the thesis.

In third place I would like to express effusively gratitude to the School of Engineering at the University of Birmingham. I am deeply grateful to Professor J.P.K. Seville for accepting me as an occasional postgraduate student in his department and for showing me how an issue can be studied from several points of view. Especially, I want to show my appreciation to Dr. Charley Wu, the person who made possible an unforgettable time of work in research under his supervision. I want to express my most sincerely thanks to him for considering my application, giving me the opportunity of joining his group, for the blind trust that he put in me from the beginning, the high interesting projects that he offered, the excellent supervision, the support, and the continuous advice. I also appreciate enormously his corrections and his contributions to this thesis.

The scholarship program conducted by *La Caixa* in co-operation with the *DAAD* has funded an important part of my stay in Germany during my PhD studies. Therefore, I would like to acknowledge these organizations since, without their support, I had never been able to initiate my project in Heidelberg.

I also want to thank the companies that have contributed to this work:

- The company Abbott GmbH & Co. KG that has funded my stay at the university over a year. Also thanks to the Department of Formulation for the measurements made with the helium pycnometre.

• The company Gerteis Maschinen + Process engineering AG lent generously the MiniPactor device to perform part of the experiments.
• The Department of *Pharma Solutions* of BASF AG put at our disposal its MiniPactor device to carry out some of the experiments.

I would also like to express my gratitude to other Schools at the University of Birmingham that made contributions to this work. Especially to the School of Material Sciences and Metallurgy, for the measurements with the micro-indenter, the reflection microscope, and the SEM; the School of Chemistry, for the development of the method and the measurements made with NIR-Imaging; and the school of Dentistry, for the determinations of density made with the helium pycnometre.

To all my colleagues and friends from both universities in recognition of the good time that I spent with them, which has become a source of motivation and a bubble of air that has brought me many times "back to earth" and has given a reason to what I have been doing during this time. My especial thanks to Joerg, for providing brilliant ideas, for pushing me to go ahead, and for his contributions to this work; to Benni, for making me feel comfortable in the department from the beginning and being always there to listen to my moaning; to my friend in need Hendrik, for his patience and readiness to lend a helping hand, even from the distance; to Christoph, for showing me why things must be done well; to Sonja, Johanna, Caroline, Johannes and the rest of people from the department in Heidelberg with whom I have shared an amazing time. From the department at the University of Birmingham, I would like to thank Yu Guo and You Van for their kindness and the good atmosphere in the office. Also Chian, Ourania, Ryan, and Isaac, deserve a very special mention. They have been great mates both inside and outside the University.

I also would like to give my deepest gratitude to Aga, who surely knows already how important has she been to me since the beginning. My work and my life in Heidelberg owe much to her. I also appreciate the support that she, Elena and Neville have given me even during the last-minute rush.

My last words go to my family. No podría acabar este agradecimiento sin dedicarle unas líneas a la mención de aquellas personas sin cuyo apoyo, comprensión, ánimo y calor no hubiera podido seguir adelante: mis padres, mis hermanos, sus familias, y Bea (y familia). Por haberme rescatado varias veces de la incertidumbre y el desánimo, por darme aliento y convencerme de lo que era correcto, por haber estado siempre ahí para escuchar, por todo lo que habéis ayudado, por todo lo que os habéis sacrificado y especialmente a Bea, por haberme dado soporte desde la distancia y la cercanía y por haber esperado con tanta ilusión (o aún mayor) el resultado y el final de este trabajo. Os dedico a todos esta tesis.

TABLE OF CONTENTS

List of figures

List of tables

Abbreviations

ADS	Ac-Di-Sol
ANN	artificial Neural Network
ANOVA	analysis of variance
API	active pharmaceutical ingredient
approx.	Approximately
ca.	*circa*
CAD	computer aided design
CADF	computer aided design in formulation
CF	compression / compaction force
CI	Carr index / compressibility index
CNS	central neural system
CP	compression pressure
DEM	definite element model/ modelling
DOE	design of experiments
DT	disintegration time
e.g.	*exempli gratia*
Eqs.	equations
ES	expert system
et al.	*et alii*
Eur. Ph.	European Pharmacopea
ext	external
FDA	Food and Drug Administration
FE	finite elements
FEM	finite element model / modelling
Figs.	figures
GMP	good manufacturing practices
i.e.	*id est*
ICH	International Conference of Harmonization
id.	*idem*
int	internal
KVA64	Kollidon VA 64
LMH	α-lactose monohydrate
LP	Ludipress LCE
MCC	microcrystalline cellulose
MLP	multi-layer perceptron
MNT	mannitol
MSE	mean squared error
NIR	near infra-red
NIRS	near infra-red spectroscopy
NMRI	nuclear magnetic resonance - imaging
PAT	process analytical technology
PE	processing element
PEPT	positron emission particle tracking
PID	proportional integral and differential control
PNE	polynomial equation
PSD	particle size distribution
QbD	quality by design
QC	quality control
R & D	research and development
RARE	rapid acquisition with relaxation enhancement
RC	roller compaction
RRSB	Rosin–Rammler– Sperling–Bennett distribution
RSM	response surface model / modelling
SD	standard deviation
SE	standard error
SEE	standard error of estimate
SLP	single-layer perceptron
SOP	standard operating procedure
TS	tensile strength
USP	United States - Pharmacopea
vs.	*versus*
X-ray μCT	X-ray micro computed tomography

Note: the definition of other symbols used in this work is correspondingly described in the text

Roller compaction of pharmaceutical ingredients

On the understanding of the compaction and the use of knowledge based applications in the formulation of tablets

Summary

Roller compaction is a dry granulation process which is still not well understood since a large number of processing variables and inherent material attributes make the description of the mechanisms involved in the process extremely complicated. Neither the intermediary compact (i.e., the ribbon) nor the final product (i.e., the granule) is normally used as dosage form. Thus, the granule is usually processed for the production of tablets. When the substance needs to be dry-granulated prior to the tablet production, not only the initial composition of the formulation, but also the processing conditions (device parameters, intermediary steps, etc.), affect the workability of the granule and, consequently, the characteristics of the produced tablets. Thus, the *development of* a *formulation* and the optimization of the production process are necessary to meet the mandatory tablet requirements that warrant the pharmaco-therapeutic success of the drug. *Expert Systems* (*ES*) are tools that result from combining experience and computing. They can simplify the task of development of new formulations in an accurate, efficient and rapid way by processing, extracting and putting to anyone's disposal data contained in their data base. This work pretends to join the effort of others on the characterisation of the compaction. The experiments described here supply key hints for the understanding of the process and the variability in the product attributes due to composition of the formulation and processing conditions. Finally, the information and the predictive models created during the experiments have been implemented in the development of an *ES* in order to demonstrate the benefits of these applications in formulation research.

For that purpose, this work reports experiments that analyze the *compact process* visually and use a critical attribute of the ribbon, the solid fraction, to evidence the interactions between the powder and the rollers, and to describe the effect of the lubrication and other compaction conditions over the dynamics and the densification of the material between the rollers. Moreover, the suitability of a number of techniques for the characterisation of the ribbon solid fraction is analyzed and compared. Furthermore, after close examination of the ribbon quality and also of the granule and the tablets produced from different pharmaceutical substances it has been shown that these product characteristics are strongly affected by the initial composition and by the parameters and the conditions of the process. Moreover, *predictive models* based on computer general *mathematic regressions* and *artificial neural networks*, have been developed using gathered experimental data. The models identify satisfactorily the underlying relationships between the independent variables (composition and process parameters) and the product characteristics, and deliver prognoses of the properties of the intermediary (ribbons and granules) and the final products (tablets). Finally the models are integrated into an *ES* that has shown to be a user-friendly application that manages the information and retrieves the models to generate a report that includes predictions of the product attributes and helpful information to be born in mind during the production. *ESs* are extremely useful tools, especially for the pharmaceutical industry, as they ease the formulation development, reducing effort and expenditures, and increasing the consistency, the quality and the efficiency of the formulation tasks. In addition they ensure the permanency and the accessibility of the knowledge and assist the work of both experienced and novice formulators.

Walzenkompaktierung von pharmazeutischen Substanzen

Über das Kompaktierungsverfahren und die Anwendung wissensbasierter Systeme in der Tablettenformulierung

Zusammenfassung

Bei der Walzenkompaktierung handelt es sich um ein Verfahren zur Trockengranulation. Nach heutigem Stand der Wissenschaft sind die zu Grunde liegende Mechanismen noch nicht vollständig verstanden, da sie von einer großen Anzahl an Prozessvariablen und inhärenten Materialattributen in komplexer Weise beeinflusst werden. Weder die durch Walzenkompaktierung als Zwischenprodukt gewonnenen Schülpen, noch das Endgranulat werden üblicherweise als Arzneiform eingesetzt. Es wird meist zu Tabletten weiterverarbeitet. Während des gesamten Prozesses treten in Abhängigkeit der Material- und Prozessvariablen eine Vielzahl von komplexen Änderungen des Materials auf, die zu einer Änderung der Endprodukteigenschaften führen können. Deswegen sind die Entwicklung der Formulierung und die Optimierung der Produktionsprozesse notwendig, um Produktspezifikationen zu erfüllen, welche eine erfolgreiche pharmakologische Wirkung des Arzneistoffes garantieren. Expertensysteme (ESe) sind Software-Systeme, die auf der Zusammenführung von (spezifischem) Wissen und Computer-Programmierung basieren. Sie erleichtern den Auftrag der zügigen Entwicklung neuer Formulierungen durch den Zugriff, die Strukturierung und die Ausgabe der Informationen, die in ihren Datenbanken verfügbar sind. Diese Dissertation liefert einen Beitrag zur Charakterisierung des Kompaktierungsprozesses. Die in dem experimentellen Teil beschriebenen Versuche liefern wichtige Hinweise für das Verständnis des Verfahrens und der Variabilität des Produktes, die durch die Zusammensetzung und die Herstellungsparameter bedingt ist. Schließlich werden die generierten Daten bei der Entwicklung eines ESs implementiert.

Zu diesem Zweck werden Versuche durchgeführt, die durch visuelle Analyse und durch die Betrachtung der Schülpendichte als kritische Charakterisierungseigenschaft des (Zwischen)Produkts die Interaktionen zwischen Pulver und Walze belegen. Ebenfalls werden der Effekt der Schmierung und der Einfluss der Kompaktierung auf die Dynamik und die Verdichtung des Materials zwischen den Walzen beschrieben. In diesem Zusammenhang werden verschiedene Bestimmungsmethoden für die Schülpendichte gegenüber gestellt und bezüglich ihrer Verwendbarkeit im Rahmen der Anwendung analysiert. Außerdem wird nach detaillierter Untersuchung der Schülpenqualität, sowie der Eigenschaften des gewonnen Granulates und der hergestellten Tabletten veranschaulicht, inwiefern Variablen, wie die Eingangszusammensetzung der Mischung, die Verfahrensparameter und die Herstellungsbedingungen, die o.g. Produkteigenschaften beeinflussen. Unter Verwendung der gewonnen Ergebnisse wird ein Expertensystem entwickelt, in das Vorhersagemodelle und weitere erstellte Richtlinien für die Formulierung eingebunden werden. Die Modelle basieren hierbei auf Regressionen und künstlichen neuronalen Netzen (ANNs). Sie legen die Beziehung zwischen unabhängigen Variablen und Eigenschaften der Zwischen- und Endprodukte fest und sagen mit Erfolg Produkteigenschaften neuer Formulierungen vorher. Zusätzlich erstellt das im Pilotmaßstab generierte ES Regeln und Anweisungen, die während des Herstellungsverfahrens zu beachten sind. ES sind dafür geeignet, in der pharmazeutischen Industrie die Formulierungsentwicklung erfahrener und unerfahrener Wissenschaftler zu unterstützen. Somit können Aufwand und Kosten gesenkt und die Konsistenz, Zuverlässigkeit und Effizienz der Entwicklung gesteigert werden.

Compactación por rodillos de sustancias farmacéuticas

Hacia la comprensión del proceso de compactación y el uso de aplicaciones basadas en la evidencia para la formulación de comprimidos

Resumen

La compactación por rodillos es un proceso de granulación seca de difícil comprensión, debido a que un gran número de variables y propiedades de las sustancias hacen la descripción del proceso extremadamente complicada. El compactado y granulado obtenidos en la compactación por rodillos no se usan normalmente como forma farmacéutica, sino que se usan como producto intermedio para la fabricación de comprimidos. La procesabilidad del granulado y por tanto las características del comprimido se ven alterados por la composición de la formulación y las condiciones del proceso (parámetros de producción, procesos intermedios, etc.). Desarrollar la formulación y optimizar el proceso de producción son así imprescindibles para cumplir con aquellos requisitos del comprimido que garantizan el éxito farmaco-terapéutico del principio activo. Los *Sistemas Expertos* (*SSEE*) son herramientas resultantes de la combinación del conocimiento y la programación informática. Facilitan el desarrollo de nuevas formulaciones de una forma precisa, eficiente y rápida a través del procesado, la extracción y la disposición de la información contenida en sus bases de datos. Este trabajo pretende contribuir al esfuerzo que otros investigadores han dedicado a la caracterización del proceso de compactación. Los experimentos aquí descritos aportan informacion clave que ayuda a comprender cómo la formulación y las condiciones de dicho proceso pueden alterar las propiedades del producto terminado. Finalmente, la información recogida y los modelos predictivos generados a partir de datos experimentales han sido empleados en el desarrollo de un *SE*, con el fin de demostrar las ventajas que estas aplicaciones tienen en la investigación de la formulación.

En primer lugar, esta tesis incluye experimentos que analizan el *proceso de compactación* visualmente y mediante la densidad del compactado, para reflejar las interacciones entre el polvo y los rodillos y caracterizar el efecto de la lubricación, la movilidad del polvo y la densificación del material a nivel de rodillos. Además se examinan en detalle un grupo de técnicas para la determinación de la densidad del compactado. Por otra parte se han analizado detenidamente las características del compactado, el granulado y los comprimidos fabricados a partir de distintas formulaciones. Como resultado del estudio se concluye que las características de los productos se ven influidas por la composición de la formulación y por los parámetros y condiciones del proceso. Finalmente, usando los datos procedentes de los experimentos, se han creado *modelos* para identificar relaciones entre variables y así predecir las características de productos intermedios (compactado y granulado) y final (comprimido) a partir de la composición de la mezcla y de los parámetros de producción. La información procedente de experimentos, junto con los modelos, se ha incluido en un *SE* que demuestra ser una herramienta de uso sencillo capaz de controlar y de aprovechar la información y los modelos integrados para generar un informe de pronósticos sobre el producto y aportar directrices que deben ser considerados durante el proceso de producción. Este *SE* desarrollado a pequeña escala pone de manifiesto el gran interés que tienen los *SSEE*, especialmente para la industria farmacéutica, ya que reducen costes e incrementan la calidad, la solidez y la eficiencia de las tareas de formulación, al mismo tiempo que aseguran la permanencia de y la accesibilidad al conocimiento, facilitando de este modo el trabajo del científico galénico.

1 INTRODUCTION

Roller compaction is a dry granulation process that boosted the interest of the pharmaceutical industry in the 1990s. After almost two decades of work and investigation, it still arouses the curiosity of pharmaceutical scientists. The large number of factors involved in the material compaction and subsequent granulation makes it a process that has not been completely characterized yet. Not only processing variables, but also inherent material attributes, are involved in an extremely complex system. For this reason, the extensive effort made by investigators from multiple scientific disciplines (Pharmacy, Chemical Engineering, Material Sciences, etc.) that has been brought in with the aim of characterizing the process, has achieved a mere approach to its thoroughly comprehension.

Dry granulation by roller compaction has three main steps: 1) material conveyance and feeding, 2) material compaction and 3) granulation. Each step is, again, influenced by a large number of variables. The compaction has shown to be the result of complex particle-particle and particle-tooling (e.g. particle-roller surface) interactions that lead to a succession of shear and normal stresses that originate the transport and the grip of material between the rollers. Any alteration of parameters or variables, that is likely to modify these interactions and the material deformational behaviour, has a significant impact on the produced compact and the final granule attributes. However, despite the fact that the description of roller compaction is one of the main focuses of this thesis, it is usually an intermediary step within the manufacture process of other solid dosage forms. The product from roller compaction, the granule, is rarely used as dosage form directly, but is processed for filling capsules or (more frequently) producing tablets.

Tablets are the most often used form of oral administration. As they are straightforwardly dosed and easy to administrate, they are the favourite drug deliver form for patients. In addition, as a cheap, clean and highly productive process, the manufacture of tablets is also preferred in pharmaceutical production. Nevertheless, from a technical point of view, *tableting,* like roller compaction, is a process in which a large number of material and processing variables result in an almost casuistic sequence of mechanisms for which a fully description and modelling is still lacking. Under the same tableting conditions, the composition of the formulation is the main source of variability in tablet properties. On the other hand, after the dry-granulation of the starting blend, not only the composition of the formulation, but also the characteristics of the obtained granules play a decisive role in the determination of the tablets attributes.

Like any other production process, the combination of roller-compaction and tableting has to meet the mandatory product requirements to warrant the pharmaco-therapeutic success of the drug. It is therefore necessary the selection of the proper components for the formulation at the same time that the process must be adequately optimised. In short, a *design* of the *formulation* and the *process* has to be built and correspondingly improved. For that purpose, experience and knowledge are crucial. Both are helpful in understanding, assessing, facing and debugging new problems that may arise during the formulation and the production. Unfortunately, the achievement of this experience happens to be a slow learning process that starts with the training of the person, develops mainly with the time that he spends working in a specific area, and grows hanging on his interests and skills. Frequently, a very large part of this knowledge disappears at the very moment that he leaves a company, as it has been

only partially or not documented at all. In order to avoid that, E*xpert Systems* (ES) become a smart alternative to be born in mind, especially in industry. ES are computational programs designed to help in solving problems in specific domains for which they have been created. They can be considered expertise and knowledge "warehouses". However, they are not simple *data bases,* though the information is stored in order to be retrieved by the user after presenting any enquiry. ES are rather interactive tools that put the knowledge at the user's disposal following structured algorithms that collect efficiently all the information from the entire pool of data prior to display it. The assortment of information sources for the construction of the data base is wide: scientific literature, know-how recorded directly from the experts, experimental data, etc. In addition, ES, in combination with models, can also be used for making predictions of product attributes.

General regression methods (GRM) and *artificial neural networks* (ANN) are suitable for the creation of models that can be afterwards included in the ES knowledge-base. They are data processing tools suitable for the identification of underlying relationships between the independent variables (i.e., composition and process parameters) and the properties of intermediary (ribbon and granules) and final products (tablets). Accordingly, the obtained models can be used as predictors of the product characteristics. GRM-modelling is based on the estimation of experimental data with mathematical expressions. The models created by means of ANN, however, generate a response resulting from the exchange of weighted information flowing through interconnected processing elements (neurons). The interconnections between neurons are correspondingly adapted so as to generate an accurate output. Regardless of the nature of the modelling methods, the performance of the models created is a function of the system complexity (i.e. number of variables involved), and the quality of experimental data. Especially for the latter, another group of computational tools demonstrates to have a very promising applicability: the design of experiment (DOE) programs. By means of selecting criteria that depend on the number of variables and the regression intricacy, the DOE application selects the experimental runs that are indispensable to generate a powerful model within a modelling space. This appears to be very advantageous in the formulation design and the optimization of processes with complex multivariate nature.

2 BACKGROUND

2.1 The tablet as a dosage form and its role

The word *tablet* comes from the French word "tablete" (13th c.), "tablette" in current spelling [1]. Originally, the term referred to a thin block of any material. In the pharmaceutical field, tablets are solid dosage forms (usually for oral administration) of variable composition, size and shape, which contain a certain dose of one or more medicinal substances and are normally manufactured by compression of particulate components. There are defined subgroups of tablets established according to the process of manufacturing (e.g. whether they are coated or not), the way of administration, and also following pharmacokinetic criteria [2, 3].

Apart from the medicinal substance, also called the active pharmaceutical ingredients or API, tablets contain other compounds that usually have no pharmacological effect: the excipients. These substances develop basically three functions:

i) to aid in the manufacturing process and the handling of the active to achieve an optimized production process;
ii) to protect the API from the ambient (light, humidity); and
iii) to control the releasing of the API in order to reach the target organ, tissue, etc. (e.g. a certain region of the gastro-intestinal tract).

Tablets are, in short, the *vehicle* for the API. They have to ensure the content of the entire dose, protect the molecule if necessary, and ensure the proper delivery of the drug. The attributes of the tablet as a dosage form depend on its physicochemical and mechanical behaviour [4]. The latter is determined by the manufacturing process parameters and the mechanical behaviour of the substances of the blend.

The true relevance of tablets is that they are the dosage forms preferred by patients and manufacturers. For this reason tablets are still the most common used oral dosage forms. From the point of view of the patient, the oral administration is the easiest and the most pleasant free from pain, odours and unpleasant flavours (in case to be coated). Moreover, the difference in shape, size and even colour make tablets easy to recognise, and even provide them with nice appearance. As for the manufacturers, the tablet is the simplest alternative of all drug administration forms:

1) Tablets are easy to produce, in large quantities and in a short time
2) The production is easy to control, and the API dosage is exact with very low tablet to tablet and batch to batch variability
3) The process is generally clean, and the conditioning and boxing up do not represent a big technical challenge
4) Finally, tablets possess long shelf life and require less attention on their storage conditions compared to other forms like gels, ointments, suppositories, oral liquids and parenteral preparations

2.1.1 The relevance of tablet formulation

In general terms, the formulation is the constitution of a cluster of elements that follows a number of rules to solve a given problem. In pharmaceutical sciences, the formulation deals with the problem of achieving a final product that fulfils certain requirements in order to become the vehicle in which the active molecule is incorporated for its administration. The rules followed, in turn, are the parameter settings and processing steps that must be implemented to ensure firstly, that the product becomes a proper dosage form with the required properties that meet quality standards described by the company, and on a larger scale, by the international Pharmacopoeias and the regulation authorities.

For most people a tablet does not hide any mystery. It is a round solid object that can be acquired in pharmacies or other premises and that will help in recovering from a complaint after being taken. Upon deeper inspection, what in a glance seems like a simple pharmaceutical product becomes, in turn, a really complex process in terms of formulation and R&D. Previous to the scale-up to industrial production, a huge investment in effort, time, staff, and consequently large amounts of funding that are spent to find out the optimal tablet formulation is required. For this purpose, the formulator or team of scientists will have to show their expertise, scientific background, and working skills.

Generally, when we talk about dosage forms, the term "formulation" is used to refer to a list of substances and their proportions processed into tablets. The galenical scientists will be in charge of finding the components, the amounts at which each substance will be added, and the optimal process parameters that guarantee the manufacture of a product that meets both, quality standards and therapeutic goals. Though tablets are widely used dosage forms with more than a century of history [4], the search for new formulations and the improvement of those that have been already developed is still ongoing. The continuous introduction of new products and new active molecules in the market, together with the need to reduce costs and increase the production without compromising the product quality, speeds up the activity in this field.

Economically, the production of the dosage form has to be feasible and cost-effective. The manufacturing costs are the major part of a company's total expenses [5]. The choice of the raw materials and the optimization of the process, with a reduction of time, energy and stuff requirements, increase the competitiveness of the product in the market. Nevertheless, the production process and the end product have to meet quality standards. The fulfilment of quality criteria is also duty of the galenical scientist, whose work should certify the development of a process with a product that fulfils all requirements. However, the process has to be also reproducible and present negligible variability. The manufactured tablets have to comply with stability criteria of storage under certain environmental conditions. They have to preserve the API from exposure to humidity, warmth and light, and at the same time they must possess certain endurance, which is necessary to avoid dosage loss and, in some cases, even the therapeutic failure due to damages in the tablet.

From the perspective of the therapeutic, to consider tablet disintegration and API release time as exclusive parameters involved in the drug bioavailability does not ensure a therapeutic success. Thus,

as a dosage form, the tablet has to carry the correct amount of drug, it has to deliver it in the desired location in (or through) the proper period of time and at a proper rate. It also has to preserve the chemical integrity of the drug until the dosage form reaches the releasing region at the gastro-intestinal tract [6], for what the interactions between substances have to be identified and established so as to detect potential chemo-physical incompatibilities. Moreover, external appearance (size, shape, colour, embossments, etc.) makes tablets easily recognizable and can help in the achievement of a successful drug therapy.

According to all arguments discussed above, the perfect formulation would be one that results in stable, regular shaped, smooth, hard tablets, manufactured in a high performance process. In addition, the tablet has to deliver efficiently the complete dose of API in order to reach therapeutic concentrations in plasma during the period of time necessary to achieve its pharmacological effect.

2.1.2 Two basic requirements for tablets: endurance and optimum API release rate

Despite all attributes mentioned previously, according to [7], the tablet hardness and the release time, together with the dosage accuracy, are the most important tablet characteristics. After their manufacture, tablets are subjected to bumps and tumbles during the conditioning into blister packs, the storage, the transport, the distribution, etc. This can damage the tablet and hazard the integrity of the dosage by attrition of tablet edges or the breakdown of the form, which would be especially dramatic for retard forms or coated tablets causing the failure of the therapy. The tablet should reach therefore at least enough endurance to avoid any defect caused by external stress. The tablet hardness is characterized by the determination of the tensile strength (σ). It measures the amount of stress applied on the tablet necessary to produce a diametrical failure in the specimen. The stress reached in a flat faced cylindrical tablet is calculated as in [8]:

$$\sigma = \frac{2P}{\pi D t} \qquad (1)$$

where σ is the tensile stress, P is the applied load, D is the tablet diameter and t corresponds to the tablet thickness. This test is standard in the evaluation of the tablet hardness, and indirectly will deliver information about the degree of material densification (see chapter 2.1.3) and the quality of the manufacturing process. The diametrical collapse of a tablet takes place at weak particle bonding regions of the tablet mass. The fracture propagates as a defect in the structure causing a crack. The propensity of a tablet to fragment is dependent on the material properties, its tendency to deform and create bonds between particles, and on manufacture parameters.

Biopharmacists consider the drug release as the first step that will limit the bioavailability of the drug. The API has to be released prior to be absorbed. The delivery of the drug from a tablet has basically two phases [9]: i) the disintegration of the tablet into smaller particles and ii) the dissolution of the API and the diffusion into the target tissue. The disintegration time depends not only on the behaviour of the formulation substances after getting in contact with the gastrointestinal fluids, but also on the

mechanical properties and the structure of the tablet. The first step of the disintegration is the penetration of water into the tablet [10]. The tablet porosity and the inter-particle contact becomes therefore an influence factor in the water uptake and the subsequent tablet disintegration. Consequently, as the densification is closely related to the tablet hardness, the formulator has to find firstly a balance between tablet cohesiveness (i.e. tablet hardness) and release time [11] before introducing any changes in the formulation or the processing parameters. Thus, a tablet cannot be extremely hard and take hours to disintegrate (if the latter is not desired). Secondly, the selection of the components is crucial to define the speed of disintegration. This has been described as an effect of the weakening or annihilation of intermolecular bonds in contact with water [8, 12, 13]. However, each material has a specific disintegration mechanism. Thus, MCC absorbs water increasing the particle volume (active mechanism), while lactose needs in first place water penetration to reduce the inter-particle force and to disperse into smaller particles that afterwards dissolve (passive mechanism). Other components present in the blend can induce variations in the disintegration behaviour. For instance, the interaction with water may change after the addition of hydrophobic lubricants, as observed by others [14, 15]. The lubricant forms a continuous film around the particle that reduces the penetration of water and extends the time of disintegration. Nevertheless, if a rapid disintegration is desired, especially in formulations with water soluble excipients (i.e., passive disintegration mechanisms), the addition of disintegrants is recommendable. These are substances that will reduce the time of disintegration actively. If, on the contrary, we need to slow down the API release (retard forms), the tablet has to present low porosity and high inter-particle bonding forces in a lattice in which also components with low water affinity are present. The binders are substances that have high contact surfaces or that are easily adsorbed around other particles surface, increasing the bonding force, the tablet hardness, and slowing down the tablet disintegration.

The proposed biopharmaceutical classification system (BCS) of the FDA [16] catalogues the drug molecules considering two factors that determine the drug bioavailability, namely the molecular solubility and the tendency to be absorbed into the system. In terms of drug delivery mechanism, though disintegration determines how the drug is spread and delivered to the system, the own solubility properties of the API will determine in what extent, and after how long, the molecule will be available for its absorption. This depends on molecular properties (polarity, pKa, solubility product, etc.) and on the shape and morphology of the API crystals. Thus, in [17], the authors observed that after re-crystallization, the dissolution properties of ibuprofen improved. Consequently, also API crystalline morphology and particle size have an important influence on the release rate.

2.1.3 Tableting process

Tableting is a compaction process through which stress is applied on material by a uniaxially displacing punch (single-punch press) or two punches approaching simultaneously (rotary press) that fit into a cavity (a die) into which the material is confined. The reduction of bulk volume and the successive changes in the material originate the consolidation of the powder or granulated material into a solid form: the tablet.

In this work we often will refer to tableting as *compression* or *uniaxial compaction*, which is a more technical term applicable to all kind of material compressed inside a die.

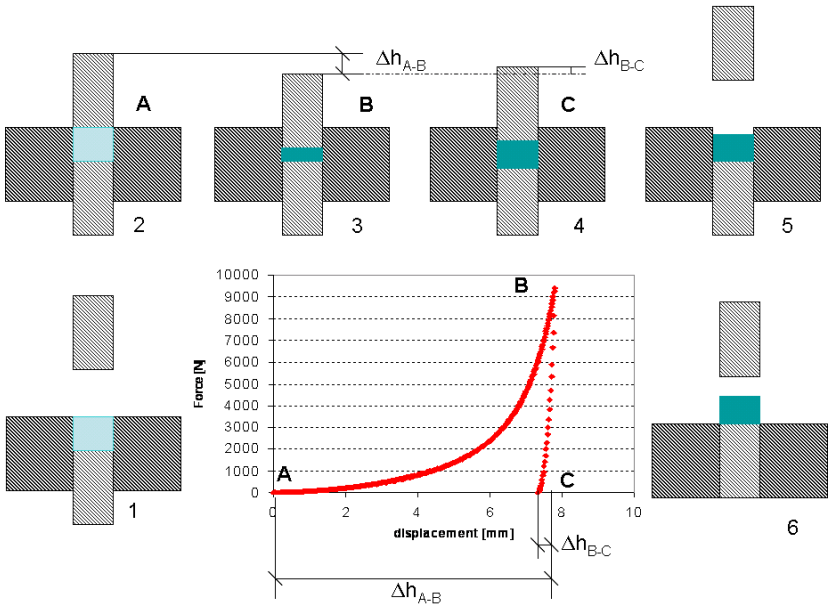

Figure 1. Representation of the compression cycle in a single-punch tablet press together with a strain-stress profile generated during the compression of MCC

In Figure 1 the different stages of compression in a single-punch tablet press are represented together with a stress-displacement plot, corresponding to the strain-stress values registered for the upper punch during the tableting process of 600 mg of MCC in a die of 13 mm in diameter. The tableting starts from stage 2 when the punch contacts the powder. At this point, no stress is exerted on the bulk yet, corresponding to the start point of the stress-strain profile (A). The existing forces between the particles are still those affecting the loose bulk density. In the next step (2-3), the downward movement of the punch forces the reduction of the bulk's volume and the material withstands the densification. As a consequence, the stress exerted by the punch to overcome the resistance offered by the material also rises. During the volume reduction, the material suffers changes similarly to those in roller compaction (section 2.2.1) until a certain level, where a maximum pressure is reached (B) and the bulk has been reduced to a minimum volume (after a displacement corresponding to $\Delta h_{A\text{-}B}$). The upper punch starts to return to the initial position and the stress starts to be released. The stress values registered in this phase correspond to the exerted by the material during its elastic recovery (relaxation) in the compression direction. The stress becomes zero after the displacement $\Delta h_{B\text{-}C}$ (4), which corresponds to the total expansion suffered by the material after the elastic relaxation. Finally, when the upper punch has returned to its original position (5) the tablet is ejected by the lower punch (6).

Environmental conditions, material properties, and process parameters determine the properties of the produced tablets. During the tableting, even the entry of the material into the die is a source of variability. The interaction between particles (internal friction) and between particles and die cavity (external friction), the origination of density gradients inside of the bulk (e.g. after segregation), the air permeability, and the shoe speed, have a strong effect on the entry of powder into the die [18, 19, 20,

21]. The flowability of the bulk is crucial to ensure a regular filling of the die, especially at high compression speeds, when the risk of tablet content variability increases.

The vertical strain drives the particles to adopt new configurations and introduces structural changes within and around them. The tendency for the compacting material to respond to these changes will influence the progress of the material compaction and the final properties of the produced tablet. This behaviour is attributed to the material *tabletability*.

2.1.4 Material tabletability

The term *tabletability* was first used by Leuenberger and Rohera [22]. They defined it as the ability of any material to be processed into tablets, and it is the result of combining two other material depending variables: the *compressibility* and the *compactability*. The same authors defined compressibility as the ability of the powdered material to decrease in volume under pressure, whereas compactability is the material's ability to be compressed into a tablet of a given strength. Both are material specific. However, they are closely related since they depend on the mechanisms occurring during the volume reduction.

The degree of cohesion and adhesion between particles is a function of the *effective compression work* expressed as:

$$W_{eff} = W_{tot} - W_{trans} \qquad (2)$$

where W_{eff} is the effective compression work. W_{tot} is the total work exerted on the powder bed and W_{trans} is the amount of work transferred to the system. W_{tot} is the sum of the stress exerted and is dependent on the magnitude of force, the rate of application and the time of application [23]. W_{trans} corresponds to the quantity of energy available to overcome frictional forces, reorganize particles, reduce the bulk volume, and overwhelm the material elastic recovery. W_{eff} will define the energy used by the system to force the failure of the particles and for the creation of new bonds.

The tabletability of a material is the sum of multiple factors: the contact surface area between particles, the number of potential effective bonds that can be established, the type of bonds and their distribution within the tablet mass. Thus, the material densification and cohesion achieved with a given compression energy will depend essentially on the following particle characteristics:

i) *Particle size* [22, 24-27]. Small particles have a larger contact surface, increasing the capacity of interacting with adjacent particles. On the one hand, it has a negative effect on the flowability and the air permeation through the bulk and increases the friction interactions. However, the smaller the particles, the greater the number of contacts per unit volume and hence, the stronger will also be the inter-particular bonds [28].

ii) *Porosity* [29- 31]. The particle deformation is controlled by the intra-particular porosity. Porous particles present higher deformability that leads to an increment of new bonding surfaces and

the creation of new inter-particle connections, increasing also the particle interlocking [32].

iii) *Shape and morphology* [32- 38]. Not only the crystalline morphology, but also the particle shape will suffer changes during the compression. Spherical, regular and smooth particles will present low friction interaction (i.e., better flowability), but also lower bonding surface. On the contrary, irregular shaped, rough particles consume more energy for the particle redistribution, and have poor flowability, but lead to a higher number of interactions and are likely to deform and to originate stronger inter-particle bonds.

iv) *Deformation mechanism* [23, 30, 35, 36]. It determines the material behaviour and the failure mechanism when normal stress is applied. Material plasticity defines the material's capacity for undergoing irreversible deformation. As for fragmentation, it describes the frequency of particle breakdown under certain compressing stress. Thus, while the particle plastic deformation increases the available contacting surface between particles, the fragmentation induces the creation of new surfaces and the interconnection between particles. Depending on the yielding stress exerted on the material, its behaviour can be plastic other brittle [39]. Finally, the elasticity corresponds to the ability of the material to recover from a deformation. If an elastic particle is compacted under the failure load it will rebound to the original shape, releasing energy (e.g. as heat).

Pharmaceutical products are normally a mixture of substances and therefore the tabletability is the result of the behaviour of the individual components and their interactions. It has to be born in mind that a pharmaceutical blend will not present only one consolidation-deformation mechanism, and that the introduction of any new component may vary the material response to deformation stresses. This is discussed in sections 6.1.3 and 6.2.3.

2.1.5 Material densification models and tableting parameters

Compression stress is the process parameter with the highest influence on the material densification. It determines the amount of energy applied on the powder and consequently will define the degree of material densification. As it has been shown previously in Figure 1, the stress-strain profile the stress achieved is a function of the punch displacement. Obviously, further displacement would have needed larger compression forces to reach larger volume reduction. Several equations have been proposed to describe the relationship between the volume reduction of the tableted material and the compression force (strain) exerted by the system. Most of them have been critically analyzed and discredited by some authors who considered that they do not give proper information about the process [40, 41]. However, Çelik [42] examined some of them and concluded that each expression can be used to approach the relationship between pressure and volume reduction at different stages of the tableting in which a compression mechanism is predominant. Two of the most frequently used models in the description of the material densification are Heckel equation [39, 43-48] and Kawakita equation [49, 50] (see 9.2 in Appendix). A third model that we would like to mention is Wiegel's [51] (see also 9.2) who developed an equation that fits profiles of densification values at a wide range of pressure levels of plastic and brittle materials successfully.

In this thesis, however, the most often used model is the one proposed by Heckel [41]. He claimed that the densification of a material follows the equation

$$\ln[1/(1-\rho_r)] = kP_a + A \qquad (3)$$

where ρ is the material relative density, k is a constant related to the material deformability, P is the compression pressure exerted and A is the intercept. According also with the Heckel hypotheses, during the material densification, the plotted values of *ln [1/(1-ρr)]* (in so called *Heckel plots*) provide information about the material deformation behaviour. In the Heckel plot of Figure 2 we plotted the values of *ln [1/(1-ρr)]* corresponding to different pressures for the compression and the decompression steps during the tableting of MCC. As depicted by the represented red line, part of the profile of the compression can be approached to the linear relationship from Equation (3). Thus, the linear Heckel plot, or to be more accurate, the linear fragment of the profile, corresponds to the pressures values for which the material deforms plastically (such as MCC in Figure 2). Moreover, the slope of this linear relationship is also used to determine the *yield stress*, i.e., the force required to deform plastically the material. This value can be calculated by the following equation:

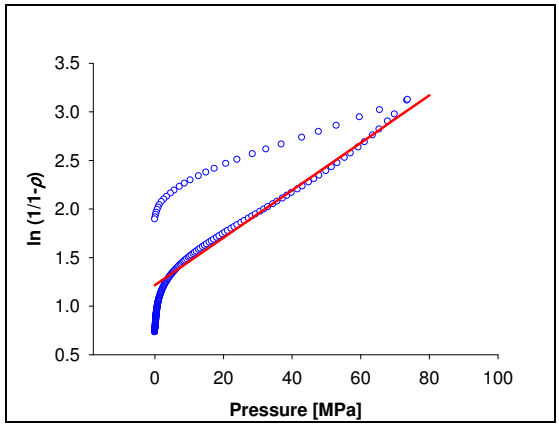

Figure 2. Heckel plot for the compression of MCC

$$k = 1/3Y \qquad (4),$$

in which k is the value of the slope and Y is the yield stress. Similarly as for the yield stress, one can also calculate the *yield pressure,* corresponding, in this case, to the pressure necessary to induce the plastic deformation of the material, which is calculated as

$$k = 1/Py \qquad (5).$$

In this equation Py is the value for the yield pressure. According to Heckel, plastic compactable materials follow linear Heckel plots which slope depicts the material ductility.

As for the tableting parameters, probably the pressure is the most relevant. Compact hardness is directly proportional to the pressure applied [23]. Accordingly, also the material densification and the hardness of the compact are directly correlated. Whiteman and Yarwood [52] and later Wong and Pilpel [36] found a linear relationship between the logarithm of the tablet hardness and the tablet density. However, this approximation seemed not to be accurate for all blends. Thus, Kuentz and Leuenberger [53], Ramirez, et al. [54] and Michrafy, et al. [55] proposed a more accurate approach in which potential and linear mixing rules were considered for the calculation of tensile strength in tablets made of multiple components.

The speed of the tableting process will affect both the die filling and the material compression. For the

former, high speed represents also less time for the bulk to fill up the die. Moreover, turbulences inside the die, irregular particle flow, and enhanced air escapement may increase the risk of mass variability from tablet to tablet. Finally, the speed of the tableting determines the time that the stress is exerted on the powder (i.e., the dwell time). Shorter dwell times will reduce the amount of energy exerted on the powder and therefore will lower the degree of particle cohesion and adhesion, producing weaker tablets [56].

Finally, other factors, such as ambient moisture can affect the material densification. The moisture content in the material is a function of relative humidity and temperature and affects the powder deformation behaviour [57]. Moisture alters the substance crystallinity [58], particle interaction and flow [59], and even the deformation behaviour, generally increasing material plasticity (see 5.2.3.1).

2.1.6 Densification heterogeneity in tablets

During the material compression, axial (vertical) and radial stress gradients are generated. Assuming the powder blend as a mechanical fluid, and picturing the bulk as a group of independent columns of powder (as in Figure 3) where the particle rearrangement is negligible, we can see that internal frictions and powder-die-wall friction gradients generate local heterogeneities in the load and shear stress vectors within the die [60]. As a result, the degree of densification of the material throughout the tablet mass is not uniform.

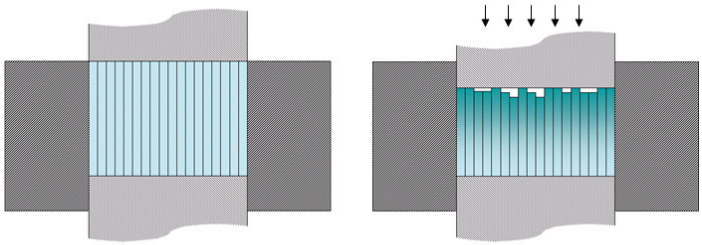

Figure 3. Representation of the origin of densification heterogeneities within the tablet mass during compression

Michrafy [60] modelled the tableting considering friction coefficients and compared the results with experimental results. The values obtained in both calculations (empirical and modelled) demonstrated that there is a difference of densification level between the top and the bottom of the tablet, elucidating thus the existence of irregularities in the stress distribution.

Variability in the axial strain was also experimentally detected by Kadiri, et al. [61], which was attributed to the particle-particle and the particle-die wall friction interactions. By analyzing the solid fraction of material layers that were stacked and compressed uniaxially in the same process, they observed that the densification of the lower layers was smaller than that of the upper ones. Another evidence of the irregularity in the densification gradients is the variability of particle sifting within the powder bed observed by Yang and Fu [62], and Nystrom, et al. [39]. The authors tracked the particle movement within the die using X-ray axial micro-tomography and observed that the particle movement was significant during the initial steps of the compression (volume reduction). Nevertheless, the particle displacement was much more evident in particles situated close to the upper punch than towards the die-wall interface. In addition, the tablet density variations originated by the

wall friction was studied by Sinka, Cunningham and Zavaliangos [12, 63]. They compared experimental density maps of tablets with FEM numerical approaches and compared lubricated and not lubricated die compressed forms. The tablets presented denser cores when no lubrication was used while the tablet edges became denser when the die was lubricated. Also Wu, et al. [64] modelled the effects of the die-wall friction on the tablet density distributions using FE and observed a heterogeneous distribution of the material densification within the tablet mass.

As a result of this gradient of densifications, the tablet possesses areas of different density, which not only affects the physical integrity and the endurance of the tablet but also can induce variability in the release of the API.

2.2 Dry granulation by roller-compaction: an intermediary process in the tablet production

The granulation is an agglomeration process in which particulate solids are bonded through solid bridges, physical adhesion or chemical and molecular forces [39] to originate larger particles with a given size, shape and structure. Compared to the original powder, the resulting granules show some advantageous qualities that are of high interest for the formulation and the manufacture of solid dosage forms [65, 66]:

i) Higher bulk density, reducing the volume occupied by the storage and easing the transport of material.
ii) Better flowability and enhancement of the material ability to fill dies and hoppers necessary to keep a constant drug content, especially at high compression velocities.
iii) Improved tabletability properties by increasing the de-aeration ratio and, in some cases, increasing the bonding capacity of the agglomerates.
iv) Reduction in the production of dust and cross-contamination.

From all agglomeration processes currently used in pharmaceutical manufacturing, *roller compaction* and *slugging* are the only two[1] dry agglomeration processes, i.e. in which no solvents are added to the compacted blend. The same principle applies to both methods: a material is consolidated applying pressure on it and is then milled into granules. For that reason, they are considered to form part of the *pressure agglomeration* processes [67]. The mechanism of agglomeration by pressure is based on physical adhesion, i.e. fragmentation, plastic deformation and particle interlocking applying a yield stress. However, the methods of material agglomeration in roller compaction and slugging differ from each other. In roller compaction the material is constricted in the gap between the rollers, whereas in slugging the material is fed in a die and then compressed. During the 50 and 70s slugging was the most frequently used dry agglomeration process in pharmaceutical industry [68]. However, the globalization and the evolution of the pharmaceutical manufacture in the last 25 years and the consequent need for higher processing rates, together with the arisen mandatory GMP specifications and QC standards, made roller compaction grow as the preferred dry-granulation. Roller compaction

[1] Spray-congealing and melt extrusion also might lead to granular particles, but are not considered particle agglomeration processes

fulfils the current requirements of the pharmaceutical industry since it is a continuous agglomeration process [69] with large production capacity, and it is likely to be automated. Moreover, roller compaction is an easily scalable process [70] that offers better batch to batch reproducibility and homogeneous granules of a better quality with lower demand of energy and operators [71]. In addition, PAT techniques such as NIR can be used for the QC and standardization of the RC process [72] increasing even more the success in the fulfilment of standard quality requirements in pharmaceutical production processes in which roller compaction is an intermediary step.

2.2.1 Dry-granulation by roller compaction

Roller compaction (RC) is a manufacturing process in which a bulk of loose material is fed between two counter-rotating rollers and forced to pass through a narrow gap to generate cohesive compacts in form of briquettes, flakes or strips (ribbons). These are thereafter milled to obtain granules of desirable size and generally processed for manufacturing capsules or tablets [73].

In the second half of the 19th century, the first compactors were used for the production of wood and coal briquettes [74]. Since then, the roller compaction became widely used in metallurgy and chemistry. Some time later, the roller compaction started to be used in the food manufacture and the pharmaceutical production [75]. However, for the latter industrial branch, roller compaction turned into the first-choice agglomeration process for the granulation of solvent (moisture) and heat sensitive substances. Moreover, the low demand for energy, staff and space, make roller compaction a good alternative to wet granulation processes like spheronisation, extrusion, fluidized-bed or high shear granulation.

There are two main steps during the roller compaction process: i) the densification of the material into compacts and ii) the consecutive milling of the compacts into granules. Figure 4 is a simplified drawing of a Gerteis MiniPactor. However the same principles and main components apply to any other roller compaction device. The elements of a roller compactor can be divided into three functional units:

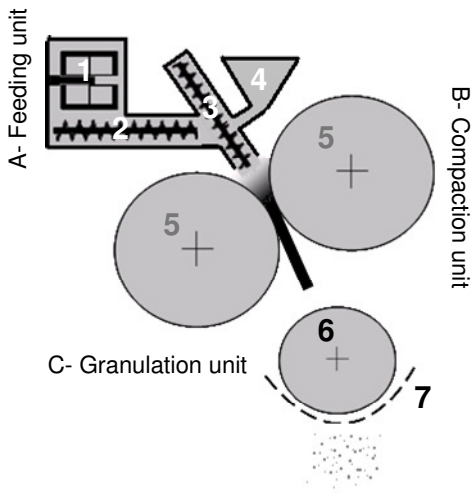

Figure 4. Sketch of the main functional units in a Gerteis MiniPactor

A- Feeding unit. The feeding unit transports the loose material from the pouring hopper (1) to the compaction unit. The pouring hopper of the MiniPactor is equipped with a winged rotor that leads the material to drop homogeneously on the horizontal feeding screw (or simply feeding screw) (2). The powder is delivered next to the vertical screw (tamping auger or *pre-compaction* screw [76]) (3), which forces the material to pass into the roller gap. In MiniPactor a small inlet funnel can be fit (4), which is basically thought for the compaction of small quantities of material. Also, though it is not represented in this figure, there is a connection at the vertical screw assembly to which a vacuum pump can be

attached.

B- Compaction unit. The compaction unit is formed essentially by two counter rotating rolls (5) the boundaries of which are confined either with rims fitted in one of the rollers, or with side plates sealing the whole compaction area (Figure 5.1) avoiding the leakage of loose material. The rollers grip the powder into a narrow gap, inducing that way material densification. The outcoming compact falls next into the granulation unit. In a MiniPactor, the right roller (or slave roller) is mounted on a movable shaft that is connected to a hydraulic system that maintains a constant compaction stress. This allows the control of the roller gap during the run. In Figure 5.2 usual roller conformations are represented. Rollers are usually interchangeable and can present different geometries and surfaces. The shape of the rollers and its influence on the compaction of material has been studied intensively. Thus, Funakoshi, et al. [77], and later Parrot [78], compared different roller designs and concluded that the use of a concave-convex roller pair improved the pass of the powder through the roller gap and originated uniform compacts.

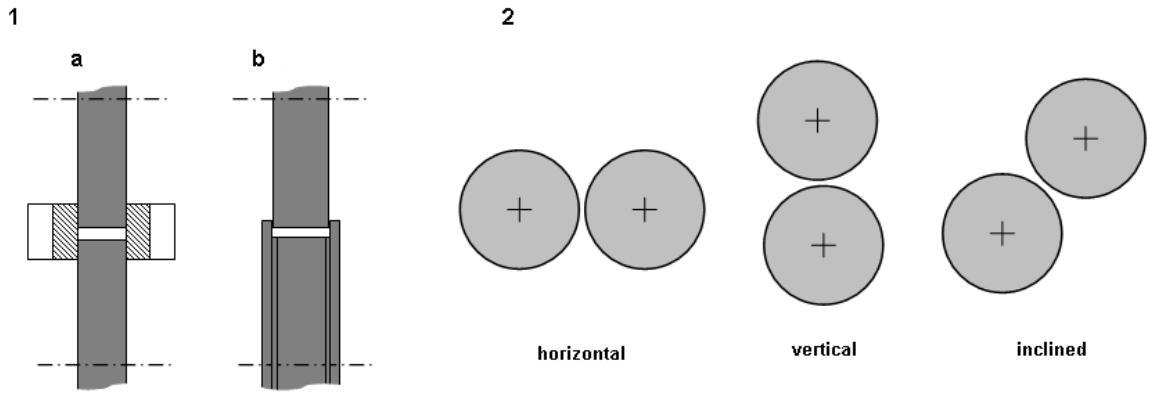

Figure 5. 1) Common sealing configurations: ***a.*** Side cheek plates. ***b.*** Sealing rims. ***2)*** Roller configurations in commercial compactors

C- Granulation unit. Milling (grinding) takes place in this unit. The oscillating granulation rotor (6) forces the compacts through a granulation sieve (7) of a given mesh size, originating the granule.

Despite the fact that each unit has different functionality, all units turn into a sole process in which a large number of parameters can be adjusted and controlled. Due to the large number of factors involved in each of the steps (some of them even not described yet), the understanding and a comprehensive description of the whole process is still lacking.

2.2.1.1 Feeding

At first glance, feeding is simply the transport of material from the hopper to the compaction unit, but during this process, and especially towards the final stages, there is a large number of phenomena occurring that influence the particle mobility, the interactions between particles, and the material compacting behaviour. Blending, homogenization, air permeation and fluidization of the bulk, particle reorganization, segregation (i.e. spontaneous sifting of small particles), interstitial air permeation, and pre-densification of the material are some of the mechanisms occurring during the conveyance of material to the compaction zone.

The different configurations of the common feeding systems in commercialized devices are represented in Figure 6. They are described in detail in [65]. As shown in Figure 6.B, in a MiniPactor the tamp auger (vertical screw) is slightly leaned.

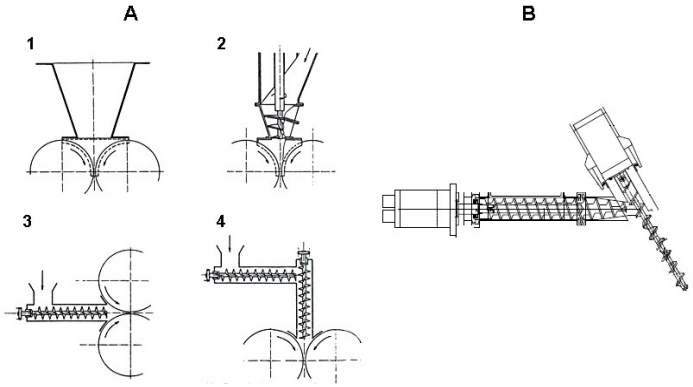

Figure 6. Common feeding system configurations. ***A)*** *1*- gravity *2*- screw forced *3*- horizontal screw forced *4*- double-screw forced [65]. ***B)*** Design of the feeder in a MiniPactor (provided by Gerteis)

However, already in the inlet hopper we find the first source of variability. The dispensed bulk material is set in motion by the rotor (also called bridge breaker [79]), which homogenizes the blend, brakes clumps and avoids particle segregation. Moreover, the mobilization and the aeration of the bulk induce a certain fluidization effect, which reduces the interstitial particle-particle interactions [80]. As a consequence, bulk materials that originally possessed poor flowability are transported straightforwardly with any need of pre-processing. While insufficient rotor velocity would not ensure a regular flow of the material towards the feeding screw, excessive rotation speed would have also negative effects. The extreme air entrapment increases the turbulences in the powder flow, the quantity of dusts produced, and can alter the material properties (e.g. particle size reduction by active grinding).

The fluidized powder is conveyed by the feeder and the tamp augers, which in addition have to ensure the uniform conveyance of powder into the compaction zone. The particle motion induced by a screw (from an extruder, though) was modelled by Moysey and Thompson in DEM -discrete element modelling- [81]. They pictured the trends of powder displacement while being transported through the screw and characterized the "solid pulsing", i.e., the irregular supply of material induced by the geometry of the screw wings, the air entrapped by the bulk, and other fluctuations in the powder flow. This "pulsing" phenomenon is also qualitatively described in [82] on the analysis of powder feeding in a roller compactor. A regular drag of powder by the horizontal screw reduces the throbbing delivery of powder to the tamp auger. However, irregularities on the flow are unavoidable. In the MiniPactor, an especial setting of the parameters allows the user to set a ratio between feed and tamp auger rotation velocity in order to keep the conveyance of material into the compaction area steadily to a certain amount.

From the two screws involved in the powder feeding in a MiniPactor, the tamping auger is of big importance since it has double functionality: feeding and pre-compacting. It does not only bear material in the compaction region, but once in there, it forces the powder to get slipped by the rollers applying stress. At this point, the particles rearrange, the air entrapped permeates and flows up, while the bulk volume is reduced and strain forces (0.4 to 1.2 MPa) are exerted on the powder [83]. The pre-densification of the powder increases the friction interaction with the roller surface and eases the gliding of the material between the rollers. The horizontal screw speed is a parameter that determines the throughput of the compaction unit [84], and along with the compaction unit parameters, it also

defines the degree of densification of the compact (density or solid fraction). Jerome, et al. [76] registered the force applied on the material during the compaction and observed the increase in the exerted stress at higher *pre-compaction* screw speeds. Consequently compact and granule properties such as friability or particle size distribution are strongly dependent on the horizontal screw parameter settings [85]. Falzone, et al. [86] attributed the strong effect of the feeding unit settings on the compaction process to its influence over the compaction pressure and the dwell time of the material in the compaction zone. The oscillations of material compaction due to the tamp auger were investigated by Simon and Guigon [87-89]. They described and modelled cyclic fluctuations in the normal stress by analyzing the compaction of the material. They registered the strain at two points of a roller which surface was equipped with piezoelectric transducers. They observed periodical fluctuations in the stress values which frequency turned out to correspond to the screw rotation speed. In addition, the same cyclic patterns were observed by tracking particle trajectories at the feeding region, analyzing the transmitted light gradients through sodium chloride compacts, and the examination of the coloration in ribbons made of lactose monohydrate blended with coal. They concluded that the geometry of the screw induces irregular pre-densifications of the material, having an important effect on the quantity and quality of pre-compacted material dragged between the rollers and the strain exerted on it.

However, not only the parameter settings and the device configuration are responsible for material feeding fluctuations. Also inherent material attributes are involved in them. For instance, particle size, material bulk density and flowability, vary the process of feeding. In some cases, the feeder screws are not capable of conveying material steadily, especially with substances of extremely low bulk density and small particle size. Here, the use of vacuum is useful in order to increase the de-aeration of the powder and ease the material transport. In Table 1, the bulk densities of virgin and roll compacted-granulated silicon dioxide (Cab-o-Sil) at different compaction specific forces are compared. Due to its extremely low bulk density, the electrostatic charge, and the high contact surface area between particles, the use of vacuum was necessary to force the entrance of material into the compaction zone.

Table 1. Bulk density values for roller-compacted Cab-o-Sil at different specific compaction forces

	Bulk density [g/cm^3]
Loose material	0.041
5 kN/cm	0.280
10 kN/cm	0.320
15 kN/cm	0.340
20 kN/cm	0.300

A regular feeding is crucial for the compaction process. It has to ensure the continuous transport of material into the compaction zone with minimal fluctuations. Figure 7 is a plot of the process parameter values during a roller compaction run. The red arrow depicts the stable value of auger rotation velocities that warrants a regular uniform supply of material into the compaction zone, and therefore, the process does not suffer large variations and reaches its steady state. In order to achieve a good roller compaction performance, the settings of the feeding system have to be adjusted at a rate that maintains the material supply at an optimal level [90]. Hervieu, et al. [91] described the need of keeping a certain ratio between screw feeder speed and roller rotation to reduce the fluctuations in the values of the process parameters and avoid the blockage of material in the roller gap. Lammens [92] demonstrated that large fluctuations in the compaction occurred if the supply of material into the

compaction area was not constant. S.Peter [82] investigated the influence of different compaction parameters (e.g., feeding auger velocity) on the amount of powder carried by the feeding unit and introduced modifications in the compaction device to achieve a regular powder supply.

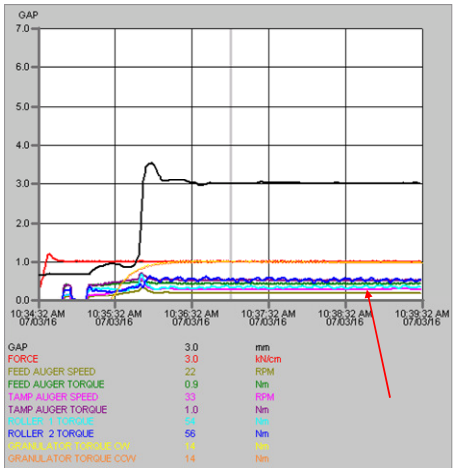

Figure 7. Steady state of the roller compaction process monitored in the MiniPactor control panel

2.2.1.2 Compaction

The compaction induces material densification. This occurs in the confined area between the rollers (the roller gap), in which they reduce the volume of the bulk and force the densification of the material. During the compaction, not only the total amount of stress, but also the effects on the material deformation induced by interstitial air and elastic recovery determine the level of densification achieved by the resulting ribbon. The process of compaction between the rollers is, therefore, a complex deformation process that involves non-linear contact and material behaviour. However, as in any other compaction process, the volume reduction under strain leads to a sequence of changes endured by the material [39, 93, 94]:

I-Particle rearrangement. It already occurs at low compaction forces. The particles reorganize themselves and move closer together to fill voids and release air entrapped.

II-Deformation and fragmentation. At higher compaction forces, and depending on the mechanical character of the substance, the particles are plastically deformed or fragmented. This originates new contacts between particle surfaces and establishes contact points, increasing thus the potential number of bonds.

III-Bonding. The particles interact with each other and form cohesive bridges. The main mechanisms are the formation of solid bridges (sintering, melting, crystallization and chemical contact), bonding through capillary and surface tension, contact between binder bridges, molecular adhesion (London and Van der Waals forces), electrostatic attraction, and mechanical interlocking.

As presented in Figure 8, the compaction zone can be divided into three regions [95]: 1) an entry other slip region, 2) a compaction or nip region, and 3) a release region. The size of these three regions and the transition between them depend on the material properties and the processing conditions.
The first region (number 1) represented in Figure 8 corresponds to the so called *slip region.* The start of this region is defined by the entry angle. The powder (partially pre-compacted) enters the slip region where particle rearrangement, permeation of entrapped air and pre-agglomeration may occur. In this region, the peripheral speed of the rollers is considerably higher than that of the adjacent material. This, together with the feeding stress of the tamp auger and the subsequent increase of powder-roller

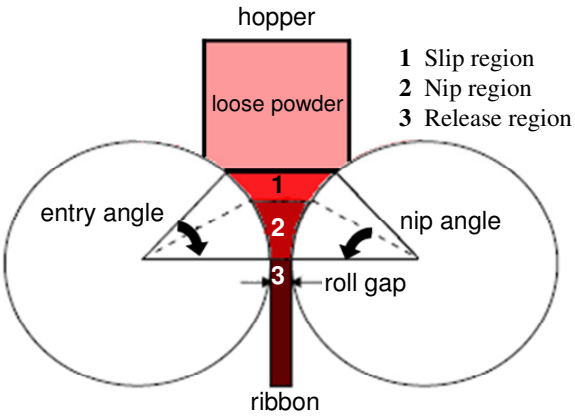

Figure 8. Regions of the compaction zone according to Johanson's model

wall friction angle, gives way to the draw of material between the rollers. Schoenert [96] studied the movement of particles in the slip region and observed that they stayed closer to the centre of the material stream rather than to the roller walls, which was attributed to the centrifugal force induced by the roller rotation. He also described a certain fluidization due to the upward flow of air squeezed out from the material bed. This was seen to compromise the throughput of the roller press when the fitted material was extremely fine. An appropriate transfer of material can be achieved using proper roller design. Daugherity and Chu [97] observed that rollers with serrated surface dragged powder more effectively and improved the performance of the compaction. Thus, the use of knurled or rough surfaces are recommendable when the friction at the powder-roller interface is insufficient [98] or when the compacted material tends to reach a high degree of pre-compaction already at very initial stages of the material slipping, becoming hard to convey into the roller gap by smooth rollers.

As the rollers continue rotating, the powder is gripped between the rollers. In a certain angular position, the velocity of the compacted material becomes identical to the rotation speed. This angle is characteristic for each process and is called the *nip angle* (number 2 in Figure 8). The angle value is a function of the internal friction of the powder, the material compressibility, and the friction between the powder and the roller surface [80]. Figure 9 represents the pressure profile as a function of the angular position of the roller. As it can be seen, the pressure exerted on the bulk starts to rise after the nip angle is reached. The material is conveyed than into the narrowest gap and is compacted as it is *nipped* between the two rollers. The pressure reaches its maximum (P_{max}) at the neutral angle, which does not necessarily correspond with the zero rotation angle [99, 100].

The compaction of the powder depends basically on the material stress-strain character, the interaction between particles (internal friction) and between particles and surfaces (see section 2.1.4). As for the *conveyance* of the powder in the slip region, factors like roller design and rotation speed can therefore alter the material densification. Jerome, et al. [76] plotted the resulting force during the compaction run and described the effects of different factors on the strain profiles. They could observe that the maximum pressure reached by the system and its fluctuation was dependent on inherent particle attributes, bulk flowability characteristics, water content of the blend, and roller surface.
The entrapped air in the bulk has been described previously to act upon the powder mobility during the feeding and the pre-compaction (see 2.2.1.1). It is also a source of variability during material compaction. Dec and Komarek [101] compared the effective compaction pressure for aerated and de-aerated powders and found that, as a consequence of the air escapement, the total load applied on the powders was lower.

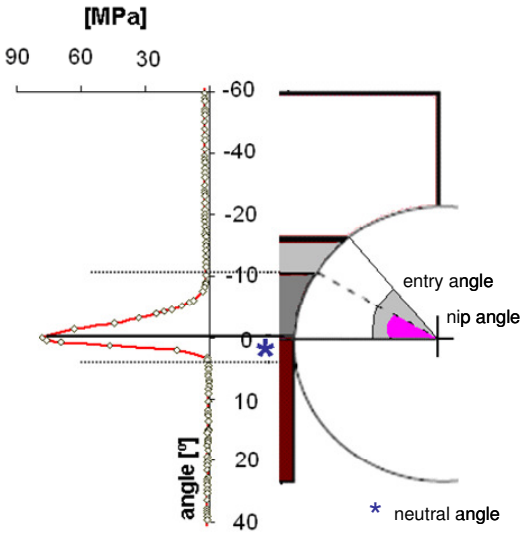

Figure 9. Pressure profile as a function of the angular position for the roller compaction of MCC and representation of the entry and the nip angle.

The large number of factors comprised here makes the distortion of the powder at the nip region almost unpredictable. However, some approaches have been made in order to improve the understanding of the compaction. Johanson [95] modelled first the pressure gradient at the slip and nip region. He was able to establish a calculation model for the transition between slip and nip region and formulated an equation to determine a compressibility factor for the compacted material. Sommer and Hauser [102] found discrepancies between the values calculated with this model and the experimental results. However, Bindhumadhavan [100] and Yusof [103] validated experimentally the model which demonstrated to deliver good estimations of their empirical results.

The material reaches its highest densification towards the neutral angle. After that point, i.e., at the start of the region known as *release region,* the compact leaves the roller gap (number 3 in Figure 8). However, certain pressure can be still registered due to the elastic recovery of the material.

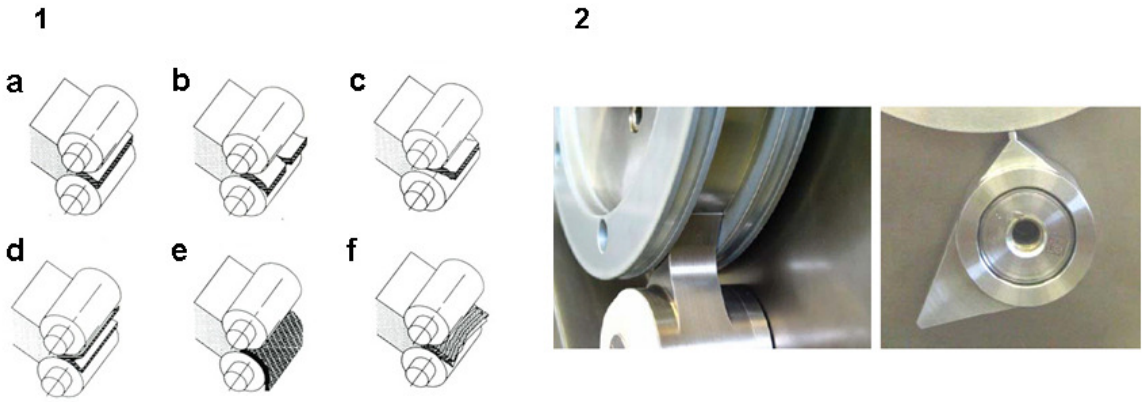

Figure 10 A) Shape patterns of released compacts according to [101]. ***B)*** Scrapers in the Gerteis MiniPactor

The compact leaving the roller gap might present different morphologies as it is shown in Figure 10.A. A regular compaction will produce continuous regular strips (*a*). Case *b* appears when the stress on the powder was not regular across the roller width and the central part of the ribbon is compacted above the material distortion failure constraint, inducing the over-compaction of material. Case *c* is due to an insufficient feeding of powder into the roller gap or can be caused also by considerable leakage of loose material at the roller edges. Cases *d* (splitting), *e* (sticking) and *f* (fissuring), might occur when there is slip-stick of powder on the roller surface.

Finally, to ensure that no rest of compacted material stays stuck on the roller surface, the compactor might be equipped with scrappers that detach possible compacted material (Figure 10.B).

2.2.1.3 Granulation

This process is also known as *milling*. The sheets, ribbons or briquettes of compacted material reach next the granulation unit in which they are milled. The granulator forces the compacts through a granulation screen (sieve). During the granulation, the compacts break at the edges by attrition and at the central parts by strain forces. The resulting particles are subsequently subjected to a large number of forces, generally inducing compression, shear and tension, crushing, cutting and cleavage.

The parameter that defines the granulation process is the *granulator clearance*, i.e. the amount of material passing through the granulation screen in relationship with the material throughput from the compaction unit. It is closely related with the residence time of the material in the granulation unit and the amount of energy required for the particle reduction.

The throughput of granulated material and the variability introduced by the compact granulation depends on the following factors:

A- Compact properties. The dimensions of the compact and its mechanical properties (hardness, elasticity, brittleness and plasticity) define the milling force necessary to overcome the cohesive forces and to fracture the material.

B- Mesh size and screen type. It defines the maximum dimensions of the particles. Due to the angular displacement of the rotor, the particle will not follow a perpendicular trajectory through the mesh, resulting in particles of smaller size than the mesh screen opening. The granulator screens can present also different configurations. Gerteis commercializes mainly two types: the interlocked wired sieve and the rasp-shaped screen. Verheezen, et al. [104] observed that the use of rasp-shaped sieves led to a finer milled product.

C- Rotor speed. High rotation speeds increase the rotator torque, i.e. the energy exerted on the particles. As a consequence of the increase of the velocity, the impact energy of the rotor blades on the particles and the number of collisions between particles rises. Also the angle of the particle trajectory through the mesh gets shallower, what reduces the effective mesh opening [105]. Thus, although the throughput of granulated material will augment, the mean granule particle size will be smaller.

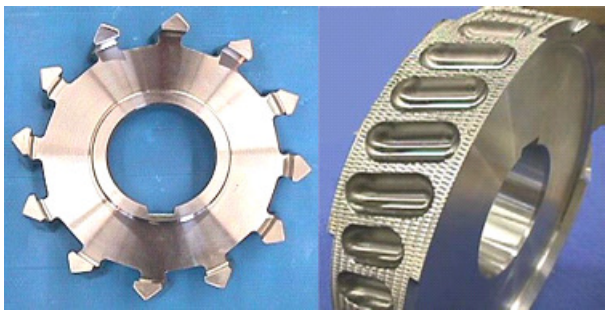

Figure 11. Rotor designs commercialized by Gerteis. Star (left) and pocketed rotor (right)

D- Rotor design and distance rotor-mesh screen. In Figure 11, the rotor designs of Gerteis are illustrated. The geometry of the rotor, along with the distance of the blades (or surface) with the granulator screen, changes the particle dynamics and the particle-particle, rotor-particle and mesh-particle interactions.

E- Feeding rate. At no time must the amount of material delivered into the granulation unit exceed the maximum clearance of the system [106]. This would end up with the clogging of the screen, the extension of the compacts dwell time in the granulation chamber, and as a consequence, the production of finer granules of uncontrollable size distribution.

Due to the apparently fortuitous character of the milling, the particle size of the end granule is normally poly-disperse [9]. The possible range of mechanisms on size reduction (crushing, attrition, breaking, cleavage, partition, screening, etc.), together with the bypass of loose material through the rolls, produce a wide span of particle sizes.

Bultmann [107] studied the effects of the mesh size and the distance between rotor and mesh and observed that larger mesh sizes resulted also in wider particle size distributions (PSD). He also demonstrated that an enlargement of the distance rotor-screen produced larger mean particle sizes. He concluded that narrower mesh openings produced smaller granules of narrow PSDs and that the distance rotor-screen should be adjusted to half the mesh size.

2.2.2 The effect of roller compaction conditions on granule properties

Table 2. List of variables involved in the granule properties

Material properties		True density Bulk density Size distribution Flow Hardness Brittleness Plasticity Elasticity Moisture content Conductivity
Ambient conditions		Relative humidity Temperature
RC Parameters	Feeding	Powder level in the pouring hopper Horizontal screw rotation Vertical screw rotation Vacuum
	Compaction	Specific compaction force Roller speed Roller gap Roller surface Roller conformation Sealing conformation
	Granulation	Rotator speed Rotation direction Rotator design Type of granulation screen Mesh size Distance sieve-to-rotor

The end product of the roller compaction process is a granulated material. Agglomerate properties such as particle size, particle morphology (shape and porosity) and mechanical deformability under yielding stresses will obviously characterize the processing behaviour and the end product attributes [108]. We have enumerated the modifiable process parameters during the roller compaction. However, as listed in Table 2, the granule properties depend not only on the roller compaction process parameters, but also on the own properties of the starting material (see section 2.1.4), on the ambient conditions, and even on factors such as the assemblage of the machine, maintenance, cleaning, etc. not listed in the table.

In Table 3 we have summarized the scientific work carried out on the study of factors and parameters of the roller compaction process that are involved in the variability of the granule properties.

Table 3. List of published studies focused on the effect of adaptable factors and variables of the roller compaction-granulation process on the end granule attributes

	Authors	Contributions
1994	Sahut Conreur / University of Lille Hervieu, et al. [91]	Impact of roller speed, feeder screw rotation speed, and the compaction force on the granule properties. Poor material feeding decreased the hardness, increased the granule friability and reduced the granule particle size.

1998	University of Gent Inghelbrecht and Remon	1- High pressure and high feeding screw speed produced optimum microcrystalline cellulose granules. The introduction of ibuprofen "disturbed the binding of the MCC fibers". The granule quality became poorer [29]. 2- Under same parameters, different types of lactose delivered different granule properties. In general, high compaction forces, slow feeding screw rotation and high roller speed resulted in the best granule quality [109]. 3- The controlled addition of water to the blend previously to the roller compaction decreased the amount of loose material leaking between rolls, reduced the granule friability, increased the granule mean size, and reduced the variance in the particle size distribution [110].
2001	University of Brussels Rambali, et al. [111]	Study of the compaction parameter effects on miconazole granules and buccal tablets. Larger mesh opening, smaller roller gap, high compaction force, and knurled roller surfaces produced larger particles but less compactable.
2002	University of Düsseldorf Woell and Kleinebudde [112]	Increasing specific compaction force resulted in larger particle sizes of lactose monohydrate placebo granules.
2002	University of Düsseldorf Grulke and Kleinebudde [113]	Sieve size has a significant influence on the granule size and therefore also on the releasing time of the tablets (larger granules release the API slowlier).
2002	University of Heidelberg Bultmann [114]	After carrying out several compaction passes, the granule mean size increased and the particle size distribution became narrower. The amount of fines decreased significantly and the flow properties improved.
2004	University of Halle / University of Düsseldorf Freitag and Kleinebudde	Micro hardness measurements and porosimetry calculations in magnesium carbonate compacts demonstrated that the increment of the specific compaction force resulted in higher micro hardness, at the same time that the percentage of fines diminished and the granules lost tabletability [34]. They also studied the effect of the variations in the blend composition on changes of particle size and flowability induced by the compaction force [115].
2004	University of Singapore Heng, et al. [116]	Roller compaction of *Baphicacanthus cusia* extract (natural indigo). Increasing PVP concentrations reduced the flow of powder and resulted into smaller friable granules. Reducing roller speed and increasing the feeding screw rotation improved granule properties.
2005	University of Antwerp Weyenberg, et al. [117]	They described the effects of compaction force, horizontal screw speed and roller speed on maize starch and ciprofloxacin granule's friability, flow properties, size distribution, porosity and density. Compaction force is the most important parameter influencing particle size. High compaction force, high feeding screw rotation and low roller speed increased the average granule diameter and decreased the granule friability, improved the flowability but decreased its tabletability.
2005	Purdue University / Bristol-Myers-Squibb Gupta, et al.[118,119]	Increasing the ambient humidity, the granules obtained from compacted MCC resulted in smaller particle sizes.
2007	University of Düsseldorf Herting and Kleinebudde [39]	Scrutiny from effects of the original material particle size, the composition and the solid fraction reached during the roller compaction on the flowability and tabletability of the granule. Porous granules had bad flowability, whereas granules from finer virgin MCC were more fluent. Blend composition also modified the granule rheology. Less porous granules led to stronger tablets.

As it can be deduced from the table above, less effort has been focused on the study of the granulation parameters during the roller compaction. Recently Am Ende, et al. [120] studied the effects of roller compaction on the content uniformity of low-dose tablet formulations and included the screen size and the granulation speed to propose prediction models for the assessment of optimal RC settings. They reported that roller force and gap width were involved in the amount of loose material bypassing at the

roller gap whereas sieve size was the main parameter influencing the particle size distribution.

2.2.3 Applications of roller compaction in tablet production

In the pharmaceutical manufacture, roller compaction has increasingly attracted the attention of formulators over the last decade [75, 93, 121]. The continuity of the process, the efficiency and the automation of the parameter control, the easy up-scale and the low operational costs turns this dry-agglomeration process into a good option when the agglomeration of the blend is needed. Table 4 lists some examples of investigations made in the field of the roller compaction and the tablet formulation.

Table 4. List summarizing the investigation carried out on the application of roller-compaction in the manufacture of tablets

	Authors	Contributions
1994 -2000	Dow Chemical Company Sheskey, et al.	In [122, 123], diverse binders were tested in niacinamide tablets. Also RC parameters were considered in the study. Release time of API was dependent on the binder concentration rather than on the process parameters. The granulation method seemed to have influence on the release of theophylline [122] as a function of the polymer concentration. In the latter work, the influence of other RC parameters such as roller surface was also analyzed. Finally, they also compared tablet properties and theophylline release after performing up-scaling [73] studies.
1998	University of Cincinnati Murray, et al. [124]	The granulation of ibuprofen reduced considerably the amount of excipients needed by the tablet formulation. Also the effects of RC parameters on the drug release were studied.
1998	University of Gent Inghelbrecht and Remon [110]	Controlled moistening of the compacted material improved the tablet properties and increased the API release rates of hydrochlorothiazide formulations.
2001	University of Brussels Rambali, et al. [111]	Optimal bio-adhesion and dissolution rates of miconazole buccal tablets were achieved through RC.
2002	University of Tuebingen von Eggelkraut-Gottanka, et al.	Optimization of *Hypericum perforatum* (St. John's wort) plant extract tablets through roller compaction-granulation. The granulation improved the flow of the bulk, reduced the generation of dust, and speeded up the tablet disintegration and the API release [125]. RC parameters impact on the granule size and the tablet disintegration time was studied [126]. Compaction force, sieve size, and also the addition of lubricant showed to have strong effect on both variables.
2004	Pfizer Global R&D Hariharan, et al. [70]	Study of the formulation composition and the release time of diclofenac tablets. MCC reduced the ability to retard the release, but increased the hardness. The addition of HPMC and Compritol slowed down the API release and led to weaker tablets.
2005	Federal University of Rio Grande do Sul Lira Soares, et al. [127]	Roller compaction and tablet production of spray-dried extract of *Maytenus ilicifolia* (espinheira santa). RC improved the flowability but reduced the granule re-workability in compression. Reduction on the tablet tensile strength was thus observed.
2008	Faculty of Pharmacy Ljubljana Bozic, et al. [128]	Roller compaction of formulations with macrolide antibiotic was investigated. Dry granulated systems exhibit better compactability and reduced capping tendency compared to the unprocessed material.

Roller compaction, however, is not always an appropriate granulation technique. The mechanism of agglomeration confers not desirable characteristics to the end granule. Arnaud, et al. [129] compared the granule properties obtained by four different granulation processes: shear mixer granulation,

fluidized-bed granulation, slugging and roll compaction. They analyzed the resulting particles and found out that in roller compaction,

1) The particle size distribution of granules has large spans (amongst other causes, due to the bypass of loose powder in the compaction unit);
2) the particles are sharp-angled with smooth surfaces;
3) their flowability is therefore poor compared to agglomerates of other methods;
4) the internal granular structure is still porous but the void mean size is smaller;
5) particles are hard, and
7) they need longer time to release the active.

For that reason, though roller compaction is a relatively cost-effective granulation process, dry-granulation is not suitable for all formulations. Consequently, the required product specifications have to be taken in consideration in beforehand prior to decide whether roller compaction is the most suitable agglomeration technique or not.

2.2.4 Focus of future research in roller compaction

Modelling the roller compaction process sheds light on the understanding of the global process and the description of the changes suffered by the material. It has been tried to model the compaction process after the parameterization of those factors that are considered to have the strongest influence on the process. The implementation of these models and the incorporation of information about powder behaviour, geometry, frictional conditions at the interfaces, and interactions into computer modelling programs is the next step on the attempt of a fully description of the roller compaction. First attempts have been already carried out in metallurgy [130]. In pharmaceutical sciences, Zavaliangos, Dec, and Cunningham [74, 131, 132] applied FEM (finite element modelling) on the simulation of the compaction and were able to predict product properties (e.g. density distribution within the compact) after varying compaction parameters and material properties. Other applications of the FEM are the calculation of internal and external temperature gradients within the material bed, the estimation of effective energy applied on the powder and the determination of elastic recovery at the compaction zone. A step further in the roller compaction modelling would be the combination of finite elements with discrete element modelling (DEM). This would provide a more accurate description of the powder compaction from the point of view of the particle (e.g. particle interactions and particle deformation) to the characterization of the bulk behaviour at the different stages of the compaction.

Another bright spot in the investigation in RC is the on-line process monitoring. As already mentioned at the beginning of this chapter, quality control has turned into a big issue in the pharmaceutical production. The ICH (*International Conference of Harmonization*) guidance discussed the principles of QbD (Quality by Design) for the management of the product quality. One of the main points dealt in these directories is the PAT (Process Analytical Techniques) to control the fulfilment of product specifications. Roller compaction is likely to adopt these measures and implement PAT to the process. It has been already studied the possibility of controlling the process by on-line determination of compact and even granule attributes using NIRS (near infra-red spectroscopy).

Finally, we believe that the formulation design based on expertise needs to grow and become a common praxis in the formulation, also in the particular field of the roller compaction. The generation of models and the creation of databases to transfer comprehensive information about properties and material behaviour under roller compaction are necessary. Çelik [4] and recently Hlinak, et al. [108] claimed that an evaluation of all the data gathered by the work of product manufacturers, excipient vendors, instrumentation companies, academic community, regulatory agencies, and standard control authorities is needed to generate the *compaction fingerprints*, i.e. a list of physical properties accessible for everyone, that would ease the development and the improvement of the current understanding of pharmaceutical processes.

2.3 Computer aided formulation through expert systems

2.3.1 Computer aided design

The term *computer aid* can be defined as the use of any computer-based tool to assist the user in speeding up any kind of operation. Computer aided design (or CAD) is the application of computational tools used for planning, drafting or modelling any activity. Architecture and engineering are the best known cases of professional branches in which the application of that kind of implements is extensive, but CAD has been actually used in a wide number of applications [133-136], that comprise from the conception and modelling of medical prostheses [137], and the chemical formulation [138], to the scheduling of timetables in public transports [139].

2.3.2 Computer aided formulation design using expert systems

The use of computer tools in pharmaceutical product formulation has gained a considerable interest among galenical scientists. A common IT tool is the knowledge based programs. Traditionally the formulator relied on his own experience to choose the preliminary components that formed part of the initial composition. Also the process parameters were set and changed based on the observations made in previous experiments. Knowledge based computer systems are problem solving IT applications through which new issues are solved by using data and information generated in the past. The information is generated based on expertise (e.g., from solving problems) and it can be used for resolving new situations by adaptation to the previous [140]. The knowledge based computer aided formulation design is the result of combining experience and computing platforms to perform the development of new formulations in an accurate, efficient and rapid way by processing and extracting data. The focus of this work will be a specific type of knowledge-based computational application, the expert system.

Expert Systems (ESs) are knowledge-based systems that simulate problem-solving capabilities of human experts. Their operational principle is based on drawing on information captured in data pools to solve a problem or to produce a response and to put it at the user's disposal [134].

As shown in Figure 12, expert systems have three main components: the knowledge base, the inference program, and the interface [141].

1- The knowledge base. It is by far the most important element of the system. It is the assembly of data and information that has been collected and organized into a knowledge bank (id. data base). The knowledge is included in form of data (i.e. facts, figures, numbers, etc.), rules or heuristic information (process descriptions, references, manuals, SOPs, etc.). The knowledge data base is not only the pillar of the ES but also the most difficult, time-consuming and tedious process of its development. Since the robustness of the information defines the power of the ES in solving problems, its collection needs to be rigorous and, therefore, has to be gathered from all possible sources.

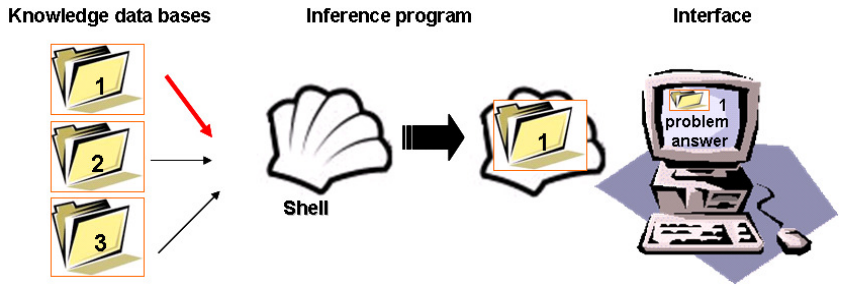

Figure 12. Components and working principle of expert systems

2- The inference program. Also denominated "the shell" of the ES, it comprehends the programming commands that organize, treat, process and extract the information from the knowledge data base. It is formed by a group of structured logic rules expressed as computer language instructions through which the information contained by the data base will flow. The inference commands are simple deductive logic rules (see Table 5) that handle with pieces of data and establish the relationship between them [142].

Table 5. Basic rules used as commands in MAX *in silico* Expert System

Rule	Type
IF	Condition 1
AND	Condition 2
OR	Condition 3
THEN	Action

The interlocking of inference commands into algorithms regulates the flow of information in such a way that the system is able to screen which information is discarded from the processing and which one is fed into the next rule. In the end, the program will draw conclusions considering only a fragment of the whole data base. In order to deal with complex knowledge, the program requires large number of rules, which obviously represents a rough work for the ES developer.

The inference strategies are classified in two different groups [142]:

i) Forward chaining: when the response of the ES is achieved through reasoning from data and information by consultation with the user to formulate the hypothesis.
ii) Backward chaining: if the process starts with the statement of a hypothesis and then the system goes through the data and information to prove or disprove the hypothesis.

Both strategies can be combined in the same inference program, hence increasing the flexibility of the system.

3- The interface. It can be considered as the stage of interaction between user and inference program. It works either as an input device or as the information displayer. It is a graphic user interface through

which the inference program asks the user for the presentation of the problem, for some additional information or for elemental guidelines in order to sort out the contents of the data base and drive the information of interest through the inference program. In the end, the system reaches the target response and presents it to the user so as to solve the problem with which it is being handled.

2.3.2.1 The sources of expertise

Where does the information integrated into the knowledge data base come from? Through our senses we perceive and become aware of the environment and the facts taking place around us increasing thus our knowledge and our skills, i.e., developing our expertise. In ESs, the source of information is the human expertise introduced into the system by the ES developers. They are in charge of embedding the information following criteria of selectivity and specificity of expertise and deciding in what form it is going to be incorporated into the knowledge base. This section describes the principal sources of expertise incorporated into an ES.

Part of the information integrated in the knowledge base corresponds to the description of materials, methods and strategies followed to perform any activity. Sometimes, the experimental information is well documented and can be easily found and incorporated into the system knowledge base. This would be, for instance, the information in experimental reports, presentations, papers, and even in SOPs. However, there is another part of the experimental knowledge for which no documentation is available. Normally it is heuristic information originated by trial and error possessed exclusively by the experts. A typical example of that is the trouble shooting. In order to collect the undocumented information, experts have to be questioned about their experimental knowledge and his tactics on problem-solving. This information is unstructured and almost always implicit, i.e. from expert to expert variable, as skills, training and problem-solving creativity are inter-individually variable [143]. This, together with the capacity of the ES developer for interacting with the expert to extract the information, becomes the bottleneck of the experimental knowledge acquisition. Finally, the knowledge is catalogued in form of lists, tables, or files to generate or enlarge the data base, normally structured in form of decision-tree algorithms [144]. The corresponding rules have to be created in the inference program so as to recall this information [145].

Mathematical equations are an abstract but highly structured source of knowledge that can be also integrated in the ES. Usually they result from the attempt to elucidate either particular or general trends of the underlying relationships between variables. Generally their origin is the numerical pool from data collected during experiments, which by approximation, regression, statistical analysis, factor analysis, data mining, etc. originate mathematical expressions, models or simply mathematic-based information that estimate the association between parameters and variables. These are then integrated into the knowledge base likewise as the experimental know-how. In order to use this information, the inference part of the ES must include decision commands to recall expressions, deliver results from calculations, and integrate them into the processing sequences while the ES is running.

Finally, in the knowledge base we can also introduce Artificial Neural Networks (ANNs). These are described in more detail in section 2.3.3. They are biologically inspired computational processing systems designed to simulate the way in which the human brain processes information. Neural networks are organized collections of processing elements -PE- (id. neurons) transferring activity (the signal) to each other via connections. They are systems with capability to learn from raw data, to establish multivariate non-linear relationship of complex nature between factors and parameters, and to draw predictions from new data.

2.3.2.2 Features of a powerful ES

Not only a robust knowledge bank is essential for a successful ES design but also a logical structure, a well-ordered sequence of commands for retrieving the information, and the inclusion of adaptation rules have to ensure the following features of a good performing ES.

A- Versatility. ES have to be able to advise, analyze, categorize, communicate, consult, design, diagnose, explain, explore, forecast, form concepts, identify, interpret, justify, learn, manage, monitor, organize, play, present, retrieve, schedule, test, tutor and verify [141]. The inference rules will define the capability of the system to carry out all these actions.

B- Dynamism. Dynamism is essential for any artificial intelligence application. The knowledge forming part of the system and the capacity of response has to be brought up to date. For this reason, the system must be adaptable.

C- Interactivity. The interaction with the user occurs in form of a dialog established during the problem solving at the inference of the system. Without interactivity, the dynamism of the process cannot exist. During the exchange of information user-ES the user introduces new data, modifies the output if the prediction does not fit to the reality, and the system takes the new information and integrates it into the knowledge base.

D- Simplicity. The presentation and the use of information should be kept simple. The user has to manage easily the program and acquire understandable information straightforwardly. This feature will determine the time spent for the problem solving and the comfort of the user on dealing with the program.

E- Accuracy and consistency. As commented before, the accuracy and the limitations of the system depend directly on the consistency of the data base. A complete, rigorous and exhaustive collection of data and information is indispensable.

2.3.2.3 Expert system vs. system of experts

As we have seen in the previous sections, the ability of an ES to debug problems derives from the human expertise. However, the principle of the ESs turns them into useful tools for the knowledge-management. Among human experts, the knowledge is lost from the moment that they leave. An ES,

on the contrary, works on reported information ensuring thus its permanency and accessibility to anyone. The information embedded into the system is furthermore easily transferable, so new staff can use it to gain experience.

Moreover, decisions and solutions displayed by ESs are fast, transparent and easy to track since they follow simple, pre-defined rules to draw conclusions. ESs are objective and logic, so there are not personal preferences or assumptions that could interfere in the results. As a whole, ESs are suitable for rapid, cost-effective and scientific reasoned problem solving which become, in turn, a permanent source of expertise. Also experts can devote more time to innovation and research, as they are freed from training and simple development tasks.

However, already in the early stages of settlement of the ESs in science, Shirley [146] described their limitations. ESs are not able to solve all kind of problems, since their biggest advantage, i.e. the knowledge base, is also their main constraint. The performance of an ES is restricted by the information present at the data base, confining the problem-solving ability to a relative narrow range of interconnected expertise domains. In order to avoid this, the developer can think of enlarging the knowledge base, but then she/he will come across with another limitation: the costs. As mentioned before, knowledge acquisition is laborious and consequently, expensive. Personal and time have to be invested to expand the pool of information, and yet it will not be enough to solve every single problem. Furthermore, to ensure the system adaptability, it has to be up-dated. The entry of new data, facts, information, etc. is vital to preserve the robustness and the reliability of the system, but becomes, in turn, a drawback of using ESs.

Summarizing and considering pros and contras, it is evident that ES contribute to improve and optimize the work in R&D [147]. However, the information retrieved from the system has to be considered merely guidelines and, conversely to what originally some authors considered feasible [148], under no circumstances an ES can suppress the figure of the expert in the company. ES are not the panacea and though they are programs considered members of the artificial intelligence applications, ES lack the creativity in problem-solving, which is exclusive in humans. Eventually, the expert takes the decisions and decides whether to accept or decline the information delivered by the ES.

2.3.2.4 Applications of ES in formulation design

Çelik [4, 149] described the potential of the ES in supporting the task of formulating dosage forms. He claimed that “fingerprints” of the components and the processes (mentioned in 2.3.2) are compulsory components of the knowledge bases, and enounced the aspects that confer these tools special interest for galenical scientists. The first applications of ES on pharmaceutical formulation appeared in the late 80s [142]. Since then, several groups have centred their effort on the development and the application of ES in formulation. The work carried out by some of them has been summarized in Table 6.

Table 6. Contributions of different investigation groups to the application of ES in formulation

	Authors	Contributions
1991-2004	University of Heidelberg Stricker, et al. [150, 151] Frank, et al. [146] PhD Thesis [51, 152-154]	Creation, development and optimization of the GSH ("Galenische Entwicklungs-System Heidelberg"). Designed for inhalation solutions, IV solutions, hard gelatine capsules, tablets [51], gas-aerosols, powder for inhalation, tablets after component granulation [153], IV preparations for peptides and lyophilised substances [152], coated tablets and pellets [154], and pellets produced through extrusion and spheronisation.
1992	Cadila Laboratories Ltd. Ramani [155]	Implement of an ES developed by the Cadila Laboratories for the formulation of tablets.
1993-2002	AstraZeneca Pharma. UK Rowe [142, 156, 157] and Craw, et al. [140]	Studies carried out with an ES developed by Zeneca for the development of solid dosage forms, parenteral preparations, and for the coating of tablets. Craw included case-based reasoning systems for tablet formulation.
1995	School of Pharmacy, London Lai, Podczeck, et al. [158]	Development of an expert system to aid the formulation of hard gelatine capsules
1996	Sanofi RD, Malvern Bateman, et al. [159]	Development and validation of an ES based on the PFES application of Logica (Boston) for the formulation design of capsules
2002	Maryland School of Pharmacy Guo, et al. [160] and Wilson, et al. [161]	Design of a hybrid ES-ANN system: an adaptive ANN-based learning ES for the design of capsule formulation containing different APIs.
2002-2007	University of Heidelberg F.C. Lintz, J.M. Bultmann [162] and S. Schmitt [144] PhD Thesis [98, 163, 164]	Development and use of AXS, a novel adaptive ES for the formulation design of aerosols, tablets made of lyophilised components and roller compacted-granulated excipients. They also a developed knowledge based ESs for the troubleshooting in nebulisation formulations and roller compaction process
2006-2008	University of Barcelona P. Pérez, J.M. Suné-Negre, et al. [165, 166]	They describe the design and the applicability a novel diagram method. An expert system for the evaluation of the suitability of substances for direct compression.

The ES created by the authors listed above presented different design, structure and features. However, all agreed that expert systems are useful tools with a wide range of applications in pharmaceutical sciences. They are highly interesting especially for industry, as expert systems shorten the time of development, reducing effort and expenditures, but increasing the consistency, quality and efficiency of the formulation tasks. In terms of knowledge, all concluded that its insertion into the system ensures the permanency and accessibility of the knowledge and assists the work of both experienced and novice formulators.

2.3.3 Artificial neural networks

Artificial neural networks (ANN) have been described previously as a source of expertise and as an enhancer of the performance of expert systems. But, how do they really work?

The structure of the smallest entity of an ANN, the PE -processing element- (also indifferently called *artificial neuron*) is represented in Figure 13. It consists of multiple input connections (s_1-s_n) arriving from other neurons, a processing node and an outgoing link from the current neuron to other PEs. Fausett [168] described in a very plain way the working principles of the artificial neuronal system. The information processing takes place in the interconnected PEs of the system. As shown in Figure

13.A, the signals are passed from neuron to neuron over the links, which have an associated weight (a numerical value) that multiplies the transmitted signal. Then, the afferent neuron receives that signal and processes it. In the first place, it adds all weighted signal of the previous PE(s), and then applies an activation function (see Figure 13.B) on the total sum before the new signal is generated. The efferent signal is transmitted and newly weighted before arriving to the next PE(s).

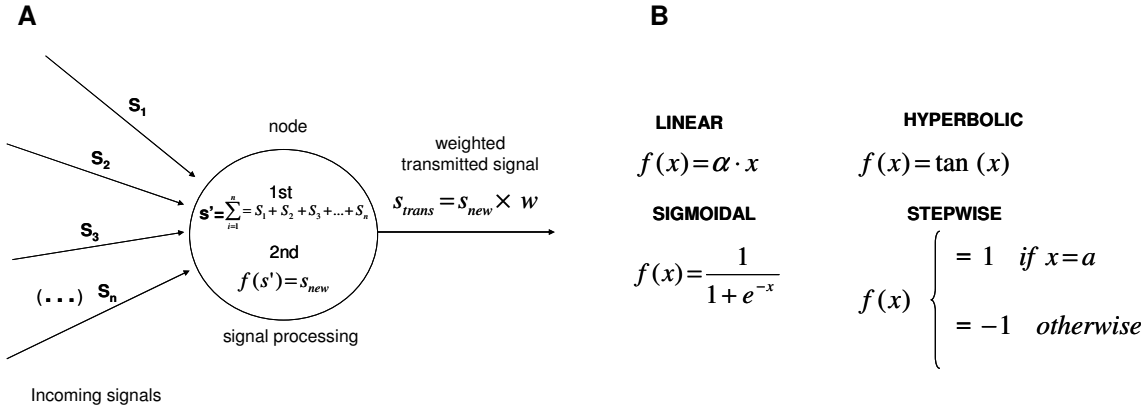

Figure 13. A) Structure of a processing element (neuron). ***B)*** Main activation functions [167]

A neural network consists of neurons lined-up in interconnected layers so that the signal of one layer is transferred to the next. The method by which they are organized and related is called the *network architecture*. A neural network has an input layer that correspond to the values or information from which the system will start the processing, and an output layer, i.e. the result achieved after feeding forward the input data through the network. The different architectures and types of ANN have been already described by other authors [167, 169, 170]. The simplest architecture is a network formed by two connected layers (single layer perceptron-SLP-), in which input and output are directly interconnected (see Figure 14.A). It was first developed by Rosenblatt during the 1950s [168, 169]. However, the most popular and successful ANN architecture is the multi-layer perceptron (MLP) [171]. As shown in Figure 14.B, in a MLP the neurons are structured in an input and an output layer. Between these layers there can be one or more intermediate layers, called the *hidden* layers, which in turn, are formed by a number of neurons (called hidden neurons) interconnected with the input and the output layer. The hidden layer becomes an intermediary processing step between the input and the output layer. This layer turns out to be necessary for those applications with extensive non-linear behaviour.

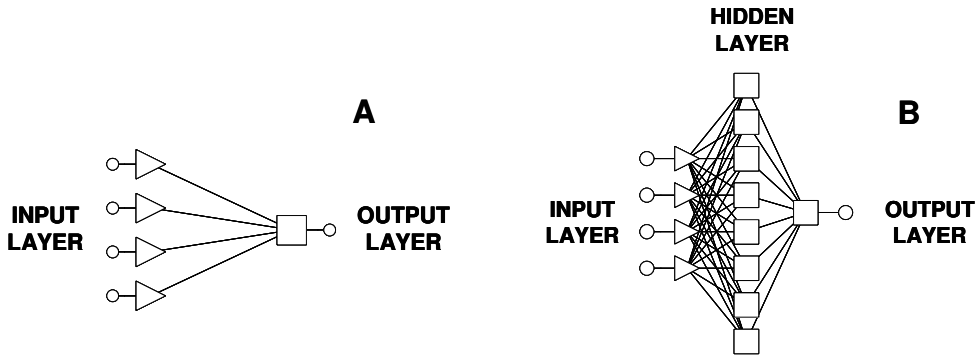

Figure 14. Sketch of a single-layer (***A***) and a multiple-layer (***B***) perceptron

The most staggering feature of ANNs is the fact that their PEs are adaptable. Thus, the system is able

to learn and fit the network response continuously. The method through which a network learns is called *training*. For the specific case of SLPs and MLPs, during the training process the data set is presented to the ANN to reduce the deviation of the network output from the target response by changing the weights of the connection between PEs. The training stops when the minimum error is reached. Once this happens, the weight values of the interconnection are stored and the ANN is *trained*. The values of weight are, in short, the "knowledge" of the ANN.

All types of training strategies have been already described elsewhere [167, 169]. In this section we describe briefly the *delta-rule back propagation* training, which is followed by the systems used in this thesis. This training has three stages [168]:

I. The feed forward of the input data to generate an initial network response.
II. The back-propagation, i.e. the estimation of the deviation between actual response and target value.
III. The adjustment of the weights for all the connections of all layers simultaneously.

These three steps are run reiteratively until the system achieves the minimal deviation between response and target value. The *iteration* is called an *epoch* and the number needed depends on parameters like learning rate and momentum [168] that control how extensively the weights are being changed after every iteration. Once the network has been fully trained, it is now able to draw predictions from new data, what means that it can calculate output values starting from new input values introduced by the user.

It has to be kept in mind that there is a maximum number of iterations allowed for the training of a system above which the ANN suffers "overtraining". If this happens, the system is not able to improve the response, and loses its accuracy. The overtraining of ANN occurs because during the training the system has memorized the input and the output values and does not have enough flexibility to predict accurate output values from new input data (this ability is commonly known with the term of *generalization* ability of a neural network).

2.3.3.1 Adaptative learning: Hybrid ES-ANN

Adaptive learning expert systems [172] or hybrid expert systems [160] possess the same structure as standard ESs but incorporate one or several ANN embedded in the knowledge base. This ANNs can be recalled by the system during the inference process when the algorithm linked to them is activated. The ES collects the output delivered by the neural network and uses it for carrying on with the data generation or for presenting it to the user through the interface. The ANNs' adaptability to the system response and their ability to establish generalisations and draw complex relationships improves the performance of the expert system. Thus, the neural network can learn from the expert system's experience and assist the expert system when it has not incorporated enough knowledge.

2.3.3.2 ANN applications as tools in computer-aided formulation

The ability of ANNs to classify, recognize patterns, predict and model from historic data has been already used in pharmaceutical research: *de novo* design and construction of combinatorial libraries of drug molecules, QSAR prognosis, pharmacokinetic and pharmacodynamic modelling, and prediction of secondary and tertiary structure of proteins, are some of the examples mentioned by Hussain [173]. Also pharmaceutical drug delivery scientists and formulators have sought the potential applicability of ANN in this field. A brief compilation of research carried out on formulation development using ANNs is presented in Table 7.

Table 7. Investigation carried out on the application of ANNs in formulation of dosage forms

	Authors	Contributions
1991-1994	University of Cincinnati Hussain, et al.	Chlorpheniramine maleate [174] and experimental API [134] matrix capsules' release profiles are modelled. Polymer component fraction and release ratio trends are directly correlated using ANN.
1996	Purdue University Kesavan, et al. [175]	Construction of two separate predictive models for granule and tablet properties respectively. Formulation, process parameters and product properties were used as training data.
1996	University of Basel Bourquin, et al. [176, 177]	Construction of predicting models for tablets out of the components and their proportions and comparison of the results obtained using regression methods (RSM) and ANN models.
1996	King's College London Richardson and Barlow [178]	First application of ANN in the description and the creation of computational fluid dynamic models of aerosol jet flow.
1997	KRKA d.d. & Ljubljana University Bozic [179]	Prediction, representation of response surfaces, and formulation upgrading of diclofenac sustained release formulations. The ANN input was the composition of the formulation whereas the output was the release time.
1997	University of Gent Inghelbrecht, et al. [85]	Description of the effects of roller compaction processing variables on the friability of compacted processed starch.
1997-2000	Hoshi University Takaoyama, et al.	Assessment and modelling of the trapidil release from sustained delivery tablets using composition, compression pressure, and release rates as training data [180]. Optimization of a ketoprofen hydrogel in cutaneous administration through establishment of non-linear relationships between the addition of ethanol and o-ehtylmenthol and the level of skin irritation [181]. Prediction of theophylline release profiles and simulation of plasma concentrations according to formulation changes [182].
1999	Marmar University Turkoglu, et al. [183]	ANNs were used for modelling acetaminophen tablet properties (friability, hardness and disintegration time) made of roller-compacted granules considering the composition and the number of granulation passes.
1999	University of Tuebingen Rocksloh, et al. [184]	Analysis of the roller compaction effects on the disintegration time of St John's wort dry extract tablets by comparing values calculated with ANN and multivariate regression models.
2000	Shenyang Pharmaceutical University Wu, et al. [185]	Formulation optimization of salbutamol sulphate osmotic pump tablets taking the concentration of polymers and the coat weight as input variables, and the release ratio as the output.
2001	Boheringer Ingelheim Vetmedica Chen, et al.[186]	Use of ANNs to correlate entire NIR spectra with the API content and the hardness of theophylline tablets.

2002	Meijo University Suanada and Bi [13]	Determination of the influence of water content, particle size and porosity on the dissolution time of tablets manufactured by wet compression and evaluation of the optimum particle size and moisture content combinations.
2003	University of Tennessee Sun, et al. [187]	Applicability and comparative studies between response surface models and ANN to the study of characteristics and the design of controlled release systems.
2005-2007	University of Heidelberg PhD Thesis [98, 163, 164]	ANN for the prediction of product properties from the formulation composition of different drug delivery systems. Tablets produced from lyophilisate proteins [163], aerosols [164] and tablets produced from dry granulated blends [98].
2008	University of Birmingham Mansa, et al. [188]	Use of intelligent software in order to correlate the ribbon density, the maximum pressure, and the nip angle values achieved during the roller compaction with two process parameters (roller speed and roller gap).

Some of the studies presented above [85, 134, 174-177, 180, 182, 187], compared the response of models corresponding to mathematical regression methods (RSM -response surface method, PNE - polynomial equations of second or third grade) with the estimations made by ANNs. In all of them ANN delivered better correlations than the mathematical estimations. This is discussed in further detail in section (6.3.3.3).

3 GOALS OF THE THESIS

The current thesis pretends to join the effort of others that have tried to shed light on the characterisation of the compaction. The experiments described in this thesis serve as evidence for the understanding of the process and the identification and description of the variability in the product attributes and the material behaviour. Moreover the obtained ES which *knowledge base* comprises information from references, experimental results, and predictive models, built by means of GRMs and ANNs, demonstrates the benefits of its implementation in the pharmaceutical research to preserve knowledge, approach it to others that might find answer to relevant issues, and to share informations with the global research community which work is centred on the issues handled here.

The work presented next is divided into three main blocks: i) the understanding of the roller compaction, ii) the systematic formulation of tablets, and iii) the development of an expert system. According to this, the aims of the thesis can be listed as follows:

I- Roller compaction

• Describe in detail the compaction, examining the patterns of particle-particle and particle-tooling interaction involved in the material mobility at this stage in order to identify sources of variability in the progress of the material densification and the characteristics of the produced ribbons.
• Study the changes of the ribbon attributes after the modification of compaction parameters and process conditions that influence strongly the aforementioned interactions and the material deformation behaviour.
• Evidence the morphologic and mechanic changes experienced by the granulated material after roller compaction in order to elucidate changes in the tabletability experienced by dry granulated substances.

II- Tablet formulation

• Detect and characterize the variability induced by the modification of the initial blend composition in the properties of ribbon, granules and tablets.
• Generate data implemented in the construction of mathematical regression and artificial neural network models for the prognosis of product attributes considering the initial composition and the process parameters.
• Test the accuracy and the predictability of the obtained models and assess the utility of both studied modelling methods on generating predictive models of good performance.

III- Expert systems

• Integrate experimental data, expertise, and predictive models into a single structured knowledge based system.
• Evaluate the resulting system and point out the benefits of its utilization in the design of tablet formulations.

4 GENERAL MATERIALS AND METHODS

4.1 Pharmaceutical ingredients

In Table 8 there is a list of the pharmaceutical substances used in different experiments of chapter 5. The corresponding sections in which the substances were used are recorded in the last column of the table. A detailed description of the manufacture process, applications and main attributes of all pharmaceutical ingredients can be found in section 9.1 in the Appendix.

Table 8. List of pharmaceutical ingredients used in the experiments

	Brand name	Supplier / Manufacturer	Experiment /s
Filler			
Crystalline α Lactose Monohydrate (LMH)	Granulac 140	Meggle, Germany	5.3
D- Mannitol (MNT)	D-Mannitol	Merck, Germany	6.2/6.3
Fillers-Binders			
Microcrystalline cellulose (MCC) PH 101 grade	Vivapur PH 101	JRS, Germany	5.1/5.2/6.1/6.2
MCC PH 102 grade	Avicel PH 102	FMC, USA	5.1/5.2
Co-processed LMH:PVP (96.5% LMH:3.5% Kollidon 30) (LP)	Ludipress LCE	BASF, Germany	6.1/6.2
Lubricant			
Magnesium stearate (MgSt)	--	Baerlocher, Germany	5.1/6.1/6.2
	Liga MF-2-V	Saville Whittle, UK	5.1/5.2
Disintegrant			
Croscarmellose sodium (ADS)	AcDiSol	FMC, Ireland	6.1/6.2
Dry-binder			
Vinylpyrrolidone:vinylacetate co-polymer (6:4) (KVA64)	Kollidon VA64	BASF, Germany	6.2
API			
Paracetamol (acetaminophen) (PL)	Paracetamol	Bayer, Germany	6.2

4.2 Other substances

As for the pharmaceutical substances, the rest of chemicals and materials used in the experiments are listed here. The numbered sections in which the substances were used are to be seen in the last column as well.

Table 9. List of other substances used in the experiments

	Supplier / Manufacturer	Experiment /s
Reactives and salts		
Hydrochloric acid 1M	Merck, Germany	6.2
Natrium hydroxide	J.T.Baker, Holland	6.2
Potassium dihydrogen phosphate	Merck, Germany	6.2
Colorants / lacquers		
Colour chalks	Crayola, France	5.2.2
Metal primer	Dupli-color, Germany	5.1
Solvents		
Dimeticone 350	Fagron, Germany	5.1
Bayol 82	Exxon-Mobil, UK	5.1

4.3 List of devices and tools

In Table 10, the devices, tools and other machines used in the experiments are classified and correspondingly numbered according to the experimental sections in which their use is mentioned.

Table 10 . List of devices and other tools used in the experiments

	Model	Supplier / Manufacturer	Experiment /s
Compaction			
Roller compactor No.1	MiniPactor M1144	Gerteis, CH	5.1/5.3/6.1/6.2
Roller compactor No.2	Laboratory-scale	University of Birmingham, UK	5.1/5.2
Compression			
Tablet press	Custom built	University of Heidelberg, Germany	5.1/5.3/6.1/6.2
Material test. machine No.1	LR30	Lloyd instruments, UK	5.1/5.2
Material test. machine No.2	4467	Instron, UK	5.3
Weighting			
Balance No.1	1006 MP 9	Sartorius, Germany	5.1/5.3/6.1/6.2
Balance No.2	3736	Sartorius, Germany	5.1/5.3/6.1/6.2
Balance No.3	71264 MP	Sartorius, Germany	5.1/5.3/6.1/6.2
Analytical balance No.1	AE 50	Mettler-Toledo, CH	5.1/5.3/6.1/6.2
Analytical balance No.2	AE 40	Mettler-Toledo, CH	5.1/5.3/6.1/6.2
Analytical balance No.3	R 180 D-#1	Sartorius, Germany	5.1
Analytical balance No.4	1702	Sartorius, UK	5.1/5.2/5.3
Analytical balance No.5	BL -210 S	Sartorius, Germany	5.3
Mixing			
Planetary mixer	MP-20	Collette, Belgium	5.1/5.3/6.1/6.2
Rotary-translational mixer	Turbula T2	WAB, CH	6.1
Rotary mixer	Lab-Mixer	Pascall, UK	5.1/5.2
Compact and tablet analytics			
Calliper No.1		Komerci OHG, Germany	5.1/5.3/6.1/6.2
Calliper No.2	CD-6”	Mitutoyo, Japan	5.1/5.2
Micrometer No.1		Komerci OHG, Germany	5.1/5.3/6.1/6.2
Micrometer No.2	Digimatic S 293	Mitutoyo, Japan	5.1/5.2
Micro-indenter	MVK-H1	Mitutoyo, Japan	5.1/5.2
Crush force tester	TBH 30	Erweka,	5.3/6.1/6.2
Hollow punch		A. Pfeiffer, Germany	5.1/5.3/6.1/6.2
Disintegration tester		Engelsmann, Germany	5.3/6.1/6.2
Dissolution tester	PTW S3	Pharma Test, Germany	6.2
Auto-sampler	PTFC II	Pharma Test, Germany	6.2
Sampler-pump	PT-PP8	Pharma Test, Germany	6.2
Bulk material analytics			
Vibratory sieve shaker	Analysette	Fritsch,	5.3/6.1/6.2
Riesel funnel	Dr. Pfrengle 3102	Hans W. Schmidt, Germany	6.1/6.2
Tamp machine	E2 71145-WF	Engelsmann, Germany	6.1/6.2
Friability tester		Engelsmann, Germany	5.3
Microscopy and imaging			
Sputter coater	SC7640	Quorum Technologies, UK	5.1/5.2/5.3
SE Microscope	XL 30	Phillips, Holland	5.1/5.3
Reflection microscope	Axioskop 2 MAT	Zeiss, Germany	5.1/5.2
X-ray axial micro-tomograph	1072	SkyScan, Belgium	5.1/5.2/5.3
NMR imaging spectroscope	DMX-300	Bruker, Germany	5.1
Digital camera	FE-740	Olympus, Germany	5.2
Spectroscopy			
UV-visible	DU 640	Beckman, US	6.2
UV-visible	ND-1000	Nanodrop technol., US	6.2

NIR (near infra-red)	NIRTab	Buechi, Germany	5.1
Other			
Drying oven	Thermo	Haeraeus, Germany	5.1
Pliers			5.1/6.1/6.2
Granulation sieve 0.5 mm		Fritsch, Germany	6.1/6.2
Helium pycnometer	AccuPyc1330	Micrometrics, US	5.1/6.1/6.2
Ultrasound bath			6.1/6.2
Moisture analysis balance	MA 30	Sartorius, Germany	5.2

4.4 Determination of the true density

A helium pycnometer (AccuPyc 1330, Micrometrics, USA) was used for the determination of the true density of all ingredients. The true density was measured in triplicate as the mean value of ten runs per determination. The resulting values are recorded in Appendix, section 9.1.10. The true density of the blends was calculated by mixing rules with the values of the single components.

4.5 Mixing

The mixing was performed in three different types of mixer: the planetary mixer, the rotary-translational mixer and the rotary mixer. The specific times of blending are given in the corresponding experimental sections. Generally, the blending of pharmaceutical excipients was performed in the first two mixer types. Figure 15.A shows the trajectories of the mixer components in the planetary mixer and the movement vectors in the rotational-translational mixer (referred here as Turbula mixer), respectively. Generally, in case of the planetary mixer the mixing time was set at 15 min for producing blends, except for the addition of lubricant (MgSt) for which the components were kept mixing for just 2 min as the mixing time of the lubricant has been found to have a significant effect on the end material behaviour [189, 190]. The rotational velocity of the planetary mixer was set at 60 rpm. The time was reduced to 10 min in case of the rotational - translational mixer for the general mixing of ingredients, whereas the addition of lubricant to the blend was kept 2 min. The rotational speed for this mixer was 42 rpm. The quantity of material being placed into the mixer vessels was also taken in consideration. Since for a proper mixing performance, the vessel should not be filled above ¾ of its total volume, the total material weight that was deposited was around 3 Kg for each batch in case of the planetary mixer, and 450 g in case of the Turbula mixer.

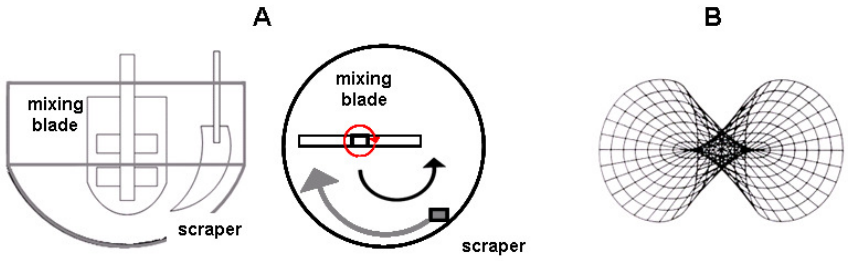

Figure 15. A) Representation of the mixing mechanism in a planetary mixer. ***B)*** Movement vectors followed by a vessel in a Turbula mixer

The third mixer type was exclusively used for the controlled addition of moisture, the coloration of MCC, and the lubrication of powder with MgSt (sections 5.1 and 5.2). The material weight being mixed and the mixing times are given in the corresponding experimental sections.

4.6 Roller compaction

4.6.1 Gerteis MiniPactor

MiniPactor is a small-scale roller compactor of Gerteis. The functional units and the principal components have been already described in section 2.2. The specific running parameters, they are described in the corresponding experimental sections in chapter 5. Figure 16 shows a picture of the roller compactor device together with the panel of control.

Figure 16. MiniPactor roller compactor and control panel

The rollers were 25 cm in diameter and 2.5 cm wide with variable surface designs. However the combination of a smooth left roller and a knurled (waffle-like) right one was used for almost all experiments. In [98], the use of this conformation was reported to be the most efficient to ensure a steady and uniform conveyance of powder into the roller gap. The distance between the rollers is variable, since the master roller is mounted on a movable shaft on which the hydraulic press is exerted. This allows the user to change the thickness of the compacted ribbons but it is also a mechanism of regulation of the densification after fluctuations on the roller gap. Thus, if insufficient amount of material is transported between the rollers or the material conveyance is not regular, the distance between the rollers will vary so as to maintain a certain level of pressure on the compacting material. The compaction zone was confined either with sealing rims fixed at the boundaries of the left roller, or with cheek side plates (see Figure 5 in section 2.2.1.2). The granulator unit was equipped with a star shape rotor (Figure 11, section 2.2.1) and a rasp sieve granulation mesh with 1 mm opening. The rotation was set at 50 rpm anticlockwise, and the distance between rotor and sieve was kept constant (1 mm).

The process was controlled on the control panel, equipped with an iFix (General Electrics -Fanuc, US) interface through which the process can be monitored in real-time and the parameters can be adjusted if needed. The computer retrieves the actual parameter value from sensors located on the motors of the feeding screws, the bridge breaker in the feeding hopper, both rollers and the granulator. Simultaneously, the distance between rollers is measured constantly by the displacement transducers installed in the roller shafts. Finally, the specific compaction force is calculated from the geometry and the position of the rollers considering the hydraulic force applied by the system after a dynamic calibration that correlates the pump hydraulic force exerted on the movable shaft and the force exerted in reality on the material considering hydraulic force and friction coefficients between the parts of the assembly. The signals produced by all sensors are transferred to the computer and are then processed by the control interface, so that they can be visualized by the user at any time. That way, the user is able to change the running parameters as required to reach a steady run. Nevertheless, in order to

automate the process control and to respond systematically to small process variations, the compaction process with the MiniPactor can be controlled with a PID (proportional, integral and differential) algorithm based parameter of control that adjusts the speed of the feeders to vary the amount of material being fed in order to keep a steady value of roller gap while keeping the specific compaction force constant [79]. All algorithm factors can be changed to adapt the feeding if small variations on the material conveyance occur [191].

The compacted powder was fed into the inlet funnel covering partially the rotor blades of the bridge breaker in the hopper (see Figure 17.A). Ribbons were sampled after the process parameters stabilized and the roller gap did not fluctuate. The first step for the ribbon sampling was the removal of the scraper from the left roller (Figure 17.B). While the roller continued rotating, a ribbon fragment remained entrapped between the sealing rims of the roller due to the elastic recovery endured by the material. Thus, the roller was left rotating until the ribbon carried by the roller reached a length of approximately 40 cm (i.e. half of a roller rotation). Thereafter, the compaction was stopped and the screws of the frontal sealing rim was slightly loosened with an Allen wrench (Figure 17.C) in order to release the ribbon fragments (Figure 17.D). A total of 3 ribbon pieces were sampled for each batch. Between sample collections the rim was screwed again, the roller scraper was set to the original position and the machine was restarted and kept running until the system reached again steadiness.

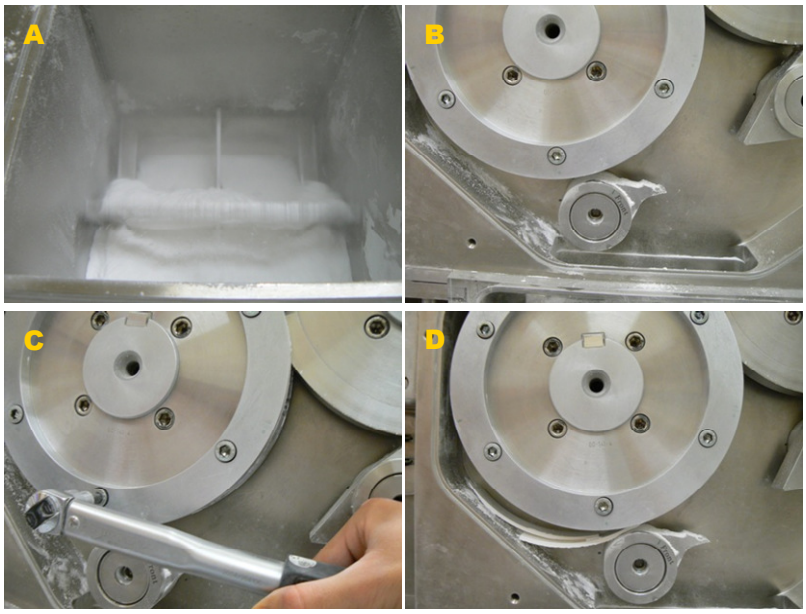

Figure 17. A) View of the inlet hopper and the bridge breaker ***B)*** Removal of the left roller scraper ***C)*** Loosening the sealing rim ***D)*** Collection of the ribbon fragment

For the collection of granules, a bag of PVP was attached to the outlet funnel. In order to avoid variability in the characterisation values of the granule induced by segregation within the bulk, the granule was collected during the run (always after the steady state was reached). Separately, a smaller amount of granule collected for the characterisation of the particle size. The weight of the samples was approx. 70 g and it was controlled using the balance No. 2. A total of three granule samples were collected and analysed.

4.6.2 Laboratory-scale compactor

Figure 18 is a picture of the laboratory-scale developed and created at the School of Chemical Engineering of the University of Birmingham by Michel [192] and Bindhumadhavan [100]. It is a simple gravity fed roller compactor with fixed rollers (i.e. roller gap remains invariable during the run). The powder is deposited in the hopper (3) and is forced by the rollers (1) into the roller gap. The rollers are 20 cm in diameter and 4.5 mm wide. They have smooth surface and their shafts are fixed to movable stages. The roller gap is adjusted screwing and loosening the side screws (9). They are loosened to increase the gap or screwed to reduce it. The gap distance is checked with steel layers of known thickness. The compaction zone is confined by two sealing side plates formed by a double layer of steel covered by Renolon POM [193]. The rollers are powered by two stepper motors (5) that can set the rollers in counter-rotation or in parallel rotation. The right roller is equipped with a pressure transducer (4) which signal is transmitted to the signal encoder (7) and amplified (8) before being transferred to the computer. The signal produced by the displacement transducer (6) is simultaneously recorded by the computer. The roller compactor can be controlled through the computer using a LabView interface (National Instruments, UK). The user can put the device in motion, control the roller parameters (basically rotation speed and rotation direction) and register the signals originated by the roller compactor sensors. The roller pressure signals for the corresponding roller positions are plotted and a "txt" file is created including data that can be further processed.

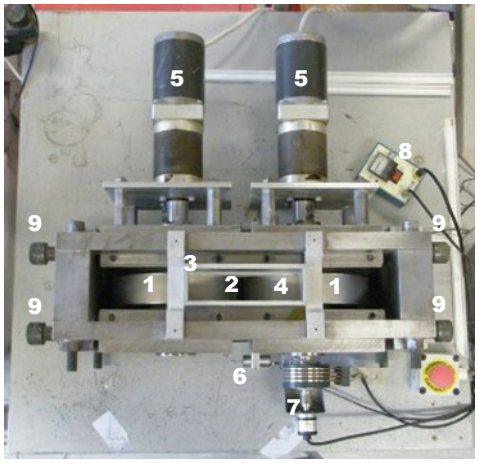

Figure 18. Gravity fed roller compaction at the School of Chemical Engineering in Birmingham

This is obviously a very simple design for a roller compaction device. Gravity fed compactors are not common in production where systems equipped with screw feeders are widely used. Moreover, the rollers are fixed and they are not interchangeable. However, it is still a very useful tool for fundamental studies and the understanding of the compaction process. The low number of influencing variables simplifies the characterization of the phenomena taking place during the material densification at the compaction zone. Moreover, the small size of the device reduces also the amount of material consumed during the experiments. Despite this, the throughput of compacted material is sufficient for the study and the further processing (e.g. milling) of the produced ribbons.

4.7 Compression

4.7.1 Uniaxial compaction

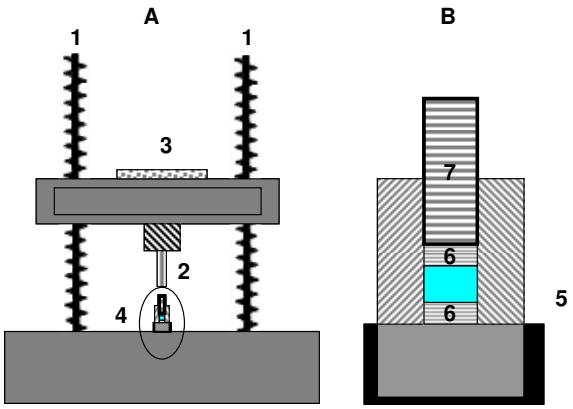

Figure 19. Sketch of a material testing machine and the assembly for the performance of uniaxial compaction (compression)

The production of part of the tablets was carried out using material testing machines. They are not exclusively used for tableting. In fact, these devices can perform tensile, compression, flexural, peel, shear, and friction tests, among others. Figure 19.A shows the main components of the double column material testing machines of Lloyds and Instron used in this work. They are formed by a stage mounted on two rotating screws (1) that drive it upwards or downwards depending on the direction of rotation. Fitted in the stage there is a force transducer (3) to which a wide ranger of grips and fixture types can be attached (2) depending on the material and the property tested.

The signal originated by the transducer is registered, processed, and recorded by a computer. Though the machine models used in this work could be entirely controlled by the user from a separated panel control, the user usually uses a program of control to set the direction, the velocity, the total stage displacement and the maximum force to be applied on the material. For the production of tablets and for the study of the material compaction, we attached a flat faced punch to the force cell. To simulate the tablet compression process, an assembly similar to the represented in Figure 19.B was used. In a detachable two-pieced die (5), a known amount of powder (bright coloured) is fed inside between two flat faced discs (6). A longer cylindrical piece (7), which function is the one of the upper punch in a tablet press, is inserted into the die. The assembly is placed on the machine bench as shown in Figure 19.A, so that the punch attached to the force cell and the "upper punch" of the assembly match perpendicularly.

Using the software, the velocity of the stage, the direction of movement and the maximal stress applied on the material were programmed. Before performing the compression, the stage was driven downwards until both punches touched each other without generating any signal. This was considered the origin point for the displacement. The compression run was then started. The "upper punch" of the assembly moved until the force reached the maximum. After this, the stage returned to its original position. Finally, the assembly was dismounted and the tablet was collected.

4.7.2 Tablet press

Figure 20 shows a custom built pneumatic tablet press that was designed and assembled at the University of Heidelberg. A single 8 mm diameter flat punch (1) is driven by a pneumatic pump (2). The pneumatic pressure of the pump is controlled through a barometer (3) to regulate the stress that

the punch applies on the tableted material. The pump is driven with a switch (4) that the user activates and deactivates manually. Two strain gages (5) have been fitted on the lateral of the punch. These generate a signal which intensity is proportional to the pressure applied on the material. The tablet die (6) is fixed on a movable platform which was kept at the same height. The lower punch (7) is mounted on a stage attached to a lever (8) used for the ejection of the tablet. The lowest point of the stage, i.e. the height of the lower punch and the die capacity, is adjustable using a screw (9) that is located at the bottom of the stage. Once the pressure of the pump has been adjusted to the desired value and the lower stage has been set at the proper height to produce tablets of a certain mass, the tableting material is hand filled. The operator activates the switcher and the upper punch starts moving downwards. As the punch gets in contact with the powder bed, the stress begins to increase. The strain gages produce a signal which is amplified by a Spider 8 (HBM AG) AD-converter/signal amplifier (10), and then is processed and recorded by the computer with a program developed by Dr. Bultmann. The values for the maximal pressure (P_{max}), the area under the curve of the stress-displacement plot and the time to reach a 10%, a 50% and a 90% of the P_{max} are then printed. The upper punch is sustained in the die for approximately 3 s. This reduces possible variability between specimens originated with different compression speeds at low and at high pump pressure. Thereafter the switcher is released and the upper punch returns to its original position. The operator can now collect the tablet by pushing the lever of the lower stage and ejecting the specimen out of the die.

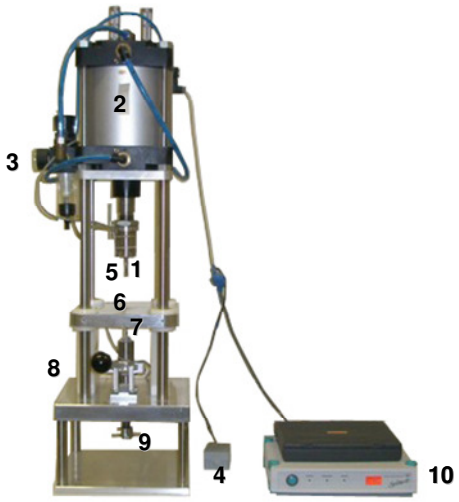

Figure 20. Custom built (University of Heidelberg) pneumatic tableting press

4.8 Determination of the flow properties

In section 2.1.4 we mentioned the importance of bulk flowability in the processing of bulk material both in roller compaction (see section 2.2.2) and in tablet compression (see 2.1.4). For the latter, the granulation provides a material with good flow attributes. Other methods described for the quantification of the material flowability are the use of powder rheometers [194], the avalanching test [195], the use of shear cells [196], or the Carr Index (see 4.9). In this work, the granule flowability was quantified by means of the technique described by the Eur. Ph. 6.0 [2] for the determination of the *angle of repose*. Approximately 50 g of the material was fed into the Riesel funnel, which opening diameter is 1 cm, fixed on its holder, while the material outlet was blocked. The opening of the funnel was cleared and the bulk started to flow and fell on the surface of a methacrylate disc with 10

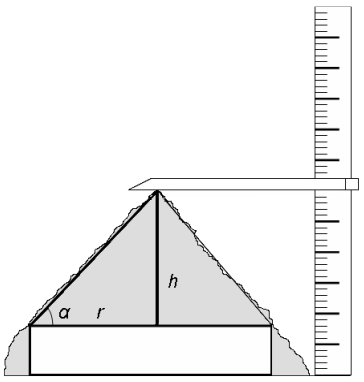

Figure 21. Determination of the angle of repose

cm of diameter. In addition, the flow time was controlled with a stop watch. After the complete content of the funnel flew through the opening, the height of the heap formed by the bulk on the stage was measured using the ruler marks on the funnel holder, as in Figure 21. The angle of repose was calculated as follows:

$$\tan\alpha = \frac{h}{r} \quad (6),$$

and

$$\alpha = \arctan\alpha \quad (7),$$

where h is the height of the heap and r is the stage radius (5 cm). Table 11 gives the classification of the capacity to flow depending on the angle of repose value [7]:

Table 11. Classification of the angle values according to the bulk flowability

Angle of repose [º]	Flow
<25	Very good
25-30	Good
30-40	Fair
>40	Poor

4.9 Carr Index

Carr index, also referred to as *compressibility index* [197, 198], is considered to provide useful information about the capacity of the bulk of reducing its volume at the first stages of the compression. Thus, with this value we can classify the substances as more or less compressible. This index was introduced by Carr [199] for the evaluation of solid flowability, and some authors still make use of it as a flow parameter [194, 200]. However, we consider and agree with Taylor, et al. [201] that the particle dynamics involved in each manufacturing process requires different flow tests, and therefore, for a complete characterisation of the material flow, a multiple scrutiny of each of the tests has to be carried out. Thus, the Carr index will be used in this work as an indicator for the classification of the material compressibility rather than a value of material flow, similarly as in [195]. The Carr index is calculated as:

$$CI = \frac{\rho_{tap} - \rho_{bulk}}{\rho_{tap}} \cdot 100 \quad (8),$$

where ρ_{bulk} is the bulk density. It is the volume occupied by a certain amount of loose poured material. For its determination, ca. 70 g of material was emptied into a 250 ml graduated cylinder with an accuracy of 1 ml. The volume occupied was measured and the density value was calculated. ρ_{tap} is the tap density. It corresponds to the volume occupied by the material after the particle rearrangement and the air escapement from the bulk. For its calculation, the same graduated cylinder with the same amount of material as for the ρ_{bulk} was tapped until there was no variation in the volume (1500 times was observed to be enough). The volume of the tapped material was measured and the CI value was calculated. As a general rule, good compressible materials present low values of CI (5-15%) whereas low compressible materials have a CI larger than 35%.

4.10 Determination of the particle size distribution (PSD)

A set of sieves of different mesh sizes was mounted on the vibratory sieve shaker. The weight of the clean sieves was recorded as tare weight. The sieves were mounted on the vibratory sieve shaker in order. The time of sieving was set at 5 min for all experiments, and the amplitude of vibration was 1 mm. After the sieving time was over, the weight of the sieves was determined. The granule size fraction was calculated as:

$$F_{size} = \frac{M_{sieved} - M_{empty}}{M\,granule_{total}} \qquad (9),$$

where the relative weight for a given size fraction F_{size} is the relationship of the amount of granule entrapped in a sieve of a given mesh size (M_{sieved}-M_{empty}) and the total amount of granule being sieved ($M\ granule_{total}$). To characterize the *PSD,* the RRSB (Rosin-Rammler-Sperling-Bennet) [202] distribution was used, which correspond to the following equation:

$$1 - D = R = 100\ \exp(-(d/d')^n) \qquad (10)$$

and after simple mathematical transformation, we have

$$\ln(\ln(D)) = n\ln d - n\ln d' = n\ln d + B \qquad (11)$$

where R and D are the cumulative distributions of residue and release (i.e. the percentage by weight of particles with diameter larger and smaller than a mesh diameter d), respectively. The position parameter d' corresponds to the diameter with a residue of 36.8% (i.e. a cumulative release of 63.2%) and indicates the fineness level of the distribution. The exponent n is a measure for the dispersion of the distribution. Equation (11) corresponds to a linear expression that can be easily used for the calculation of size fractions. The representation of the PSD for two experimental batches is shown in Figure 22. For all experiments presented in this work, the PSD of the granules has been successfully approached by a RRSB distribution with good correlation coefficients (≥ 0.96).

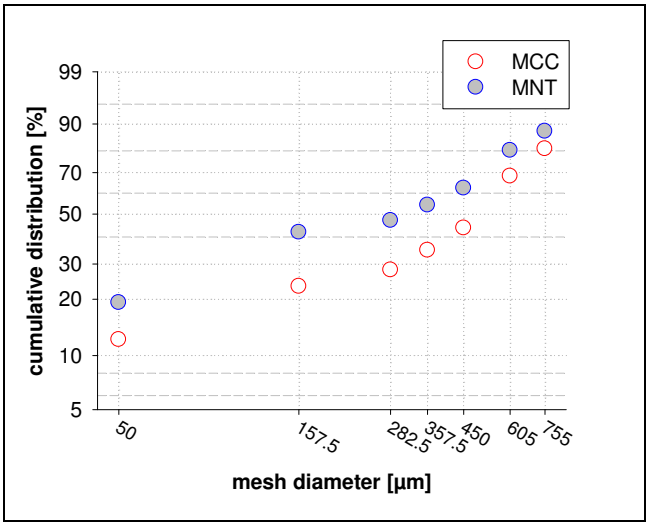

Figure 22. RRSB particle size fraction distributions for the granules of two different substances

4.11 Compact tensile strength determination

The determination of the toughness of the compacts to break was carried out in a crush tester. The tensile strength of the tablets was measured applying a diametrical compression load. The tablet was placed on the stage of the crushing tester and the load was applied diametrically on the tablet, until it crushed (see Figure 23). The value of tensile strength was calculated from the value of load producing

the failure of the tablet and the tablet dimensions, applying the equation of Fell and Newton [203]:

$$\sigma = \frac{2 \cdot P}{\pi \cdot d \cdot t} \qquad (12)$$

where P is the value of the failure load, d is the tablet diameter and t is the tablet thickness.

To estimate the cohesiveness of the roller compacted ribbons, a three point beam bending test was carried out. A 2.0 cm long piece of ribbon was placed on the stage of the crush tester, vertically leant on the fixed arm which was equipped with a piece formed by two knobs separated from each other 1 cm. During the run, the piece of ribbon was approximated to a third knob that fitted between the other two protuberances of the fixed arm (as shown in Figure 23). This way, the fracture of the ribbon was induced. The strength of the ribbon was expressed as [219]:

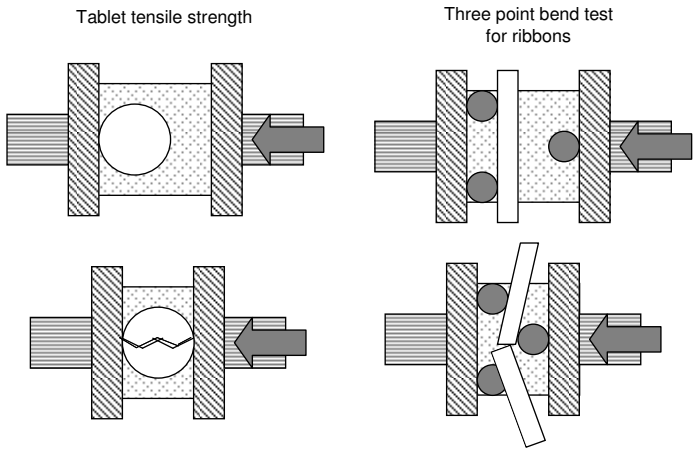

Figure 23. Representation of the methods to exert crushing strain on tablets and ribbons for the determination of their tensile strength.

$$\sigma_{comp} = \frac{2 \cdot P \cdot S}{3 \cdot W \cdot t^2} \qquad (13)$$

where the cohesiveness of the compact σ_{comp} is directly proportional to the load of failure P and the distance between the knobs of the movable arm S (1.0 cm), and inversely proportional to the ribbon thickness t, and the ribbon width W.

4.12 Disintegration time

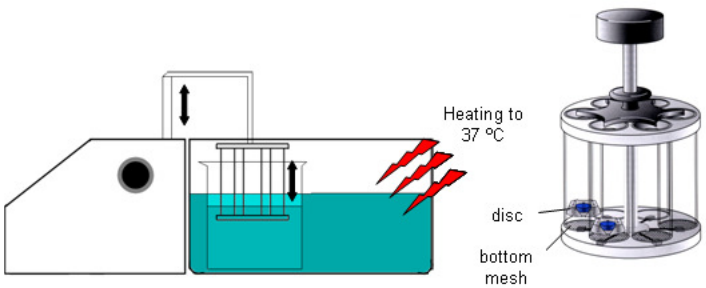

Figure 24. Disintegration test according to Eur. Ph. 6.0

The time taken by the tablet to disintegrate in water at 37 ºC was estimated by means of the device described by the Eur. Ph. 6.0 [2] (Figure 24) The bottom of the six testing tubes of the basket was equipped with a sieve of 1 mm mesh. A 900 ml beaker with 750 ml of water was left in a water bath at 37 ºC. The temperature of the water contained inside of the beaker was controlled with a thermometer. After the desired temperature was reached, six tablets were individually placed into the six tubes of the basket with a disc on each of them to avoid the free flotation of the tablet. The basket was thereafter

immersed in the water, and the disintegration tester was turned on. The vertical movement of the basket was of 20 immersions per minute. The time was controlled with a stop watch. The tablet was considered to be disintegrated when no fragments were left in the testing tube. The time after which the tablets were disintegrated was recorded and the mean value was calculated. The measurement was considered invalid when the tablet stuck to the flotation disc.

4.13 Dissolution time

The dissolution time, also referred to as release time, is the amount of API released by any delivery form in a given medium at a given time. In this work we estimated the dissolution time of tablets containing paracetamol as active substance. According to the USP 31 [3] paracetamol (acetaminophen) tablets have to have released at least 80% of the API within 30 min of dissolution time in 900 ml of a phosphate buffer (pH 5.8) in a paddle tester. Thus, in this work, the release time of the tablets was estimated in a dissolution tester with paddles as stirring elements (i.e. type 2) as described in [2] and [3].

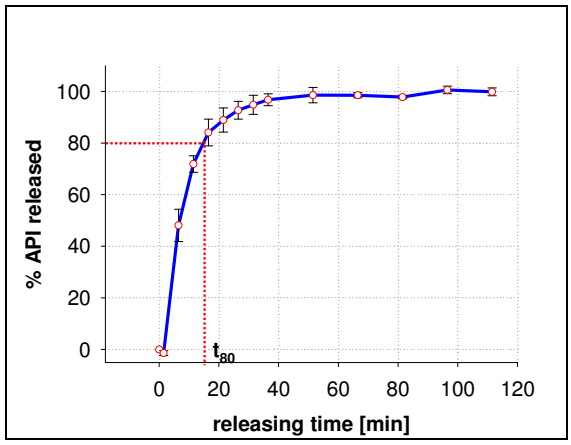

Figure 25. Determination of the t_{80} value from the dissolution profile of a tablet containing 20% of paracetamol

The phosphate buffer was prepared using bi-distilled carbon dioxide-free water as specified by the USP 31 [3] (monograph about reagents and solutions) and the corresponding substances from Table 9. The pH value of the buffer was controlled using a pH-meter. 900 ml of buffer were poured in each one of the six dissolution vessels. The temperature of the bath was set at 37 ºC and the temperature inside of the vessel was controlled with a thermometer. The test was initialized when the desired temperature was reached. In order to take samples of the dissolution media, an auto-sampler was used. It extracted 1.5 ml of the solution from each of the dissolution vessels and dropped it into sample vials. During the first 30 min of test, the sampling was carried out every 5 min. Thereafter the time passing between sample and sample was 15 min. The dissolution was extended until the tablet was entirely dissolved or completely disintegrated.

The determination of API released was carried out with a Nanodrop UV-Vis spectroscope. A calibration curve to estimate the concentration of paracetamol was obtained by using different dilutions of paracetamol in phosphate buffer. The resulting curve was:

$$PL_{conc}[mg/ml] = 193.64 \cdot A - 1.1914 \qquad (14)$$

where A is the value of absorbance detected at a wavelength of 243 nm. The content of API for each vial was then calculated from the absorption values detected. The dissolution profiles were recorded and the time of dissolution of 80% of the theoretical content of the tablet (t_{80}) was determined as in Figure 25 and was used as reference value.

5 ROLLER COMPACTION OF PHARMACEUTICAL SUBSTANCES

5.1 Solid fraction: product property for monitoring the compaction process. Methods of determination.

5.1.1 Introduction

If we consider a compact as a system of entrapped air within a solid lattice, the term *solid fraction*, also referred to as *relative density*, corresponds to the proportion of solid material in the total compact volume. It is expressed with the following ratio:

$$\rho_{rel} = \frac{\rho_{app}}{\rho_{true}} (\cdot 100) \qquad (15),$$

where ρ_{rel} is the solid fraction (relative density), ρ_{true} is the true density (referred to as particle density), i.e. the density of 100% solid material, and ρ_{app} is the apparent density that corresponds to the mass (M_{comp}) of a certain compact volume (V_{comp}) if assuming the mass of embedded air as negligible:

$$\rho_{app} = \frac{M_{comp}}{V_{comp}} \qquad (16).$$

The solid fraction of a compact is a property that describes the degree of densification achieved by a compacted material. Also the term *porosity* (ε) is commonly used to describe material densification. This corresponds to the fraction of the compact occupied by air entrapped in pores or voids, and is calculated as:

$$\varepsilon = (1 - \rho_{rel}) \qquad (17).$$

The main effect of the compaction process -and the tableting- (see 2.1.4 and 2.2.1.2) is the overall volume reduction of the material. As a consequence the inter- and intra-particular voids are reduced and simultaneously the number of inter-particle bonds is increased. This is described by Riepma, et al. [37] who observed proportionality between tablet hardness and porosity, and with recent studies [204-206] in which the authors demonstrated that the cohesiveness and the strength of compacted pharmaceutical materials depend primarily on their solid fraction.

In tablets, the determination of the achieved solid fraction provides, in the first instance, information about the tablet hardness and the tendency to disintegrate, though the latter is also strongly composition-dependent. In addition, the study of the relationship between volume reduction and ρ_{rel} achieved by the material allows the characterization of its capacity to be compressed into cohesive tablets (see 2.1.5). Moreover, the determination of the density distribution within the tablet, evidences in what extent factors such as the wall or powder lubrication, the filling speed, the compression speed, etc., have induced the production of tablets with irregular cohesiveness (as described in 2.1.6).

For ribbons, the determination of the solid fraction is a valuable source of information about the quality of the process and the granule attributes. As it is observed in tablets, solid fraction and hardness are directly correlated. In turn, ribbon hardness is closely related to almost all critical properties of the produced granules [117, 207]. Thus, denser, and consequently, stronger ribbons lead to larger granules that presented less internal porosity. These two compact properties (i.e. hardness and internal porosity) determine the granule PSD, the flowability and its tabletability. Consequently, as it has been mentioned in 2.2.2, changes in granule attributes have a strong impact on the tablet properties, so any modification in the ribbon densification has a direct impact on the end tablet characteristics. Thus, from the ribbon properties, one can establish a qualitative control of the whole production process.

The solid fraction reached by a given material under certain roller compaction parameters is a function of the quantity of material being slipped between the rollers and the total stress applied on it. As a consequence, solid fraction is strongly determined by the compaction parameters. Thus, it is affected in minor extent by the feed-auger / tamp-auger velocities (in compactors equipped with screw feeders), and extensively by compaction force, roller rotation and roller gap settings [188, 208, 209]. Hence, for the same material, if parameters such as roller speed, roller gap and roller force are kept invariable during the run, solid fraction fluctuations would suggest, for example, irregularities on powder feeding [86]. The origin of variability in the stress distribution on the compacting powder induced by the powder feeding, and the consequent solid fraction fluctuations within the ribbon has been already described in 2.2.1.1. Within the compaction zone, the nip angle and the pressure level exerted on the powder define extensively the ribbon solid fraction (see 2.2.1.2). The former determines the dwell time of the powder in the compaction region, while the latter is an indicator of the level of normal stress exerted on the powder. These two parameters are determined in a very complicated manner by both the inherent powder properties (internal friction, cohesion and the friction between the powder and the tooling), and the processing conditions such as roller speed and roller gap [79, 100, 117, 188, 210].

Although ribbons with homogeneous density distribution are desirable in pharmaceutical processing, it is a challenge to produce them. Funakoshi, et al. [77] observed that the pressure applied on the powder in the middle region of the rollers was higher than at the edges in smooth flat rollers and, agreeing with [78], they obtained much more uniform stress distributions when using concavo-convex rollers. Zinchuk, et al. [211] compared the ribbons produced using a laboratory scale compactor with the tablets produced by uniaxial compression with a compactor simulator. They found out that ribbons presented much larger variations in tensile strength and solid fraction values than tablets. This was attributed to the non-uniform stress distribution across the roller length and width during the roller compaction process. The non-uniform stress distribution across the ribbon width was investigated by Katashinskii and Vinogradov [212], Lubjuhn, et al. [213] and Busies [214]. They reported that there is a two-dimensional pressure distribution across the ribbon width which is heavily dependent on the type of lateral restriction of the roller gap. Thus, the use of cheek plates as sealing originated higher stress towards the middle region of the rollers whereas using mounted rims increased the stress exerted

at the roller edges. This is also observable in gravity fed roller compactors [215] with fixed rollers.

One can conclude then, that ribbon properties reflect the progress of the roller compaction. Especially the solid fraction provides usual information about how the material densification has taken place. In the following sections we describe and compare different methods used for the determination of the compact solid fraction and present some examples of results obtained for ribbons characterized using each of the techniques. Other methods used for the determination of the solid fraction in compacts that are not included in this study are the powder pycnometry [211], the helium pycnometry [216], the mercury porosimetry [13, 98, 217]), and the calculation of density considering roller compaction throughput for given process parameters [218].

5.1.1.1 Geometrical determination

In this method, the compact volume V_{comp} is calculated from the compact dimensions. After the determination of the compact mass M_{comp}, the estimation of the compact relative density is directly calculated with Equations (15) and (16). It is a primary determination method widely used and commonly accepted to deliver accurate values for tablets [45, 49, 205, 206, 219, 220].

For roller compaction, this method has also been extensively used [98, 118, 211, 221, 222]. However it is not accepted as a standard method for the determination of the solid fraction because, unlike tablets, the geometry of a ribbon fragment is not perfectly regular, being this a source of error. In this work we used two different methods for the geometrical density determination in ribbons: the sectioning and the punch method.

5.1.1.2 Buoyancy (suspension-floating technique)

According to Archimedes' principle, the weight of an object in a flotation medium diminishes proportionally to the weight of the volume of medium displaced by the object. Thus, the determination of this weight reduction in case of a completely immersed compact allows us to calculate the compact volume as:

$$V_{comp} = \frac{(m_1 - m_2)}{\rho_m} \qquad (18),$$

where (m_1-m_2) is the difference of compact mass outside (m_1) and immersed into the flotation medium (m_2), and ρ_m is the medium density. The solid fraction is then calculated using Equations (15) and (16).

The determination of relative compact density of compacts by buoyancy has been performed in works not only from the pharmaceutical sciences [209, 221, 223] but also from the metallurgy [224-226].

5.1.1.3 Near infra-red spectroscopy (NIRS)

NIRS is an analytical technique that measures the changes suffered by the electromagnetic radiation at the wavelength domain between 800 and 2500 nm after the interaction with the analyzed specimen. Since NIR spectra are a mixture of overtones and signal combinations, the intensity at a given wavelength does not necessarily respond linearly to a change in the attribute monitored. Normally, multiple regression techniques are therefore used for the interpretation of the spectral data.

NIRS is a non-invasive and non-destructive technique with no need of sample preparation and short measurement time. This makes this technique likely to be used in at-line, on-line and in-line monitoring. In the last three decades, NIRS has gained a lot of interest in the pharmaceutical manufacture. During the last years NIR has experienced a boom as PAT for pharmaceutical processes, especially after the issue of the guidance for industry by the FDA in 2004 [227]. The successful introduction of NIRS in production by big drug manufacturers encouraged even more the work of analysts in the research on NIRS applications [228]. Morisseau and Rhodes [229] and Reich [230] did an extensive and detailed review of the current applications. For the production of solid dosage forms, NIRS applications embrace from the characterisation of the raw materials [220], through the monitoring and control of manufacture processes such as blending [231] or granulation [232], to the analysis of the tablet content uniformity [233, 234].

As a secondary analytical technique, NIRS presents a considerable drawback: the calibration. This presupposes the correlation of spectral information with the specimen attributes. The identification of specific spectrum bands, the detection of band-shift variations after changing process parameters, and the discrimination of those spectrum profile variations that give real information, needs a detailed and often tedious analysis. Simple approaches employing the spectra band shifting at a certain wavelength were extremely sensitive to local band shifting. Therefore the best-fit line through the spectra was thought to be a better alternative [235, 236], since it integers the local spectral variations in the analysis. However, multivariate analysis becomes the most useful correlation strategy when trying to characterize intricate processes. It provides flexible models with tolerability upon unexpected variability, and can be as robust and accurate as a simple linear model. Nonetheless the multivariate analysis demands a huge pool of data and becomes a challenge for the analyst's expertise. However, the quality of the models is also determined by the accuracy of the values of reference. This makes the selection of the method of reference a key aspect to be taken in consideration.

Though NIR has not been yet established as a standard PAT for the control of the roller compaction process, it is considered as a potentially useful tool for the quality control in that process. Miller [237] firstly described NIR as an analytic method that was able to detect qualitatively variations on the product induced by changes in process parameters such as roller pressure level and the de-aeration of the compact zone. He observed that though the spectra profile did not change significantly, high roller pressure and the use of vacuum increased the absorbance detected for the specimen. After this work, the number of studies carried out on the application of NIRS to the monitoring of ribbon and granule properties has been increasing. From studies of simple models that consider the base-line shift slope to

predict the ribbon hardness [236], to works with complex multivariable models to predict both, ribbon, and granule properties screening other influence parameters [222], there is a fair number of published studies that deal with the construction of NIRS predictive models of ribbon and granule characteristics produced in roller compaction processes [72, 118, 119, 238-240].

The instrumentation of roller compaction devices with NIRS, and the implementation of the processed spectral data for the regulation of process automation algorithms used in most of the commercialized models, would create an optimized real-time adaptable performance capable to minimize product variability and to optimize those manufacture processes in which roller compaction becomes an intermediary step.

5.1.1.4 Micro-indentation

Micro-indentation is a technique for determining the hardness of materials in micro-scale that quantifies the resistance of a material to plastic deformation. Figure 26.A depicts the process of indentation of a specimen. During the micro-indentation test, an indenter of known shape and size is pressed into the material to be tested with a specified force ranging 9.8mN-9.8N (2). After the indenter is removed from the sample, an impression (indentation) remains on the surface (3) (Figure 26. B). The indentation size depends on the dimensions of the indenter, the applied load, and the hardness of the sample. The latter can be therefore determined by means of the following expression:

$$H = \frac{P}{A} \tag{19}$$

where H is the hardness of the material, P is the applied load, and A is the indentation area.

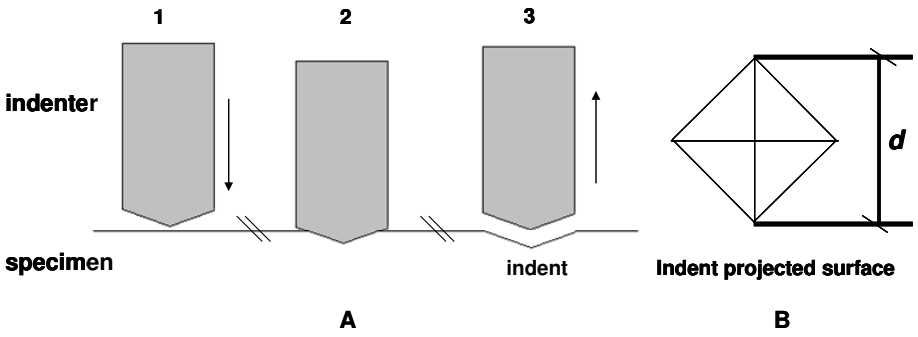

Figure 26. A) Indentation of the material. ***B)*** Projected surface of the indent observed under microscopy and measurement of the indent diagonal

In this study, we employed the Vickers test. It is a micro-indentation test in which the indenter is a diamond of square-base pyramidal shape with an angle of 136º between adjacent faces that makes a square indent. The indentation size is generally measured using a reflection microscope. The choice of micro-indentation upon other indentation techniques was reinforced by the fact that the forces used in macro-indentation (10 to 100 N) could be too high for low density regions, which would induce a crack in the sample. The indent size was large enough for its detection even by naked eye and it has a regular shape that was easy to identify and measure.

During the Vickers' test both diagonals of the indent (Figure 26.B.) are measured and the mean of these values is used to calculate the projected surface area *A* as follows:

$$A = \frac{d^2}{2 \cdot \sin(136° / 2)} = \frac{d^2}{k} \tag{20}$$

The indent area is therefore proportional to the diagonal lengths, and so is also the projected area imaged by microscopy:

$$A \propto \psi = k' d^2 \tag{21}$$

where ψ is the projected area and *k'* is the constant of proportionality between projected and real area. By combining Equations (19) and (21), we have that

$$H = \frac{P}{\psi} \tag{22}$$

Indentation tests have been recently performed to characterize the mechanical properties of solid dosage forms. Leuenberger and Rohera [22] analyzed the hardness of tablets through indentation. Later, Rohera, et al. [241] determined the endurance of polymeric film coating of ibuprofen tablets. Freitag, et al. [34] explored the effect of compaction parameters on the ribbon hardness. The tablet hardness was analyzed by Busignies, et al. [242] with micro-hardness and correlated it with the tablet porosity. Sinka, et al. [63] used the micro-hardness to obtain density distribution maps of tablets manufactured with lubricated and unlubricated die. Recently, Lee [243] characterized the structural heterogeneity in lactose tablets produced at different compression forces.

5.1.1.5 X-ray micro-computed tomography (X-ray μCT)

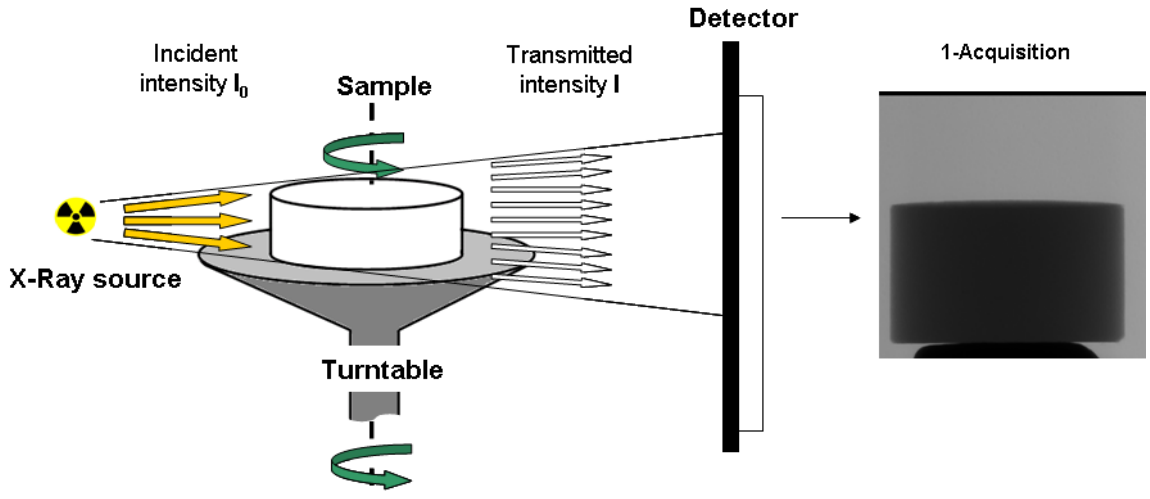

Figure 27. Image caption through X-ray μCT

X-ray μCT is a non destructive imaging technique that provides micro-structural information of materials by acquisition of cross-sectional images in planes through a sample with a resolution of

several microns. As illustrated in Figure 27. X-ray μCT systems consist typically of an X-ray source (emitter), a detector, and a turntable that rotates stepwise in a well controlled manner. During the test, a sample is attached onto the turntable. An X-ray beam of an incident intensity I_0 (i.e. the energy of photons per unit area in a unit of time) is then originated and directed to the sample. Once the X-ray passes the sample, some X-ray photons are attenuated (absorbed), while the rest transmit through the sample and are detected by the sensor that produces a signal with a proportional value to the transmitted X-ray intensity I. According to Lambert-Beer's law, the transmitted intensity I is proportional to the incidental intensity I_0 and the linear attenuation coefficient μ. For a beam of X-ray passing through homogenous materials,

$$I = I_0 e^{-\mu \cdot t} \tag{23}$$

where t is the thickness of the sample along the X-ray path. For non-homogenous materials,

$$I = I_0 e^{\int_0^t [-\mu(x)]dx} \tag{24}$$

where $\mu(x)$ is the value of the linear attenuation coefficient at various positions along the X-ray path and x is a distance variable along the X-ray path.

The linear attenuation coefficient μ represents the absorption ability of a material to the X-ray photon energy (30-100 keV), which is related to the photon interactions of X-rays with the atom of the materials. This attenuation coefficient depends upon the material density ρ, the atomic number Z and the X-ray energy E. For a given X-ray energy and a compact of a single-component material (i.e. Z is constant), the linear attenuation coefficient is proportional to the solid fraction.

Generally, the X-ray μCT test involves three steps: 1) acquisition; 2) reconstruction; and 3) visualization. During the image acquisition, the transmitted X-ray intensity is registered by the detector after every sample rotation, which is processed to a shadow (radiographic) image (see Figure 28). Hence a set of shadow images are gathered. As illustrated in Figure 28, after that, the shadow images are used for the reconstruction of a virtual slice through the sample (the red line across the sample). A data set is generated for the virtual slice using a sophisticated reconstruction algorithm (e.g. the modified Feldcamp cone-beam algorithm). During the process of reconstruction, the data set is included into a floating matrix for the linear attenuation coefficients of the corresponding cross section. These are converted linearly to 256 grades of gray and ordered so that the entire floating data matrix is then transformed into a cross section image (tomography) as pictured in Figure 28. Furthermore, the integration of the floating matrix of a cluster of section slices throughout the sample allows the creation of 3D structural models of the specimen.

Hancock and Mullarney [244] presented a review and exemplified the applications of that technique in formulation studies. X-ray μCT has been used for the study of the structure and the interconnections between voids forming part of the internal structure of granules [245]. Yet it has been widely used for

the examination of properties of tablet properties, including the density distribution [246-250], and the study of crack and fracture patterns inside tablets [251]. Nonetheless, although in [244] it was described that the cracks and irregularities within the ribbon mass can be identified using X-ray μCT, the application of this technique for the quantitative analysis of the density distribution in roller compressed ribbons has not been reported yet.

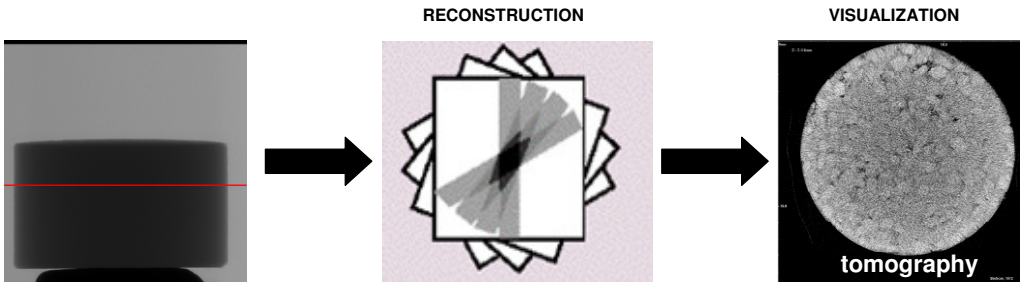

Figure 28. Steps of the sample characterization with X-ray μCT

5.1.1.6 Nuclear magnetic resonance imaging

NMRI is a non-invasive inspection technique that provides images from the tested specimen through the processing of NMR signals originated by a sample placed in a magnetic field after the irradiation with radio frequency. In the magnetic field the H^1-nuclei of the material molecules have a spin, an angular momentum of ½. The nuclei population is distributed between two levels of spin. The addition of radio frequency radiation to the system during the excitation pulse induces the perturbation of the distribution between levels by the interaction of the radiation with the nuclei. After the interruption of the pulse, a radio frequency NMR signal is detected as the equilibrium between the two levels is restored. The signal detected for a period of time is then transformed into a frequency signal via Fourier transformation and is then processed [252]. NMRI uses magnetic fields to spatially encode the NMR signal. The imaging through NMRI has, similarly as for X-ray μCT, three steps: image acquisition, reconstruction and visualization. For the acquisition the magnetic fields are originated in special coils. In order to derive the information in 3D, the additional fields derive in defined gradients: Gx, Gy, Gz. Gx is called the read-gradient and corresponds to the resonance frequency along the sample. Gy is the phase gradient and corresponds to the signal dependent upon the location in the direction of the second gradient. Applying the phase gradient orthogonally to the read gradient we can already generate a 2D matrix that is derived by Fourier transformation and originates a 2D image corresponding to a cross section (visualization). The gradient Gz is the one originated for a selected slice during the excitation-pulse. The integration of the three gradients originates a matrix that divides the sample in 3D voxels of given dimensions that contain the signal value for each spatial coordinate.

Nebgen, et al. [253] and Djemai and Sinka [254] argued that the key parameters for the imaging by means of NMR are the strength of the magnetic field gradient B_0, and the times of relaxation T_1 and T_2. Increasing the magnetic field gradient B_0 will amplify the signal, and consequently will increase the image resolution. The relaxation times characterize the dissipation of energy to return to the equilibrium state. T_1, the spin-lattice relaxation, depends upon the magnetic polarization of nucleus and affects the rate at which data can be accumulated from successive NMR signals. T_2, the spin-spin

relaxation, is the time needed to lose the magnetic moment that defines the time of the signal decay. T_2 affects the achievable spatial resolution and the signal-noise ratio.

The interest of the application of NMRI in the characterisation of solid dosage forms were reviewed by Melia, et al. [255]. Nebgen, et al. [253] published the first study that dealt with the characterization of tablet density using NMRI. They visualized the heterogeneity of the porosity distribution within the tablet. Djemai and Sinka [256] also used NMRI for the characterization of tablets solid fraction. They observed differences in the densification induced by different die-punch geometries and by the presence of lubricant. Both studies pointed out that the anisotropy of the particle movement within the die is the cause of the irregular powder densification within the tablet. However, as it also happens with X-ray μCT, it has not been published yet any work in which this technique is used for the determination of the solid fraction in roller compacted ribbons.

5.1.2 Materials and methods

5.1.2.1 Materials

Microcrystalline cellulose -MCC- PH101 grade and PH102 grade- were used as supplied for the manufacture of ribbons and tablets. Magnesium stearate -MgSt- was punctually used as external lubricant when needed (especially for the ejection of tablets). The metal primer and the silicon oil were used for the buoyancy method as sample coating substance and flotation medium respectively. The true density of the dried metal primer (2.021 g/cm^3) was measured with helium pycnometry (see 4.4) while the density of the flotation medium (i.e. silicon oil) was determined by fluid pycnometry at 22 ºC (0.969 g/cm^3). For the NMR imaging, Bayol 82 was used for the visualization of voids.

5.1.2.2 Sample preparation

Table 12. Parameters and settings for the sample manufacture

		Material	Lub.	Device	Parameters	Samples	Method
TABLETING	**A**	MCC PH101	Yes	Tablet press 16 mm flat faced punch	Press force 3/5/7/10/12/16/21 kN	40 per press force	Geometrical Buoyancy Punch
	B	MCC PH102	No	Material testing machine No.1 13 mm flat faced punch	Press force 3/6/9/12/15/18 kN	3 per press force	X-ray μCT Micro-indentation
ROLLER COMPACTION	**A**	MCC PH101	No	Roller compactor No.1	Compaction specific force: 2/3/5/7/8/9/10 kN/cm Roller gap: 3 mm Roller speed: 2 rpm PID: on Sealing of compaction zone with side cheek plates	80 ribbon fragments per compaction force	Geometrical (punch) Buoyancy NIRS
	B	MCC PH102	No	Roller compactor No.2	***I*** ***II*** Gap 1.0 mm 0.9 mm Speed 3 rpm 6 rpm Side cheek plates	100 cm ribbon per compaction setting	Geometrical (sectioning) X-ray μCT Micro-indentation NMRS

In this experimental part, MCC PH101 and PH102 were used as main components for the manufacture of tablets and roller compacted ribbons. MgSt was used for the external lubrication of tooling in some cases (generally during the tableting). Table 12 summarizes the different devices and parameters used for the sample manufacture. The last column of the table lists the corresponding method of determination of sample solid fraction used in each case.

5.1.2.3 Geometrical determination of solid fraction

Three different methods based on the calculation of density from the sample mass and dimensions were used: the geometrical, the sectioning and the punch method.

For the calculation of tablet solid fraction geometrically -exclusively for tablets-, the height was measured with a micrometer (No.1 or No.2). The value of tablet height was the mean of a total of five measurements. The tablet diameter was assumed to be the same as the die diameter. The mass of the tablets was determined on an analytic balance (No.2 or No.4) and the solid fraction was calculated using Equations (15) and (16).

The sectioning method was carried out with ribbons obtained with the method of roller compaction B II (see Table 12). As shown in Figure 29, the division of about 20 pieces of ca. 1 x 1 cm was drawn on a ribbon segment of approximately 6 cm long. The segments dimensions were measured using the calliper No.2 and the micrometer No.2. Thereafter, the segments were cut out meticulously with a scalpel and were weighted on the analytic balance No.4. Equations (15) and (16) were then used for the calculation of the solid fraction of each small fragment. Though the attempt to section the ribbon fragments evenly, the ribbon (see Figure 29), and the resulting fragments, presented irregular edges causing measuring errors.

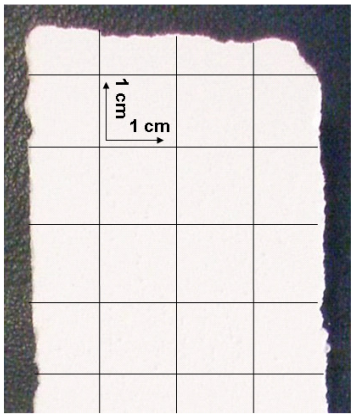

Figure 29. Representation of the divisions made on a ribbon sample for the sectioning method

The steps followed in the punch method are represented in Figure 30. This method was used for the determination of the solid fraction with ribbons produced by the roller compaction *A* (Table 12). For the performance of the measurement, the ribbon sample was segmented in 2 cm fragments across the ribbon width (2.5 cm) with pliers. Then, the height of the cut fragments was measured with the micrometer No.1 (1). The mean height value of five measurements was taken for the calculations. Previous to the punching, the analytical balance No.1 was zeroed with the punch leaned on a piece of cardboard (2). The ribbon was thereafter placed on the piece of cardboard and a circular section was punched out of the sample with a 16 mm diameter punch (3). The material remaining around the punch was wiped with a brush and the piece of cardboard with the punch containing the portion of ribbon was weighted (4). That weight was assumed to be the mass of the fragment enclosed within the punch boundaries. Finally, the ρ_{app} of the fragment was calculated as:

$$\rho_{app} = \frac{M_f}{\pi \cdot r^2 \cdot h} \tag{25}$$

being M_f the mass of the punched fragment, and r^2 and h the punch radius and the fragment height respectively. The solid fraction of the fragment was calculated using Equation (15).

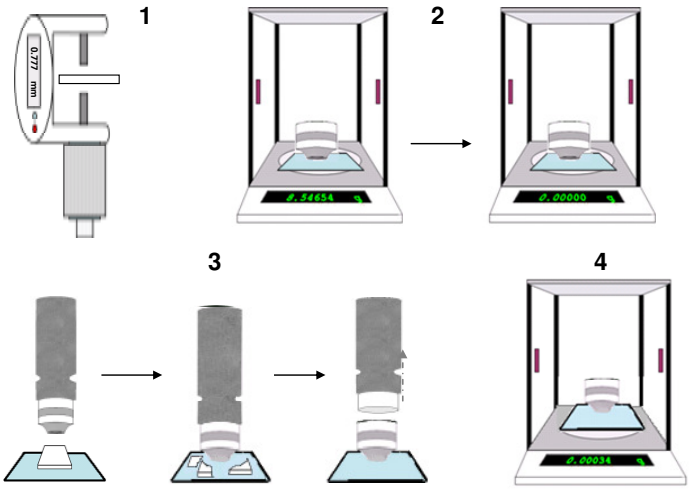

Figure 30. Determination of the solid fraction of a ribbon fragment with the punching method

5.1.2.4 The buoyancy method

This technique was used with the ribbons produced with the roller compaction *A* (Table 12). The ribbon samples were fragmented as for the punch method. The weight of the fragments was next determined with the analytical balance No.1. To know the weight in flotation-immersion, there could not be any kind of interaction between compact and medium. For this purpose, the sample was coated prior to the measurement. To extend the time of penetration in case of small discontinuities in the sample coating, viscose silicon oil was used as medium. The sealing was carried out by spraying a metal primer over the sample several times on each side. Between metal primer applications, the specimens were put to dry in a drying oven at 45 ºC for at least 1 h. Once both sides were coated, the primer was applied and carefully scattered on the ribbon edges where there were still uncovered spots. The coated ribbon fragments were let in the drying oven at higher temperature (50 ºC) for at least 2 hours, until the primer was completely dry. Thereafter, the weight of the coated fragment was determined.

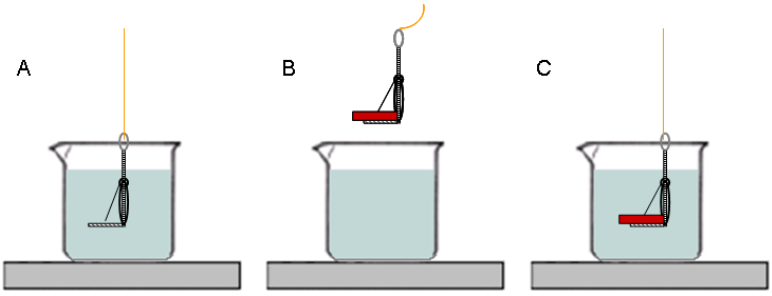

Figure 31. Determination of the solid fraction of a ribbon fragment with the buoyancy method

To measure the weight in immersion, the analytic balance No.3 was placed on a wooden support. Balance No.3 was equipped with a hook attached to the balance plate, to which a sample holder was tied. A 250 ml beaker filled with 200 ml of silicon oil was placed underneath the balance, so that the hanging holder could be immersed in the medium. The distance between balance and holder (35 cm), as well as the immersion depth into the flotation medium (1.5 cm) were kept constant for all measurements. The balance was zeroed while the holder was kept in the medium and the weight value stabilized (Figure 31.A). The holder was taken out of the medium and the sample was fixed to it (Figure 31.B). Then, holder and sample were immersed again and the flotation weight was measured when there were no weight fluctuations (Figure 31.C). A sudden increase on the weight indicated extensive medium penetration, in which case the specimen was rejected.

The compact volume was calculated by means of the modified Equation (18):

$$V_{comp} = \frac{(m_T - m_b)}{\rho_b} - \frac{(m_T - m_0)}{\rho_p} \qquad (26)$$

where m_0, m_T, and m_b are the initial mass of the ribbon fragment, the mass of the coated fragment and the mass of the immersed fragment respectively; and ρ_b and ρ_p are the density of the buoyancy medium and the metal primer in that order. The solid fraction was calculated with Equations (15) and (16).

5.1.2.5 NIRS

As shown in Figure 32.A, the NIR spectra were acquired by transmittance. The focus opening was set at 1 cm. The NIR source was equipped with a 100 W tungsten lamp. A high intensity of emission was chosen as high absorption and scattering of the light by the samples was expected. NIR transmittance spectra were acquired with the NIR spectrometer device against a 4 cm thick cylindrical biplane *Spectralon* tablet of 13 mm in diameter. The wavelength range between 870 and 1760 nm was scanned with a spectral resolution of 1 nm. For every sample, a total of 32 scans were performed.

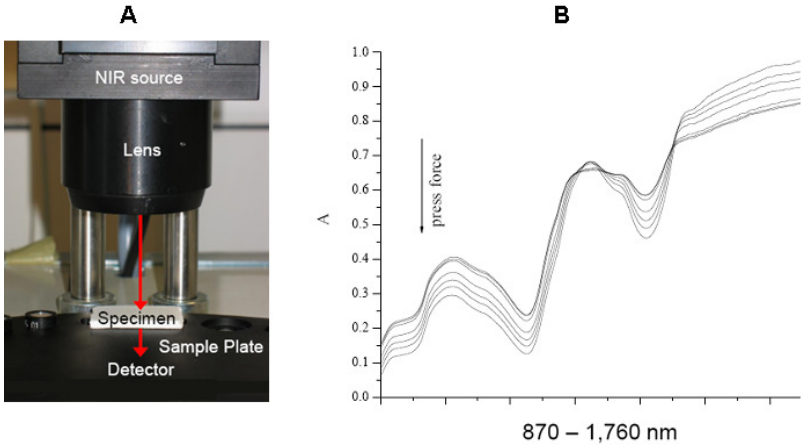

Figure 32. A) Representation of the NIR beam pathway through the sample in transmittance measurements ***B)*** Example of spectra obtained for ribbons from different densification levels.

By contrast with the previous techniques, NIR spectra need reference values to correlate spectral changes with the solid fraction variation. For the calibration, the measured solid fraction by punch and buoyancy method respectively, were assigned to the spectra as reference values. The MCC PH101 ribbons produced during the roller compaction *A* (Table 12) at 2,3,8,9 and 10 kN/cm were fragmented

in 2 cm wide fragments. The corresponding NIR transmittance spectra were obtained. The fragments were than divided into two groups. The solid fraction for the samples from the first group was determined with the geometrical punch method whereas for the samples from the second, it was determined with the buoyancy method. The NIR raw spectra were transformed to the logarithmic inverse of transmittance (i.e. absorbance) (see Figure 32.B). The pre-processed spectra were then analysed using the NIRCal 4.21 chemometrics software package (Büchi Labortechnik). Multivariate analysis correlations were made through partial least square (PLS) regression with 4 primary factors using the solid fraction values calculated using the punch and the buoyancy method as reference to create two separate predictive models. The accuracy of the obtained models was checked by calculation of the standard error of estimate (SEE), defined as standard deviation of the observed and the predicted relative densities.

In order to test the predictability of the obtained models, transmittance spectra of a total of forty ribbon fragments with unknown solid fraction were acquired, so as to calculate the density of the specimens using the calibrated NIRS models. Thereafter, the same specimens were again divided in two halves for verification of the solid fraction again with the reference methods. The NIRS predicted values and the measured values were then compared.

5.1.2.6 Micro-indentation

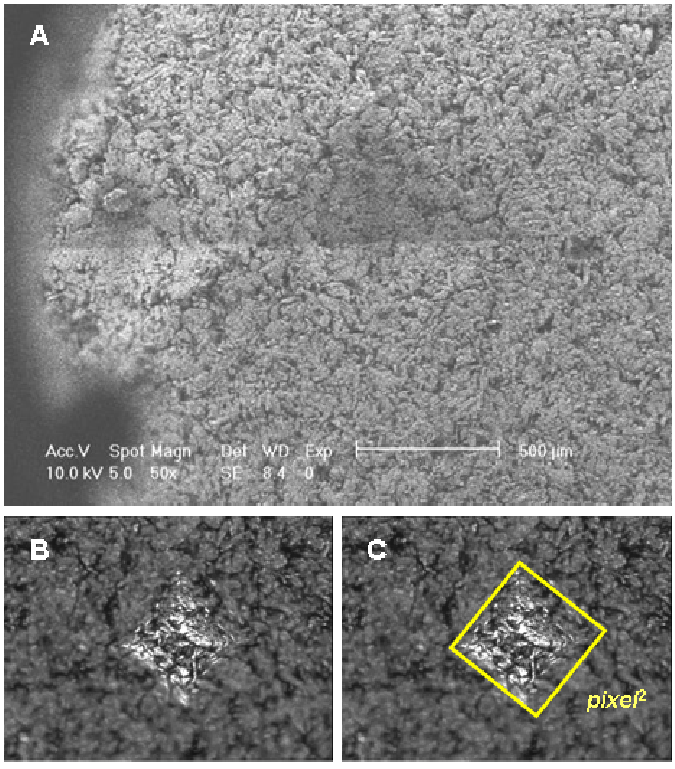

Figure 33. A) SEM of two adjacent indentations ***B)*** Visualization of an indentation in a reflection microscope after coating of the sample with gold ***C)*** Measurement of the indent area

The indents were made with the micro-indenter. For that purpose, the specimens were fixed on the sample stage of the device and the surface was repeatedly indented applying a force of 300 gf. For the measurement of the indent size, the indent had to be visualized. However, since MCC is a reflecting material, the direct observation of the indents with the reflection microscope incorporated to the micro-indenter could not be done. The specimens were therefore coated with a 75 nm gold layer in the sputter coater. This permited to observe the indents with SEM (Figure 33.A). But the unclear localization of the indents in the SE microscope, made necessary the use of another microscopy device in which the handling of the specimen is simpler. Finally, by means of the Zeiss reflection microscope we were able to localize, visualize and store digital images from indents, as it can be seen in Figure 33.B and C. The image acquisition was carried out under a magnification of x5. The images were then analyzed using the image processing software *ImageJ*

created by the US-NIH (National Institute of Health). As shown in Figure 33.C the indent projected area was measured and expressed as pixels^2. The indent area is directly dependent upon the compact hardness, which at the same time is proportional to the material solid fraction.

In order to find out the relationship existing between the material solid fraction and the size of the indents, we performed a calibration model. The reference samples were MCC PH102 tablets (calibration discs -CD-) manufactured with the tableting method *B* (Table 12). Then, a total of 15 indents in average were made on each of the 3 tablets manufactured for each compression force. Afterwards they were coated with gold in order to visualize and measure the indents. Table 13 is the record of the solid fraction values and the indentation areas obtained for the calibration tablets.

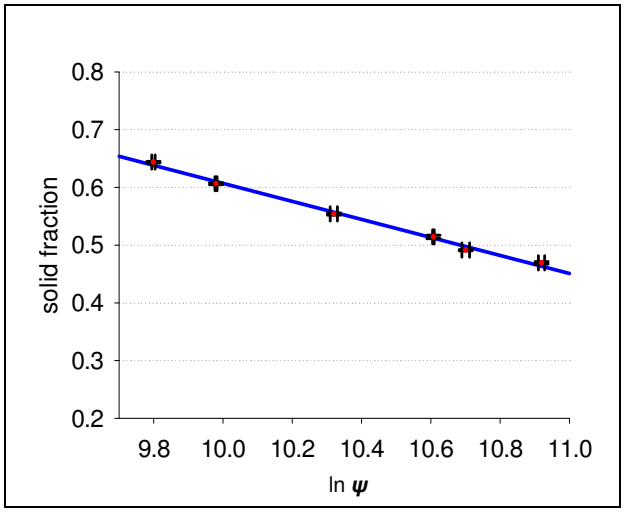

Figure 34. Calibration curve for the calculation of the solid fraction out of the indentation area

Table 13. Indentation and solid fraction reference values for the calibration

	Comp. pressure [MPa]	Solid Fraction	Indentations /specimen	Indentation area [pixels^2]
CD 1	37.67	0.481 (±0.46%)	15/15/16	55222.2 (±7.95%)
CD 2	45.20	0.504 (±0.20%)	15/14/17	44392.04 (±6.12%)
CD 3	52.74	0.527 (±0.58%)	15/16/15	40426.39 (±6.75%)
CD 4	67.81	0.568 (±0.32%)	16/15/16	30317.15 (±10.45%)
CD 5	90.41	0.622 (±0.27%)	14/16/15	21592.13 (±8.39%)
CD 6	113.01	0.660 (±0.20%)	16/16/15	18018.55 (±8.11%)

As illustrated in Figure 34, the logarithm of the projected area was found to be linear with the tablet solid fraction through the following expression:

$$\rho_{rel} = -0.15597 \ln\psi + 2.167 \qquad (27)$$

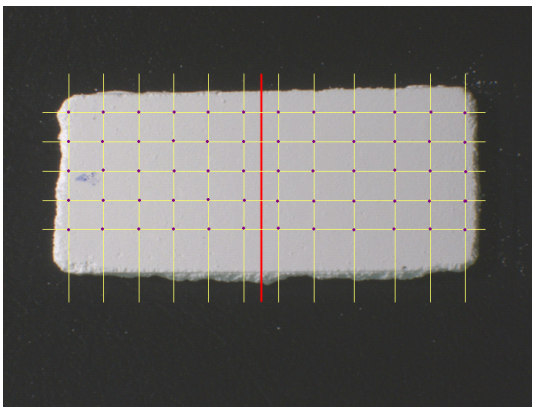

Figure 35. Localization of the indentations made on the ribbon sample

where ψ is the projected area of the indent. The correlation coefficient of this linear relationship is 0.994. Equation (27) was used for the calculation of solid fraction out of the indent projected area.

The compacts produced with the roller compaction *B-I* (Table 12) were sectioned in 1.5 cm long fragments across the ribbon width (ca. 4.2 cm). As the maximum size of the sample fitting in the micro indenter was 2.5 cm x 2.5 cm, the ribbon fragment was divided in two pieces of 2.1 cm. A total of 30-35 indentations distributed grille-likely were made on each of the fragments (15 to 17 each half) (see

Figure 35). The indent area was determined as for the calibration tablets. The solid fraction of the compact for the indented region was then calculated using Equation (27).

5.1.2.7 X-ray µCT

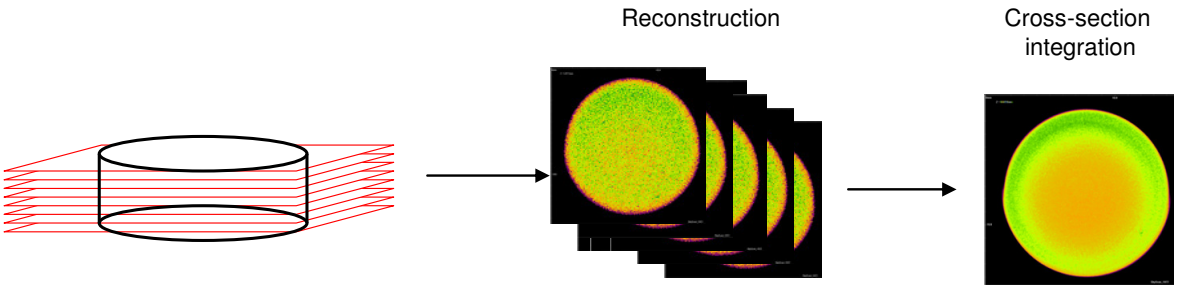

Figure 36. Acquisition of the integrated image of a calibration tablet

The ribbons produced with the roller compaction *B-I* (Table 12) were also examined using the X-ray µCT system. The X-ray beam was set at 50 kV and 98 µA. The total sample rotation was set at 180º with an interval of 0.9º (i.e., the sample was scanned every 0.9º rotation). The spatial resolution was 11 µm/pixel (i.e. a magnification of x19.10). The reconstruction was carried out using the NRecon software (Skyscan, Belgium). For all reconstructed images, a colour filter was activated in order to achieve better contrast (see Figure 36), in which the different colours represent the different attenuation coefficients. The pixel values ξ in each reconstructed X-ray µCT image were determined using again the *ImageJ* software. For the determination of the average value pixel values $\bar{\xi}$ of each sample, the 2D cross section images were stacked and an integrated µCT image was created with the average pixel values of all stacked 2D cross sections (integrated cross-sections). The integrated image shows hence the average pixel values (hence the linear attenuation coefficients) over the entire thickness of the sample. For the image processing parameters used in this section, the higher the attenuation, the higher the pixel value (i.e. the colour is brighter).

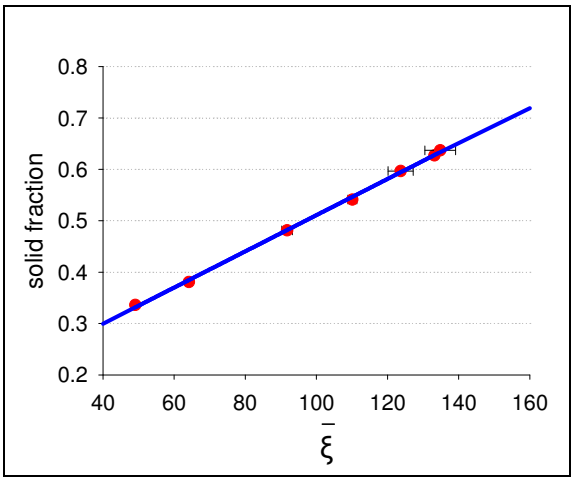

Figure 37. Calibration curve for the calculation of the solid fraction out of the mean grey value of the compact

X-ray µCT, needs also reference values to correlate a given pixel value with the corresponding solid fraction. For this purpose, calibration experiments were also performed. The calibration tablets (discs) produced by the tableting method *B* at different compression pressures were examined using X-ray µCT. As aforementioned, acquisition and reconstruction parameters were kept constant. It is observed that as the maximum compression pressure increases, the overall pixel value grows, indicating that the average attenuation coefficient becomes larger as the powder is compressed at higher pressure. The relationship between the average pixel value over the tablet ($\bar{\xi}$) and the reference solid fractions of the calibration discs (determined geometrically) is shown in Figure 37. It is clear that the

average pixel value is linearly proportional to the relative density, which is consistent with the analysis of Sinka, et al. [248] and Busignies, et al. [249]. The variables are correlated by

$$\rho_{rel} = 0.00352\bar{\xi} + 0.1584 \qquad (28)$$

with r2 = 0.999. It is interesting to note that Equation (28) results in ρ_{rel} = 0.1584 for the minimum density, which is identical to the value of solid fraction for loose MCC PH102 (0.16) reported in [200]. Equation (28) was used to convert the pixel values in the reconstructed µCT image of the ribbons into relative density values.

For each batch of ribbons, a 5 mm wide sample was cut along the ribbon width and was further sectioned into blocks of approximately 5x5 mm. The fragments were stacked and attached to the turntable of the X-ray µCT device. The image acquisition and the reconstruction were then performed using the same parameters as for the calibration tablets. For each specimen, reconstructed µCT images were obtained and an integrated image was created. A typical integrated image for ribbon samples is shown in Figure 38. The images were further processed to generate density maps of the whole specimen as follows: grey values of these integrated images were averaged every 100 pixels over the sample width and were taken as data points for the generation of a density map (i.e., a contour plot with the corresponding density values measured). Using the calibration curve (Equation (28)), the corresponding relative density for each data point was determined and the density map could be plotted together with the x- and y- coordinates of each measured point.

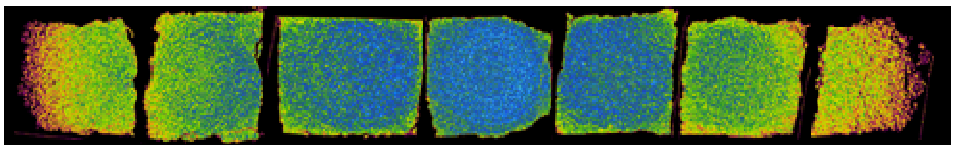

Figure 38. X-ray µCT integrated images of a fragmented ribbon section

5.1.2.8 NMRI

The intensity of the NMR signal is proportional to the resonance of H_1. In order to detect the internal voids, which basically would produce any signal as such, a fragment of ribbon produced with the roller compaction *B* (Table 12), of 1.5 cm length and 4 cm width was immersed in Bayol 82 under vacuum for at least 4 h. The sample was then deposited into a sample cylinder, which in turn was introduced in the detector coil, and was inserted into the NMRI device. For the imaging, the field of view was 4 x 1.4 cm resulting in a spatial resolution of 156 x 109 µm/pixel. The image was acquired with a fast spin-echo sequence called RARE (rapid acquisition with relaxation enhancement). A single echo was collected from each excitation. The final signal was generated from the average of 16 signals. The repetition time (time between excitations) was 2.0 s, whereas the echo time (i.e. the time between excitation pulse and signal acquisition) was 4.954 ms. The total time of the image acquisition was around 1 h.

The solid fraction determination with NMRI was performed for a single sample of ribbon produced during the roller compaction method *B-II*. As a result of the NMRI processing, we obtained an image

in which the pixel value corresponded to the intensity of the resonance signal. For the calculations of the solid fraction, the highest pixel value (253) was assumed to be a 0% of solid fraction (i.e. voids) whereas the lowest pixel value (0) was considered to be a 100% of solid fraction (0% porosity). The mean pixel values of a 0.8 cm wide ribbon fragment were determined by means of the *ImageJ* software.

5.1.3 Results and discussion

We have divided the resulting data into three main groups. The geometrical method and the determination of solid fraction using buoyancy were assessed and were implemented as reference methods for the calibration of NIRS-models. In addition, another group of results gathered from the determination of the solid fraction by means of the sectioning, the micro-indentation and the X-ray µCT are presented and compared. Finally, we present the data for the solid fraction determined with NMRI. We evaluate the results obtained with this technique by comparing them with determinations made with X-ray µCT.

5.1.3.1 NIRS prediction models calibrated with the punch and the buoyancy methods as reference.

In the first place, we report the validation of the reference methods for the model calibration. We evaluated the methods to demonstrate that the values of solid fraction delivered corresponded to real values. We used the values of density from tablets of known solid fractions (geometrically) and calculated it with both reference methods. For the validation of the methods we compared both sets of data. Then, we report and discuss the values of density for all samples determined with the reference methods. Finally, we present the resulting NIRS-models and compare their performance as a function of the reference method used for the model calibration.

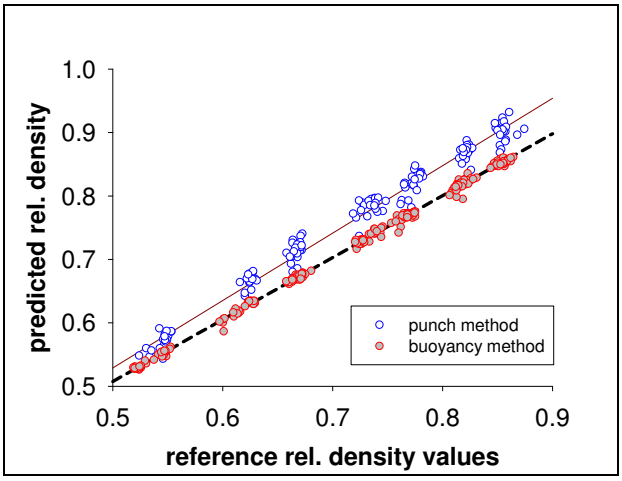

Figure 39. Comparison of the reference density values with the measured with the punch and the buoyancy method

The validation of the reference methods was carried out as follows. The relative density of the 40 tablets (tableting *A* -Table 12-) produced for every compression force was determined geometrically. It was assumed that the value obtained for an almost geometrically perfect form such as a tablet may deliver an accurate value close to the reality. In order to evaluate the capability of punch and buoyancy methods to estimate the solid fraction to be used as reference methods for the calibration of NIRS models, the density values of the produced tablets calculated geometrically was contrasted with the values delivered by the other two methods. Thus, after the geometrical determination, the density of half of the specimens was determined with the punch method and the rest with the buoyancy method.

In Figure 39 the resulting linear correlations of the geometrical density values for the tablets and the values calculated by the reference methods are compared. The linear expressions of the correlation for each method are listed next:

$$\rho_{pred} = 0.97621\rho_{ref} + 0.0195 \quad (29)$$

for the punch reference method, with $r^2 = 0.98216$, and

$$\rho_{pred} = 1.06255\rho_{ref} - 0.0031 \quad (30)$$

for the buoyancy reference method, with $r^2 = 0.998$.

The solid fractions estimated by both reference methods show good correlation with the reference values. Thus, one can consider that both methods are suitable for the determination of compact solid fraction. Nevertheless, a higher correlation coefficient indicates a better accuracy of the buoyancy method upon the punch determination. The punching of the tablet generates cracks and attrition in the compact mass and on its borders increasing the appearance of determination errors. The buoyancy method has a long list of potential error sources: imperfections on the coating, irregular film formation, interference of the value due to formation of bubbles, pendulum motion of the sample stage during the measurement, etc. However, the results showed better accuracy and proximity to the reference values.

Moreover, the intercept value of the correlation for the punch method differs significantly from the axis origin, whereas for the buoyancy method the intercept value is closer to 0, revealing that there has been a systematic error during the measurements with the punch method. Figure 40 illustrates the cause of the divergence of the intercept value between both methods. Tablets present higher densification levels towards the central region [63, 64, 248, 249, 251, 256]. Considering that the determination of density by punch method only contemplates a fragment of the whole tablet, usually corresponding to centre of the tablet, there is a continuous over-estimation of the real density value. Buoyancy method determination, on the contrary, integrates the whole tablet mass and delivers more accurate density values.

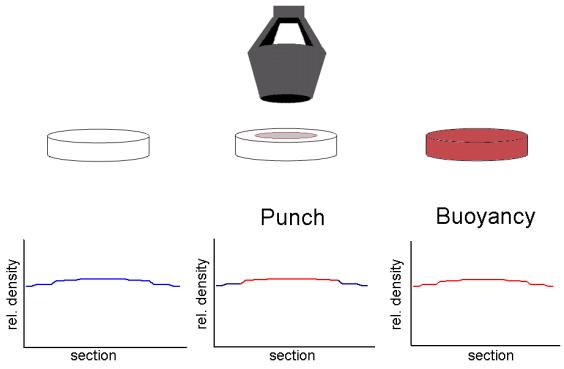

Figure 40. Representation of the over-estimation of the density value using the punch method

The solid fraction of ribbon samples was next verified for both methods. The correlation of the ribbon solid fraction value delivered by the reference methods and the logarithm of the specific compaction force was observed to fit linearly as showed in Figure 41. The fit equations for each one of the methods are:

$$\rho_{rel} = 0.16788 \cdot \ln(CF) + 0.49408 \quad (31)$$

for the punch method, with $r^2 = 0.968$, and

$$\rho_{rel} = 0.15337 \cdot \ln(CF) + 0.396479 \qquad (32)$$

for the buoyancy method, with $r^2 = 0.986$.

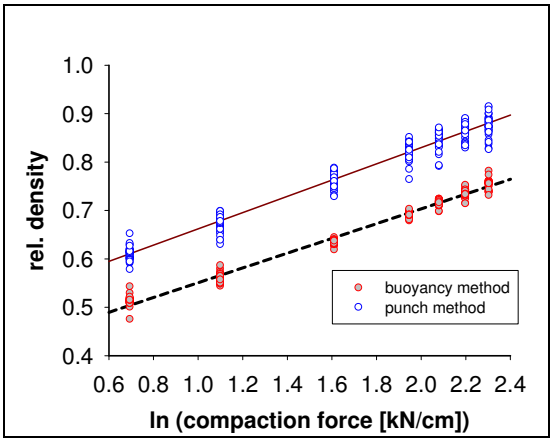

Figure 41. Comparative of densification curves for the punch and the buoyancy methods

For both methods, a proportional linear increase of the densification level as a function of the compaction force has been observed. Nevertheless, and as for the validation of the methods, the buoyancy seems to deliver more accurate estimations. The sample manipulation and the alteration of the compact integrity during the punching, increases the variability of the values obtained. Although the slope of Equations (31) and (32) are similar, the difference of intercept values between the two methods is observed again. In case of roller compacted ribbons produced in a process in which the compaction zone is sealed with cheek plates, the ribbon density distribution has higher densification levels towards the middle region (see Figure 44). Thus, the same way as for the tablets, and as represented in Figure 42, the punch determination method is prone to deliver over-estimated solid fraction values, whereas the buoyancy method values are closer to the real solid fractions.

The NIRS models were calibrated with the values of density measured by the two reference methods separately. The end regressions of the NIRS models with the two reference methods are summarized in Table 14. The correlation coefficient and the standard error (SEE) of the model calibrated with the punch values correspond to a weaker model. Buoyancy offers better reference values and therefore it was expectable that the resulting model gives also better performance.

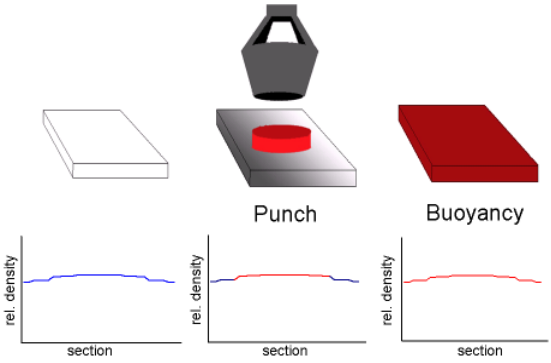

Figure 42. Representation of the density over-estimation in ribbons using the punch method

Table 14. Evaluation parameters for the calibrated NIRS models

	Slope	Intercept	r^2	SEE	rel. SEE [%]
Punch	0.1319.	0.3881	0.9687	0.0135	2.22
Buoyancy	0.1533	0.3995	0.9787	0.0124	1.88

To confirm the latter, the NIRS models generated were tested. Each model was used to predict the density of 20 ribbon samples of unknown density. Figure 43 shows a diagram in which the NIRS model predicted values are compared with those measured by the reference techniques. The linear correlation of measured and predicted values resulted in the following expressions:

$$\rho_{pred} = 0.9350917\,\rho_{ref} - 0.0363625 \quad (33)$$

for the NIRS model calibrated with the punch method values, with $r^2 = 0.847$, and

$$\rho_{pred} = 0.959906\,\rho_{ref} - 0.017973 \quad (34)$$

for the one calibrated with the buoyancy method values. In this case the $r^2 = 0.924$.

Both models are able to predict the solid fraction values. The approach to the real values for the solid fraction, however, is differently accurate. The average of deviations of the predicted values from the NIRS model calibrated with the buoyancy reference values (6.70 %) is smaller than the deviation of the predictions made by the model calibrated with the punch values (11.16%). Also the correlation coefficient indicates that the accuracy of estimation for the former is better than for the latter. This demonstrates that in order to create a NIRS model with acceptable performance, the reference method used for the calibration needs to be reproducible and accurate.

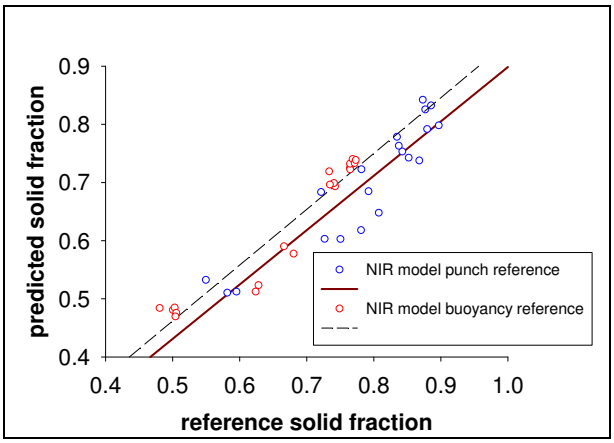

Figure 43. NIRS model predictions compared to the values measured by the reference methods

5.1.3.2 Determination of solid fraction through X-ray µCT, micro-indentation and sectioning

Using the sectioning method, X-ray µCT and micro-indentation, one can generate density maps as shown in Figure 44. In the figure, we can see 2D contour plots of relative density distributions for ribbons produced with the roller parameter settings *B* (see Table 12). In these figures, the same colour scale is used in order to be easily comparable. Thus, the minimum solid fraction value is set at 0.16 and the maximum is set at 0.85, covering the entire range of solid fraction expected for ribbons made of MCC PH102 with these process parameters. For the representation of the contours, the horizontal position was normalized by the ribbon width, so that the x-axis values correspond to the relative distance from the centre of the ribbon width ($r = 0$). The y-axis value is the ribbon length, which is variable for every method.

Figure 44.A, B, and C correspond to the solid fraction distributions determined by means of the sectioning method, the micro-indentation technique, and X-ray µCT respectively. The map for the sectioning method was created representing the relative density value of each sectioned ribbon segment over the x-, y- coordinates of the segment centre. The contour plot of relative density distributions obtained using the micro-indentation was represented by ordering the solid fraction value calculated for each indent with its coordinates. As for X-ray µCT, the contour was plotted out by considering the average pixel value every 100 pixels in both axes.

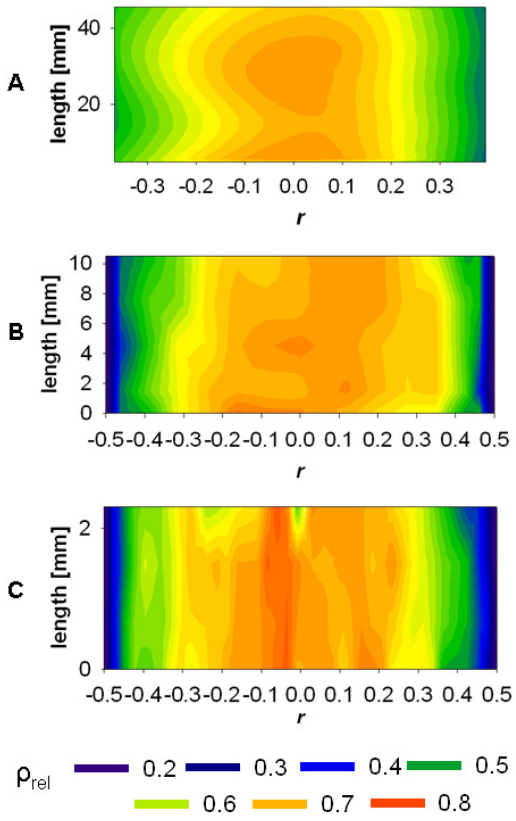

Figure 44. Contour plots corresponding to the solid fraction maps calculated with ***A)*** Sectioning (geometrical) method. ***B)*** Micro-indentation. ***C)*** X-ray µCT

From Figure 44, it is clearly observable that the overall patterns are similar independently of the method of determination used. The same densification patterns have been detected with the three techniques. Thus, high densities were observed towards the middle of the ribbon while the edges possessed lower density. This is in agreement with the observations of several authors (as reported in 5.1.1). After close examination of the solid fraction distributions, one can find that variations of the local density distribution in a particular ribbon can be depicted with more detail using micro-indentation and X-ray µCT, which is due to the fact that the spatial resolution in these methods is much smaller than the size of the segments measurable using the sectioning. However, no significant difference in the solid fraction distribution along the ribbon length were observed, implying that for the roller compaction performed with the gravity feeding, the density variation along the rolling direction (ribbon length) is negligible.

As we have seen in Figure 44, the solid fraction in the middle of the ribbon is higher than that close to the edges. This is further examined by plotting the average solid fraction along the ribbon length against the position across the width. The density profiles obtained with all techniques for a ribbon sample produced with the roller compaction method *B-I* are shown in Figure 45. Here, the data obtained using the different methods have been superimposed. It is noticeable that all three methods deliver essentially identical results. However, as it also happens in the contour plots (Figure 44), the number of points calculated depends again on the spatial resolution, which is small for the sectioning method. The sudden value fluctuation in the density profiles curves obtained using X-ray µCT are due to fluctuations of the pixel values at the edges of the segments. It is clear that for all cases the average densities in the middle of the ribbon width are higher than that at the edges, implying that denser regions are produced in the middle of the ribbon width.

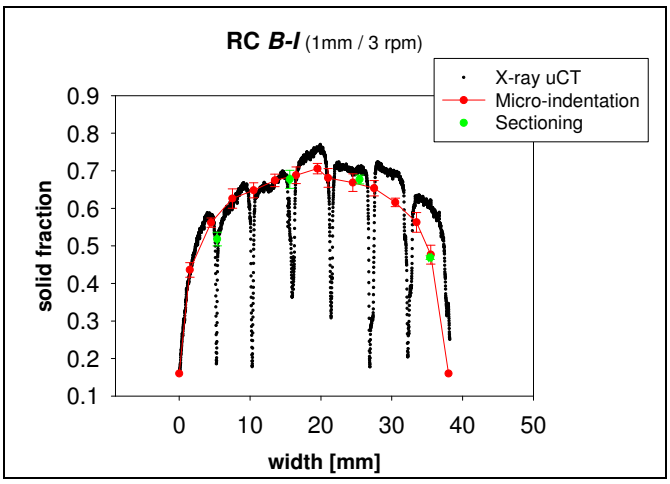

Figure 45. Comparison of the density profiles across the ribbon width determined with all three methods for a ribbon sample obtained from the roller compaction method *B-I*

5.1.3.3 Determination of solid fraction through NMRI

The processing of the NMRI signal resulted in the image of Figure 46.A. It can be observed that the ribbon edges present a higher pixel value (brighter colour) than in the central region. The more voids at a given ribbon region, the more increased is the presence of silicon oil and, subsequently, the more intense becomes the resonance signal. As shown in the figure, the highest pixel values (the brightest zones of the picture) are found towards the bottom of the sample tube, at which silicon oil deposited. Considering the sample, the two extremes (i.e. the ribbon edges) seem brighter than the centre, depicting a much denser structure at this region. The square represented in the same figure corresponds to the sample area considered for the density calculations (40 mm x 8 mm). Thus, the mean value of the pixel value for each vertical position of this square (i.e. across the ribbon width) was calculated from the average of all values at the same height.

In order to estimate the accuracy of the solid fraction determination by NMRI, the values estimated are compared to those delivered for a ribbon sample obtained under the same conditions (roller compaction method *B-II*) with X-ray µCT. As shown in Figure 46.B, the density profile plotted with the NMRI depicted the same tendency of solid fraction distribution across the ribbon width as the observed in Figure 45. The NMRI profile delivers density values similar to those measured by X-ray µCT. However, the maximum solid fraction values detected are slightly higher. This can be explained by the following reasons:

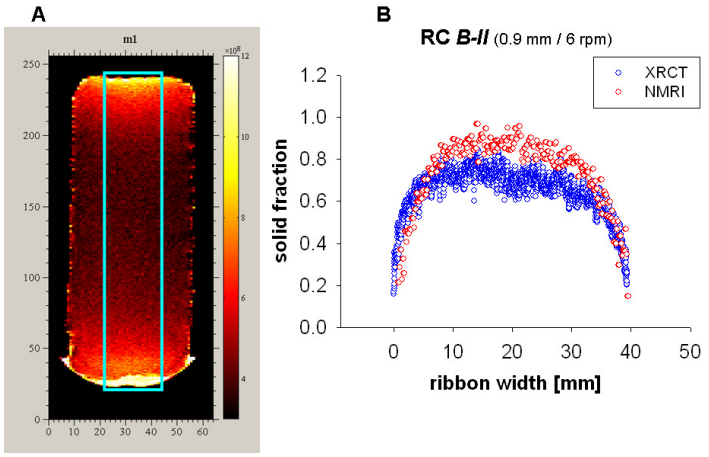

Figure 46. A) NMRI acquisition from the ribbon sample produced with the roller compaction *B-II*. The squared region was taken for the calculations. ***B)*** Comparison of the density profiles resulting from the measures performed with X-ray µCT and NMRI

I) The possible batch to batch variability between samples.

II) An incomplete migration of silicon oil to the central region of the sample, resulting into an overestimation of the solid fraction of that region.

III) The elution of the silicon oil to the bottom of the sample glass cylinder reducing its concentration at the central region and weakening the detected signal.

Since the determination of solid fraction by NMRI was made only once, the sample preparation, the signal acquisition and the image processing need to be optimized to achieve more accurate measurements.

5.1.3.4 Evaluation of the different techniques

A comparison of all methods is summarized in Table 15. The methods considered in this section are compared according to different criteria based on the method (equipment requirements, sample

preparation, calibration and time consumption), the versatility (on-line determination, mapping and imaging), and the accuracy of the measurement. Three main groups of techniques can be unequivocally differentiated:

1- Geometrical techniques and buoyancy do not offer the possibility of detecting in detail local solid fraction distributions. They do not require especial equipment and in general are carried out easily. An obvious benefit is that these techniques do not require calibration. However, the accuracy of these techniques is compromised as sample manipulation and irregularities of the sample may introduce estimation errors.

2- NIRS is the only technique likely to be used for on-line measurements, which makes it suitable for PAT-monitoring of the process. The measurement is fairly easy and fast, but the calibration is a time consuming task on which the accuracy and reliability of the technique are dependent. Though it was not studied here, some NIR devices offer the possibility of being used in imaging of samples detecting local solid fraction fluctuations, in a similar way as Lyon, et al. [257] reported for the application of NIR imaging techniques for the evaluation of the tablet content homogeneity.

3- Micro-indentation, X-ray μCT, and NMRI are in essence laborious techniques. They require specific equipment, which in case of NMRI is extremely expensive. Moreover, the techniques are time consuming because they require calibration or, as for NMRI, the sample preparation and the measurement take long. Though micro-indentation is laborious, the variability between data induced by the acquisition and the processing parameters is negligible. For X-ray μCT and NMRI, however, the settings of acquisition parameters and the image (or the signal) processing have to be meticulously tuned to ensure the quality and reproducibility of the determination.

Table 15. Assessment of the techniques for the solid fraction determination presented in this section

	Equip.	Sample prep.	Calibration	Time	Map	Imaging	On-line	Accuracy
Geometrically	-	-	-	-	-	-	-	+
Punch	-	-	-	-	-	-	-	-
Sectioning	-	-	-	-	+	-	-	-
Buoyancy	-	++	-	+	-	-	-	+
NIRS	++	-	++	*	*	*	+	*
Micro-indent.	+	+	+	++	+	-	-	+
XRCT	++	-	+	++	+	+	-	++
NMRI	+++	+	-	++	+	+	-	++

* see text

A compromise between the requirements, the information gained through the measurement, and the applicability of the technique has to be established before choosing the one that meets our interests. Thus, fast and simple determinations, which in turn deliver global evolution patterns and approaches to the ribbon quality, are enough for rough analysis (or monitoring). However, more tedious determinations will produce extensive information with detailed and accurate values, useful if thoroughly information is required, for instance during the characterisation of small changes introduced in the ribbon quality (e.g. by slight changes in the feeding or the compaction parameters).

5.1.4 Conclusions

The ribbon solid fraction is a product attribute that gives valuable information about the roller compaction process and the granule properties. The ribbon solid fraction value depends on the stress applied on the material and, therefore, almost any variation in the process parameters will have effect on it.

A number of methods for the solid fraction determination are studied and evaluated here. All have demonstrated to be capable of estimating the compact solid fraction. However, they are distinctly accurate, and deliver information of the sample densification with different resolution. In order to evaluate the implementation of a technique, certain selection criteria must be established considering equipment requirements, performance issues, versatility, accuracy and nature of information gathered.

Those techniques that permit the acquisition of a density map of the ribbon provide valuable information about the local density variability. It has been found that the solid fraction of ribbons produced in a roller compaction zone sealed with side cheek plates present a common pattern in which the ribbon central region presents higher densification. The same densification pattern has been detected with all mapping techniques.

5.2 Roller compaction of pharmaceutical substances

A process is generally considered well understood if (1) all critical sources of variability are identified and explained; (2) the process variability can be completely managed; and, (3) product quality attributes can be accurately and reliably predicted over the design space established for the used materials, the process parameters, and for manufacturing conditions (environmental and others). At first glance, the densification of material through two rotating rollers follows fairly simple principles but, in fact, it involves non-linear and disordered phenomena that turn roller compaction into a complex process still far from being completely characterized.

In this section we present a series of studies through which we attempt to describe and demonstrate some of the phenomena occurring during the roller compaction of powdered material. We demonstrate that, even if it is a compaction process like tableting, the densification mechanisms occurring between rotating rollers are more intricate than within a die. In addition, by visually analyzing the behaviour of the powder during the compaction and the characterization of the obtained ribbons at different parameters we demonstrate that not only the processing conditions, but also the inherent attributes of the material, have a significant impact on the material compaction.

5.2.1 The analogies and contrasts between roller and uniaxial compaction

5.2.1.1 Introduction

In sections 2.1.3 and 2.2.1 we have described the manufacture of tablets (in that section referred to as *uniaxial compaction* or *die compaction*) and ribbons as two agglomeration processes in which the volume of the bulk is reduced to form a dense, cohesive *compact.* The materials being consolidated in both processes experience similar changes: the reduction of volume originates particle rearrangement that turns into particle deformation and attrition after the volume of unaltered particles achieves a minimum. This particle distortion originates a system in which solid bridges, particle attraction, and mechanical interlocking occur. These mechanisms determine the compact *cohesiveness.*

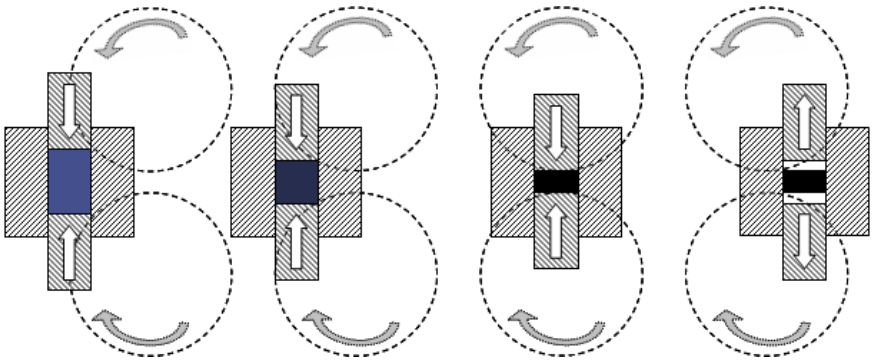

Figure 47. Representation of the analogy between the uniaxial die compaction and the roller compaction

In Figure 47 it has been represented the analogy between the roller compaction and the uniaxial compaction. When considering the roller compaction as a lateral unconfined compaction, the different

stages in the compaction zone could be directly compared to the different stages in the *in die* compaction process if both, upper and lower punch, move axially simultaneously (in a similar way as it happens in rotary tablet presses) at a linear speed that approaches the speed of the strain in the roller compaction. During roller compaction, the material volume reduction reaches its maximum at the neutral angle. This would correspond to the shortest distance between punches during uniaxial compaction. The resulting product of both processes is a rigid form of given porosity: a compact. In case of the roller compaction the compact is unconfined, whereas for the uniaxial compaction its shape is well delimited.

The study of the similarities between both compaction processes, and the attempt of simulating roller compaction using uniaxial compression has been made by several authors from different fields. Michel [192] compared the compacts produced with both methods. He contrasted the solid fraction achieved by the compacts produced from aluminium particles of different size under same amount of pressure. The author concluded that, even if the way of applying force on the material was divergent, similar values of stress produced similar densification. Applying the same principle, Gereg and Cappola [223] made predictions on the suitability of new pharmaceutical ingredients for roller-compaction. They monitored and made approaches about the behaviour of the substance using uniaxial compaction to simulate roller compaction. Also Zinchuk, et al. [211] and Gupta, et al. [118] compared the attributes of compacts produced in a compactor simulator and a roller compactor and concluded that compacts of the same material compressed to the same solid fraction, exhibited equivalent mechanical properties independently of the compaction process. Yusof, et al. [103] studied a method to model the roller compaction of maize powder through values obtained during uniaxial compaction. Following the theories of Johanson [95], who concluded in his work that at the nip region the powder behaviour obeys the laws as in a simple uniaxial die compaction., the authors were able to predict the profiles of roller force as a function of roller speed, roller gap, amount of powder and friction angles by means of the values of compressibility, internal friction, wall friction and applied pressure-volume relationship measured during the uniaxial compaction experiments. Perera [215] considered the size of the rollers, the nip angle and the roller compaction parameters to calculate the equivalent uniaxial compaction parameters (i.e. compaction speed, punch displacement and powder amount) in order to gain compacted discs of similar properties. He compared compacts produced with both processes and found out that the solid fraction and therefore their mechanical properties were not significantly different. Finally, Guigon, et al. [75] presented in page 268 a plot in which the solid fraction of Avicel PH102 compacts as a function of the amount of pressure applied is compared to that of uniaxially compacted Avicel. The values for both compaction techniques converged in the same curve, demonstrating the findings of the other authors.

In this section we compare the compression profile of uniaxial and roller compacted MCC to describe at which extent different mechanisms and material behaviour in two processes that induce material densification can result in products of similar characteristics.

5.2.1.2 Materials and methods

Avicel PH102 was used as supplied for all experiments. For the lubricated powder, MgSt 0.5% (w/w) was blended with MCC in the rotary mixer for 2 min at low speed.

Unlubricated and lubricated MCC blends were separately roller compacted using the roller compactor No.2. The rotational velocity was set at 3 and 5 rpm and the roller gap was 1 mm. The initial amount of powder was the same for all runs. The hopper was completely filled up and the excess of powder at the top was levelled off. Ribbons were collected and the solid fraction was verified by sectioning (see 5.1.2.3). A total of 3 ribbons for each compaction settings were analyzed.

Unlubricated MCC was uniaxially compacted by means of the material testing machine No.1. The powder was fed into a 13 mm diameter die and then compacted at different compression forces as described in 5.1.2.6. The thickness of the compacted tablets was ca. 1 mm. This was chosen as it was also the roller gap set for the roller compaction. The quantity of material and the compaction forces used for manufacturing tablets of approx. 1 mm thick are listed in Table 16. A total of three compacts were compacted uniaxially for each compression force. The mean thickness of the obtained compacts is also recorded in Table 16. The solid fraction of the manufactured compacts was geometrically calculated as described in 5.1.2.3. For the compacted ribbons, exclusively the central region of the ribbon was considered, since the pressure sensor is located in this region. Finally, a second batch of uniaxial compactions was carried out for which the quantity of powder fed into the die was approximately 600 mg.

Table 16. Parameters set for the compaction and resulting thickness of the MCC tablets (uniaxial compacts)

Comp. force [kN]	APH102 amount [mg]	Compact thickness [mm]
1.5	90	1.217
3	105	1.224
6	130	1.250
9	145	1.252
12	160	1.275
15	170	1.254

The force-displacement profiles during the compaction in both compaction devices were recorded. The data gathered with the LabView software for the roller compactor was processed using MatLab in order to calculate the pressure values. The Lloyds software for registering the data from the material testing machine, in turn, delivered the information of strain and displacement automatically.

5.2.1.3 Results and discussion

The different compaction regions are described in section 2.2.1.2. Figure 48.A shows the typical profile of a rotational compaction corresponding to the compaction of MCC at 3 rpm without lubrication. The stress exerted by the roller on the powder increases as the material reaches the neutral angle, at which the compaction pressure is maximal. As pointed out in section 2.2.1.2, this angle does not correspond to the rotation angle 0° [258]. After the maximum pressure (P_{max}) is reached, the material is released and the pressure detected on the roller surface decreases. The relatively gradual decrease in the pressure value is due to the material relaxation. The pressure returns to 0 when the rollers keep rotating.

A compression-decompression cycle profile from a uniaxial compaction of 600 mg of MCC to a pressure of ca. 80 MPa is plotted in Figure 48.B. The process is represented as a function of the punch displacement and the pressure registered by the strain detector. As the punch moves downwards, the increase of stress is detected and exhibits an exponential character until the maximum pressure set for the process is reached. Then, the punch is driven upwards. At this point, a certain amount of pressure is still detected. This is, as for the roller compaction, the pressure exerted by the material during its elastic relaxation.

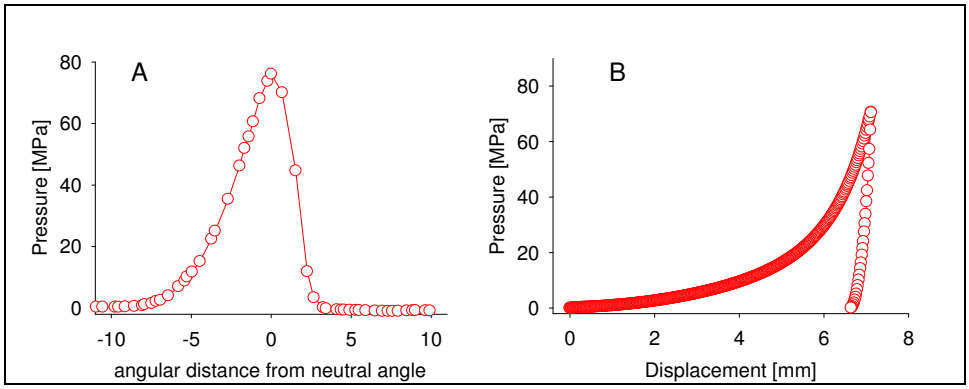

Figure 48. Pressure-displacement profiles of A) roller compaction B) uniaxial die compaction

The angular displacement for the roller rotation can be transformed to a linear vector. Thus, the angular position of the rollers can be transformed into a linear displacement value through the following equation:

$$\ell_{\phi} = 2 \cdot \{R - [R * \cos(\phi)]\} \qquad (35)$$

where ℓ_{ϕ} is the corresponding linear distance from the axial centre of the roller gap at the angle Φ considering both rollers, and R is the roller radius. Considering the angle Φ from which the pressure starts to increase as the origin, and assuming that this angle is the same for both rollers, the plot of Figure 48.A can be transformed into the one showed in Figure 49.

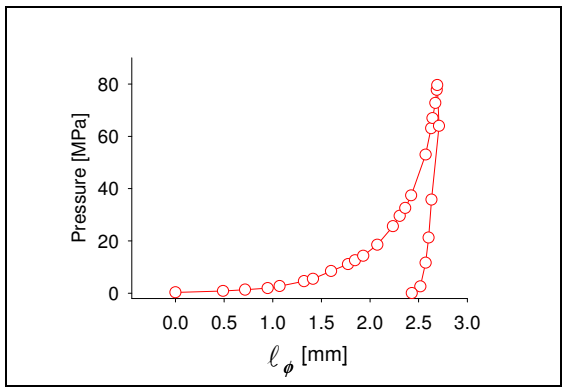

Figure 49. Converted pressure- angular displacement data to a pressure-linear displacement profile

Analyzing the resulting graph and comparing it with that of Figure 48.B, it is evident that there is a parallelism between the stress exerted during rotational and uniaxial compaction. The profile follows a similar curve evidencing the exertion of load and the release of it occurring during both processes. However, in the rotational compaction the stress is defined by the sum of settings and parameters that influence the material compaction, the feeding of material, the pressure exertion and its distribution. Altogether it makes the control of that stress to be more intricate than for uniaxial compaction.

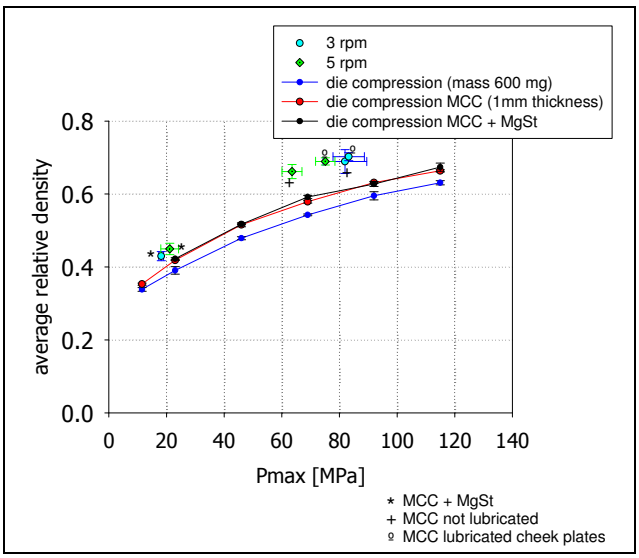

Figure 51. Compressibility patterns of MCC and lubricated MCC at different compaction conditions. Comparison of uniaxial compression and roller compaction.

In Figure 51 the solid fractions of compacts produced by both methods are compared as a function of the maximum compaction pressures and the solid fraction achieved by the material. The line plots correspond to the densification in uniaxial compaction. Three curves are drawn: 1) the compaction of a constant mass of 600 mg of unlubricated MCC resulting in different tablet thicknesses; 2) the uniaxial compression of lubricated and 3) unlubricated MCC in different amounts of powder to reach a similar ribbon thickness of approx. 1 mm. There is no significant difference in the densification behaviour between the lubricated and the unlubricated MCC. This is owing to the very small amount of MgSt (0.5% w/w) added, which according to [259] and [260], resulted in similar porosities for unlubricated and lubricated microcrystalline cellulose powder, when compressed at a certain load. The results for the rotational compaction are represented by single symbols. In a similar way as it is observed for the uniaxial compacts, the average solid fraction of rolled compacted ribbons increases with the maximum compression pressure. Moreover, the results for the two different roll speeds coalesce to form a single master curve, what evidences that the solid fraction is a function of the pressure exerted on the powder (regardless of the compaction parameters). The values presented here belong to the roller compaction of lubricated and unlubricated MCC which densifications, as seen before, also drawn a sole curve. Moreover, the different conditions of compaction (i.e. comparing not lubricated cheek plates with the lubricated) make increase the final maximal pressure. This is attributed to the conveyance of a larger amount of material into the roller gap.

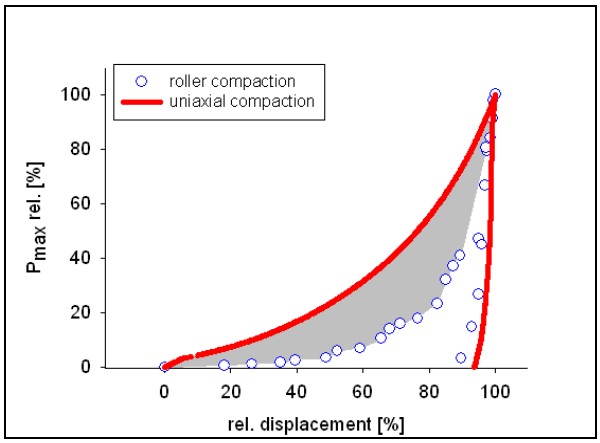

Figure 50. Comparison of the force-displacement curves (normalized) for a roller compaction and a compression process

Nevertheless, it is noteworthy to point out that the curve profiles of roller compacted and uniaxially compacted materials are parallel. Back to Figure 51, it is shown that tablets made with 600 mg of material reached a lower level of densification than if a smaller amount of material is compacted so as to obtain 1 mm thick tablets. In turn, the curve drawn by the density values of ribbons is above the one of the 1 mm thick tablets. It appears that one dominant factor of the level of densification is the amount of material being compacted. In Figure 50 we compare the force-displacement profile for the uniaxial compaction of 600 mg of MCC (with and end thickness of around 3 to 3.5 mm) with the roller

compaction of MCC (producing ribbons of approx. 1 mm). The maximal pressure reached in both compactions was ca. 80 MPa. In order to make the stress-strain profiles comparable, we have normalized the displacement and the pressure values between 0 and 100%. As depicted by the grey area, the relative work (expressed as the area under the curve) made by the punch was more extensive than the one exerted by the rollers. It is therefore clear that the compaction of a larger amount of material requires more energy in order to achieve a certain level of densification. However, when combining the results from Figure 51 and Figure 50, one can observe that even if the total work applied on the material is considerable larger (Figure 50), the relative density achieved by the 600 mg MCC tablets was smaller than the one of the ribbons (Figure 51). For the production of the 600 mg tablets, the punch needs a longer displacement to reach the same value of pressure (longer displacements) during which the volume reduction, the wall-friction and the particle friction [12, 23, 60, 63, 64, 80, 217] induce the dissipation of energy and reduce the cohesiveness achieved, since a big part of the energy has to be used to overcome a larger number of friction interactions and elastic recovery undergoing by more particles simultaneously. Thus, even if the quantity of work and displacement are much larger than in the roller compaction, the system achieves lower densification levels.

In addition, the duration of the time of permanence of the material at stages of high pressure (i.e., the dwell time) is different for uniaxial and roller compaction. According to [261], the densification does not suffer large variations at a wide range of dwell times. However, it was proved by others [65, 86, 188, 210] that in roller compaction the rotation speed and the dwell time of the material determine significantly the level of material densification and, consequently, the hardness of the ribbon. In Figure 52 we compared the time-displacement profiles of both processes. The diagrams of this figure correspond to the profile displacement-time for the *in die compaction* (1) and the transformed "linear" displacement-time diagram of the profile for a roller compaction at 6 rpm (2), which is a relatively fast rotation speed. The diagrams on the right are a magnification of the encircled areas. The global time of the uniaxial compaction is longer than for the roller compaction. However, as it can be concluded after comparing the diagrams on the right, it is not clear exactly how long the real "dwell times" last, since the frequency of data recording does not allow its accurate determination. Nevertheless, roller compaction has apparently longer dwell times than the uniaxial compaction. This would be consistent with the higher densifications achieved by the ribbons observed

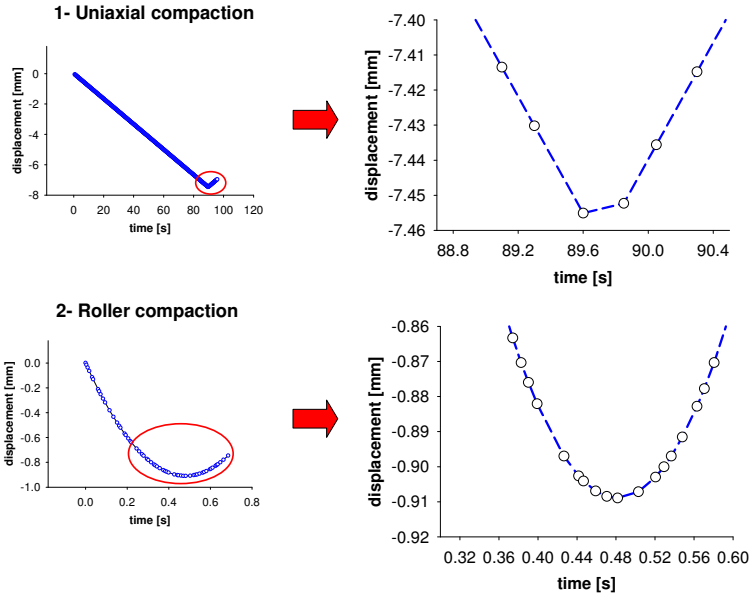

Figure 52. Time-displacement diagrams of the uniaxial compaction and the roller compaction of MCC

in Figure 51, demonstrating why tablets of the same thickness (1 mm), and produced with the same pressure levels as the ribbons, presented lower solid fractions.

Finally, other reasons for the different level of density achieved by the material in both processes (Figure 51) is attributed to the fact that the sequence of mechanisms and phenomena occurring in both processes might be less similar than as reported by others [103, 192, 215]. Our experiments demonstrate that during the uniaxial compaction we could not manage to simulate the compaction conditions of the roller compaction. Firstly the powder confinement is different. The roller compaction with side cheek plates as sealing is unconfined, i.e., as if the material were uniaxially compacted without one of the die walls and changing the other wall by one of low rigidity. In addition, the width-wise confinement of the material induces a non-homogeneous distribution of the material across the roller surface (5.2.2) and, since it is not a completely closed space, there is leakage of uncompacted material. Furthermore, the way the pressure is exerted on the material is different for the two compared systems. In roller compaction both rollers exert pressure on the material symmetrically, while in the uniaxial compaction performed here only the upper punch induces the volume reduction. For this reason, the simulation of the pressure for the rollers can be simulated exclusively in a system in which both punches are moving simultaneously (as depicted in Figure 47 and as described in [211]). Thus, a totally confined assembly in which only one punch exerts stress on the powder, might not match the conditions taking place in roller compaction.

The densification conditions between the rotating rollers are therefore less predictable and the process becomes far much more complicated than the simulated *in die*. Consequently, only if similar (if not identical) strain-stress conditions are generated during the material densification, the produced compacts will show similar attributes regardless of the compaction process [118, 211].

5.2.1.4 Conclusions

The compaction of material follows the same sequence of volume reduction mechanisms and particle deformation regardless of the method used. Roller compaction can therefore simulated and compared with an *in die* uniaxial compaction process if similar strain-displacement conditions are achieved. We have demonstrated that the amount of powder (even if it is compacted to an equivalent pressure level), the differences in dwell time, and the way in which the material is confined produced compacts of different attributes. Though both processes result in the compaction of material, the simulation of roller compaction using uniaxial compaction demands a large number of parameters to be considered in order to simulate similar conditions and mechanisms of volume reduction.

5.2.2 The material behaviour during roller compaction

In this section, a series of studies is presented, in which irregularities in the powder mobility during material compaction that have an effect on the properties of the ribbon are described and analysed. Two methods of visualisation of flow patterns were used in order to follow the gradients of powder flow and material transport at the roller compaction regions: 1) analysis of the appearance of the ribbons produced using colour powder; and 2) observation of the powder flow in the hopper on video.

5.2.2.1 Analyzing the conveyance of material at the compaction zone through examination of patterns of coloured MCC on ribbons

5.2.2.1.1 Introduction

As described in section 2.2.1, there is a large number of factors involved to a major or a minor extent in the progress of material compaction. The conveyance of material into the compaction zone and the movement and distribution of powder at the slip and the nip regions is one of them. The conveyance of powder is the result of shear stress, strain and interface interactions between the instrument and the powder bed. But in contrast to non porous, continuous materials, which transport only depends on these interactions, in granular materials the internal friction (i.e. the one originated between particles) is also crucial for the understanding of the material conveyance. The movement of powder at the compaction zone is originated by roller surface-bulk friction transferred across the bulk by particle-particle interactions [262]. Thus, during the roller compaction we need to distinguish four different frictional components that generate the transport of powder into the compaction zone: the internal friction below and above the nip region, and the external friction (i.e. between particles and tooling) below and above the nip region [263] as well. The internal friction depends on particle shape, particle size, size distribution, particle porosity and molecular forces (e.g. electrostatic charge). The external friction, in turn, depends also on the roughness of the tooling surfaces. The friction interactions and the gradients of powder flow generated when the material enters the compaction region are reflected in the distribution of densification in the produced ribbon.

The material dynamics at the compaction area is induced by the rotation of the rollers. The rotational movement originates shear at the interface between bulk and roller surface, which causes the material motion. The particle trajectory at this stage was controlled by Schoenert [96] with a fast camera. He reported that the particle displacement was smaller than the radial velocity of the rollers, evidencing that the particle movement depends not only on the friction with the roller walls, but also on particle interactions. In his work, Perera [215] tracked the particle movement at the different compaction stages with PEPT and observed that the particle velocity in early levels of the compaction area is lower than at the nip region, where the speed was equal to that of the rollers. Moreover, the motion of the particles at a given height of the powder column is affected by strain and shear resulting from the powder feeding. Simon and Guigon [88] also tracked the particle trajectories at the slip region and observed that they presented irregular patterns originated by the feeding system. Thus, in systems with screw feeders, the transference of energy between particles is proportional to the inherent coefficient

of friction and the normal stress applied by the auger on the bulk. In gravity fed systems, however, the conveyance of powder into the compaction zone has been observed to be largely affected by the height of the powder (i.e. the own bulk weight) for materials with large bulk density [192, 264].

The frictional interaction between powder and tooling is another source of variability in the particle motion. Thus, the irregular axial distribution of material densification across the roller gap is attributed to the friction of particles with the side walls that seal the compaction zone [77, 193, 209, 213-215]. The material transport towards the edges of the compaction gap is opposed by the frictional force generated by the side wall. The gap between the rollers is less filled with material (i.e., less particles are present) and, consequently, the densification level reached by the material becomes lower.

In this work we try to investigate how these irregularities in the material transport at the compaction zone appear in a gravity fed compactor. By using coloured MCC, we could analyze qualitatively, how the material is being transported by the rollers and what are the fluctuations undergone by the transport of the powder after the modification of roller compaction parameters (i.e. rotation speed), compaction conditions (i.e. tool lubrication), and powder internal friction (i.e. powder lubrication).

5.2.2.1.2 Materials and methods

MCC PH102 was used as principal component. Colour chalks were used for staining the powder and MgSt was used as lubricant. A suspension of 5% MgSt (w/w) in ethanol was prepared for the application of MgSt as external lubricant.

The colour chalks were pulverized using a granulation sieve with 0.5 mm opening and a porcelain mortar. The ground chalks of different colours were mixed with 900 g of MCC PH102 for at least 30 min, in a Pascall rotary mixer, until a homogeneously coloured mixture was produced. Four different coloured powders were produced (see Figure 53.A). Part of the coloured powder was thereafter blended with a 0.5% MgSt again in the rotary mixer for 2 min at intermediate speed.

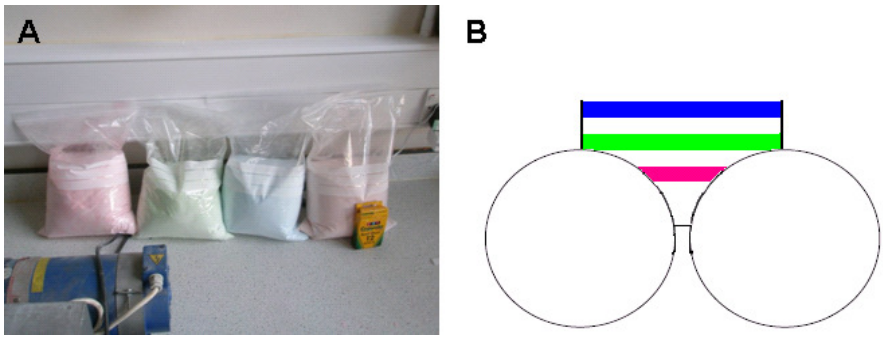

Figure 53. A) Chalk coloured MCC. ***B***) Layout of the colour layers within the compactor hopper before starting the run

Different compaction experiments were carried out, for which the coloured powder combinations and the compaction parameters were different. In a first experiment, the hopper was filled up with powder as shown in Figure 53.B. MCC blends of different colour were deposited in layers in the hopper with virgin MCC in between. The same volume of powder (100 ml) was deposited on each layer. This amount was kept invariable for all runs. The roller compaction was carried out on the roller compactor No. 2 with a roller gap of 1 mm and a rotational speed of 5 rpm. Three different runs were performed. For the first

run, the powder and the compaction was performed normally. For the second run, the MgSt suspension was applied on the hopper walls and the side cheek plate and was let dry before filling the hopper. For the third run, the powder blends were lubricated with 0.5% MgSt prior to deposit them into the hopper. During all three runs, the produced ribbons were carefully collected for a later analysis paying especial attention on the order of sequence and the sample orientation.

In a second group of experiments, the hopper was only fed with rosy and white (virgin) MCC, in this order. 200 ml of each powder type was deposited into the hopper forming two layers. This time three compaction runs at different rotation speeds, at 2, 3, and 5 rpm, were performed. Moreover, the compaction was made with and without external lubrication of the roller press. The entire ribbons produced were also collected.

Using a digital camera, we took pictures during the compaction run from the top of the hopper in order to observe and capture the patterns and conformations formed by the powder. Finally, also the produced ribbons were pictured for further analysis.

5.2.2.1.3 Results and discussion

During the compaction runs, the produced ribbons were collected and arranged in order to measure the length at which the different colour bands appeared. Figure 54 shows the typical patterns of colour observed in the ribbons for the transitions between layers. Independently of the roller compaction parameters and/or conditions, the appearance of the next layer starts before the totality of the current layer has been completely conveyed through. It can be seen clearly (Figure 54), that part of the material corresponding to previous layers remains towards the ribbon edges while the next colour appears towards the central compact region. This indicates that the transport at the central region of the roller gap is faster than that closer to the cheek side plates, which is consistent with the observations made by the authors listed in 5.2.2.1.1 and with Kuleshov [264], who observed that during the compaction in a gravity fed compactors, lower stress were detected at the lateral regions of the rollers due to the formation of a discharge channel generated by faster transport of material at the centre of the roller gap.

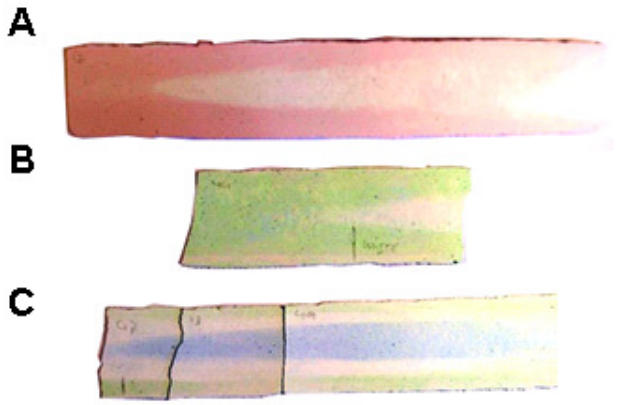

Figure 54. Colour patterns observed for the collected ribbons. ***A)*** Transition pink to white (third layer). ***B)*** Transition green to white (fifth layer). ***C)*** Transition white layer to blue layer (last layer)

Moreover, as it can be seen in Figure 54.B, the brighter colour that corresponds to the penultimate layer ("white" MCC) in the first batch of experiments, has adopted a slight tone of blue. This proves that during the transport, there has been an exchange of material between layers. This is the evidence that already at early stages of the compaction there is certain mobility of particles between powder levels due to irregular trajectories and intricate patterns followed by the material during the transport.

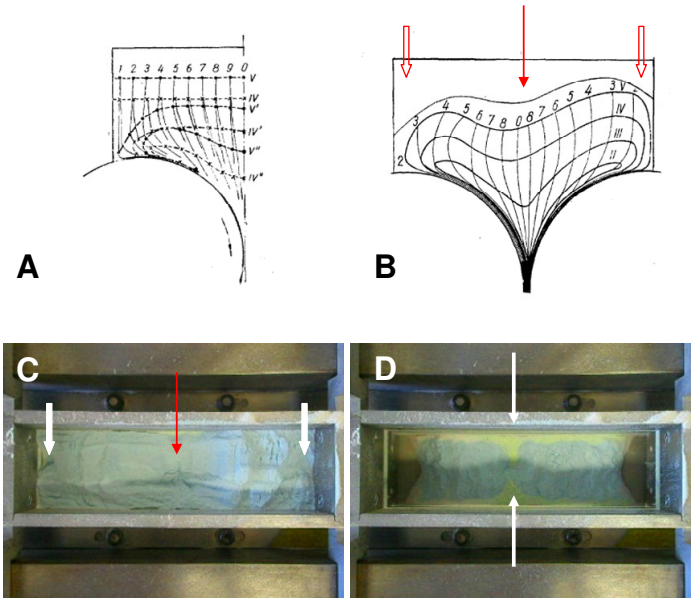

Figure 55. Bulk flow in the hopper of the gravity roller compactor. ***A)*** Evolution of the powder distribution at different compaction stages [265] ***B)*** Irregular distribution gradient from the edges to the central region of the hopper [265]. ***C)*** Distribution observed during the experiments. ***D)*** Evidence of the opposition of the side plates to the powder feeding towards the edges of the compaction area.

Vinogradov and Katashinskii [265] studied the trajectories of lead particles while being roller compacted by means of X-ray imaging. They described that, within the hopper, the particles moved differently at the different regions. Thus, particles at bulk regions away from the roller gap initially move slowly, while their speed increases as they approach the compaction area. The central powder column, however, flowed with constant axial velocity induced almost exclusively by the rotational speed (see Figure 55.A. [265]). This irregular flow is also the reason for the exchange of material between layers. The irregular movement of the particles provides the bulk with a shape similar to the shown in Figure 55.B. Comparing Figure 55.B and Figure 55.C, it can be seen the theoretical quantification made by the authors are in agreement with the heaps and dips (also known as *rat holes*) observed by us from the top of the hopper. The arrows drawn in Figure 55.B and Figure 55.C point at the similar patterns observed in our experiments and these reported by Vinogradov and Katashinskii. Another trend observed from the top of the hopper which is also consistent with the geometry of the colour transition bands in the ribbons of Figure 54 is depicted in Figure 55.D. The colour of underlying layers becomes visible on the top of the bulk, especially towards the regions of contact with the side plates at the gap between rollers (see white arrows). This indicates again, firstly, that the transport at the central regions of the hopper is faster than towards the edges, and secondly, that the side walls hinder the powder to move forward.

Figure 56 presents the ribbon lengths at which the transitions of layers with different colour appeared for different compaction conditions. Each bar corresponds to ribbons produced during the first block of experiments (i.e. with constant rotation speed of 5 rpm). It has to be highlighted that, though the appearance of a new colour was more or less evident, in some cases, the interlocking of colours reached such an extent that the identification of the beginning and the transition of some layers became difficult (see Figure 54.C).

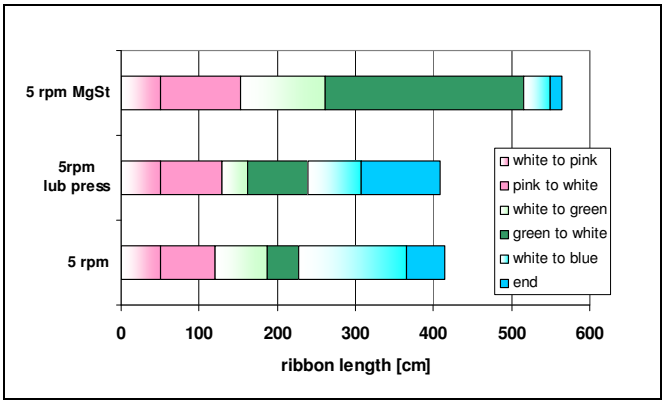

Figure 56. Ribbon lengths at which the transition between layers appeared

The total length of the ribbons, the distance between layers and the length of the transitions at which virgin powder could be identified as such or mixed up with coloured powder vary when the compaction conditions change, as it is depicted in Figure 56. An obvious result that can be extracted from the figure is that the total ribbon lengths vary as a function of the compaction conditions. However, this will be discussed below. After the analysis of the lengths for the different colour bands, one can see that during the process without lubrication (bottom bar) longer white-colour transitions are followed by shorter colour bands. The ribbons produced with the lubricated side wall, however, present shorter white-colour transitions, and longer colour bands. Finally, the ribbons of lubricated powder have generally longer bands for both, transition and colour fragments. However, since the material of the last layers was strongly mixed, the identification of the last bands was not evident. Two factors of the material mobility at the compaction area can be concluded from these results:

1) The interaction of the material with the side walls, accentuates the delay of transport of material at this region, causing the simultaneous compaction of virgin MCC and coloured MCC for longer with not lubricated side walls than after being lubricated. Thus, the reduction of the interaction of material with the side walls after lubrication diminishes the interlocking between layers.

2) The friction components (both, internal and external) are of crucial importance in the material transport induced by the rollers. Internal friction seems to be also involved in the particle mobility between different levels of the material column. Thus, low internal friction (e.g., after powder lubrication) increases the particle mobility and eases the exchange of material between layers, which results in a heterogeneous mixture of colours at the final ribbon fragments. The external friction, on the other hand, defines the extent of material interaction with the side walls and the roller surface, which determines the amount of powder drawn by the rollers towards the edges of the roller gap.

The lubrication of the powder decreases the coefficient of friction between individual particles and between the bulk surface and the roller surface [266]. This induces a decrease on the material amount being born into the roller gap at each rotation and consequently the ribbons are longer but also less dense, which explains the total length observed in Figure 56 for ribbons produced from lubricated powder.

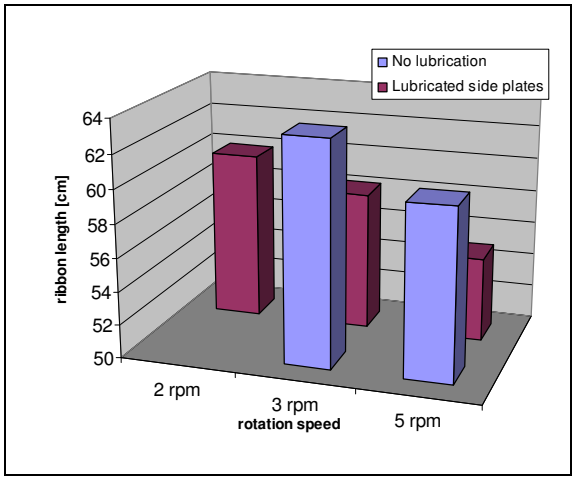

Figure 57. Total ribbon length as a function of the roller rotation speed and the powder lubrication

The results obtained for the second block of experiments (i.e., compaction of only a layer of pink stained MCC and virgin powder) are shown in Figure 57. The histogram compares the ribbon lengths at which the band of virgin MCC appeared for different rotation speeds for the roller compaction of lubricated and unlubricated side walls. Though the results for the compaction at 2 rpm for the unlubricated press are missing, the general trend shows

that the white band appears after shorter lengths of ribbon for increasing rotation speeds. As observed by Vinogradov and Katashinskii [265], the velocity of the central powder column is directly proportional to the rotational speed and therefore, the up-regulation of the roller speed induces an early appearance of the next layer at the central region of the ribbon. In addition, wall lubrication enhances the overall transport of material (i.e. both towards the borders and the central region), hence increasing the amount of powder conveyed into the roller gap. For this reason, as it is shown in Figure 57, the external lubrication of side walls enhances the early appearance of the white band regardless of the rotation speed.

5.2.2.1.4 Conclusions

The transport of loose material from the hopper into the compaction zone is the result of interactions between the bulk and the surface of the rotating rollers and is strongly influenced by the interaction between particles (internal friction) and by the interaction with the side walls (external friction). In this study, the colour pattern observed in compacted ribbons demonstrates that the material transport in roller compactors with side plates sealing the compaction zone is faster at the centre than towards the edges of the compaction gap. This is attributed to the opposition of the side wall against the material transport in that region. The results of this study show that the lubrication of the powder reduces both internal and external friction. As a consequence, less material is conveyed into the compaction zone and the ribbons obtained possess lower density. It has been also observed that increasing the rotation speed enhances the transport of powder dragged through the centre of the roller gap. Finally, the lubrication of the side walls improves the flow of powder through the rollers increasing the quantity of material being compacted and resulting in a more uniform distribution of the compacted material across the roller gap.

5.2.2.2 The drag angle and the homogeneity of the ribbon densification

5.2.2.2.1 Introduction

In the previous section (5.2.2.1) we have demonstrated by analyzing the colour patterns of ribbons that the transport of material in the compaction zone is not homogeneous across the roller gap, which is consistent with the results reported by others. In addition, we have also reported certain mobility of particles within the bulk that resulted in a blending effect of the loose powder deposited in the hopper. We have also seen that the particle motion at the first stages of the compaction depends largely on the friction interactions. Since the quantity of material and the degree of densification define the friction interactions in the system, any change in the roller compaction parameters, the process conditions and the inherent bulk attributes will have a strong effect on the powder feeding. Obviously, non-uniform feeding of material will cause discontinuities in the pre-densification stages of the compaction that are also transmitted to the compaction zone, generating ribbons with heterogeneous solid fraction distributions.

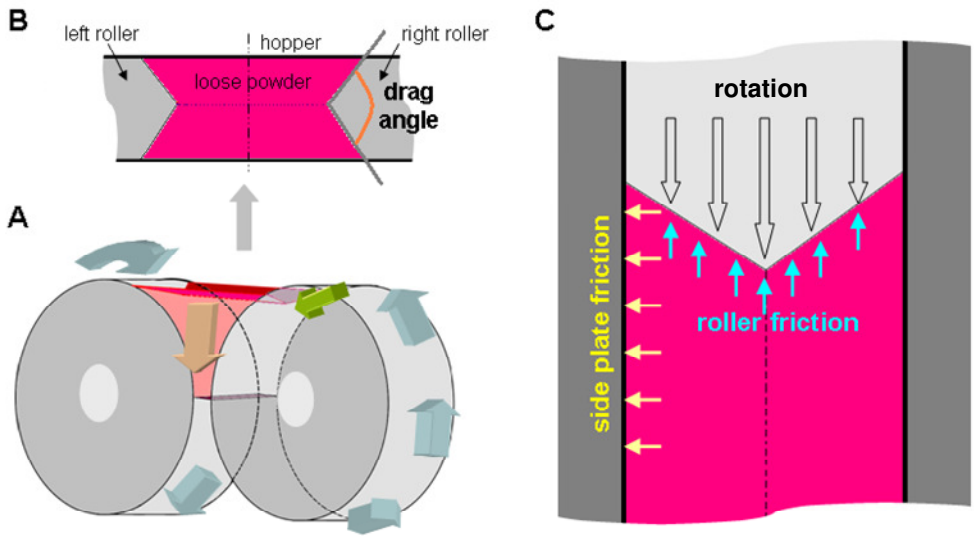

Figure 58. A) Origin of the visualized *drag angle* at the upper regions of the powder in the hopper before entering the compaction zone ***B)*** Sight of the angle formed from the top of the hopper ***C)*** Friction interactions involved in the origin of the pattern

In this section, the transport of the material induced by the rollers taking place in the hopper was visually observed. Schoenert [96], Simon [88] and Perera [215] tracked the bulk movement at the compaction zone and described respectively the trajectory, turbulences and velocity of the material conveyed in the compaction zone. However, they examined and pictured the bulk mobility from a lateral perspective of the rollers. Since the device used for this study is a gravity fed compactor, the analysis of the powder behaviour from the top was feasible. Through examining the powder in the hopper during the roller compaction from the top we have already reported in 5.2.2.1.3 the formation of irregularities in the bulk, and the apparition of underlying (coloured) layers at the contacts with the side walls as a consequence of the different gradient of powder transport at the side walls and the

centre of the hopper. However, another pattern has been observed to take place at the upper levels of the bulk, in which the powder still loose. As it is represented in Figure 58.A, while the rollers rotate, the loose powder of the hopper forms a dip towards the centre, which is due to the differences in material conveyance at the side walls and *mass flow* (orange arrow) produced by the rotation of the rollers. In addition, the powder forms another pattern on the roller surface: a "v-shape" corresponding to a gradient on the material conveyance, this time caused by the difference of powder mobility between the central part of the rollers and the side walls (green arrow). When the hopper is observed from the top (see Figure 58.B), the two dimensional v-shape resulting from the sum of both angles is referred here as the *drag angle*. As depicted in Figure 58.C, the drag angle drawn by the loose powder in contact with the surface of the rollers is therefore originated by two gradients:

i) the gradient wall-roller centre, due to the difference of the mass flow downwards as the hopper is emptying; and
ii) the gradient wall-to-roller centre of the *core flow,* which is directly related to the interaction of the powder with the roller surface.

We have observed that these gradients determine how powder is gripped into the roller gap and how it distributes across the roller width, which is also directly correlated with the distribution of the density in the compacted ribbon. Moreover, the effects on the material compaction due to changes in the friction at the contact between the powder and the side walls and between the powder and the roller surface have been monitored.

5.2.2.2.2 Materials and methods

MCC PH102 was used as compacted material. For the lubrication of the powder, MgSt 0.5% (w/w) was blended with MCC in the rotary mixer for 2 min. For the external lubrication of the cheek plates, as for the previous section, a suspension of 5% MgSt (w/w) in ethanol was prepared. Not lubricated and lubricated MCC PH102 were separately roller compacted by means of the roller compactor No.2. The rotational velocity was set at 3 and 5 rpm and roller gap was 1 mm. The initial amount of powder was the same for all runs, i.e. the hopper was completely filled up (see Figure 59.1) and the excess of powder at the top was levelled off. Runs with and without external lubrication of the side walls were also carried out. A total of three runs for each roller compaction settings were performed. On the top of the hopper walls ruled tape was stuck in order to have a reference of the distances travelled by the powder. During the roller compaction the process was recorded from the top with a digital camera fixed in the same position. Images of the process were recorded as shown in Figure 59.1-3. For each

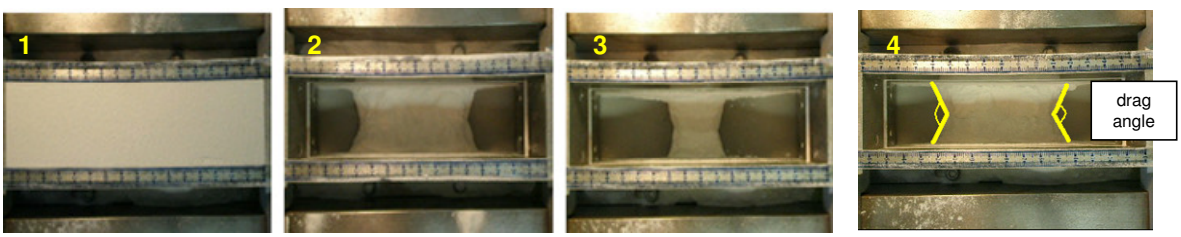

Figure 59. Imaging and measurement of the drag angle

run, a total of seven shots corresponding to the powder displacement at 2, 2.5, 3, 3.5, 4, 4.5 and 5 cm from the hopper left wall were acquired from the recording. The obtained pictures were analyzed using the software *ImageJ*. The angle formed by the powder on both rollers was measured for each one of the slices as in Figure 59.4.

A total of three ribbon samples were collected for each of the compaction settings. The solid fraction of the samples was determined as described in section 5.1.2.3. The ribbon samples were sectioned into 20 fragments which solid fraction was verified geometrically (5.1.2.3).

5.2.2.2.3 Results and discussion

The averaged drag angles resulting from each one of the run conditions are represented in Figure 60. Narrower angles indicate a larger gradient of powder transport from the laterals toward the central region of the roller gap. In absence of lubrication, the angles were the narrowest. This is attributed to the frictional forces on the side walls. They oppose the particle transport into the compaction zone, as reported in previous experiments (5.2.2.1).

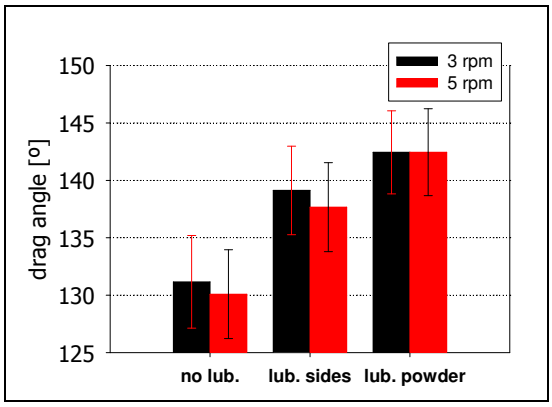

Figure 60. Average drag angle values

An increase in the rotation speed generates even narrower angles. As higher rotational speeds increase, the kinetic energy of the particles grows. Consequently the energy dissipated by the collision of particles with themselves and with the side wall increase [267]. As a consequence the gradient of bulk transport edge to middle is incremented and, therefore, the drag angle becomes narrower. When the side walls are pre-lubricated, the particle-wall friction decreases and, consequently, the drag angle becomes wider. It has been shown again that faster roller rotation increases the unevenness of material transport towards the centre. Moreover, the lubrication of the powder decreased both the internal friction between the particles and the particle-wall friction. As it can be seen in Figure 60, the angle values confirmed, firstly, that the particles are transported more homogeneously across the roller surface, and secondly, that the reduced particle-surface interactions when the powder is lubricated are less sensitive to the intensification of the rotation speed than non-lubricated material.

The solid fraction values of the ribbon fragments for each width position were averaged as shown in Figure 61.A. The solid fractions are shown and compared in Figure 61.B and C. All samples characterized show the typical pattern of denser middle regions and looser ribbon edges. In addition, in Figure 62 two SEM images of a fragment of a ribbon of no lubricated MCC produced at 3 rpm are compared. It can be seen that for the same specimen, the image from the edge (left picture) and the middle part of the ribbon (right picture) reveal the different level of densification across the ribbon width. Moreover, in the left SEM, we can observe the irregular edge of the ribbon, which is due to the loss of uncompacted material from the roller edges and the scratching with the sealing cheek plates.

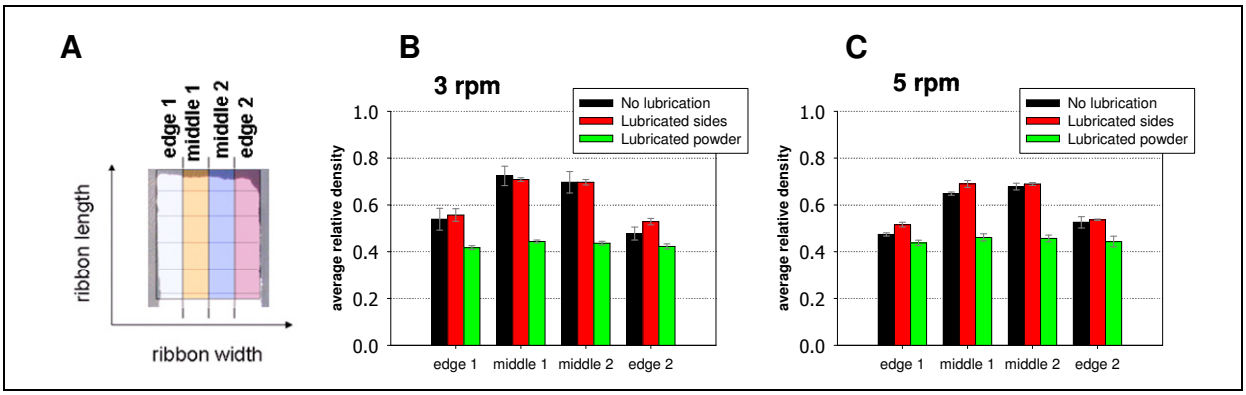

Figure 61. Distribution of the density across the ribbon width at different compaction conditions

The gradient of densification edge-to-centre is in agreement with findings of other authors [268] and with results presented in other experimental sections of this thesis (5.1.3 and 5.2.3.3). Nevertheless, the compaction of unlubricated powder generated ribbons with less dense edges, whereas powder lubrication reduced the gradient of density between edge and centre of the ribbon. Obviously, the values of solid fraction for lubricated MCC ribbons decreased abruptly, for reasons already mentioned in 5.2.2.1.3.

However, the lubrication of the compactor side walls induced, in addition, a slight increase of the density. As the solid fraction is directly related to the amount of powder being conveyed between the rollers, the lubrication of the side walls enhanced the material transport and, as a consequence, the densification achieved becomes larger. Comparing the values of solid fraction from Figure 61.B and Figure 61.C one can observe that, in general, the values for ribbons produced at 3 rpm are higher than those produced at 5 rpm. Decrease in the powder densification due to higher roller velocities was also observed by [193], [209], and [215]. They attributed this to a reduced stress applied on the material at faster rotation.

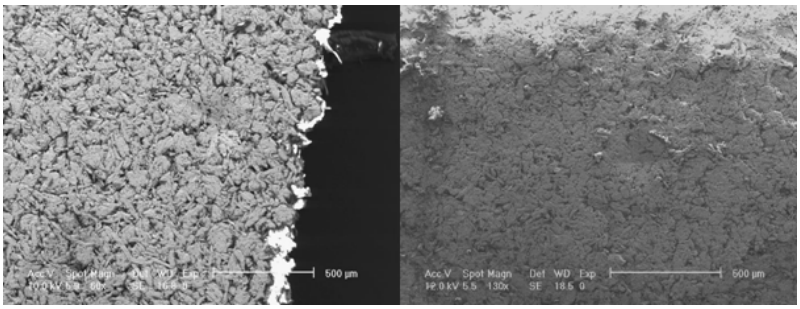

Figure 62. SEM of the edge (left picture) and the middle region (right picture) for the same ribbon sample. In the picture on the left, the irregular edges in the ribbons produced

In order to depict in what extent the gradient of central and external solid fraction changed for the different runs, the slope between values was normalized as follows:

$$\delta = \frac{\rho_r \max - \rho_r \min}{\overline{\rho}} \qquad (32),$$

where ρ_r *max* and *min* are the values of solid fraction at the centre and the ribbon edges respectively, and $\overline{\rho}$ is the average of the solid fraction.

In Figure 63, the values of δ are represented for each compaction condition. The δ values for the not lubricated system are the largest. The gradient of density edge-to-centre becomes more or less important depending on to two factors: the roller speed, and at a much larger extent, the lubrication. The slightly lower δ-value for increased rotational speed is partially due to the reduction in the dwell time of the powder in the roller gap. This diminishes the amount of stress applied on the powder, especially at the centre (see 5.2.1.3). As a result, there is a smaller density gradient edge-to-centre. On the other hand, the δ-value is also reduced after using lubricant. Thus, the lubrication of the wall improves the transport of material at the gap edges, so that a larger amount of material is present and the densification level increases at that area. Finally, as pointed out in Figure 61.B and C, powder lubrication reduced both, the δ value and the overall density. The former is due to the reduction of the interaction between the powder and the side plates (as it happened with the lubricated side walls), as for the latter, the lower external friction of the lubricated powder with the roller surfaces, reduces the conveyance of material into the roller gap, hence decreasing the densification level achieved by the system.

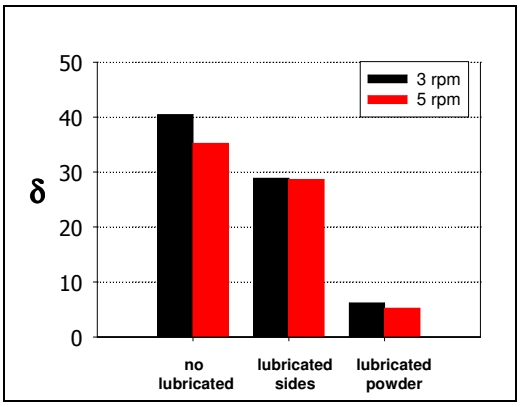

Figure 63. δ - value for the density distribution within the ribbon sample at different compaction conditions

The values of δ against the drag angles measured for each one of the runs are shown in Figure 64. There is an obvious relationship between both variables. An increase in the drag angle seems to be a sign of homogeneous distribution of the material across the ribbon width, which seems to be reflected by a uniform densification of the material in ribbons with a lower δ-*values*. On the contrary, narrower drag angles are linked to irregular distribution of the material at the compaction zone and result in ribbons with larger δ.

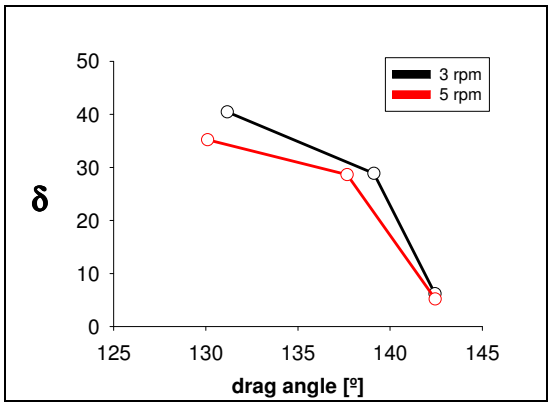

Figure 64. δ - value as a function of the drag angle value

5.2.2.2.4 Conclusions

The irregular feeding of material into the roller gap is reflected in the end ribbon densification. The shear forces generated through friction interactions between material and roller surface induce the transport of powder between the rollers. The interaction with the side walls counters the motion of powder and reduces the entrance of material at that region. Thus, in devices with fixed rollers and with cheek side plates sealing the compaction zone, material densification is enhanced if the interaction with the side walls is reduced, and the interaction with the roller surfaces is increased. Accordingly, the use of rims for the sealing of the compaction zone is strongly recommended, since this system allows the production of more homogeneous ribbons.

The *drag angle* proposed here is a pattern drawn by the powder on the roller surface resulting from the interactions aforementioned. These originate an irregular transport of the material over the roller surface and produce alterations of the densification throughout. Narrower angles are originated when the interaction with the side walls increases. A direct correlation of the density distribution across the ribbon width and the drag angle value measured has been established. As the drag angle decreases, the powder in the central roller region is gripped in the compaction zone at a much higher rate. Consequently, more powder is compressed at the middle than at the edges of the roller resulting in ribbons with larger edge to centre gradient of solid fraction.

5.2.3 The effects of the roller compaction conditions on the compact characteristics

The roller compaction of powder materials is a process in which a large number of variables play a decisive role in the resulting product properties. In the introduction (see 2.2.2) we have already listed and discussed those parameters that investigators have found to have a strong influence on the compaction process. Among them, there are not only processing variables, but also inherent material properties and ambient conditions. Also in previous experimental sections (5.2.2.1and 5.2.2.2) we have seen that one source of variability is the powder conveyance into the compaction zone and that this is established by process factors. Logically, these parameters define a complex system of variables and interactions involved in the compaction process. In Figure 65 there is a list of the main device parameters affecting the compaction process in a Gerteis MiniPactor. For compactors in which the material is transported to the compaction zone actively, the variables are split into those due to material feeding, and those introduced by the compaction itself as it is depicted in the figure.

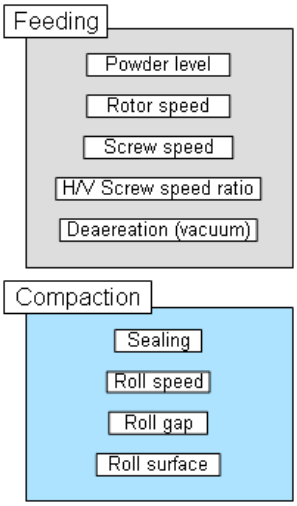

Figure 65. Main device parameters involved in the compact properties

5.2.3.1 Introduction

In this section we study the changes experienced by the material during the roller compaction, and subsequently the variation of the ribbon properties, originated by the modification of the process parameters (roller speed and roller gap), changes in the frictional interaction between compacted powder and device (lubrication), and after the controlled addition of moisture to the powder.

1- Roller gap: The opening between the rollers has a direct effect on the amount of material that is being gripped by the rollers. However, the significance of this variable is slightly different in a device with movable or with fixed rollers. While for the former the gap varies as a function of the material conveyed in order to maintain the value of specific compaction force invariable, for the latter, the steady roller gap will determine, firstly, the level of densification achieved by the material, and secondly, the homogeneity of the stress distributions across the roller width due to the interaction of the powder with the roller surface and the sealing plates.

2- Roller speed: The roller rotation speed determines the "dwell time" (see 5.2.1.3) of the material in the compaction zone [86, 191] which influence the number and the strength of the bonding points between particles. Furthermore, it has a significant impact on the amount of air escaping from the powder bulk [227] and the number of interactions between particles and between particles and compactor [267]. As a result, increasing the compaction speed produces a fluidization-effect of the compacted powder, magnifies the number of particles interacting with the compactor walls and reduces the time available for deforming and establishing bonds.

3- Lubrication: Lubricants are materials of extremely low frictional coefficients. Within the formulation, the lubrication ensures a steady flow of material and avoids sticking on the roller surface [125]. However, it introduces changes in the internal and external friction, modifying the material flowability and the extent of the interaction with the roller surfaces and the side walls.

4- Moisture: There is a large number of studies about the effects of humidity on the material workability [58, 111, 119, 239, 269] and the end tablet properties [57, 59, 270] after a given time of storage and under certain ambient conditions. Nevertheless, Inghelbrecht and Remon [110] first reported that the addition of water to the compacted powder in a controlled manner reduced the amount of dust produced and improved the ribbon properties, the granule particle distribution and hence, the quality of the tablets. They took the idea from [271, 272]. In these works, the authors presented a novel dry granulation process using high shear mixer agglomeration during which the granule moisture was absorbed by externally added components instead of performing a drying step after the granulation. Thus, the controlled addition of water enhances the material compactability reducing capping and improving the material compressibility [269, 273]. In case of roller-compaction, this would result in granules with better tabletability.

The effects observed after changing the compaction conditions have been studied in the following section by processing the material in the gravity fed roller compactor. There is a much lower number of variables involved in this device, as it has been already reported in 4.6.2. For instance, we can neglect all powder feeding variables and reduce the number of factors to the compaction unit parameters: roll speed, roll gap, roll surface and sealing conformation. Two monitoring variables, the nip angle, and the maximum pressure applied on the powder, are used for the characterisation of the compacting process. Moreover, the solid fraction of the produced ribbons has been characterized in order to analyze the variations in the compaction of material introduced with changing process conditions, as it has demonstrated to be a critical process attribute that delivers information on the degree and the quality of the powder densification during the process (5.1).

5.2.3.2 Materials and methods

Avicel PH102 was roller compacted as commercialized in all experimental blocks which dealt with the effects of the conditions related to the device parameters. However, in order to study the effect of the lubricant addition to the powder, the same MCC grade was blended with 0.5% MgSt using the rotary blender for 2 min at 18 rpm prior to the roller compaction. Finally, for the study of the controlled addition of moisture, water was added gradually to the same MCC grade in the rotary blender. The corresponding amount of water (see Table 17) in a total mass of 500 g was sprayed at a low rate (1-5 ml/min) whilst the mixer was rotating. The rotation speed was set at 6 rpm for “low” water-addition mixtures (2.5%-7.5%) and 18 rpm for high water content mixtures (10-15%).

Table 17. Amount of MCC and water used for the production of blends with controlled water content

	MCC [g]	Sprayed water [g]
0%	500	0
2.50%	487.5	12.5
5%	475	25
10%	450	50
15%	425	75

Once the totality of water was added, the blending was prolonged for 20 min at 60 rpm. To ascertain that the controlled water addition was successful and to verify that the water distribution in the bulk was homogeneous, the final water content was monitored in triplicate by determining the loss of water with the moisture analysis balance.

The roller compactor No.2 was used for all experiments presented here. The same amount of powder was used for all runs (i.e. the hopper capacity). The ribbon samples were collected for further analysis. However, the parameter settings were different for each block as listed next:

i) Roller speed. MCC was roller compacted at 1-6 rpm. The roller gap was kept at 1 mm.
ii) Roller gap. The distance between rollers was set at 0.9, 1 and 1.5 mm. In this block, the roller speed was 6 rpm.
iii) Lubrication. As in 5.2.2.2, we studied separately the effects of lubricating the roller press and the powder. Thus, for the former, a suspension of 5% (w/w) MgSt in ethanol was brushed on the side cheek plates, whereas for the latter, the lubricated powder was dispensed as usually in the inlet hopper. The compaction was performed at a rotation speed of 3 and 5 rpm and with 1 mm opening between rollers.
iv) Moisture. The moisturized MCC blends were all compacted at 6 rpm and 1 mm gap.

The ribbons produced were sampled for the determination of their characteristics. For 1, 3 and 4, the pressure versus the angular position values during the roller compaction were registered with the LabView control-panel interface and were automatically stored in the computer. Using MATLAB command algorithms, the values of nip angle and maximum pressure were calculated. The drag angle was also imaged and measured as in 5.2.2.2.

The relative density (solid fraction) of the sampled ribbons was determined next. Three methods described in section 5.1 were applied for this purpose: the sectioning method, the micro-indentation method and the X-ray micro computer tomography (X-ray μCT). The density of ribbons for all batches was measured with all three methods except for ribbons made of lubricated and moist powder, for which only the sectioning was used. The methods considered have been already described in sections 5.1.2.3, 5.1.2.6, and 5.1.2.7, respectively.

For the performance of compactability studies of moisturized MCC, the blends with different water content were compacted *in-die* using the material testing machine No.2 (see 4.7.1). For each compaction 600 mg of material was placed into an assembly with a die of 13 mm in diameter. After the “upper punch” was fitted into the die, the total height of the assembly was noted in order to know the initial point of displacement. The testing machine was programmed to exert a maximum force of 9 kN and the punch displacement speed was set at 1.5 mm/min. The “upper punch” was attached to a 30 kN (± 0.1) force transducer that was fixed to the movable upper stage of the machine. During the compaction, the punch displacement and the stress force exerted on the powder were registered and stored in data files. This information was then processed for the representation of *in die* Heckel plots (see 2.1.5).

The apparent density of the produced tablets (n=3) from each blend of moisturized MCC was determined geometrically (i.e. considering the weight and the tablet dimensions). Also the tablet strength was measured. The testing machine No.1 was used for this purpose. The tablet was placed on its side onto a metal stage. The force transducer at the upper movable stage was changed for one of 1 kN (± 0.01). The run for the axial crushing was programmed with a punch displacement of 3 mm (enough to ensure the tablet crushing). The maximum force value applied on the tablet was noted and the strength was calculated using Equation (1).

5.2.3.3 Results and discussion

5.2.3.3.1 Roller speed

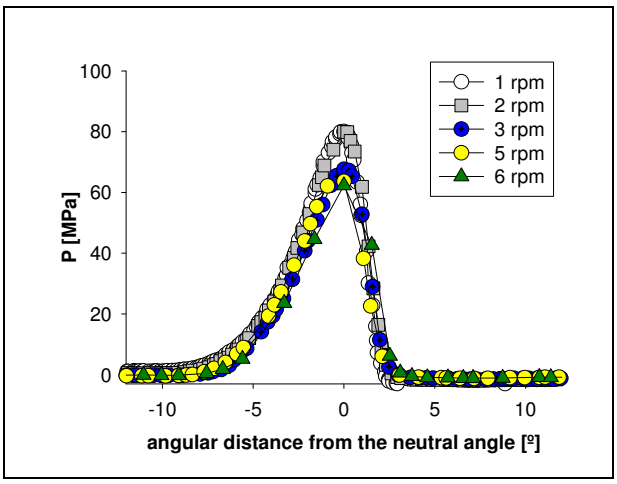

Figure 66. MCC compaction profiles at different rotation speed

The strain-angular position profiles at the compaction zone for five roller speeds are shown in Figure 66. As shown, the faster the roller rotation, the smaller is the area under the compaction curve and the lower is the value of maximum pressure exerted on the material. The peaks reached lower values of pressure and this was applied on the material during shorter ranges. These results were also reported by other authors [188, 193, 215, 274] who observed the same effects on the compaction profile when the rotation speed was modified. The increase in the roller rotation speed induces, as a first effect, a weaker adhesion of the particles to the roller surface. This is partially due to the mobilization of particles at the contact surface, reducing the interactions with the roller surface [103]. A fall of this friction interaction restricts firstly, the capacity of the rollers to convey loose material into the compaction zone, and secondly, reduces the amount of partially denser material that is being gripped between the rollers [74]. Nevertheless, there is a second effect on the powder behaviour induced by the roller speed that may cause a reduction of the material compaction. According to findings of other studies [96, 275, 276], faster rotation increases the particle mobility which induces the fluidization of the material. The air entrapped in the bulk tends to escape from the powder mass. Faster rotation intensifies the air mobilization, which again reduces the conveyance of powder into the compaction zone. Thus, the transport of powder induced by the rollers diminishes as an effect of the roller rotation speed. This is due to: 1) the opposite movement vectors of the escaping air and the powder displacement, and 2) the reduction in the adhesion of the powder to the roller surface.

The air permeation and the lower particle-roller surface interaction reduce the feeding of powder into the compaction area [277] but it has a second effect: the material compaction starts after wider angular positions. In other words, as the powder-roller interaction decreases, the minimal frictional stress necessary to grip the material between the rollers (see 2.2.1.2) is reached later. Consequently, the nip

angle values decrease as the roller rotation speed increases, as shown in Figure 69.B (page 96). Thus, the sum of a smaller amount of powder being gripped between the rollers due to the lack of feeding, and the reduced duration of the strain exerted on the material at higher roller speed reduce the values of stress applied by the rollers on the material [208].

The mobility of the powder at the compaction zone is originated by the roller rotation. However, not only the interaction of powder and roller surface, but also the powder movement at the edges of the compaction gap and the corresponding generated interactions with the hopper walls and the cheek side plates are altered by the rotation speed. In section 5.2.2.2 the concept of *drag angle* has been introduced as an indicator of this interaction. It has been proved that its value is, furthermore, closely related to the homogeneity in the stress distribution across the compaction width. In Figure 67 the values of the drag angle for the compaction of powder at different rotation speeds are represented. The angle formed by the powder on the roller surface becomes narrower at higher rotation speeds. This is attributed to the increment in the particle interaction with the walls that intensifies the gradient of particle mobility between the regions close to the side cheek plates and the central part of the rollers.

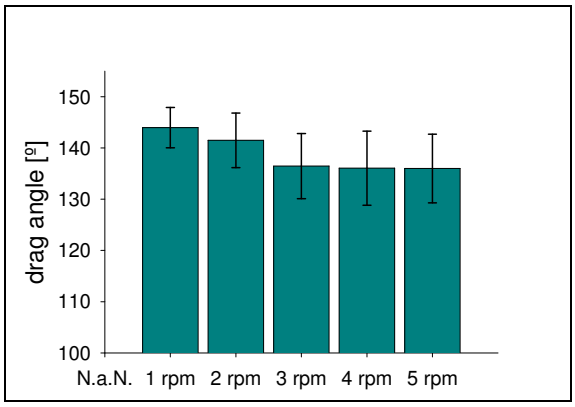

Figure 67. Drag angle values measured at different rotation speeds

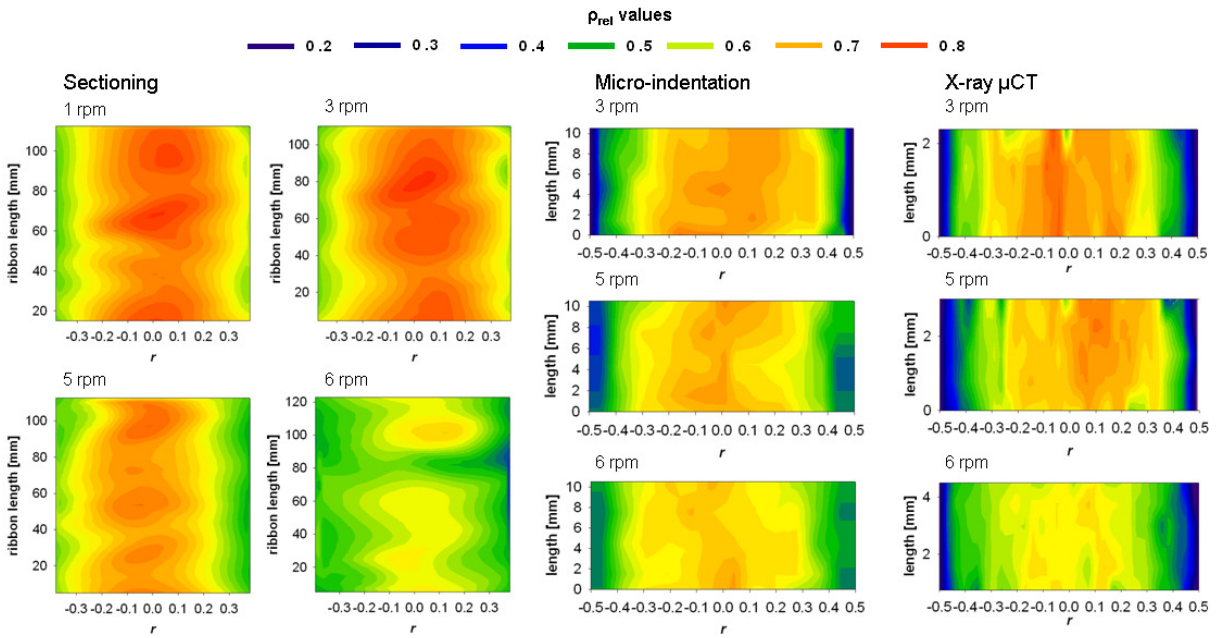

Figure 68. Colour maps of the solid fraction measured on ribbon samples produced at different roller rotation speeds by means of three different methods of density determination

As it has been discussed in section 5.1.1, the solid fraction of the ribbon provides information about the progress of material densification taking place during the roller compaction and, therefore, can be used as evidence of the main effects induced by the factors studied here. All methods used in aid of performing the density measurement demonstrated to deliver the same basic information, although, as

described in section 5.1.3, they possess different spatial resolution. The same was observed for the maps of relative density (contour plots) drawn for the ribbon samples for the three methods. Correspondingly, the solid fraction maps for the different samples produced at different roller speed represented in Figure 68 show basically the same trend: the compacts become looser at larger rotational speeds. The same findings were reported in a considerable number of works [86, 103, 109, 192, 193, 208, 209, 215, 240, 274]. Some of them claim that roller speed has a very important effect on the dwell time influencing the type and the number of bonds between particles [86, 109]. According to that, faster rotation, i.e., shorter dwell times, would reduce the deformation of particles and would generate looser and more brittle compacts. However it is considered that when the roller speed increases, reductions in the friction between powder and roller press, the induction of powder fluidization, and the consequent lessening amount of stress exerted on the material, are the cause for lower densification levels [103, 192, 193, 209, 215, 274]. In other words: faster rotation reduced both, the pressure level exerted on the powder, and the dwell time during which the powder is compacted.

5.2.3.3.2 Roller gap

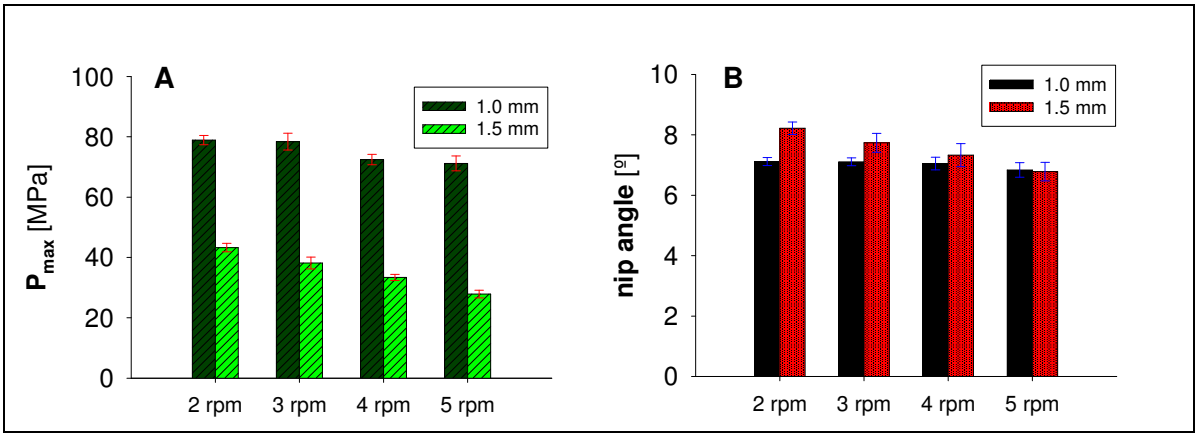

Figure 69. Comparison of the mean A) P_{max} and B) nip angle values for roller compaction runs at two different compaction gaps and different rotation speeds.

The roller gap defines the thickness of the compacted ribbon. The opening distance between rollers, however, determines also the thickness of the powder column that is being gripped in the compaction area. Changes in the interaction between material particles and the roller surface, and modifications of the material behaviour at different dynamic conditions become hence the main influencing variables affected by the roller gap. In Figure 69.A and B, we compare the fluctuation in the maximum pressure and the nip angle values for two roller gaps and four roller speeds. The same trend is observed for the two roller gaps independently of the rotation speed settings. Thus, as shown in Figure 69.A, the values of P_{max} for larger gaps are significantly smaller than for 1 mm. Similar findings were reported in [74, 99, 100, 193, 209, 215, 258, 274, 278]. All authors observed that the value of pressure reached during the compaction decreased for wider gap openings. As the column of compacted powder over the roller gap becomes thicker, the number of particles at any cross section of the gap increases. This raises the requirement of stress exerted by the rollers on the material to reach the same densification level as with a smaller gap. In turn, there is much more energy that undergoes dissipation, since a large part of it is lost in particle-particle friction, elastic recovery and thermal diffusion. In devices such as the

MiniPactor, the feeding parameters are auto-regulated (e.g. increasing the tamp auger speed) so as to counteract the decrease of densification due to the variation of the roller gap. This does not occur in the gravity fed compactor used here, in which the change in the roller gap is immediately reflected in the ribbon properties.

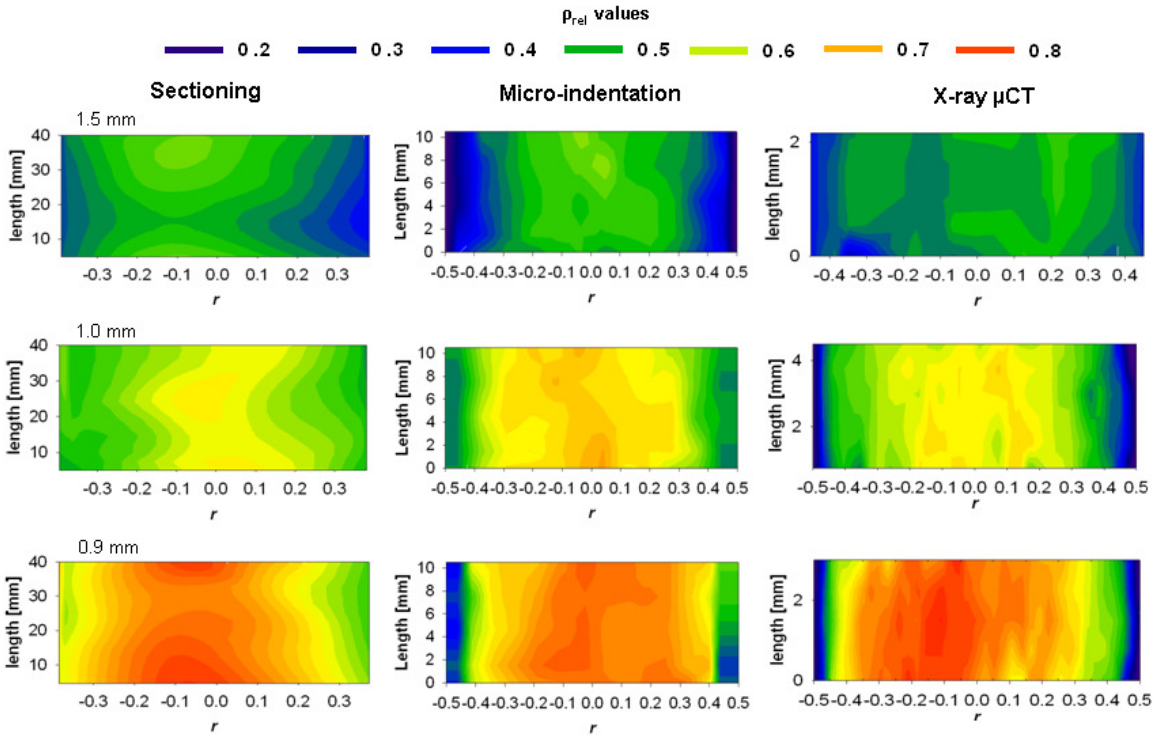

Figure 70. Colour maps of ribbon solid fraction measured on samples produced at 0.9, 1.0 and 1.5 mm roller gap by means of three different techniques of density determination

The enlargement of the compaction gap makes the nip angle wider (also observed by Bindhumadhavan, et al. [100] and Perera [215]). If the space between the rollers grows, the column above the rollers widens and the entrance of material at the nip region begins at earlier rotational stages than in narrower gaps [279, 280]. Considering that the nip angle depends basically on the relationship of particle-particle and particle-roller surface friction coefficients [281], the effective friction needed to force the material between the rollers for a larger number of particles at the material-roller interface is reached at larger angular positions (wider nip angles).

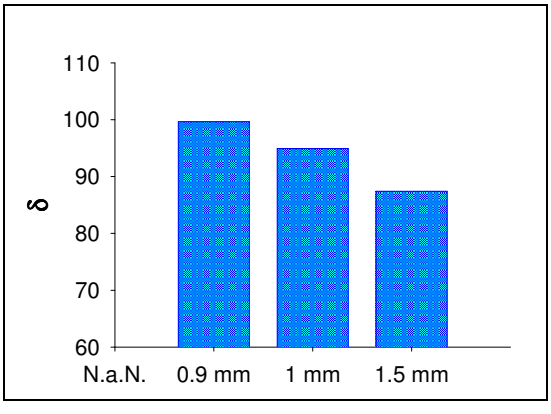

Figure 71. δ values for the span of density for ribbons of different thickness

However, though at first glance one could think that the widening of the nip angle, which involves an extension of the dwell time of the material at the compaction area, would lead to denser ribbons, the negative effect of the roller distance on the densification level of the material is dominant. In Figure 70, the solid fraction maps of ribbon samples produced at three roller gaps are represented. The level of densification suffers a sharp reduction when the gap between rollers increases. This is mainly due to the lower normal stress exerted on the material [280]. Moreover, it has also been observed that the low pressure levels reached during the compaction

reduce the gradient of densification across the ribbon width. In Figure 71 the δ values of density distribution homogeneity (5.2.2.2.3) for the same samples of Figure 70 become smaller for wider roller gaps. It shows that the span of densification levels is reduced in ribbons produced at larger roller gaps.

5.2.3.3.3 Lubrication

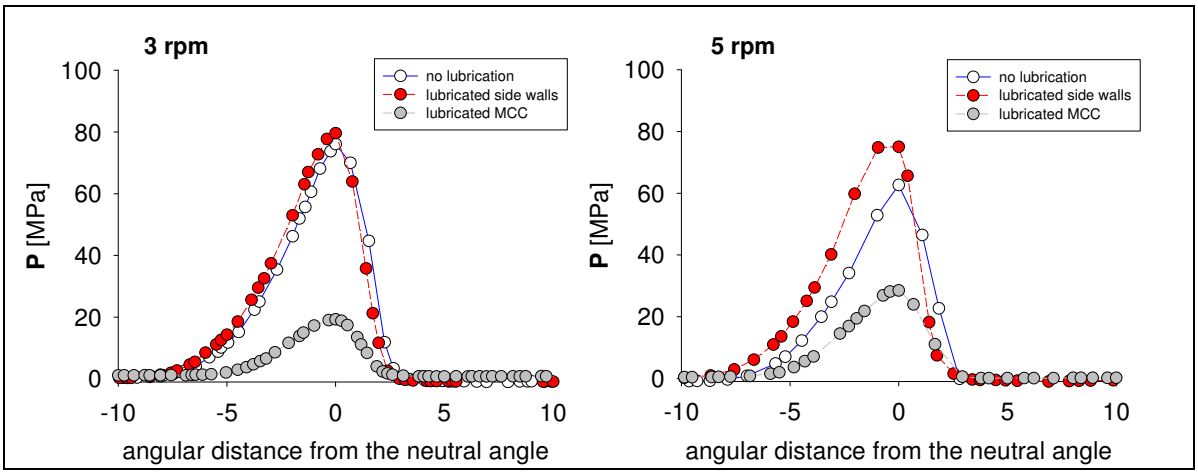

Figure 72. Changes in the compaction profiles introduced by the use of lubrication at two roller speeds

The lubricant reduces drastically the friction coefficients at the interfaces where it is available. The effects of the lubrication have been described in 5.2.2. As shown in Figure 72, the compaction profiles change as a function of the situation of the lubricant. Thus, either on the cheek side plates or within the compaction material, the lubrication affects the compaction process differently. The lubrication of the cheek plates increased (slightly at 3 rpm and markedly at 5 rpm) the pressure achieved by the rollers. As the interaction with the side walls decreases, the quantity of material being dragged into the compaction gap rises, causing the growth of the shear stress needed to pull the material through the rollers [267],. This is in turn more evident at faster rotations since the reduction of the interaction of the particles with the cheek side plate result in a stronger improvement in the material transport. The lubrication of the powder, however, reduces the overall normal stress exerted on the material. The lubricated powder presents low frictional coefficients, both internal and external [266]. Accordingly, the adhesion of the powder to the roller surface is weaker [282] and the active forces involved in drawing the powder into the roller gap are reduced (i.e., slipping of material occurs) [74, 283]. As a consequence, less material is dragged into the compaction gap, which reduces the pressure exerted on the powder by the rollers.

The average of pressure values achieved for the whole compaction processes are represented in Figure 73. The same trends as observed in Figure 72 for the compaction profiles are found here. The lubrication of the cheek plates increases the value of pressure exerted on the material whereas the lubrication of the powder reduces it drastically. This is in agreement with other observations reported [282]. The variations in the nip angle values represented in the figure can be explained with similar arguments as for the roller gap. The wider nip angle in case of the lubricated sealing is due to a growing number of contacts between material and roller surface as more material is being fed between

the rollers. The lubrication of the compacted material, on the contrary, lowers the value of nip angle because the efficient frictions at the powder-roller interface required to overcome the material slipping and force the powder to pass between the rollers, are reached closer to the neutral angle [107, 281]. The lubrication of the compacted material introduces, therefore, two negative effects on the material compaction: the reduction of the pressure level achieved by the system and the shortening of the dwell time of material in the compaction zone.

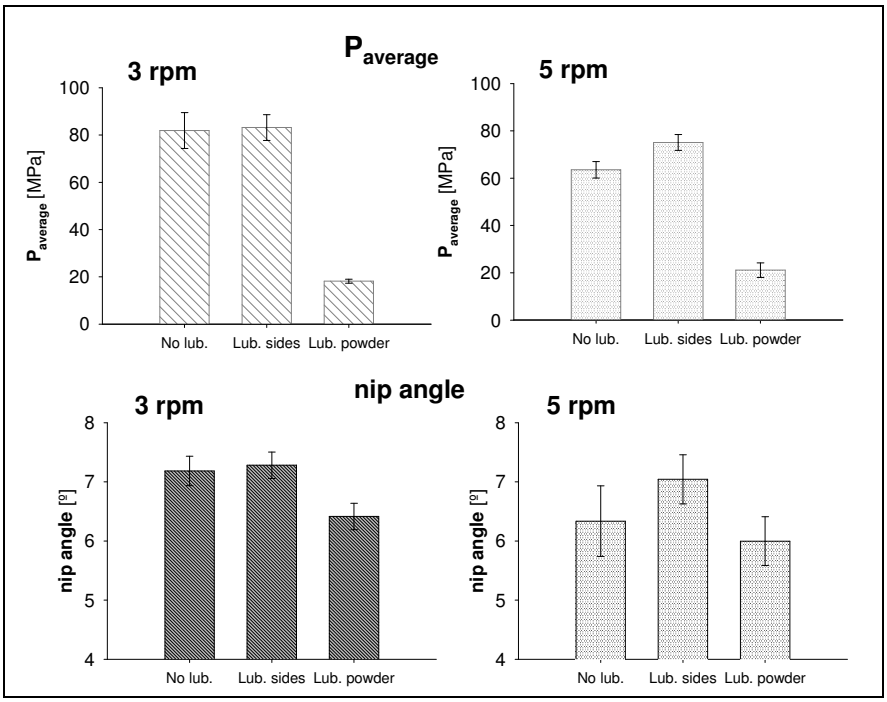

Figure 73. Average of maximum pressure values and nip angles for the roller compactions at 3 and 5 rpm

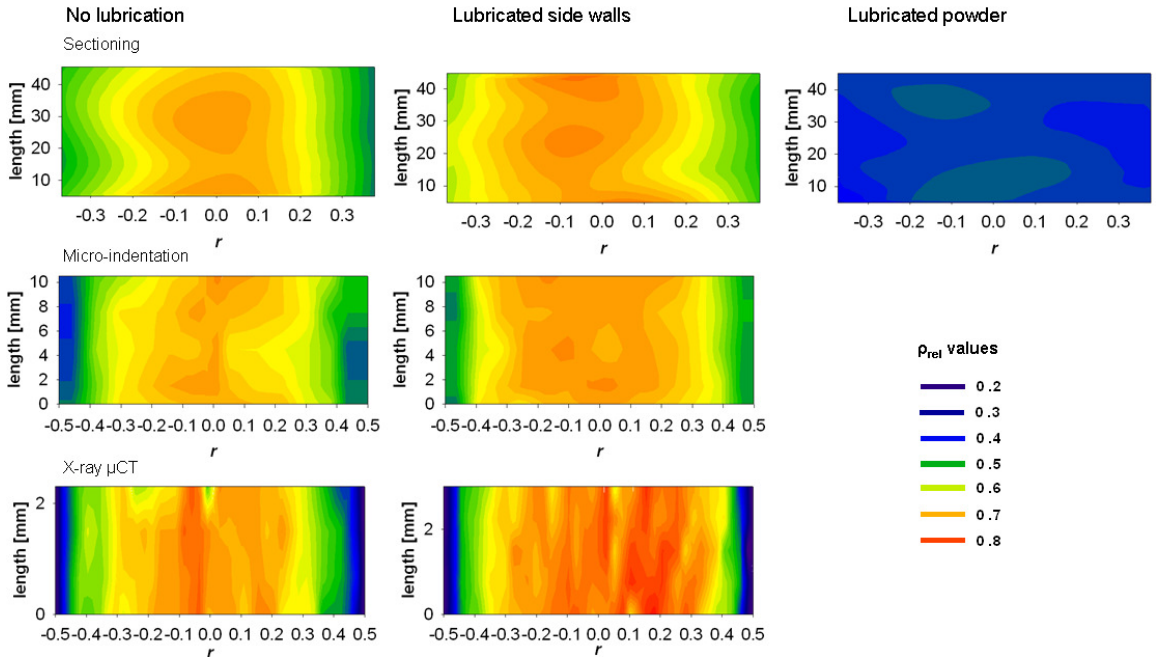

Figure 74. Colour maps of ribbon solid fraction measured on samples produced at different levels of lubrication by means of three different techniques of density determination

Similarly as for the rotation speed and the roller gap, in Figure 74 one can compare the contour plots of density maps from ribbons produced with different kind of lubrication with those from ribbons produced without lubrication. Again, we assume that the pressure exerted by the system is directly related to the densification degree reached by the material. As expected considering the results of the monitoring variables and according to other studies [215], the lubrication of the sealing plates leads to

denser compacts than those produced with unlubricated walls, whereas the addition of lubricant to the powder resulted in compacts where the densification was notably lower.

The lubrication of side plates and powder also changed the interaction of the material with the hopper walls and sealing plates. In section 5.2.2.2 we have already described and discussed how the lubrication affects the *drag angle* and heterogeneity of the distribution of density across the ribbon width. The lubrication increases the value of the drag angle, meaning that the gradient of the material conveyance edge-to-centre is reduced, leading to more uniform ribbons.

5.2.3.3.4 Moisture content

The mean values of moisture contents determined for the blends and its correlation to the amount of water added are represented in Figure 75. The linear correlation between values (r^2 = 0.994), and the small deviation between measurements indicate that the addition of water has been successful and the moisture is homogeneously distributed throughout the blend.

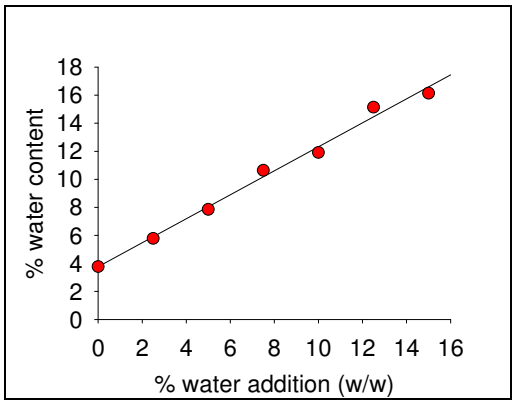

Figure 75. Moisture content of the blend after adding different amounts of water

To understand the changes of the material densification behaviour of the powder in roller compaction due to the content of water, we analyzed first the response of the material in uniaxial compaction. Figure 76 compares the *in-die* Heckel plots for moist MCC with different water content calculated from the strain-stress diagrams recorded during the material compaction. Analyzing the represented profiles, it can be seen that the growing moisture content allowed the material to reach higher densification values at lower stress levels. According to the literature [76, 269], water enhances the material compressibility and compactability by two mechanisms. First, water reduces the friction due to its lubricating effect, reducing the interaction between particles. Secondly, the presence of water disrupts the hydrogen bonds of the cellulose hydroxyl groups of surrounding molecules, increasing the plasticity of cellulose [284, 285]. Thus, both effects reduce the energy needed to rearrange and approach particles at the same time that increase the ductility, the particle interlocking, and thus, the inter-particle bonding, generating denser and stronger tablets for a same amount of stress exerted on the powder.

The results presented in Figure 76 are entirely consistent with the conclusions of [286] and [287] for different MCC grades. The authors observed that MCC became more deformable under the same pressure when the moisture content was larger and, consequently, MCC reached higher densification with lower strain level (i.e., the yield pressure diminishes). The enhancement of the particle plastic deformation by water increases the packing of the powder and reduces the size of the voids between particles. Hence, the compacts become denser. However, after a certain content of water, the material starts to present stronger elastic character [284]. The slope of the Heckel plots represented in Figure 77 increased with the water content. This is attributed to the enhancement of the plasticity deformation of

the moist MCC. However, after large water additions (say over 10%), the densification profile exhibits an exponential character. Heckel plots resulting from *in die* compactions with exponential profiles were described when compacting elastic materials elsewhere [288]. The initiation of this elastic deformation behaviour, in turn, appears at different compaction pressures depending on the water content. This is represented in Figure 77. As it can be seen, the Heckel plots of the material densification between 0 and 100 MPa for MCC with a 10% and a 15% of added water present exponential profile. However, it appeared at lower pressure values when compacting MCC with 15% water addition. Hence, the larger the amount of water added, the stronger is the elasticity of the blend.

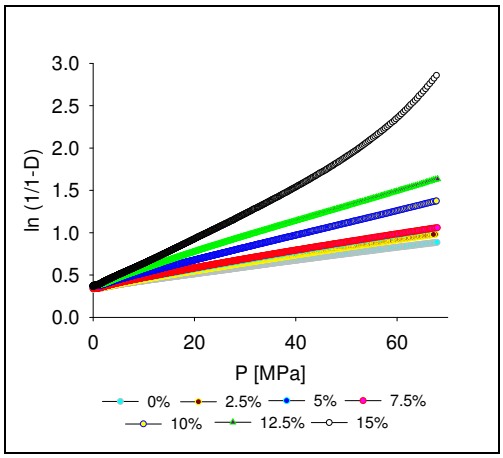

Figure 76. Heckel plots of MCC blends with different amounts of moisture. The values listed in the figure correspond to the % (w/w) of water added

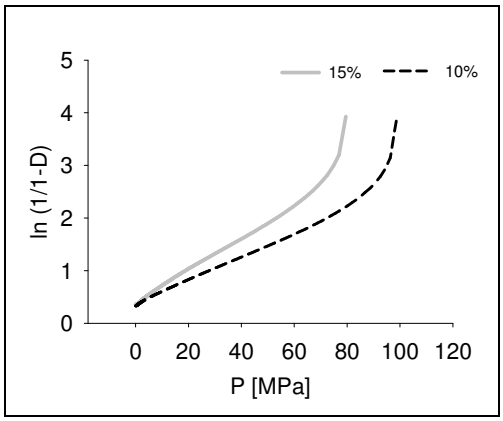

Figure 77. Comparison of Heckel plots of MCC blended with 10% and 15% of water

The apparent density of tablets manufactured from MCC with different quantities of added water at a pressure of 70 MPa and the corresponding tensile strengths are presented in Figure 78.A and B. Both histograms follow a similar trend. The densification of the material and the strength of the tablets seem to increase with larger addition of water. However, after 10%, the value of both variables decreases. As stated before, water addition allows particles to yield more easily resulting in compacts with denser structure. As a result, closer inter-particle contacts enhance the number of bonds, which causes the formation of stronger compacts. An excess of water, on the other hand, augments the elastic character of the material, producing less compacted structures due to elastic recovery. Moreover, part of the contained moisture condenses around the particles, reducing the inter-particle bonding [273]. As a sum of all effects, the resulting tablets of blends with high water contents are less dense and more brittle.

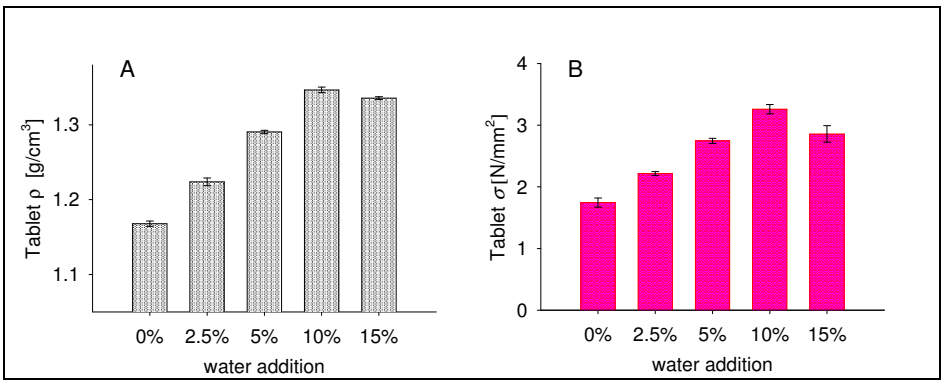

Figure 78. Densification and tensile strength values of tablets produced from different blends of moisturized MCC

The characterization of the compaction of moisturized MCC is used next in order to interpret the results obtained during the roller compaction of the same moisturized MCC blends. The compaction profiles for all blends are represented in Figure 79. The tips of the peaks are represented separately in order to depict better the pressure values reached by each blend. The general tendency observed is that the stress exerted by the rollers on the material is higher at increasing powder moisture content. As for the base of the peak, it becomes narrower.

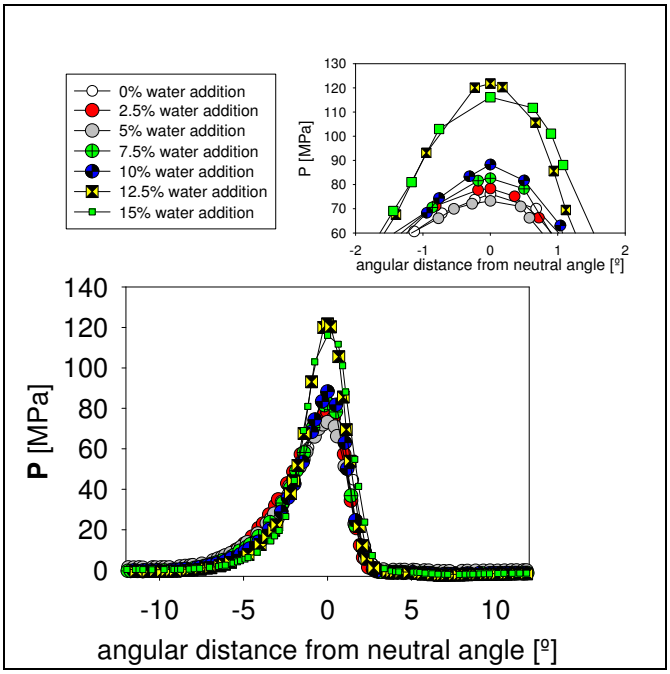

Figure 79. Roller compaction profiles of moisturized MCC blends. The diagram on the upper corner of the figure corresponds to the top part of the peaks

The average pressure values reached and the compaction nip angle measured during each run are presented in Figure 80.A and B, respectively. The P_{max} value decreases gradually up to 5% water addition. After that, the value starts to increase again gradually. However, at 12.5% water addition the pressure grows abruptly and drops again at a 15%. As for the nip angle values, they decrease continuously as more water is added to the MCC.

As we have seen for other compaction conditions, the pressure level and the value of the nip angle are closely related to the quantity of powder drawn between the rollers. This is, in turn, strongly influenced by the flow properties of the material and the interface interactions as a function of the particle-particle cohesion and the friction coefficient at the material-roller interface. The water adsorbed around the particle reduces the external friction coefficient and increases the slippage of the material over the surfaces [273]. As a consequence, in a similar way as for the addition of lubricants, the angular position at which there is a sufficient shear stress to pull the powder into the roller gap is reached at later stages (i.e. the nip angle becomes narrower). Furthermore, the rollers are not able to drag the material efficiently and as a consequence, a smaller amount of material is transported into the roller gap and the value of pressure exerted on the powder by the rollers decreases. However, as more water is added (over a 10%), the amount of

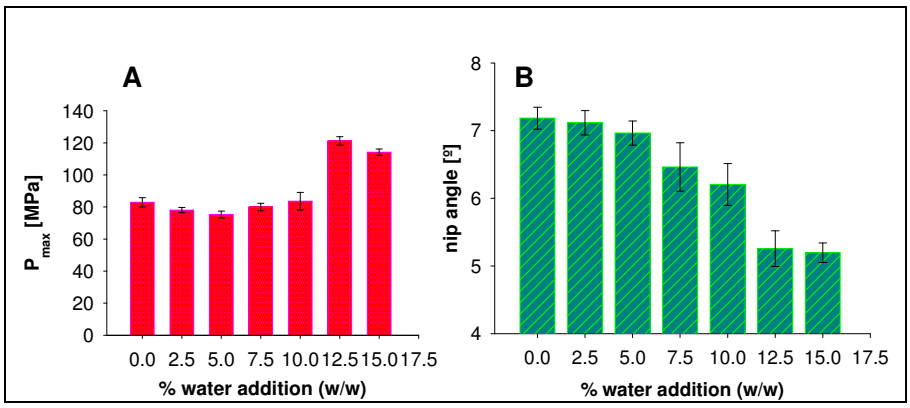

Figure 80. Maximum pressure and nip angle values calculated from the compaction profiles of moisturized MCC

material conveyed into the roller gap increases again. Moisture strengthens the particle-particle cohesion [285]. The particles become adherent, tend to aggregate and, if the moisture continues growing, even to form cakes [269]. Although the bulk volume being gripped by the rollers might be reduced, the moistened material, which bulk density is large, moves forward as a block partially pulled by the rollers and by the contact with the material of lower levels dragged into the roller gap. Consequently, a larger amount of material is compacted and the pressure value registered grows.

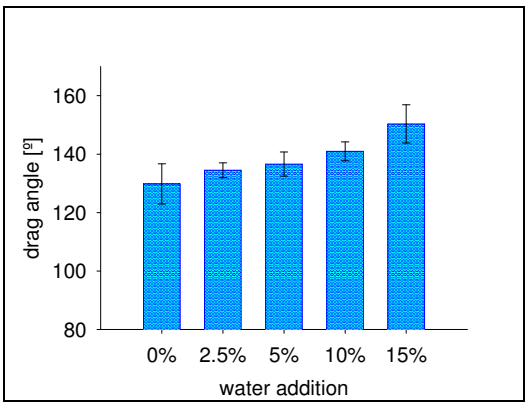

Figure 81. Drag angle values of moisturized MCC

The *drag angle* values of Figure 81 evidenced the lubricating effect of water. Its addition reduces the friction of the material with the hopper walls and the cheek side plates. The gradient of powder movement between the edges and the central region of the roller width becomes smaller. This increases the amount of powder that is gripped towards the roller edges and induces the formation of ribbons with uniform density distributions.

The densification maps measured for the ribbon samples of the moisturized MCC are represented in Figure 82. Here, the apparent density, and not the relative density is given as a value of densification. Similarly as we have seen previously for the uniaxial compacts, the addition of moisture enhances the material compaction. The density values measured become larger after increasing moisture contents. Moreover, the dense regions at the central part of the ribbons become wider, which is coherent with the drag angle values observed in Figure 82 and demonstrates that ribbons of moisturized MCC

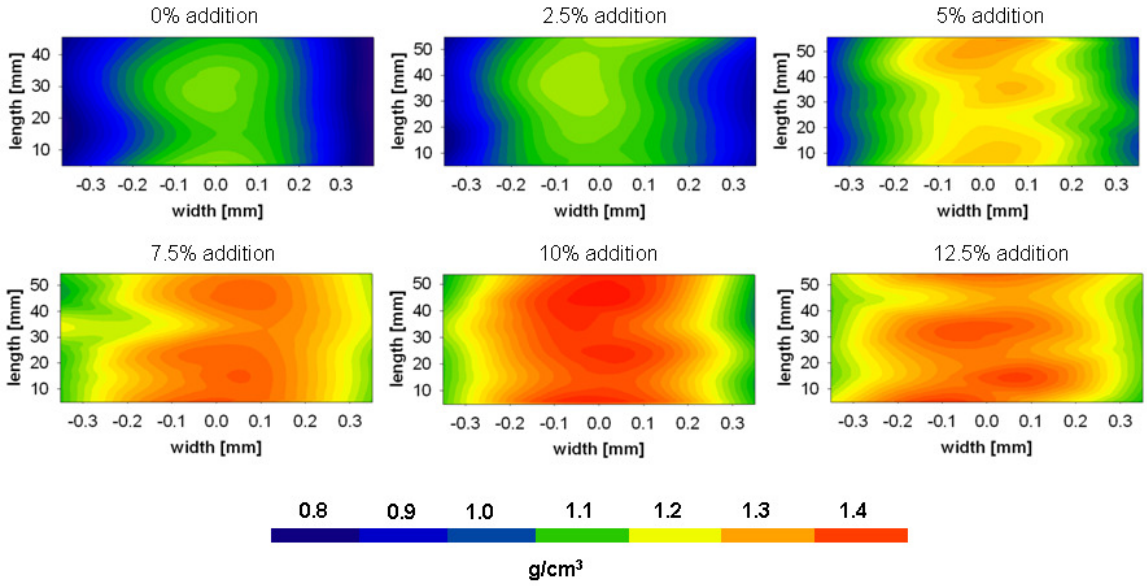

Figure 82. Colour maps of ribbon solid fraction measured on samples produced out of moisturized MCC blends using the sectioning method

present more uniform density distributions. Although the pressure values measured for blends of 0-5% water addition at the roller compaction decrease slightly, the ribbons reach higher densification levels. Again, this is due to the enhancement of the plastic deformation induced by water. However, the

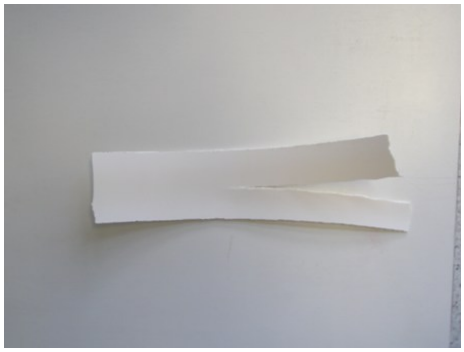

Figure 83. Ribbon split up in two halves obtained after roller-compacting a blend of MCC with 12.5% water addition.

improvement in the particle deformability reached its maximum at a 10% water addition. The blend with 12.5% of added water did not form regular ribbons. The effect of a large addition of water to MCC on the ribbons is in Figure 83. The ribbons resulting from the compaction of blends with more than a 10% of water addition were collected split in two halves. This is believed to be due to an overcompaction of the material. The pressure registered for the blends with 12.5 and 15% water was above 100 MPa, which is over the "critical pressure" value after which the elastic recovery of the material appears. Thus, the elastic character of the material and the weaker material bonds at the central region (in which the maximum pressure is exerted) cause material failure and originate the breakage of the compact. The produced ribbon pictured in Figure 83 also presented a brown tone towards the central region, which is due to the extensive pressure exerted on the powder that also might alter the chemical nature of the substance (e.g., by partial hydrolysis of the cellulose). However, the chemical changes undergone by the material were not examined.

5.2.3.4 Conclusions

The material compaction results from the combination of shear stress and normal stress (pressure) exerted on the material at the compaction zone. These forces vary depending on the material feeding, the roller parameters and the friction between the material and the confining boundaries, i.e., roller surface and side sealing. On the other hand, the degree of densification is directly related to the amount of stress exerted and the inherent deformation character of the compacted material. The modification of compaction parameters and material properties, such as deformation behaviour and friction components, caused fluctuations on the progress of material densification and resulted in compacts with dissimilar properties.

Increasing roller speed results in a less effective contact of the powder with the roller surfaces and a higher interaction with the hopper and the sealing walls. Furthermore, it also augments the rate of air escaping from the bulk. As a result, less material is fed between the rollers and the values of pressure and nip angle decrease, inducing a lower level of material densification.

A wider roller gap increases the material volume between the rollers. Though the effective friction and the powder pre-densification start earlier and last longer, the stress exerted by the rollers is reduced and the ribbons are less dense and weaker.

Lubricants reduce the internal and the external friction of the material. Adding lubricant to the material lowers shear forces at material-roller interface and reduces the material densification.

Moisture acts as a plasticizer and as an external lubricant. The addition of water to MCC also increases the elasticity and the powder cohesion. Generally, increasing moisture content up to a certain amount enhances the material conveyance between the rollers (though it reduces the friction of powder),

reinforces the material deformability and result in denser, harder and more uniform ribbons. However, for some formulations the addition of moisture is not desirable. The moistening of the material requires a drying step, which is always avoided in order to simplify the production process. Moreover the addition of water reduces the shelf life of the dosage forms due to microbiological proliferation and might compromise the stability of the API. Accordingly, the moistening of the compacted blend is not the first option considered for the optimization of the process.

The material compaction and the compact attributes are dictated by changes in the process parameters, by the behaviour of the material at the boundary interfaces, and by modifications in the material deformability. Accordingly, any process optimization must go through the consideration of all parameters and all factors that may contribute to these changes.

5.3 Re-workability of roller-compacted substances

5.3.1 Introduction

During the material compaction, two principal stress components are applied on the material by the rollers: the shear stress and the normal stress (i.e. pressure). The former, which depends on the interaction between the material and the roller surface, sets the powder in motion and grips the material into the compaction region. On the other hand, the normal stress is mainly responsible of the material densification. The value of this stress component depends on a large number of factors and parameters that have been discussed in previous experimental sections (5.2.3). Moreover, we have also seen in section 5.2.1 that the cyclic compaction has many similarities with the uniaxial compaction (i.e. die compaction or tableting). Accordingly, both processes are presumed to result in compacts of similar properties if the compaction conditions (strain vectors, amount of material and dwell time) are similar. However, if the tableting parameters are kept constant, tablets produced from dry-granulated material will not show the same properties as tablets produced by the direct compression of the unprocessed material, since the obtained granule has different tableting properties to those of the starting substance.

In section 2.2.1.2 we have listed the alterations that the material experiences during the compaction process. We generally assume that the compaction stress induces the energy necessary to reduce the volume of a particulate system until a certain level of densification is achieved. This energy is generally used to overwhelm all interactions in the system and to produce particle deformation. We have also described the tendency of the material to form stable dense compacts, referred to as *tabletability*. The main mechanisms involved in the powder compaction and the dominant factors and variables have been discussed in sections 2.1.4 and 2.2.1. It is widely accepted that the capacity of a dry granulated material to be compressed is inferior to that of the virgin material. The extent to which the material still can be compressed after its dry granulation is defined as the *re-workability* of the granule, i.e., the ability to be compacted a second time. This is sometimes called *re-processability* or *re-compactability.*

The study of the re-workability for excipients has attracted the attention of pharmaceutical scientists during the last two decades. In particular, in the field of the dry granulation, the study on how the roller compaction, and the subsequent comminution into granules, affect the material compressibility and the attributes of produced tablets has been the main focus of many work published [24, 26, 34, 114, 129, 275, 289-295]. All observed that when compared with the original material, the dry granules showed different deformation behaviour. The general trend observed was that the material withstood particle deformation and the end compact strengths from dry granulated material was reduced (i.e. particle bonds became weaker). However, diverse hypothesis about which particular alterations on the material determine the particle deformability are stated. Thus, recently it has been debated whether particle size enlargement or the initial material properties cause in more extent the reduction of the material tabletability [296, 297].

To see the relevance of the study of the granule *re-workability*, we put forward five works that, made interesting contributions to the understanding of the changes in the tabletability of dry granulated materials.

(1) Malkowska and Khan [289] introduced the term "*work hardening*", which had been widely used in Engineering and Material Sciences since the 1950s [298]. They claimed that the *work hardening* increases the resistance of the pharmaceutical excipients to permanent deformation (i.e. reduces plastic deformation of the particle). Since plastic deformation is irreversible, it becomes more difficult to cause further material deformation due to a *hardening* of particles. The *work hardening* theory gained acceptance among pharmaceutical scientists [22, 29, 107, 121, 292, 299].

(2) Bultmann [114] studied the changes suffered by the dry granulated MCC after undergoing multiple compaction runs. He described the variations in the compaction process and the effects on the obtained product attributes, i.e., he characterized the resulting ribbons, granules and tablets. He found that the material re-processability was reduced from run to run and consequently ribbons and tablets could be considered to present deteriorated quality after three re-compaction cycles. Moreover, he found out that, after each compaction-granulation cycle, the obtained granules were denser, had a reduced fraction of fine particles and showed improved processing features such as flowability. The hypotheses presented in this work were reaffirmed by others [25, 107, 121, 216].

(3) Sun and Himmelspach [294] argued that providing that the material deform mainly plastically, the particle enlargement of the resulting granule, rather than the *work hardening* endured by the material, is the main cause of the loss of tabletability observed for dry granulated MCC. They compacted and granulated MCC and set apart two granule size fractions. They re-compacted the material three times and from the second and the fourth compaction run, they separated the same size fractions as for the first granule. They found out that regardless of the process steps undergone by the material, the tensile strength of tablets produced from small size fractions was always larger than that of tablets produced with coarse particles.

(4) However, the hypothesis defended by Sun and Himmelspach was recently questioned by Herting and Kleinebudde [24]. In their work, they reported that the initial particle size of the compacted material plays a very significant role on the granule tabletability and demonstrated that *work hardening* has to be considered when elucidating changes in tabletability.

(5) Farber, et al. [295] studied the effect of the dry granulation (roller compaction-granulation) on the material re-workability. They introduced the theory of the *unified compaction process*. Straightforwardly explained by the authors, the resulting granules "remember the compaction step experienced during roller compaction". Thus the deformation behaviour and the strength level achievable by the granules are proportional to the total work exerted on the material, as illustrated in Figure 84. Given a tableting process after the granulation, the maximum tablet strength (σ') reached by the compact after the granule compression is inversely proportional to the amount of work previously

exerted on the material during roller compaction. Thus, the material densification coalesces into a single curve independently of the compaction processes involved.

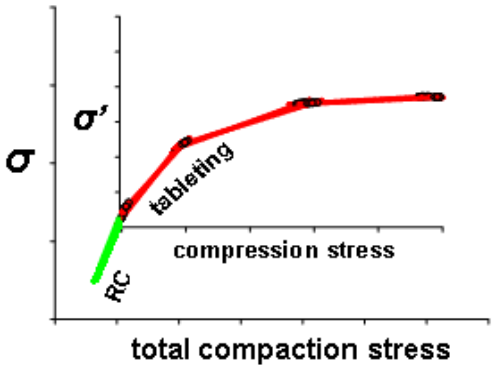

Figure 84. Unified compaction process theory. Adaption from [295]

It is clear that there has been an increasing interest in exploring the effect of dry granulation on tabletability because a complete understanding of these phenomena not only helps to improve the comprehension of the mechanisms of material deformation occurring during roller compaction, but also identifies the factors that need to be taken into account during the design of the formulation and the establishment of the steps and the parameters of the process. In this section we investigate the changes in tabletability of lactose monohydrate after being processed using roller compaction-granulation. We analyze the changes experienced by ribbon, granules and tablet attributes, after undergoing consecutive cycles of roller compaction-granulation, and describe what the evident modifications in the material processability are.

5.3.2 Materials and methods

Though crystalline α-lactose monohydrate (LMH) is not commonly used neither in DC nor in roller compaction, it was chosen as a model substance with brittle deformation. The design of the experiment was similar to the described in [294]. The LMH was lubricated with 0.5% MgSt in the planetary mixer for 2 min and was subsequently roller compacted using the MiniPactor. The compaction parameters are listed in Table 18. The lubricated LMH underwent four consecutive roller compaction-granulation cycles at each specific compaction force similar to the methods described in [114]. The roll gap had to be reset at the fourth compaction cycle from 3 mm to 2.7 mm so that compacted strips of enough strength could be produced. Ribbons and granules were collected during the first, the second, and the fourth compaction-granulation passes.

Table 18. Parameters used for the roller compaction - granulation of LMH

Specific compaction force	5 and 15 kN/cm
Rotation speed	2 rpm
Roller gap	3 mm (sporadically 2.7 mm)
Roller conformation	Knurled (slave) and smooth (master) rollers
Sealing	Rims (master roller)
PID[2]	Activated
Horizontal-tamp auger velocity ratio	150 %
Granulator - rotation	50 rpm anticlockwise
Granulator - sieve	Rasp sieve 1 mm mesh opening

The sample collection of ribbons and granules has been already described in 4.6.1. The relative density and the tensile strength of the sampled ribbons were determined using the methods described in sections 5.1.2.3 and 4.11, respectively. The granule size distribution of the collected granules was measured as in 4.10. From the whole granule bulk, we sorted out two granule fractions through selective sieving: a coarse one corresponding to the fraction between 800-1000 µm, and a finer

[2] Proportional Integral and Differential control of the feeding that adjusts the speed of the feeders so as to keep a steady roller gap in the MiniPactor (see section 4.6.1)

between 200-315 µm. Moreover, in order to quantify the granules' resistance to shear forces, the attrition (friability) of the granules was also determined. 50 g of granule were set into the standard friability tester. After 40 rotations at 10 rpm, the content of the drum was emptied and the new particle size distribution was determined.

The morphology and the structure of the granules were also examined using, SEM and X-ray µCT. The SEM images of the granules were taken in order to characterize the shape and the surface of the particles. The SEM magnification was set between x120 and x130 for all acquisitions. In addition, the internal granule porosity was qualitatively examined by analyzing the X-ray µCT cross section images (see 5.1.1.5). The imaging and the reconstruction of the tomographies were carried out using a similar approach to that for the ribbon samples discussed in section 5.1.2.7. The image resolution, however, was set at 3.85 µm/pixel for coarse granules and 2.96 µm/pixel for fine granules.

In order to investigate the material deformation behaviour and the tabletability of the granules of the size fractions considered from the recycled granules, tablets were produced and characterized. The tablet production was carried out in two different devices. The study of the material deformation was performed in the Instron material testing machine. 800 mg of the corresponding granule were fed into the die of the compression assembly. The compression of the material was programmed to achieve a maximal force of 9 kN (i.e. 70 MPa pressure) with a compaction speed of 1 mm/min. The strain-stress profile was recorded during each process. This data was interpreted using the *in die* Heckel plots (see 2.1.5). The relative density and the tensile strength of the tablets obtained in the previous step were measured. The relative density was calculated from the dimensions and the tablet mass while the tensile strength was determined through diametrical compression tests (5.2.3.2). For these tablets, X-ray µCT imaging was also performed. Vertical and horizontal cross sections of the tablets were qualitatively analyzed.

As for the characterisation of the granule tabletability, tablets were produced at different compression pressures. 200 mg of granulated material were pressed into tablets with the pneumatic press, equipped with the 8 mm diameter die, at 33, 54, 100, 200 and 300 MPa. The density of the tablets was calculated whereas the crush strength was measured by means of the tablet crush-tester (4.11).

5.3.3 Results and discussion

5.3.3.1 Ribbon properties

As it can be seen from Figure 85, increasing the specific compaction force produces higher ribbon densification. Logically, the internal structure of the ribbons becomes denser if the material is compacted under higher pressure but, in addition, the re-processing of the granules in roller compaction induces a progressive increase in the solid fraction. The evolution of the material densification is dependent on the specific compaction force used. It is clear that the material densification can be improved more significantly in ribbons produced at low compaction forces. The results observed here are in agreement with the findings of [114], in which, the multiple compaction of MCC also produced ribbons that were denser after every re-compaction cycle. This is attributed to a

constant consolidation of the material particles into denser structures. Ribbons produced at high compaction forces, however, do not experience that large increase in the densification from cycle to cycle. The particle density after the first compaction has achieved a high density so that particle porosity will only suffer any large variation with further compaction.

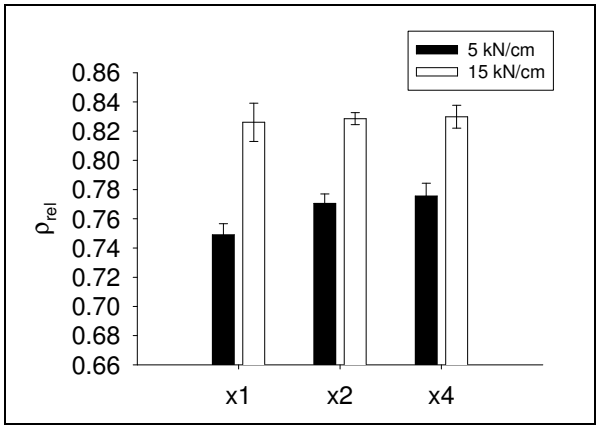

Figure 85. Relative density values for the ribbons collected after different RC-granulation cycles

In addition, the ribbon strength for the same ribbons, as presented in Figure 86, was dependent again on the specific force applied on the material and the number of RC cycles. Generally, denser ribbons are also harder. Nevertheless, this is not observed here. Denser ribbons that were produced after two and four roller compactions present, contrariwise, reduced tensile strengths, in spite of possessing higher relative density (Figure 85). This would support the idea that the granule loses the capacity of establishing bonds when the particles become denser. However, one could also justify the observed reduction of the ribbon strength with the variations in the granule size distributions after each RC cycle, as it is discussed next.

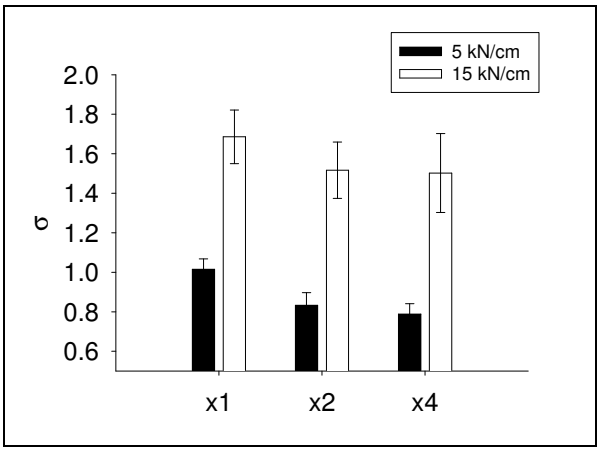

Figure 86. Tensile strength values for ribbons collected after different RC-granulation cycles

5.3.3.2 Granule morphology

The particle size is a material property that has been observed to have big influence on the end compact properties [22, 27]. When finer bulks are compacted, the number of particle-particle interactions that are established is larger than in coarser bulks. The resulting structure is less porous and the contact between particles is tighter.

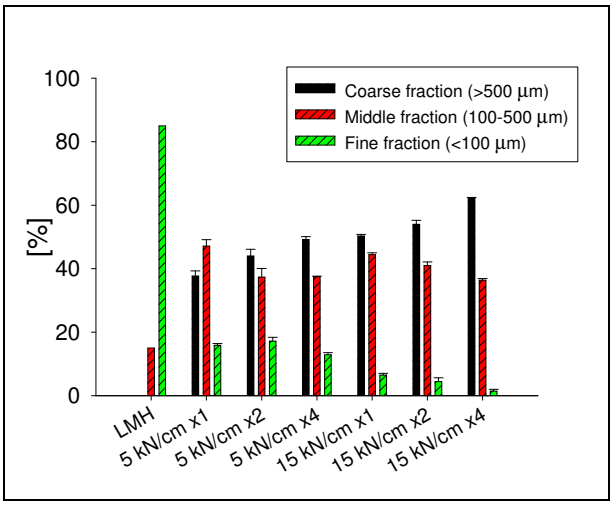

Figure 87. Changes in the particle size as a function of the number of RC-cycles and the specific compaction force used

All fraction sizes were classified into three groups: fine particles (< 100 µm), medium size particles (100-500 µm), and coarse particles (> 500 µm). As it can be seen in Figure 87, the amount of fines becomes smaller by increasing both, specific force and number of recycling. Increasing the compaction force produces granules with more quantity of large particles and reduced

fractions of fine and medium particles [300]. The granule recycling accentuated this trend even more. Thus, the reduction of fines became extremely significant after the granule recycling at 15 kN/cm. These results are in agreement with [114] and [301]. Hein, et al. [301] showed that consolidated lactose compacts generated granules with larger mean particle sizes. As smaller particles produce stronger compacts [24-27], the decrease of the granule fine fraction and the generation of coarser particles explains partially explain the progressive reduction of the ribbon strength showed in Figure 86.

The resistance of granules against attrition induced by shear stress and impact tested in the friability device is shown in Figure 88. Since the method is not originally developed for the testing of granules, some results appeared incongruent. Thus, non-collected fine particles from the drum are the origin of the wrong fine fraction reduction in granules of the second recycling at 15 kN/cm after the friability test. Nevertheless, from Figure 88 one can observe that granules generally possess higher endurance proportionally to the compaction forces and the frequency of recycling. Accordingly, particles are less prone to break and present reduced capability to fracture during packing and rearrangement (i.e. they lose compressibility).

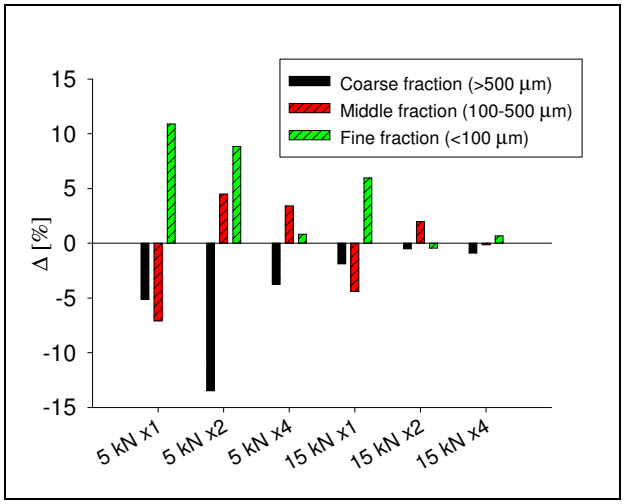

Figure 88. Variations in the particle size fractions after testing granule friability

In Figure 89 and Figure 90 SEM images of the granules produced at different compaction batches are shown. The SEM pictures of the fine particles are in the left column of the figures, whereas the pictures from the right correspond to the coarse particles. The images in Figure 89 are from granules of dry-granulated LMH produced by milling ribbons compacted at 5 kN/cm and after the RC recycling processes. Regardless of the manufacture conditions, all particles present irregular shape with rough, drusy surfaces scattered with very tiny particles. Nevertheless, re-processed granules (x2 and x4) present more regular edges with less pitted surfaces than the first granules.

The particles produced at 15 kN/cm (Figure 90) are more regular, smoother, and less bumpy than the granules produced at 5 kN/cm. Contrariwise as it is observed for the granules produced at low compaction forces, the changes in the morphology of the granules after each compaction cycle are more noticeable after each pass at high compression forces. The particles adopt more regular shapes and smoother edges, at the same time that surfaces become significantly smoother after each re-compaction step.

Finally, the particle internal porosity was analyzed using X-ray micro computed tomography. Figure 91 shows the cross-section images of isolated particles from each batch. The same trend as extracted

from the ribbon densification values in Figure 85 is observed also here. Accordingly, the granule porosity decreased with progressive increase in the compaction specific force and the number of RC-passes. This is consistent with the findings reported in [129]. As it can be seen, the internal structure of the granule shows smaller voids and higher attenuation with increasing the number of compaction cycles. However, for granules produced at 15 kN/cm, the progress of the densification level is less appreciable than for the granules produced at 5 kN/cm. This is also consistent with the values for the ribbon solid fraction in Figure 85 in which the growth of ribbon densification is also less substantial at high compaction forces.

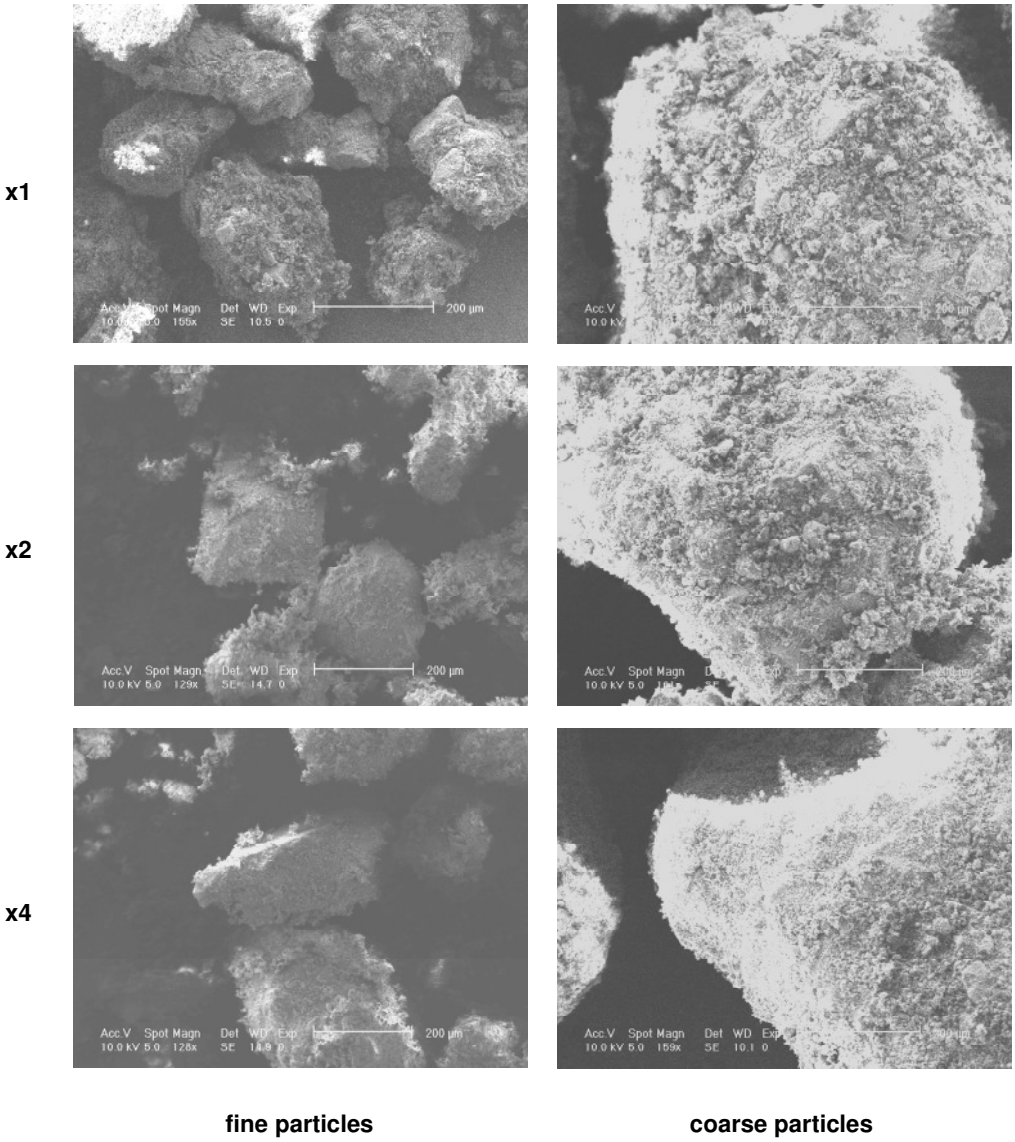

Figure 89. SEM images (x120 – x130) of granules produced at 5 kN/cm. The fraction and the processing number of re-processing cycle are correspondingly labelled

It has been shown that granule attributes are affected by the processing conditions. Particle size, shape, porosity and surface smoothness are altered as a function of the initial compaction force and the recycling. These changes affect the behaviour of particle consolidation under compaction and compression, since material volume reduction, deformation behaviour, and the establishment of inter-particle bonding, are strongly controlled by these particle characteristics [23, 32, 33].

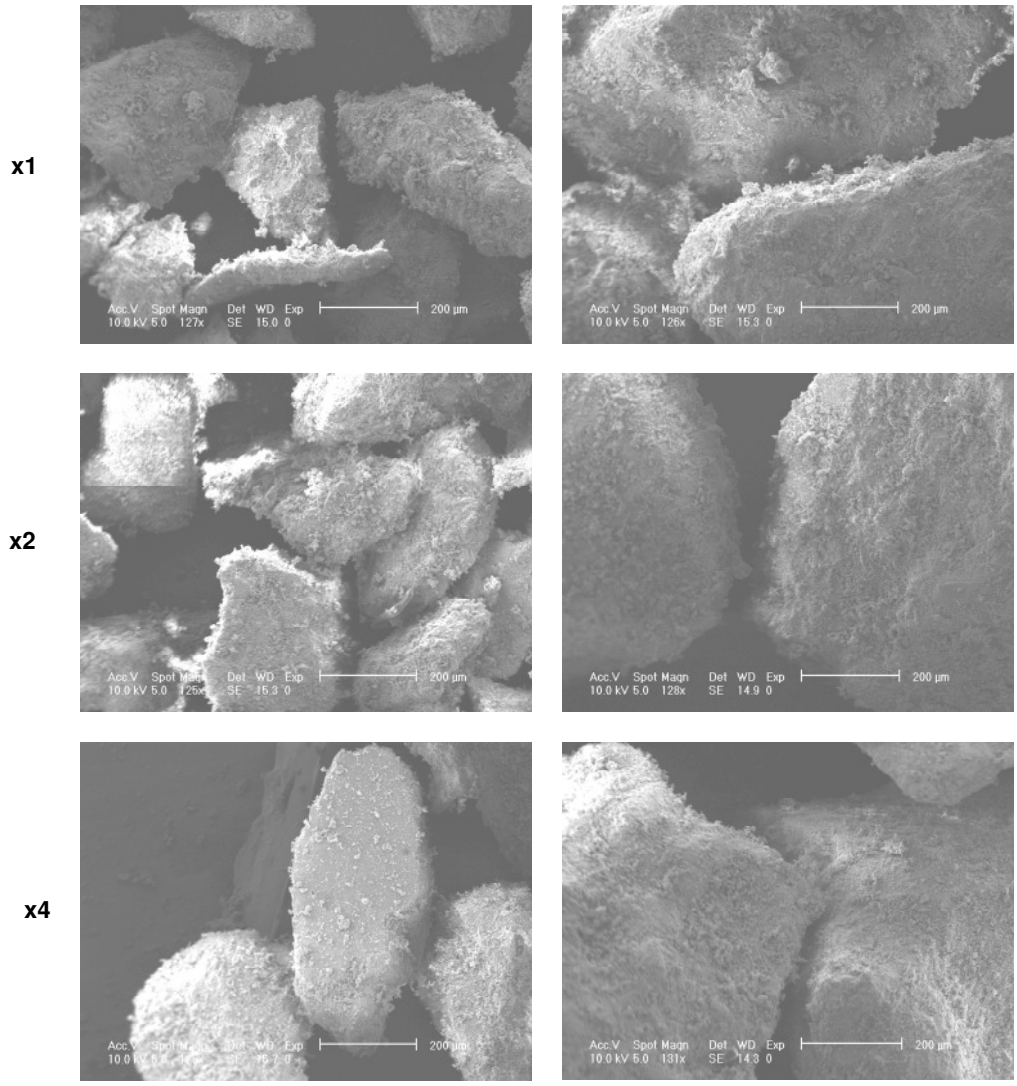

Figure 90. SEM images (x120 - x130) of granules produced at 15 kN/cm. The fraction and the processing number of re-processing cycle are correspondingly labelled

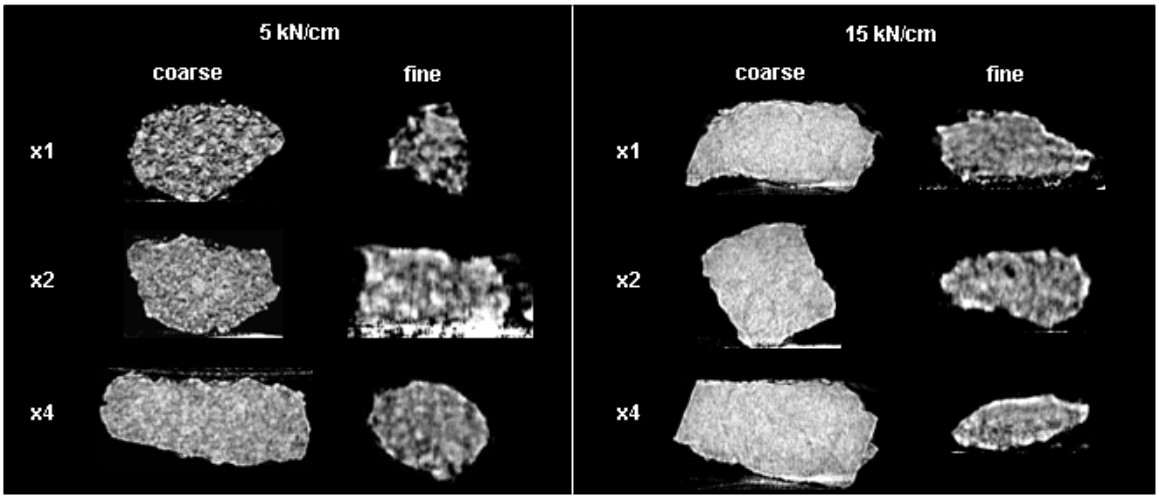

Figure 91. X-ray cross-section images of single granules from the two particle size fractions of all granule batches generated.

5.3.3.3 Compression behaviour

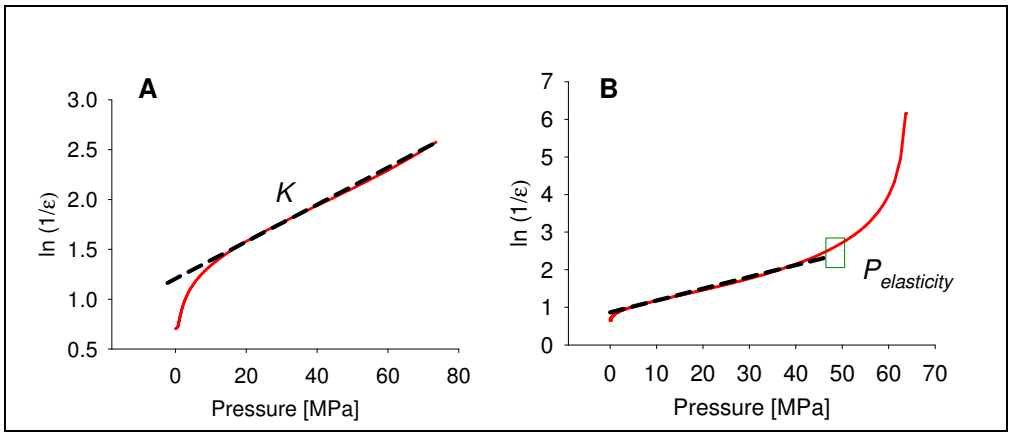

Figure 92. Determination of the *K* (A) and the $P_{elasticity}$ (B) value from *in die* Heckel plots. The two profiles correspond to different granule batches

The deformation behaviour of the different granules was characterized using the data from *in die* strain-stress profiles gathered during the uniaxial compaction of granulated LMH. Two values were calculated for the granules of each batch. The first was the *K* value (see section 2.1.5), corresponding to the slope of the regression fitting the linear region of the *in die* Heckel plot (see Figure 92.A). This value is directly proportional to the material plasticity [302], and is considered to be the inverse value of the mean yield pressure of the material (i.e., the pressure out of which the material deforms plastically -see 2.1.5). The second value obtained from the Heckel plots was the pressure value above which the plot profile suffers deviation from the linearity (see Figure 92.B). This value was also determined in [45] and appeared at earlier stages of the compression for materials with higher elastic modulus values (i.e. materials with stronger elasticity). Here, this value is denoted as $P_{elasticity}$ and is considered an indicator of the material elasticity.

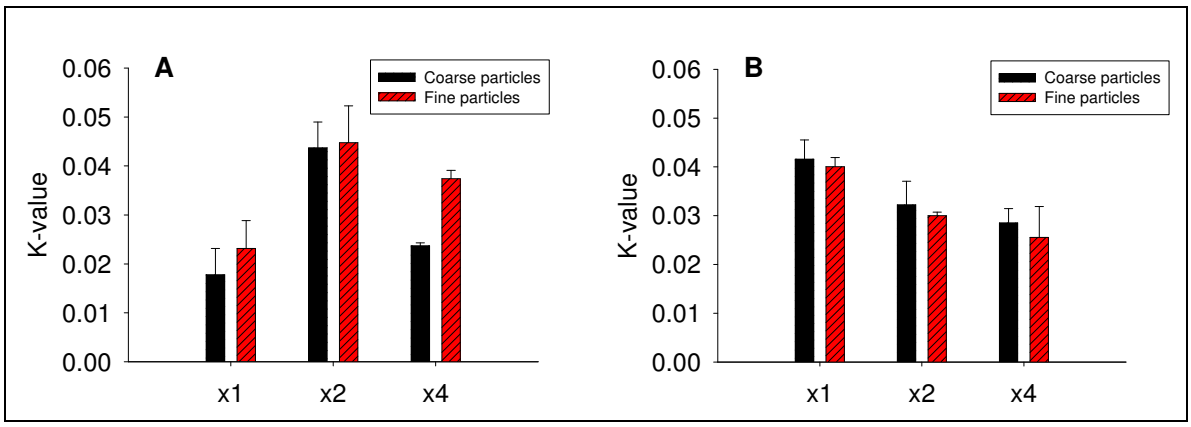

Figure 93. *K* values of the different granule batches calculated out of the *in die* Heckel plots. A) Compaction force 5 kN/cm B) Compaction force 15 kN/cm

The *K* values of fine and coarse granules produced at the different compaction runs are shown in Figure 93. As it can be observed, all factors, i.e., initial specific compaction force, granule recycling, and granule size, seem to be involved in the particle deformation behaviour. Initially, the compaction at low forces (Figure 93.A) generates granules with the lowest plasticity but after undergoing multiple compaction-granulation passes, LMH granules become more plastic. However, the particle plasticity

increases substantially after the second recycling and adopts lower values after the fourth granule re-processing. Figure 93.A also shows that for granules produced from low force compacted LMH, fine particles present higher *K* values. In fact, the difference of the value between coarse and fine fractions is especially significant after the fourth re-compaction. Interestingly, the *K* value for the granules produced at the second recycling (at 5 kN) was extremely large (even larger than for granules produced at 15 kN). This can be explained by a sudden change in the deformation behaviour of LMH at a certain level of densification (as reported in [303]). Thus, an abrupt change from brittle to plastic deformation mechanism could accentuate the particle plasticity, which decrease again with further material recycling (due to the *hardening* of the particles).

As for granules produced at high compaction forces (Figure 93.B), the first RC pass of virgin LMH (x1) produces granules which plasticity is similar to that of the granules after the second recycling at low compaction forces. In this case, however, small particles exhibit less plasticity. Moreover, the re-cycling of the granules reduces the material plasticity gradually (as it probably occurs after the second cycle compaction at low compaction forces). LMH is a material which initial particle deformation mechanism is dominated by the fragmentation [36, 52, 304, 305]. However, the initial processing of the substance seems to generate granules with greater deformation capacity [36]. Thus, a gradual increase in the plasticity is originated when re-compacting porous granules at low compaction forces, whilst the granule plasticity increases abruptly already after the first RC and then decreases gradually.

The $P_{elasticity}$ values of the granules are represented in Figure 94. Low values of $P_{elasticity}$ are linked to a marked material elasticity, since it means that the pressure at which the material is elastic appears at earlier densification levels. Material recycling induces the elastic behaviour of LMH. The bars in Figure 94 labelled "*>70 MPa*" depict that during the *in die* compaction to a maximum pressure of 70 MPa, the Heckel plot did not deviate from the linearity, showing that the granules are not elastic. Comparing *K* and $P_{elasticity}$ values, we can see a direct relationship between them. Thus large *K* values seem to be linked to low $P_{elasticity}$. Similarly as for the moisturized MCC studied in 5.2.3.3.4, the enhancement of the plastic material deformation also reduced the pressure level that induced the elastic behaviour of the material.

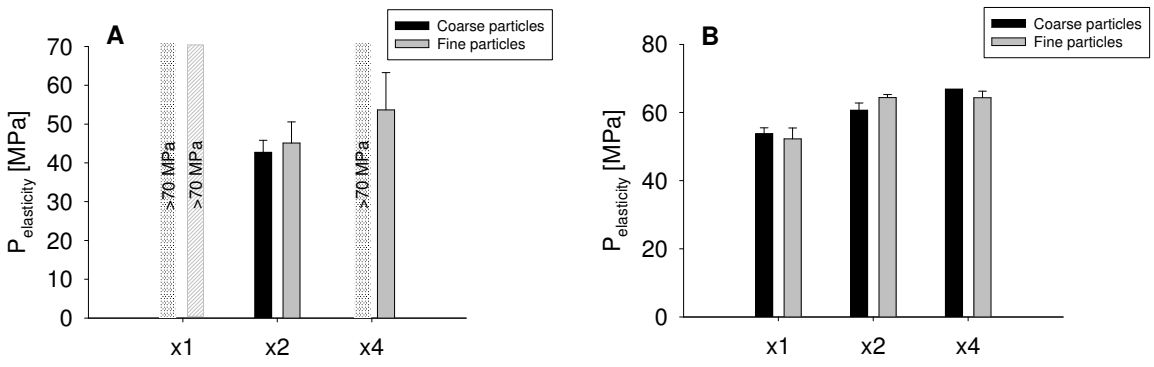

Figure 94. $P_{elastic}$ values of the different granule batches calculated from the *in die* Heckel plots. A) Compaction force 5 kN/cm B) Compaction force 15 kN/cm

The LMH granules from the first RC pass at low specific compaction pressures (Figure 94.A) do not present elastic behaviour at a pressure of 70 MPa. After the second re-processing, on the contrary, the material deforms elastically at 40-45 MPa. Nonetheless, the material loses its strong elastic character again after the fourth re-compaction. The strong elastic character of the granule after the second RC cycle was evidenced after the analysis of a tablet cross section image acquired using X-ray µ-CT. As shown in Figure 95, from the two stacked tablets made with fine and coarse granules compressed at 70 MPa, the one made of fine granules showed a failure in the tablet mass. The pressure used for the tablet production was above the $P_{elasticity}$ (see Figure 94), and therefore the elasticity of the material can be the cause for the capping [64].

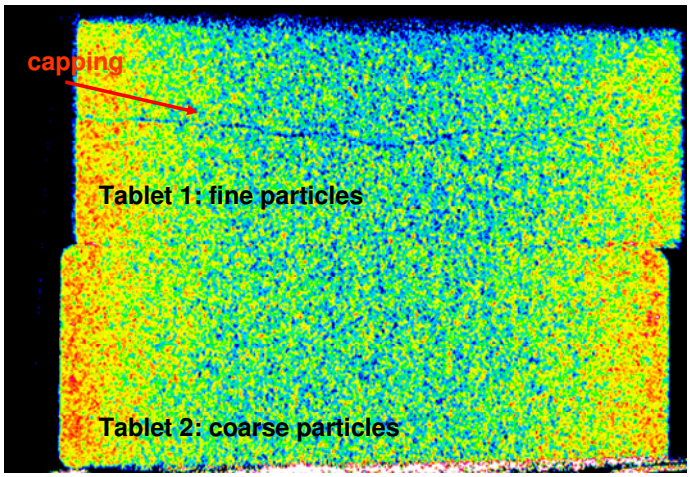

Figure 95. X-ray µCT section of two stacked tablets. The upper one, produced with the fine fraction of granulated LMH after two RC cycles, presented a failure in the tablet mass due to tablet capping

As shown in Figure 94.B, the compaction at high forces induces the elastic behaviour of LMH granules already after the first RC-cycle. However, unlike it happens at low compaction forces, the re-processing reduces the material elasticity. It has been demonstrated that the deformation behaviour of granulated LMH deviates from the one of the original material. Changes in the deformation behaviour of LMH as a function of the processing conditions were also reported in [33] and [288]. The authors observed that, during compaction processes, LMH changed from an originally brittle and low ductile material, to a material with more accentuated plasticity and elasticity. In [36] the authors also found that unprocessed LMH became plastic and subsequently elastic as the compaction pressure increased. Moreover, they also attributed the enhancement of the material plasticity to the presence of larger fractions of fine particles. Other authors [32, 306], in turn, claimed that LMH densification behaviour does not depend directly on the particle size since it is a brittle material. Nevertheless, we have observed that this seems not to be the case of dry-granulated LMH. Our results show that particle size, and also porosity, affect the bulk deformation character. Thus, the plasticity of fine granule fractions (and re-processed granules) from ribbons compacted at low forces (i.e. porous granules) is slightly larger than that of larger granules (i.e. dense granules). Moreover, small granules of processed LMH show also a more marked elasticity than coarse granules, while the opposite has been reported on the particle ductility of unprocessed lactoses [28].

The general pattern observed for the deformation of roller compacted LMH is that the granulated LMH presented different behaviour depending on the roller compaction conditions. At low compaction forces, the generated porous granules are less plastic and less elastic (i.e. they still keep the brittle character of LMH). In fact, studies have elucidated that fragmentability is related to granule porosity, so that porous particles of LMH are more brittle [30]. High compaction forces, in turn,

generated denser granules that deformed plastically and presented marked elastic characteristics. Moreover, the recycling of the granules in roller-compaction caused fluctuations in the material consolidation behaviour in a different manner, depending basically on the RC specific force settings. The RC re-processing of porous granules at low RC pressures enhanced the plastic behaviour and reduced the pressure threshold for the elastic deformation. However, higher RC pressures reduced the particle deformability, and the tendency of elastic recovery. We presume, therefore, that the deformation of the material processed under the latter conditions is attributed to brittle fragmentation above certain pressure levels.

5.3.3.4 Tabletability

The values for the relative density and the tensile strength of tablets produced with both size fractions from all granule batches at three compression pressures (54, 100 and 300 MPa) are presented in Figure 96 and Figure 98 (page 119), respectively. The relative density (ρ_{rel}) of tablets made from all granule batches increased as the pressure exerted on the material increases. As it can be seen in Figure 96, the tablets generally become less dense after each RC re-cycling. The reduction of densification is much more evident for tablets produced with granulated compacts at high compaction forces. This will be discussed further by comparing the X-ray µCT cross-section of tablets produced with each batch of granule. Moreover, at high compression pressures (say, 300 MPa), the variation of the tablet densification do not suffer large variations, so that the reduction of material densification between granules produced with different number of recycling diminishes.

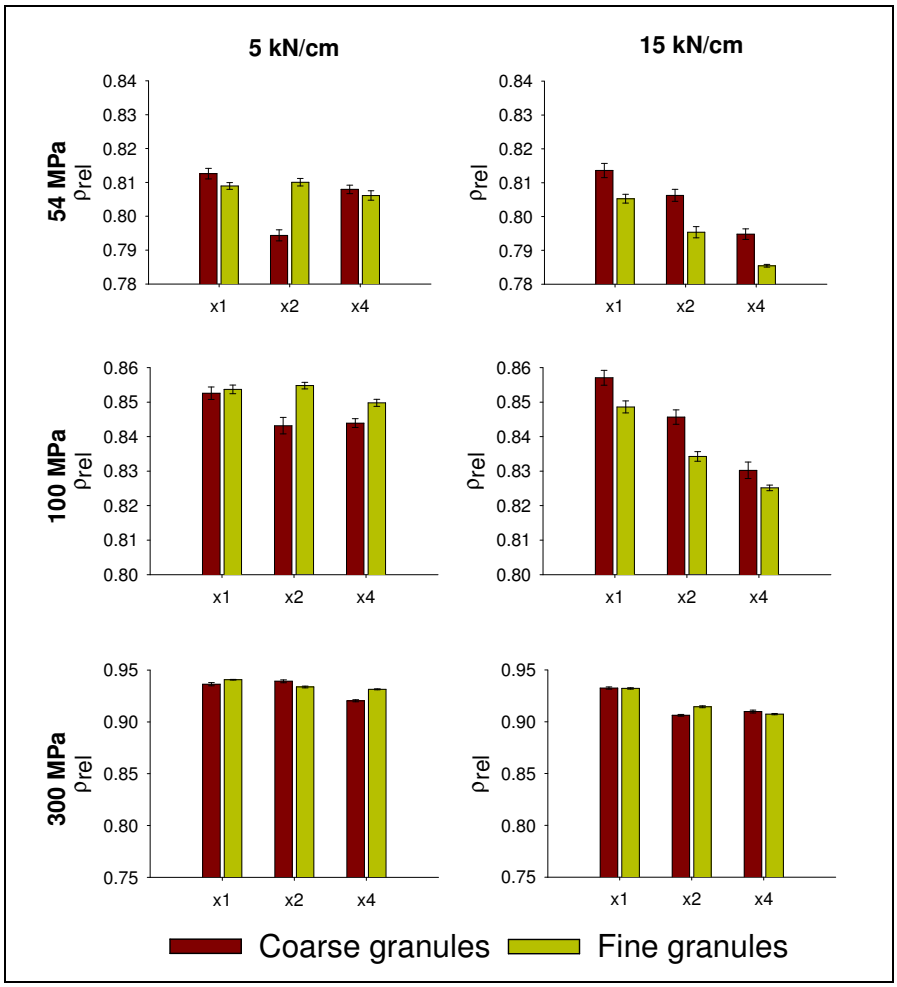

Figure 96. Relative density of tablets produced at three different compression pressures with each of the granule batches

As it is shown in Figure 96, the granule size affects the material densification. However, this varies depending on the granule porosity. Tablets produced from fine porous granules obtained at low

compaction forces generally have higher densification levels than those with coarse granules. The same trend was also observed in [26]. In this work the authors reported that finer porous granules produced tablets with higher density and smaller pore sizes, whereas tablets made of dense fine particles (produced at high RC compaction forces) had lower solid fractions and large pore mean sizes.

In order to examine the differences in the tablet densification, X-ray μCT was used to visualize the internal structures of tablets. The corresponding X-ray images obtained for tablets made of all granule fractions at a compression pressure of 70 MPa are shown in Figure 97. As it can be seen, porous granules can be compressed into denser tablets. Comparing tablets produced from granules obtained with the same RC specific forces, smaller granules are compressed into tablets of reduced inter-particle porosity. However, there is no perceptible difference in the interparticle porosity between tablets from the fine fractions of the different runs. Analyzing the tablets made of coarse particle fractions, it is clear that the inter-particle porosity increased with both, the number of RC cycles and the RC specific force. Thus, denser granules tend to conserve their identity after the compression [30, 33], and form larger inter-particle voids. However, the overall porosity achieved depends on the porosity of the initial particles. When the same pressure is applied on coarse porous granules, they tend to fragment, producing similar internal structures as to the one formed by fine granules, but with a larger overall porosity. As for coarse dense granules, they deform plastically but have low threshold of elasticity. Thus, after each RC pass, the internal granule porosity is reduced, while the inter-particle porosity of the produced tablets increases.

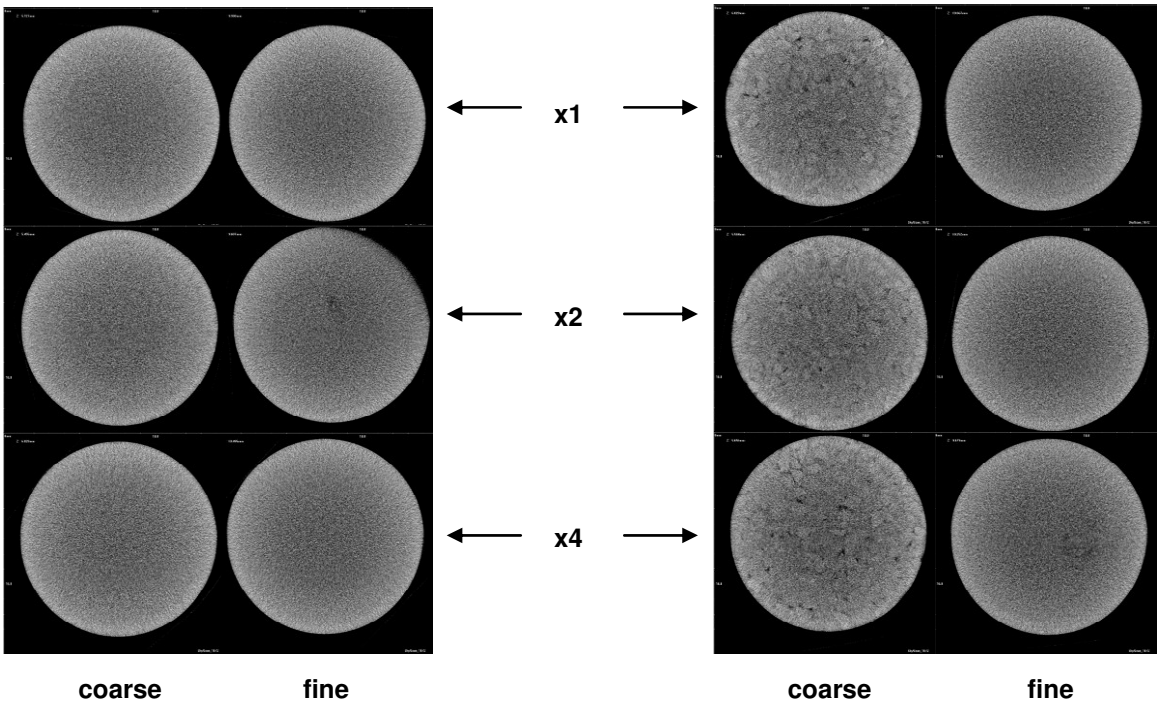

Figure 97. Cross section X-ray μCT images of tablets produced at 70 MPa with all granule batches

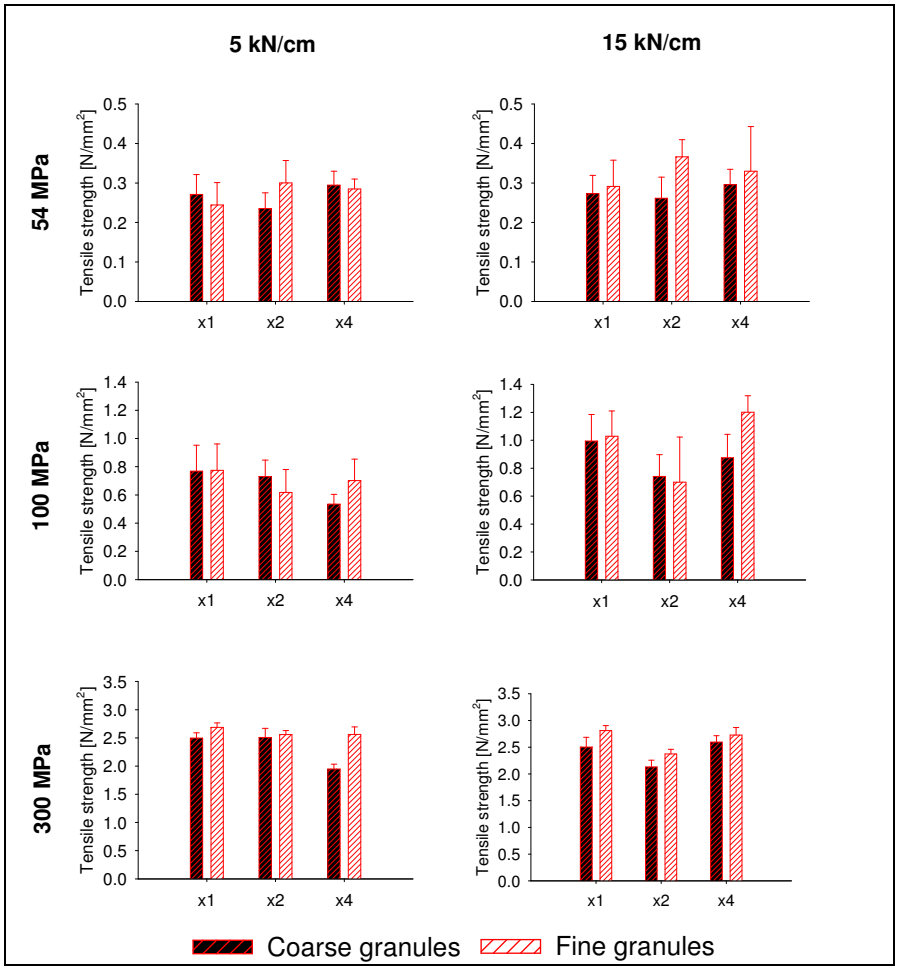

Figure 98. Tablet tensile strength values of tablets produced at three compression pressures with all granule batches

Figure 98 shows the values of tensile strength for the tablets produced at different compression forces. It is clear that tablet strength (σ_{tablet}), like ρ_{rel}, grows with increasing compression pressure. However, LMH exhibits relative low compressibility in comparison to other materials [52], so that the tensile strength values are relatively low. In almost all cases, small size fractions result in stronger tablets since they possess larger bonding areas and reduce the inter-particle porosity [28], augmenting therefore the number of contacts and the strength of bonds between particles [26]. Interestingly, even having lower solid fractions, the tensile strength of tablets from dense granules is larger than those produced with porous at low compaction pressures (up to a compression pressure of 100 MPa). This was also observed in [26]. Densely granulated LMH presented larger values of σ_{tablet} than unprocessed LMH. As we have demonstrated previously, denser LMH granules (and consequently, the corresponding tablets) exhibited plastic deformation behaviour, whereas virgin LMH and porous LMH granules have strong brittle characteristics. Thus, while the crush failure in tablets of dense granules occurs at the inter-particle space, in tablets made of porous granules the origin of failure occurs at the internal particle structure, reducing the tablet strength. At high compression pressures (300 MPa), however, the extensive pressure exerted on the material, forces the material to achieve a similar densification level independently of the initial granule attributes (similarly as it happens with ρ_{rel}), so that the mechanical properties of the resulting tablets become similar.

The effect of granule recycling on σ_{tablet} depends on the compaction pressure. For instance, at 54 MPa, re-processed granules under both RC compaction forces, deliver stronger tablets. On the contrary, at 100 and 300 MPa, tablets become more porous if produced with further RC-cycles. In addition, apparently different patterns are observed for granules of porous and dense compacts: the reduction was gradual after each re-processing in tablets made of porous granules, similarly as it has been

observed for the ribbons, whereas it can be seen that, after the fourth recycling at high compaction forces, the values of tablet strength are partially restored. We can see here that the difference between σ of tablets made of granules produced at 5 kN and 15 kN, decrease as a function of the tableting pressure. This is in complete agreement with the theory of the unified compaction curve reported by Farber, et al. [295]. At 300 MPa the pressure exerted on the powder is enormous so that the different level of densification induced by the recycling in roller compaction becomes of less influence. Thus, independently on the specific force used in the production of the ribbon, the produced tablets achieve similar values of strength.

As we have mentioned in the introduction of this experimental section, the observed reduction of the tablet tensile strength after granule re-processing corresponds to the phenomenon of *work hardening*. This is attributed to the loss of tabletability due to a reduction in the material capacity to undergo "defects" [294] or "dislocations" [289] during the plastic deformation at a compression level. However, we have demonstrated that the processing (roller compaction) of LMH improves the tabletability of the unprocessed LMH (see values of σ in Figure 98). Moreover, we have also found that *work hardening* in LMH is proportional to the granule internal porosity (Figure 97), and it is manifested in increased material elasticity as it can be seen in Figure 94.

With our results we demonstrate that in order to know whether the resulting RC dry granules for a given production process may have experienced a slight or a strong reduction in compactibility one has to consider three main aspects:

1) that the compaction behaviour of a particulate material depends on the particle morphology, internal porosity, and the main mechanism of deformation initially [26];
2) that the deformational characteristics of the material changes along the different stages of compression (or material compaction) [23, 39]; and
3) that the roller compaction and the tableting have to be considered as complementary densification steps if both are part of the same production process [295].

The properties of the resulting tablets depend upon the behaviour of the RC-granules during the tableting (flowability and deformability), which in turn are influenced by the behaviour of the starting material during the compaction (again flowability and deformability). Accordingly, in order to claim whether the granule particle size [307], the particle size of the initial particles [24], the particle porosity [304] or the work hardening [289] is the main contributing factor to the loss of tabletability after dry granulation, one has to take into account all factors: the attributes of the starting materials, the processing conditions during the roller compaction, and the tablet compression parameters. Thus, the optimization of the dry-granulation parameters and the processing steps is essential in order to avoid an excessive reduction of the material tabletability due for instance to too high pressure at the RC step, or to the recycling of sieved fine fractions with modified compaction behaviour.

5.3.4 Conclusions

The re-cycling of LMH granules in RC modifies the characteristics of the intermediary products (ribbons and granules) and the final tablets. This is attributed to changes in the deformation behaviour of the granulated material after every RC pass. Thus, the density and the tensile strength of tablets produced from the re-processed granules depend upon the properties of the starting granule (material), the conditions of the RC process, and the pressure for the tablet production.

The LMH deformation behaviour varies when the particle attributes (shape, surface smoothness, size, and internal porosity) are modified after roller compaction-granulation. Generally, dry granulation at high RC specific forces produces larger and denser granules that tend to deform plastically but experience elastic recovery. Low specific forces, in turn, generated smaller and more porous granules that, in spite of their ductility, still conserve the original brittle character of LMH. Porous granules can be compressed into denser tablets and are more brittle initially than dense granules. Apparently, LMH granules that have undergone further roller compaction-granulation processes increase their elasticity and reduce their compressibility due to *work hardening* effects.

The results obtained in our experiments are in broad agreement with the hypotheses found in the literature for the explanation of the "loss of re-workability" owing to dry granulation. Thus, as we have demonstrated, a material changes its deformation behaviour as a function of the process parameters. For this reason we believe that all mechanisms proposed in the literature (*work hardening*, changes in granule size, starting particle size, and total level of compaction) have to be born in mind when examining the changes in the tabletability experienced by the material after roller compaction-granulation.

6 SYSTEMATIC FORMULATION AND PREDICTIVE MODELS

The relevance of the tablet formulation and the importance of finding the most suitable combination of components and optimizing the processes for the manufacture of suitable solid dosage forms have been already discussed in section 2.1.1. Concerning the formulation, the excipients cannot be considered as inert components but as functional constituents that provide the blend and the final product with specific attributes. Moreover, as seen in previous experimental sections, the production parameters have also a big impact, since the behaviour of the substances and the interactions between them vary as a function of them.

Excipients can be defined as substances forming part of a formulation which addition has been intentional for acquiring a dosage form that fulfils the requirements imposed for the success of the drug therapy. Among over thousand substances used as excipients, only around two hundred are recorded in monographs [308, 309] in which there is information about physical-chemical properties, functional categories, handling precautions, and also technical data such as compressibility, water content or particle size distribution. However, the information delivered is brief and concerns normally the use of excipients as single components, which is not of much help for the formulator since a formulation corresponds usually to the combination of at least one excipient and one API. In addition, it has to be considered that the performance of the dosage form is dependent on the process variables which determine the attributes of the dosage form to a very large extent. Altogether, in order to select the proper combination of substances [309], it is obvious that a detailed description of the excipients during the formulation for the different production phases is necessary to reveal the behaviour of the components in interaction with other substances.

For that purpose, we carried out studies on the *systematic formulation* for the production of tablets from dry-granulated blends, in order to describe thoroughly the modifications of product characteristics induced by changes in the type and/or the quantity of substance added to the initial formulation. Moreover, we describe the impact of the processing steps followed and the process parameters set for the tablet compression on the end properties. A total of three sets of formulations were considered in this section:

1- MCC granules with external additives. In these formulations, granules of lubricated microcrystalline cellulose were blended with different amounts of other components before the production of tablets.
2- Multicomponent blend - formulation (group) 1. All components of the formulations, in which MCC was the main component, were blended together prior to the dry-granulation.
3- Multicomponent blend - formulation (group) 2. In this case, the main component was mannitol (MNT).

We also compared the trends followed by the product characteristics after the modification of the formulation with the response graphs generated using *artificial neural networks* (2.3.3). The networks created were trained with the initial composition as independent variable (*input*) and the corresponding

characteristic as response (*output*). This way, we could assess whether ANNs were able to model and approach their response to the changes in the product properties due to modifications in the composition. On one hand, the description of the trends was used in the knowledge base. On the other hand, the experimental results were collected as data sets to be processed so as to develop prediction models which development is focus of the work presented in 6.3.

6.1 The effect of extragranular addition of components

The workability of the granules obtained through roller compaction into tablets is inherent to changes suffered by the raw material during the processing and the behaviour of the new obtained granule. The mixture of the initial substances and the subsequent compaction-granulation lead to the formation of a new material *identity* with own mechanical characteristics. Assuming a granule as a homogeneous bulk, it can be assumed that the dosage forms manufactured will not present significant inter-individual variability in their characteristics. However, the extra-granular addition of components to the granule will modify the response of the resulting blend to the processing and will originate dosage forms with changed properties. The differences in the blend workability are induced, in principle, exclusively by the addition of the new substance. Nevertheless, the intricacy of interaction mechanisms established between substances can vary the product properties unexpectedly.

6.1.1 Introduction

The extragranular addition of components is commonly used in the manufacture of tablets from wet granulated substances [10]. Generally, previous to the compression, formulators add other excipients to the granule to facilitate the tableting. The excipients that are frequently added extragranularly are lubricants [10] and disintegrants [310]. The former aim the reduction of variability in the content uniformity, whereas the latter enhance a rapid disintegration of the tablet (and consequently, the fast delivery of the API). Also in roller compacted granules, the addition of lubricant extragranularly is also common [34, 117, 125, 126] though some authors consider that there is no need to do so [183]. Nevertheless, the extragranular addition of other kinds of excipients has also been studied by Li, et al. [311] and Hausman [312]. They found out that the addition of MCC improved not only the flow of the granules but also their compressibility. Inghelbrecht and Remon [110] examined the benefits of adding a disintegrant extragranularly to roller compacted granules and observed an extension of the tablet disintegration. Also Turkoglu [183] studied formulations with extragranular MCC and detected that external MCC increased the tensile strength of acetaminophen tablets produced from dry agglomerated blends.

The extragranular addition of Aerosil 200 (A200), Ludipress LCE (LP) and unprocessed Avicel PH101 (MCC) to granules obtained by roller compaction of lubricated MCC is studied next. The extragranular components were added as single component and as a combination of MCC with A200, MCC with LP or A200 with LP in different proportions. After varying the components and the amounts added extragranularly to the MCC granules, we analyzed the changes in the blend processability and the end tablet properties. The general trends observed were qualitatively compared

with response graphs generated by ANN models created for the same variables using experimental data. Finally, we compared the differences in processability and in resulting tablet characteristics of two component formulations with identical composition, depending on whether the second substance was added externally to the MCC granule or it was blended together with MCC before being dry granulated.

6.1.2 Materials and methods

MCC (Vivapur PH101) was mixed with 0.25% MgSt for 2 min in the planetary mixer. The blend was thereafter dry compacted and granulated in a Gerteis MiniPactor. The roller settings were the same as in section 4.6.1. The compaction specific force was 5 kN/cm and the gap between the rollers 3 mm. The rotational speed was set at 2 rpm. The granulation unit was assembled and configured as in 4.6.1. After the gap variation approached ± 0.1 mm and the parameter values did not experience significant fluctuations, the granule was collected. A small part of the granule was taken for its characterisation and the production of tablets while the rest was blended with external components. As for the production of the granules with two components, MCC was blended with the corresponding amount of the second component in a planetary mixer for 15 min and was mixed with 0.25% MgSt for 2 min. Thereafter, the blend was roller compacted and granulated using the same RC parameters.

As shown in Table 19, different blends of the granulated MCC with variable amounts of A200, LP and MCC were produced. In case of the extragranular addition of component(s), they were added individually or as combinations of A200 with LP, A200 with MCC or LP with MCC. Under no circumstances three components were added to the granule simultaneous. The percentage values listed in Table 19 are relative to the total weight. Nevertheless, the detailed compositions of the blends are listed in Table 35 in section 9.3 of the Appendix. The blending of the extragranular component(s) was carried out in a Turbula mixer for 10 min at 42 rpm. Thereafter, 0.25% MgSt was added on and mixed also in the Turbula mixer at the same rotational speed for 2 min. The angle of repose (see 4.8) and the Carr Index (CI) (see 4.9) of the final blends were estimated a total of three times. The mean values are presented in the next section. From each blend, tablets were produced using the single punch pneumatic tablet press, equipped with the 8 mm diameter punch, at five different compression pressures: 33, 54, 100, 200 and 300 MPa. At least 17 tablets were produced for each compression pressure. The tablet mass was kept at 200 mg (± 10 mg). The tests for the diametrical tensile strength and the disintegration time of the tablets were performed using the measurements described in sections 4.11 and 4.12, respectively.

In addition, the ANN software Statistica Neuronal Network Package v. 4.0 (StatSoft Inc., US) was used for the creation of models able to approach the effect of the composition on the tablet characteristics. Separate models to those created for section 6.3, were generated here for a single compression pressure (54 MPa), in order to show the tendency of the variations induced exclusively by the formulation, without considering the tableting pressure. Thus, the formulation (i.e., components and amount) was the network *input* and the value for the modelled attribute (tablet tensile strength and disintegration time) the *output,* or model response. Several networks of variable architecture were

tested and trained using the data sets produced with the experimental results. From all collected networks, only those with the best performance were chosen. The accuracy of the networks was estimated with the correlation coefficient calculated from the comparison of the estimated and the real values.

Table 19. Percentages of components added to the MCC granules

		LP ext[3]					MCC ext				
		0%	2.5%	5%	10%	30%	0%	2.5%	5.0%	10%	30%
A200 ext	0%	✓	✓	✓	✓	✓	✓	✓	✓	✓	✓
	0.25%	✓	✓	✓	✓	✓	✓	✓	✓	✓	✓
	0.75%	✓	✓	✓	✓	×	✓	✓	✓	✓	✓
	1.25%	✓	✓	✓	✓	✓	✓	✓	✓	✓	×
	2.5%	✓	✓	✓	×	×	✓	✓	✓	×	×
LP ext	0%						✓	✓	✓	✓	✓
	2.5%						✓	✓	✓	✓	×
	5%						✓	✓	✓	✓	✓
	10%						✓	✓	×	×	×
	30%						✓	×	✓	×	×

6.1.3 Results and discussion

6.1.3.1 Flowability and compressibility

The modifications in the flowability and the compressibility attributed to the addition of a second component extragranularly to the MCC granule are shown in Figures 99 and 100 respectively.

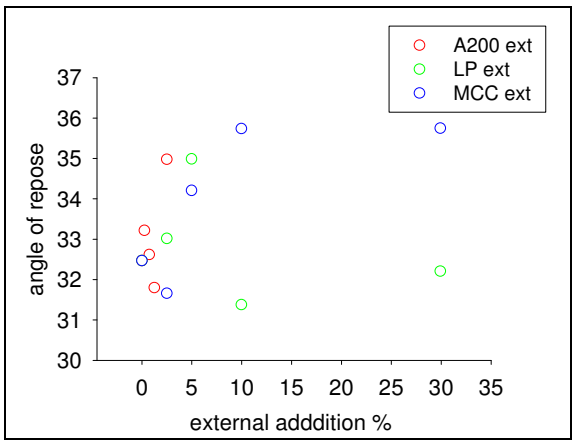

Figure 99. Angle of repose after adding a second component extragranularly

Particle-particle frictional interactions are well known to regulate the bulk flowability. This is widely accepted to be basically determined by the particle size and shape [80, 195, 313], which define the internal friction coefficient of the bulk [314]. However, the particle surface determines also at large extent the particle mobility. As it is shown, the addition of a substance with a large specific surface, such as A200, enhances the bulk flow already at low concentrations, and has a negative effect when the quantity grows (Figure 99), as observed by Van Veen, et al. [315], and Jonat, et al. [307]. Both studies reported the gliding effect of colloidal silicon dioxide which, when added in small quantities extragranularly (up to 0.75%), had a positive effect on the powder flowability, whereas increasing amounts (2.5%) worsened the flow. Due to its enormous specific surface, A200 forms a film around the particles and reduces significantly the particle-particle friction. However, the formation of thicker layers of A200 (i.e. at higher A200 concentrations), increases the number of contact points between particles, and thus, enlarges the internal friction. When analyzing the addition of LP (Figure 99), an increase in LP generally enhances the bulk flow. According to product specifications [316], LP possesses a fairly coarse mean particle size. Thus, an

[3] The abbreviation *ext* and *int* used here are referred to the extra- and intragranular location of the formulation components in the final blend

increase in the coarser fractions of particle systems improves the flowability. In turn, it is clear that MCC generally has the contrary effect. Because of the relative small mean particle size of unprocessed MCC (ca. 50 µm), its addition reduces the particle mobility.

The *Carr index* (CI) quantifies the ability of the powder to rearrange within the tableting die during the die filling and the first steps of densification [317]. A200 seems to affect the material compressibility as a function of the amount present in the formulation (Figure 100). Intermediate concentrations (0.75-1.25 %) show negative effects on the blend compressibility. However, very low amounts (0.25%) and large amounts (2.5%) of A200 enhance the blend compressibility, confirming the observations made by Chang, et al. [318]. The authors stated that the colloidal silicon dioxide facilitates the material densification and improved the packing properties. The other two substances, on the contrary, show a clear positive effect on the powder compressibility. Both LP and MCC enhance the packing of the material. The effect induced by LP is attributed to the spherical morphology of the LP particles [319] that, in contrast to needle-like particles, facilitates the particle rearrangement. As for MCC, though the observed effect is similar to the addition of LP, the better packing behaviour of the blend is induced by the sifting of the fine particles passing through the coarses to fill up voids. On the other hand, addition of large quantities of LP and MCC induces an increment in the CI. If LP amount keeps on growing, the reduction in the proportion of fines limits the number of particles slighting through coarser particles and filling up voids, whereas after a large addition of MCC, an excess of fines reduces the interparticular mobility and, as a consequence, the ability of the bulk to pack impoverishes.

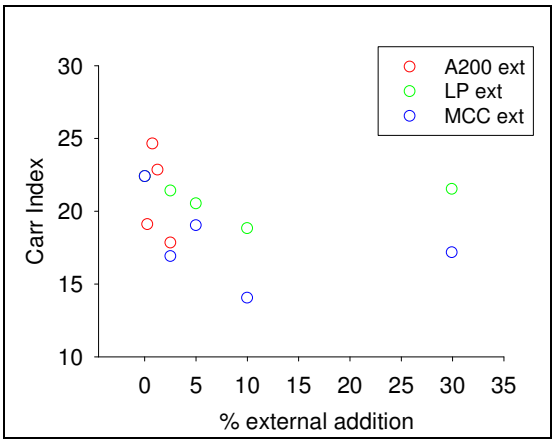

Figure 100. Compressibility index after the extragranular addition of a second component

6.1.3.2 The effects of extragranular addition of single components

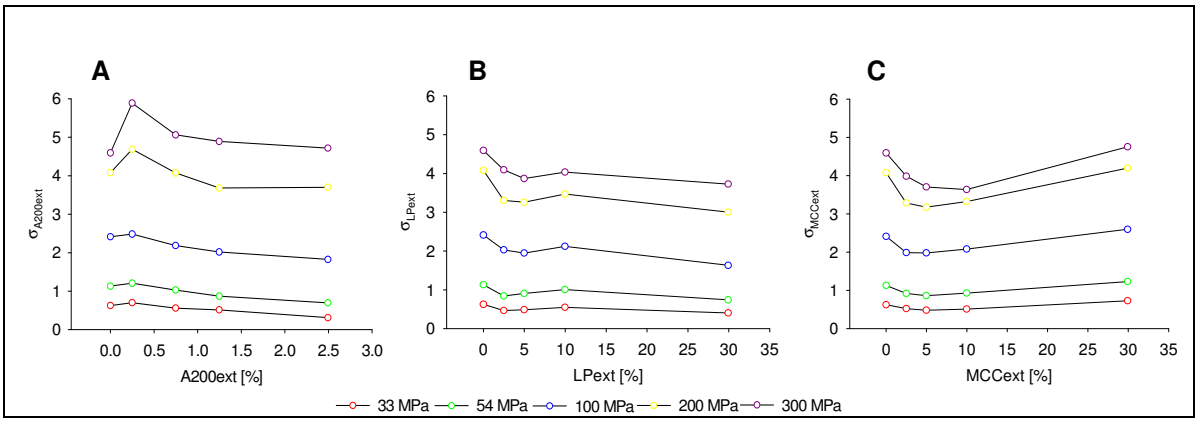

Figure 101. Tensile strength variation after the extragranular addition of different substances

We have considered the tensile strength (TS), represented as σ, and the disintegration time (DT), represented also as t_{dis} to study the effect of the external addition of a single component on the

properties of the end product. In Figure 101 the TS of tablets from formulations in which the second component was added extragranularly are represented for different compression pressures. Interestingly, the main patterns have almost parallel profiles between pressure levels.

Similar trends as presented in Figure 101.A after the addition of A200 have been reported in multiple studies [307, 315, 318, 321]. They all reported that A200 enhances the tablet strength (i.e. it facilitates the densification) in small quantities, while the opposite effect is observed if the amount of A200 increases. In addition, all our observations are in line with the report of Edge et al [320] and thus, Figure 102 has been extracted from their work. The profiles of the tensile strength values after progressive addition of A200, match entirely the profiles presented in Figure 101.A. Thus, the specific contact between particles is extended, enhancing the particle interaction and multiplying the number of bonds. Hence, as shown in Figure 102, the tablet strength increases when 0.25 to 0.4% A200 is added externally and it tends to decrease after exceeding these values. At low concentrations, A200 form a layer on the particle increasing the "surface roughness" and enhancing the particle interaction and the establishment of bonds. However, again the formation of thicker extragranular layers of A200, which is a very low compressible material, reduces the interaction between granules, and enlarges the number of potential failure points.

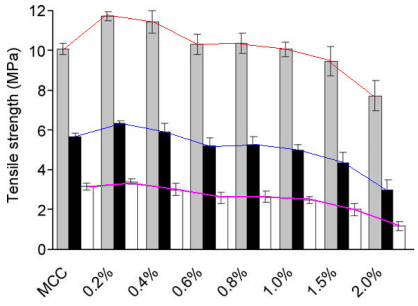

Figure 102. Tensile strength values after the external addition of A200 (adaption of Edge, et al. [320]) for three compression forces

The addition and the increasing amount of LP, reduces the tablet strength (Figure 101.B). LP was described by Kolter [319] as a very plastic material. It is precisely the excellent material plasticity what seems to cause the decrease of the tensile strength values observed. As the only mechanism of inter particular cohesion in plastic materials occurs by means of the contact surface extension during particle deformation, the inexistence of particle interlocking increases the number of potential failure surfaces [28], which, in addition, are very sensitive to the addition of lubricant [313]. Thus, as during the elaboration of the blend 0.25% MgSt is added in a last step, the number of weak contacts in the tablet increases. Finally, the external addition of MCC initially reduces the value of strength. This observation is partially contradictory to reported results [183, 311, 312] which can be explained by the fact that phenomena like segregation, unsteady die filling due to bad flow, and air entrapment, occur more frequently in systems of fine particles. For that reason, the tablet quality worsens up to a certain percentage of MCC added externally. However, when larger amounts of MCC are added to the granule, the tablet strength is improved again (see Figure 101.C) as it was reported by the aforementioned authors.

Similarly to the effects on the tablet endurance, the profiles of tablet disintegration times after the extragranular addition of one component showed similar patterns for the different compression pressures (Figure 103). A200 clearly reduced the disintegration time (see Figure 103.A). Nevertheless, this effect was only noticeable at higher compression pressures, at which the disintegration time of the

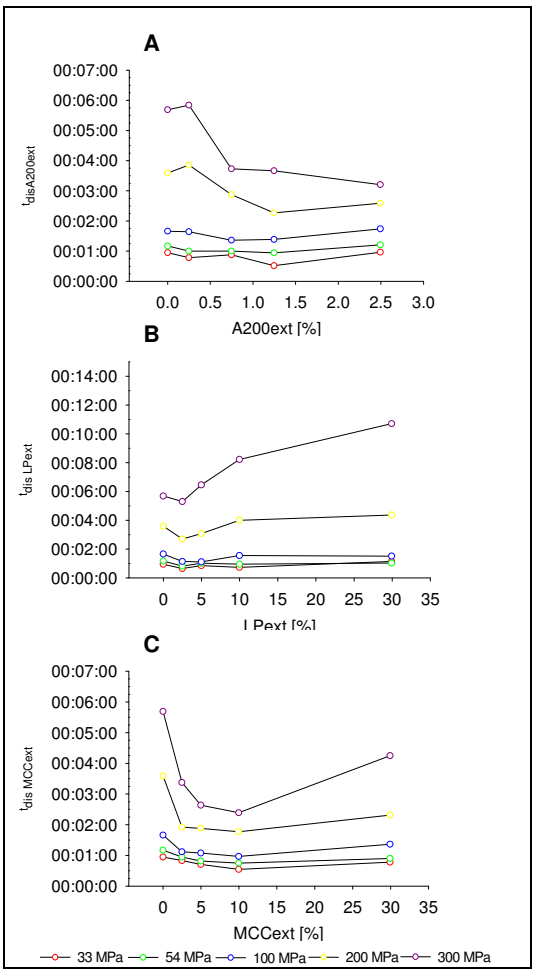

Figure 103. Disintegration time variation after the extragranular addition of different substances

tablets made of MCC granules suffer a significant extension. Due to the active disintegration mechanism of A200 and the wicking effect induced by its hygroscopic behaviour [318], A200 works as a moisture scavenger. Thus, the water uptake by the tablet mass is enhanced and the migration of water towards the tablet core becomes rapid. The extragranular presence of this substance ensures the formation of a canal-like network around the MCC granules that distribute water rapidly.

On the contrary, extragranular LP slows down the tablet disintegration, as depicted by Figure 103.B. Though low percentages seemed to enhance it, above 5% of LP reduced the disintegration rates. LP is a co-processed excipient which major component is lactose monohydrate [316], and as already mentioned, it presents a high plastic deformational behaviour. Moreover, it also contains a 3.5% of Kollidon 30, a binding agent. As a consequence, the extension of the disintegration is due to a sum of factors. First, the disintegration mechanism of lactose is functioning mostly by breakage of interparticular bonds, habitually exclusively by dissolution, which is a passive, slow mechanism [322]. Second, the binder included in the excipient must cause strong bonds between particles that are not easily breakable in contact with water. Third, the plastic deformation of the particles might reduce the tablet internal porosity, reducing the permeability of water into the tablet. Finally, at high compression forces, LP particles might present brittle character, inducing, in addition, the formation of a more dense mass of extremely reduced porosity. Figure 104 shows the evolution of the ρ_{max} value (i.e. the maximum value of solid fraction achievable by the material), obtained after the iterative optimization of the compressibility plot calculated using the Wiegel's equation (see Appendix 9.2). As it can be seen, external addition of LP induces the increment of the solid fraction (i.e. the porosity is reduced) reached by the compressed blend, which hinders the water uptake of the tablet by capillarity.

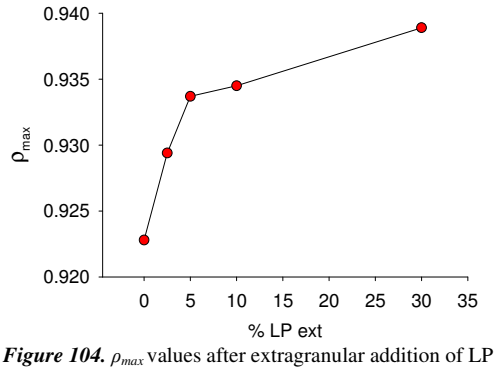

Figure 104. ρ_{max} values after extragranular addition of LP

Finally, Figure 103.C shows how the addition of raw MCC reduces the tablet disintegration time observed also by others [8, 311, 312]. In these studies, the authors reported that the tablets made of granule and external MCC had better release rates. In contact with water, MCC swells [13, 322], becoming an active disintegrant. As a consequence, MCC works in a similar way like A200, i.e. as moisture

scavenger, and enhances the penetration of water into the tablet [323]. The later extension of the time at higher MCC quantity (Figure 103.C) is, again, attributed to the generation of low porosity tablets through which water cannot permeate that easily.

6.1.3.3 The effect of extragranular addition of two components simultaneously

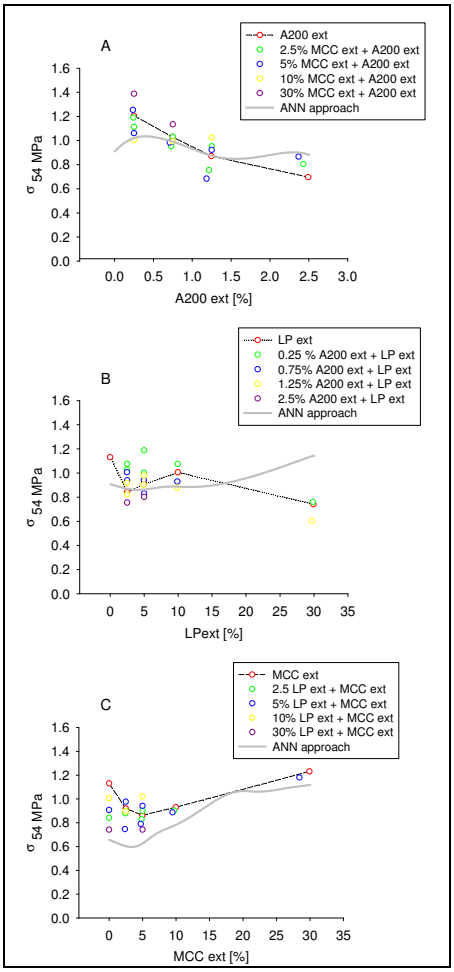

Figure 105. Evolution of the tensile strength values of tablets produced at 54 MPa after changing the composition. The gray line correspond to the ANN calculated response

A combination of variable composition, formed by two components, was added extragranularly to MCC. The changes of the tablet attributes (σ and t_{dis}) as a function of the composition are presented here (shown in Figure 105 and Figure 107, respectively). However, we considered the values for tablets produced exclusively at 54 MPa. Moreover, the experimental results were compared with the response graphs originated with ANNs models, created exclusively for the assessment of the trends observed in the experimental results of this section.

In Figure 105, experimental values (open symbols) and ANN values (continuous line) for tablets manufactured at 54 MPa are plotted together. Though the 2D representation of the experimental values only allows the representation of one of the two possible substance combinations for each component (MCC-A200 in Figure 105.A, A200-LP in Figure 105.B, and LP-MCC in Figure 105.C), the ANN models were generated with the complete set of data for the corresponding compression pressure (i.e. with all combinations of external additives listed in Table 35 in Appendix, section 9.3). The resulting ANN models for the tablet characteristics were multilayer perceptrons (MLP) (2.3.3) with 4 inputs (MCCint, A200ext, LPext and MCCext), 2 outputs (σ and t_{dis}) and one hidden layer with 13 neurons. The ANN was trained with back-propagation iterations until the regression correlation achieved reached its maximum, which was 0.929 for the output σ, and 0.915 for the output t_{dis}. The ANN response graphs plotting the value generated for the corresponding tablet attribute after the addition of each one of the external components were created and exported for its representation together with the experimental data.

In case of the output σ, it seems that the estimations made by the ANN models match the general trend followed by the experimental data. Due to the large order of the approach function generated by the ANNs, the profiles are tortuous. However, the curve lays close to the experimental values represented, meaning a satisfactory approach of the trend. It is shown that A200 tends to reduce the tablet tensile strength (Figure 105.A), similarly as it has been observed for its addition as single additive. Hence, even in combination with other substances, A200 induces the tablet cohesiveness at low

concentrations, this becoming stronger if added together with higher proportions of MCC (Figure 105.A). The corresponding ANN response graph also depicts a slight increase in the tensile strength around 0.25% of A200. However, at higher concentrations, A200 reduces the tablet strength (as it has been also seen when added as a single extragranular component). The same trend was followed by the response graph generated by the ANN model. Generally, increasing concentrations of LP increase the tablet strength in combination with the second component (A200) (see Figure 105.B). At higher concentrations, however, the effect is the opposite. Analyzing the trend drawn by the ANN response graph, on the contrary, contradicts the last observation. Finally, MCC (in combination with LP) improved the tablet tensile strength, which is in the line with the ANN response graph for this substance.

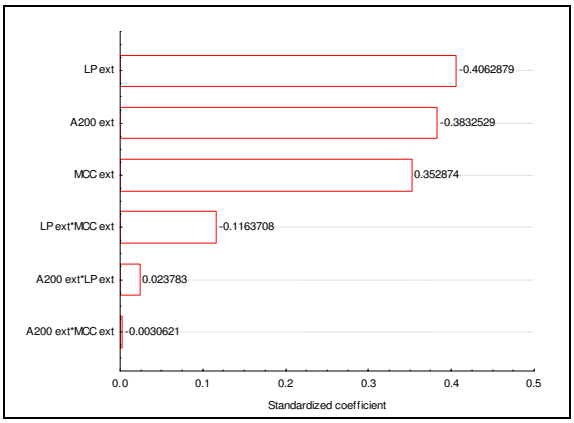

Figure 106. Pareto chart. Response surface of the external addition of the substances and the value of TS for tablets produced at 54 MPa

The trends of the tablet strength observed for the extragranular addition of components in combination with a second substance are similar to those observed for the addition of single components. This reveals that the tensile strength is strongly influenced by the effect of the individual substances. To prove this, Figure 106 corresponds to a Pareto chart and shows the standardized coefficients for the factors of a calculated general regression of the relationship between the extragranular amount of components and the tablet tensile strength. Here, the standardized coefficients for each factor are represented. It has to be remarked that though the correlation of the response surface is low (0.675), the coefficient values are in agreement with the general trends observed in the experimental results. Thus, A200 and LP present negative coefficients, i.e., they reduce the tablet strength while MCC has a positive coefficient (i.e., it improves the tablet strength). Furthermore, the variables of the regression that present larger coefficients are the individual components, whereas, the interaction between components has a relative little effect on the end strength value. Thus, by this analysis it has been evidenced that the effects induced by the combined substances on the tablet tensile strength is the "sum" of the individuals whereas the interaction between components is negligible.

The diagrams of the disintegration times for the tablets of the same formulations are presented in Figure 107. Differently as for the tensile strength, the trends observed for the extragranular addition of combined substances are not always similar to those described for the external addition of the single substances. As depicted in Figure 107.A, the enhancement of the disintegration observed for the addition of A200 as single component does not appear in combination with MCC. Large amount of A200 (2.5%) even extends the disintegration time. Figure 107.B also shows a different evolution of the disintegration time values after the addition of LP when combined with A200, compared to the addition of LP as a single extragranular component (Figure 103.B). Thus, at low LP concentrations, the tendency is to shorten the disintegration times while this swops over at higher LP amounts. Only

changes on the table disintegration rate induced by the addition of MCC in combination with LP (Figure 107.C) presented the same patterns as added alone (see Figure 103.C). MCC increased the disintegration rates at low concentrations while the effect becomes the contrary at high percentages.

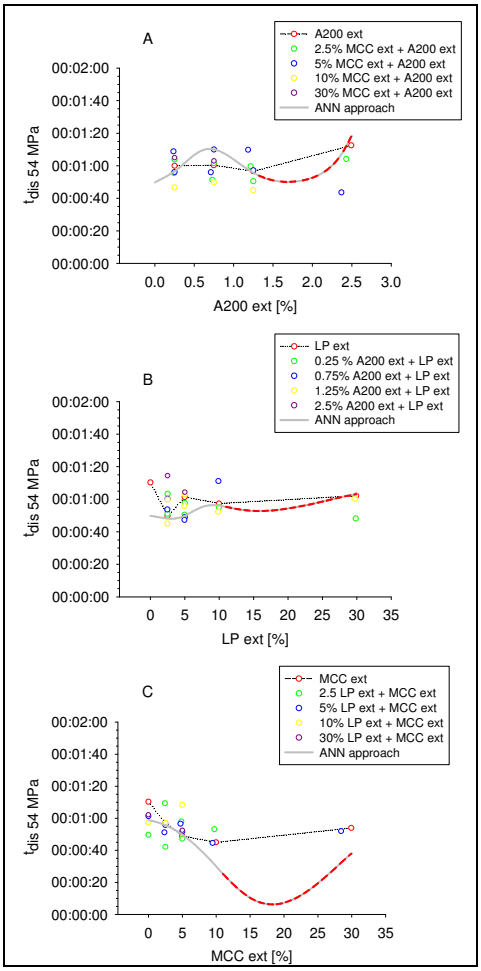

Figure 107. Evolution of the tablet disintegration rates of tablets produced at 54 MPa after changing composition. The gray line correspond to the ANN calculated response

From the ANN approaches represented in Figure 107, it is clear that all presented tortuous profiles. Though they converged with the experimental results, there is a range at which the curve shows unexpected variations, as depicted by the segments highlighted in red. These rates correspond to those for which a lack of data produced the establishment of the network weights by chance, without following any logical criteria. Thus, though the progress of the curve is good in Figure 107.A and B, the ANN delivered a curve of aberrant values in Figure 107.C.

We have shown that when adding a combination of two components extragranularly, in case of tensile strength, this tablet property is still largely determined by the single components, whereas for the tablet disintegration, the interaction between the components acquires especial relevance. The establishment of contact networks between particles of different nature, which conformation presumably changes by reducing or increasing the proportion of the components, modifies the affinity of the end blend to the water uptake, which is different to that of the individual substances.

6.1.3.4 Extragranular addition versus intragranular addition

In order to analyze and compare the effect of the addition of a new component either within the granule or added extragranularly, we studied the tablet properties of formulations with the same composition but manufactured following different production steps. Hence, the second component was blended extragranularly with the MCC granules for the first formulation, whereas for the second, both MCC and the component were blended together prior to be dry-granulated.

In Figure 108 two separate plots are represented corresponding to the variation of the tablet tensile strength by progressive increment of LP and A200 as a function of the location of the second component (i.e., intragranularly or extragranularly) for tablets produced at 54 and 200 MPa. It is clear that there is a noticeable deviation of TS values between batches. Hence, in Figure 108.A, not only the total tensile strength is increased, but also the patterns vary depending on whether LP is part of the granule or not. Thus, when LP is component of the granule, the tablet strength suffers an abrupt

increase already at low LP proportions (Figure 108.A). When LP is granulated together with MCC, the plasticity of the substance increases the compressibility of the blend, which can deform more effectively than the granule made of 100% MCC. However, extragranularly added, the plasticity of LP reduces the tablet strength. This could be due to the high sensitivity of the blend to the addition of a lubricant, as LP lowers the propensity of the blend to establish particle interlocking and thus generates weaker bonding contacts.

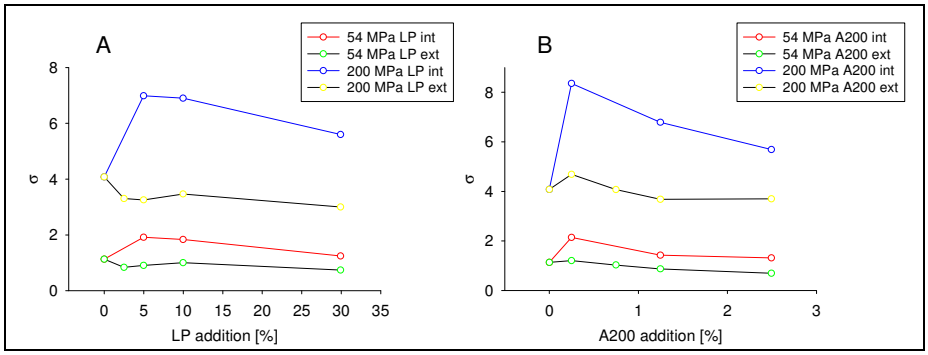

Figure 108. Tablet tensile strength values of batches with the same quantity of second component added intragranularly (*int*) and extragranularly (*ext*)

As for A200 (Figure 108.B), the profiles of the internal addition are parallel to those of extragranularly added A200. However, when A200 is added intragranularly, the steeper increase in tensile strength and the higher values kept through all A200 concentrations point to a much more accentuated enhancement of the particle bonding. When both components are mixed together, a bigger number of MCC particles of smaller size than the granulated MCC get in contact with A200, which results in granules with higher compressibility. The surfaces of the granules possess free A200, which also increases the potential number of granule-granule interactions. As a result, the tableting of compressible granules with a large number of contact points produces more cohesive tablets. Larger amounts of A200 again formed thick layers of free A200, and lowers the interaction between MCC particles reducing the material tabletability.

The values of tablet disintegration time are compared in Figure 109. Again, there are evident differences as a function of the location of the second component. Nonetheless, it is clear that these differences become more substantial at higher compression pressures (Figure 109.A). One can see that while the diagrams of dissolution time with increasing concentrations of LP are close to each other for tablets produced at low pressure, the difference of values becomes larger for the produced at high compression pressures. For substances that disintegrate by dissolution (e.g. LP, LMH, MNT), similar intermediary tablet solid fractions (0.74 in both cases at 54 MPa) ensure the water uptake by the tablet in a very similar extent. However, at higher compression pressures, the porosity is reduced and the water uptake depends almost entirely on the material inherent capacity of interacting with water. In that case, while the extragranular LP delays exclusively the intergranular dispersion of water, the intragranular LP slows down, in addition, the intragranular dispersion, which results in a much more marked extension of the disintegration time.

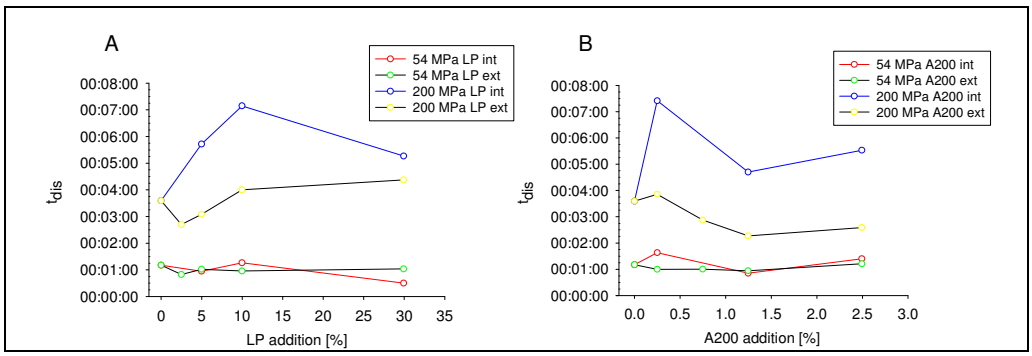

Figure 109. Tablet disintegration time values of batches with the same quantity of second component added intragranularly (*int*) and extragranularly (*ext*)

In Figure 109.B we can observe a similar trend for the addition of A200. At low compression pressures, both batches present similar profiles, while for tablets produced at 200 MPa (i.e., less porous) the difference between intra- and extragranular A200 are more extensive. This is owing to the fact that in denser tablets, if A200 is granulated with the MCC, the complex distribution of A200 within the granules, between small size particles of MCC, results in a slow distribution of water throughout the tablet mass.

6.1.4 Conclusions

The properties of produced dosage and the blend processability change after any modification in the formulation. The variations introduced by the extragranular addition of substances shows that not only the interaction of the external additive and the granule, but also the interaction of the external substances with each other (in case of the addition of more components simultaneously) causes changes in the behaviour of the formulation and the resulting properties of the product. In case of the extragranular addition of two components, the changes in the tablet tensile strength are the sum of the effects produced by the external substances individually, whereas for the variations in the disintegration the interaction between substances plays an important role.

Formulations of identical composition can result in dosage forms with dissimilar properties as a function of the processing steps followed for their production. Thus, the addition of the same amount of components intragranularly or extragranularly originated tablets with divergent tensile strength and disintegration time values. The effect of the addition of one or more components in the granulating blend (i.e. the generation of granules made of multicomponent mixtures) is studied in the next section.

ANNs have demonstrated to be able to process complex data with no evident correlation between variables in order to draw relationships between them. In this section they have revealed that they can decipher general trends in the end tablet properties due to modifications in the composition from the experimental data. However, the accuracy of their predictions depends on the ANN architecture, the amount of data and the inherent complexity of the relationship between variables.

6.2 Multicomponent formulations

6.2.1 Introduction

The task of developing and optimizing formulations is restrained in one hand by the lack of recommendations of a standard strategy to be followed for the selection of substances during the formulation. On the other, the extensive research done in formulation has been carried out mainly for single components or very simple blends. Hence, the influence of the composition on tablet attributes has been widely studied for single model excipients and binary mixtures [44, 53, 292, 324, 325]. Only a little effort has been focused on the study of multicomponent formulations. Moreover, the studies present in the literature dealing with this kind of formulations are centred rather in the establishment of excipient-drug compatibility [326, 327] or, as we are going to see in 6.3.1, they simply used the experimental data to model the composition effects on the end product attributes. As we have shown in the previous sections, there is a large number of variables that are involved in the conformation of a solid dosage form. This complicates extraordinarily the visualization of the effects introduced by the components of the formulation. Moreover, the system becomes extremely intricate for each further component added to the formulation. Accordingly, changes in the component proportions, as seen in 6.1, generally do not follow any linear or evident pattern, although estimations and rough calculations can be done by fitting mathematical regressions and by creating ANN models (see section 6.1 and 6.3).

In this section we consider multicomponent mixtures for the identification of the effects originated by the variation in the formulation on the product properties. In order to elucidate this, we have structured the analysis so as to neglect dry-granulation and tableting variables. Hence, process conditions are kept constant for all experiments and only one tableting pressure (100 MPa) has been taken. The trends drawn by the experimental points were compared to the approaches calculated by ANN models. As a result, we obtained information about the behaviour of the components and we learned in what extent they are involved in the modulation of the product attributes.

6.2.2 Materials and methods

As described in page 122, two different groups of formulations for multicomponent mixtures were considered. For each of them the principal components (i.e. the substance present in larger quantity) were microcrystalline cellulose (MCC) in case of the *group 1,* and mannitol (MNT) for *group 2*. The other components and the proportions present in each batch are listed in Table 20. The exact composition for the batches is furthermore listed in the Tables 36 and 37 in the Appendix, section 9.4. An especial remark is that in this section we also introduced paracetamol (PL) as API in some of the formulations.

The corresponding amount of each substance was calculated so as to reach a total weight of 2 Kg of material. The bulk was blended for 15 min at 60 rpm in the planetary mixer. Thereafter, MgSt was added as a lubricant and was mixed for 2 min. The variable corresponding to the quantity of MgSt

added was neglected in the analysis since the same amount was used for all blends (0.5% w/w). The blend was next roller compacted and granulated. The roller conformation and the assembly of the Gerteis MiniPactor were as described in 4.6.1. The compaction specific force was set at 5 kN/cm and the gap between the rollers was 3 mm. The rotational speed was set at 2 rpm. The granulation unit was assembled and set as in 4.6.1. After the gap variation approached ± 0.1 mm, ribbon samples were taken as described in 4.6.1 in triplicate. Also the produced granule was collected for its characterization and the production of tablets.

Table 20. Composition of the multicomponent fomulations

MCC - group 1-	A200	LP	ADS	PL
	0%	0%	0%	0%
	0.25%	5%	2.5%	10%
	1.25%	10%	5%	20%
	2.5%	30%		40%
MNT -group 2-	KVA64		ADS	PL
	0%		0%	0%
	1%		2.5%	10%
	2%		5%	20%
	4%			30%
				40%

The relative density (solid fraction) was measured with the punch method (section 5.1.2.3). The relative density of a total of 10 ribbon fragments was determined. The compact height was measured at 5 different points of the specimen and the hollowed fragments were weighted with the analytical balance No. 1. The tensile strength of 10 ribbon fragments was calculated as specified in 4.11. The ribbon width (*W*) was assumed to be 3.5 cm (corresponding to the roller width). The ribbon thickness was measured with the calliper No.1.

As for the granules, the same characterization tests as in 6.1 were carried out. Moreover, a sieve fractioning for the determination of the size distribution of the granules (see 4.10) was performed. The mesh opening sizes of the sieve set were 800, 710, 500, 400, 315, 250 and 100 μm. The cumulative distributions were fitted to RRSB distributions from which the parameters *d'* and *n* (see also 4.10) were chosen for the characterization of the granule size. Finally, tablets were produced for each batch at 5 different compression pressures and were characterized (tensile strength, disintegration time). For this section, however, the data generated exclusively for tablets produced at 100 MPa was considered. Finally, the API-release profiles for the tablets were obtained. For that purpose, dissolution tests were carried out as described in section 4.13. The t_{80} value was employed as a characterization value for the release rate of the formulation.

The data collected was organized in worksheets in order to simplify its representation and to structure the data sets that had to be part of the ANN modelling for the evaluation of the trends observed in the experimental results. The same ANN software as in section 6.1 was used here. Separate ANNs were created for the estimation of each variable. The architecture used in all cases was the multilayer perceptron (MLP) (see 2.3.3). The optimization of the number of nodes in the hidden layer was evaluated by examining the performance of the networks generated (i.e. checking the correlation coefficient for the relationship between predicted and observed values). The end architecture of the ANNs for each modelled characteristic is reported in the results. The response graphs generated by the

corresponding neural network and the experimental values were plotted together in order to contrast the approached with the empirically observed trends.

6.2.3 Results and discussion

For each attribute, an ANN was generated in order to evaluate and confirm the trends observed. Therefore, the corresponding diagram of responses predicted by the ANN was plotted together with the experimental values as it also was done in 6.1.3.3. The architecture and the performance of each ANN are listed next in Table 21 and Table 22 , respectively.

As it can be extracted from Table 21, in general, a lower number of variables also needs a reduced number of neurons in the hidden layer. As for the performance of the network, almost all obtained ANNs presented an acceptable performance. The major part presented good correlation coefficients and low standard error values (Table 22). However, the networks corresponding to the group 2 show better accuracy, which was unexpected, considering that the number of cases studied (n = 15) is much lower as for group 1 (n = 30). Also the deviation of the estimations is smaller for the approaches made by the ANNs from the second group.

Table 21. Record of the architecture of the generated ANNs

	Variable	Input layer		Hidden layer		Output layer
		Group 1	Group 2	Group 1	Group 2	Both
Ribbons	ρ_{rel}	5	4	6	6	1
	σ	5	4	3	13	1
Granules	n	5	4	3	2	1
	D'	5	4	7	3	1
	rep .angle	5	4	6	5	1
	CI	5	4	8	7	1
Tablets	σ	5	4	11	7	1
	t_{dis}	5	4	3	6	1

Table 22. Performance of the generated ANNs

	Variable	r^2		SE	
		Group 1	Group 2	Group 1	Group 2
Ribbons	ρ_{rel}	0.9051	0.9830	0.8160	0.2601
	σ	0.8290	0.9893	0.1811	0.0194
Granules	n	0.6773	0.9238	0.0165	0.0102
	D'	0.7260	0.8233	37.4584	26.0023
	rep .angle	0.9208	0.9937	0.7277	0.1170
	CI	0.9085	0.9999	0.0165	0.0021
Tablets (100 MPa)	σ	0.9360	0.8542	0.25	0.0593
	t_{dis}	0.8662	0.9588	0.0019 (00:00:17)	0.0001 (00:00:10)

6.2.3.1 Ribbon properties

The neural networks corresponding to the modelling of the ribbon properties for groups 1 and 2 presented acceptable coefficient of correlation. As shown in the corresponding figures (Figures 110 and 111 for the ribbon density and Figures 112 and 113 for the ribbon strength), the ANN response graphs match the general profiles observed in the experimental data. Nevertheless, the fitting of the predicted plots seemed to be more accurate for group 1, though the r^2 and the SE values of the ANN predictions of Table 22 point at the contrary.

The effect of each component on the density of the ribbon from formulations of the group 1 (main component MCC) and the group 2 (main component MNT) is shown in Figures 110 and 111.

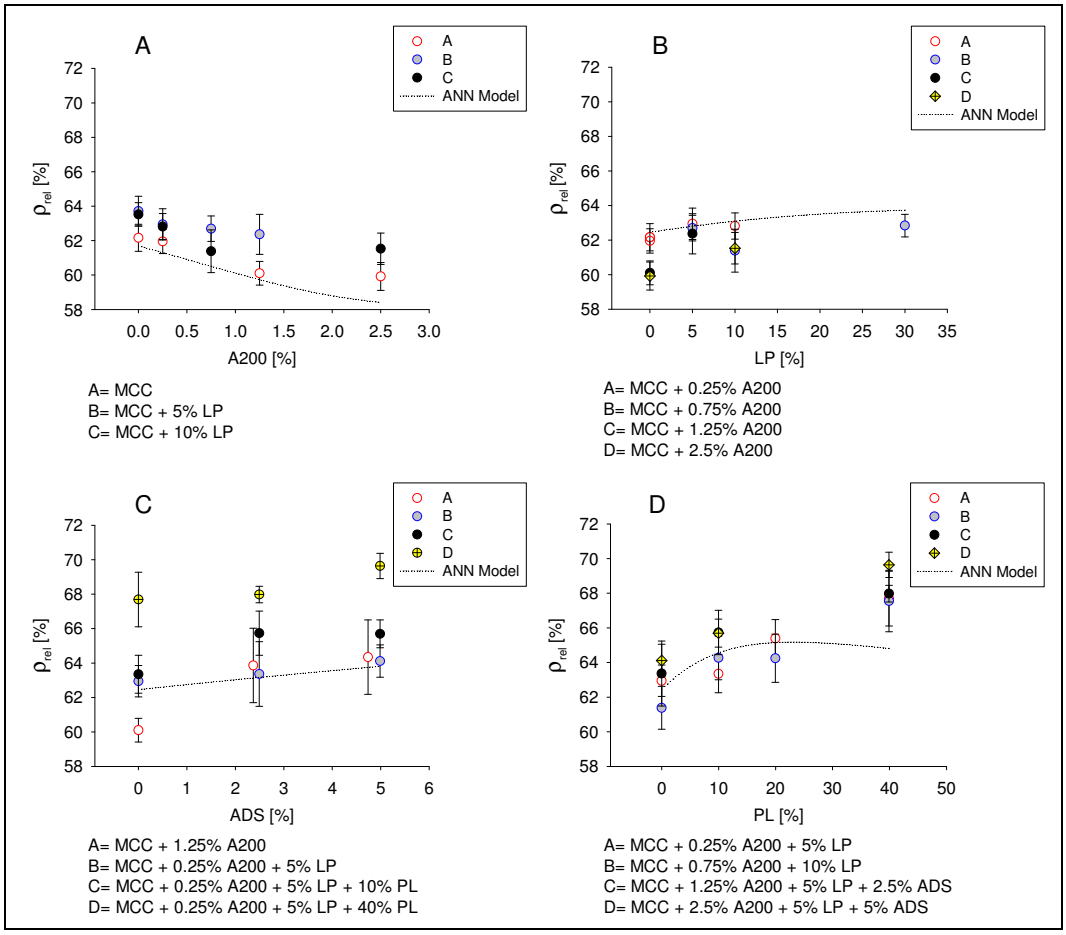

Figure 110. Group 1. Response of the ribbon tensile strength values to the modification of the formulation

As it can be seen in Figure 110.A, A200 reduces the compact solid fraction. The high specific surface of this substance increases the number of interparticular contacts, strengthening thus the internal friction and reducing the compactibility of the blend. Moreover, the low compressibility of A200 reduces the capacity of forming cohesive ribbons. On the contrary, as observed in Figure 110.B, the good compressibility of LP, reduces the minimum distance between particles so that the system reaches high densification levels. Increasing the amount of ADS improves the material densification (see Figure 110.C) which is in conformity with Ferrero, et al. [328]. They reported that ADS induced the reduction of the overall porosity of tablets as the plastic behaviour of cross-linked cellulose derivates reduces the inter-particle distance and increases the powder densification. However, as shown in Figure 111.B, in combination with fragmenting materials such as MNT and PL, the introduction of ADS seems to hinder the densification.

The increase in PL in the formulation resulted into denser compacts (Figure 110.D and Figure 111.C). Though having low compressibility [246, 329], PL volume reduction occurs mainly through particle fragmentation [330, 331] what enhances the formation of narrower inter-particular contacts and decreases the volume of the voids. In turn, the plastic deformation behaviour of KVA64 induced the reduction of the compact porosity (see Figure 111.A). However, high quantity of binder caused the contrary effect. Similar observations are described in [116]. The authors justified a decline in powder densification values by the negative impact of KVA64 on the powder flowability. An unsteady flow of

powder hinders the regular conveyance of material into the roller gap, diminishing the total amount of powder, and therefore, reducing the densification level of the material.

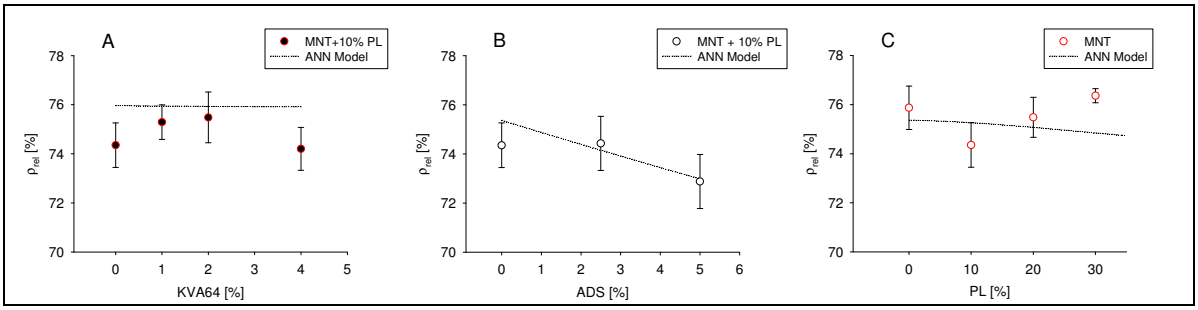

Figure 111. Group 2. Changes in the ribbon relative density by varying the formulation composition

The ANN response graphs for the ribbon density of both formulation groups match up satisfactorily with the experimental values. Although the architecture of the networks was the same for both formulation groups (Table 21) and the regression coefficients of Table 22 point at the contrary, the curves from the group 1 converge better with the experimental points.

The other ribbon property studied in this section is the tensile strength (σ), which values are presented in Figures 112 and 113. In previous sections (5.1.1) we have mentioned that the compact tensile strength is proportional to the densification level reached by a given material. Nevertheless, as we prove next, when comparing different materials, the formation of denser ribbons does not produce necessarily harder compacts. A first evidence of this is the dissimilar cohesiveness achieved by compacts of the main components, MNT and MCC. MCC ribbons are less dense, but the ribbons are harder than those of MNT (compare the range of the y-axis between Figures 112 and 113). The characteristics of both materials were studied by Majuru and Wurster [332]. They compared the bonding capacity of MCC and MNT, among other substances, and noticed that MNT particles do not establish as strong interactions as MCC, resulting into weaker compacts. In a similar way, there are cases in which variations of composition originate denser ribbons that are looser.

The effect of A200 on the ribbon strength is shown in Figure 112.A. As commented previously (6.1.3), A200 possesses poor compactability properties which have a double consequence. It does not only hinder the achievement of denser ribbons, but also weakens the bonds between particles, and deteriorates the ribbon strength. As for plastic deforming materials such as LP, they enhance the material densification, but as no interlocking between particles is produced, the strength of particle interaction depends exclusively on the bonding forces at the contact surfaces, resulting usually in weak compacts (Figure 112.B). A similar effect is yielded by ADS in both groups (Figure 112.C and Figure 113.B, respectively). Unexpectedly, as seen in Figure 113.A, KVA64 shows no binding effect in formulations of group 2. Thus, low KVA64 concentrations even reduce the strength value. Nevertheless, at larger amount of KVA64, there is a certain trend of incrementing the tensile strength of the ribbon. As for paracetamol, the poor compressibility and the reduction of the strength induced by the addition of PL (Figure 112.D and Figure 113.C) is attributed to the combination of poor particle cohesiveness and bad compressibility characteristics, due to the extreme elastic recovery

experienced by the material [329, 333]. Consequently, most of the energy applied on the material is employed to overcome the particle elasticity and the resulting ribbons are also looser.

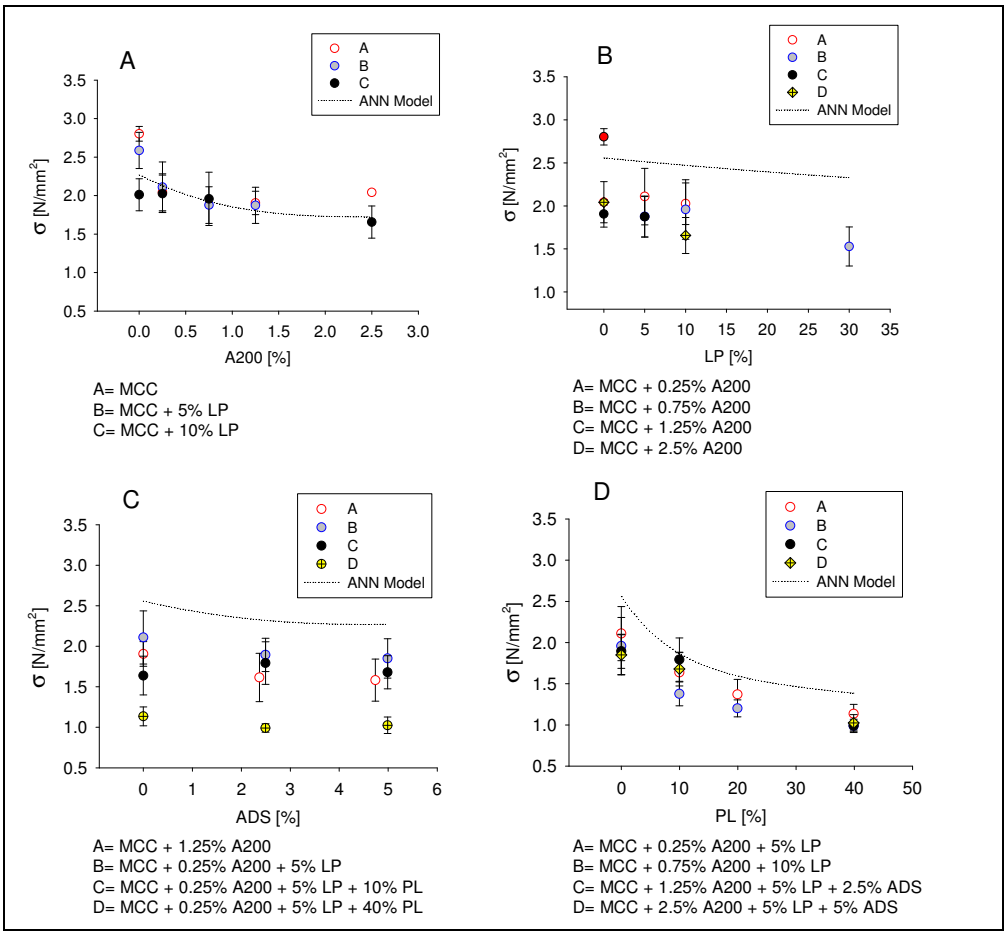

Figure 112. Group 1. Response of the ribbon tensile strength values to the modification of the formulation

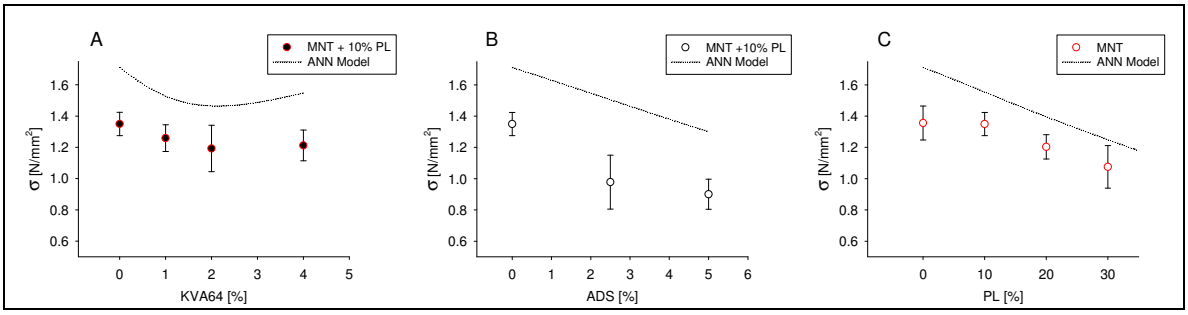

Figure 113. Group 2. Tensile strength changes introduced by the alteration of the composition

Again, the ANN response curves converged with the experimental data. However, as it happened with the ANN response graphs for the ribbon tensile strength, the ANNs created for the formulation group 2 show larger deviations from the experimental values. A very large number of hidden neurons (13) (Table 21), for a small number of cases, might have caused that the ANNs create the response from memorized relationships.

6.2.3.2 Granule properties

We have already described in section 2.2.2 that the attributes of the produced granules are defined by the properties of the ribbon resulting from the compaction process. We also have discussed in section 5.3.3 to what extent granule particle properties (PSD -particle size distribution-, porosity, mean size, particle morphology, etc.) influence the workability of the granule into tablets. Considering these aspects, in this section we analyze the effects that a modification in the formulation has on the PSD, the flowability and the compressibility of the produced granule.

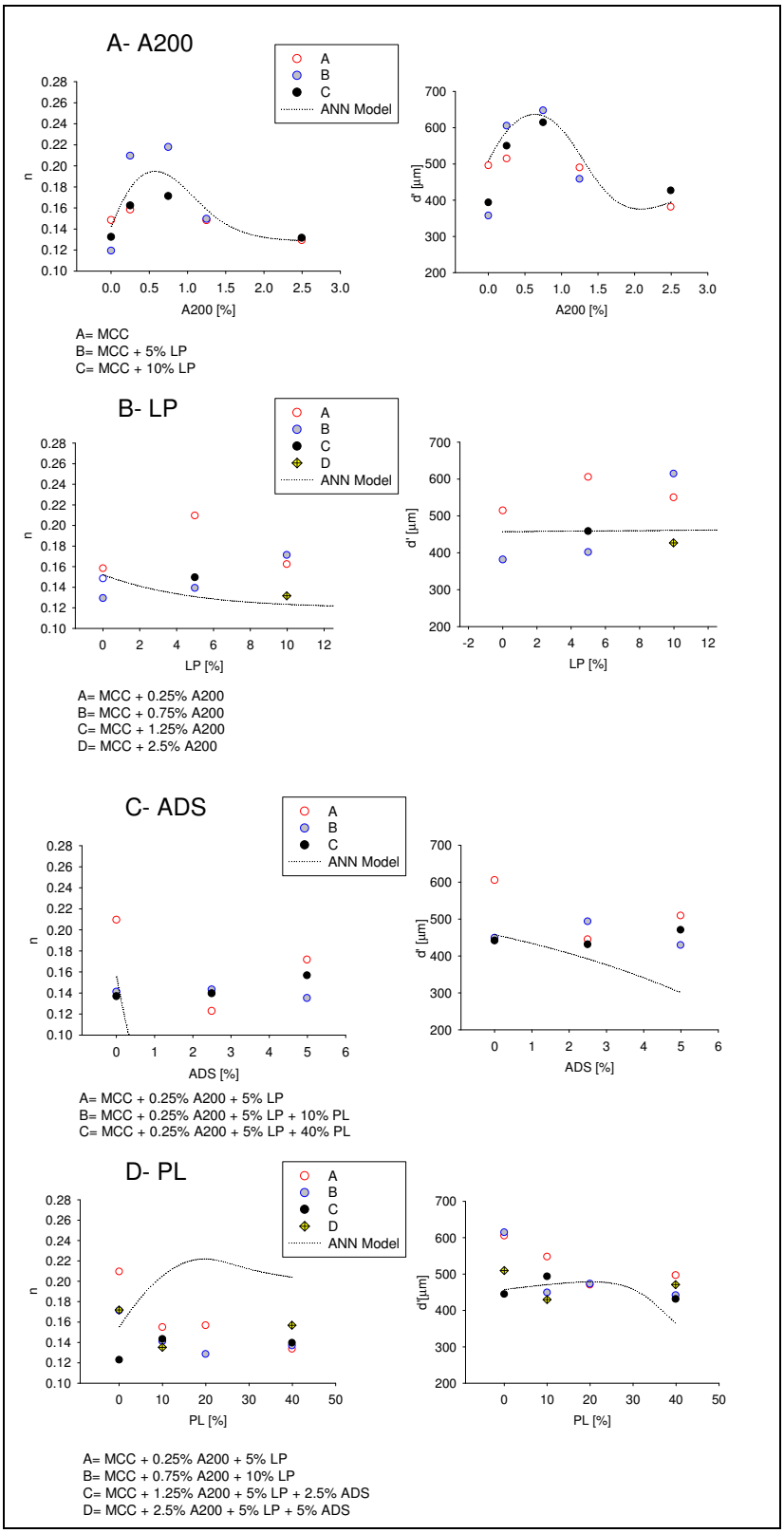

Figure 114. Group 1. Variations on the PSD induced by altering the composition

For the study of the PSD, the cumulative distribution of the particle size fractions of both formulation groups were fitted into a RRSB distribution presenting good linearity values ($r^2 \geq 0.97$). The parameters *n* and *d'* (4.10) together with the ANN response curves of both formulation groups are presented in the Figures 114 and 115.

The particle size distribution of the resulting granules is strongly influenced by the properties of the compact. Thus, a hard compact produces coarser granules with narrower distributions (i.e. larger values of *d'* and *n*). It can be seen in Figure 114.B, C and Figure 115.B that ADS and LP produced granules with wider distributions (*n* -value is reduced) and smaller size (*d'*-

values are also reduced). This is clearly attributed to the reduction of ribbon tensile strength experienced after increasing the amount of these excipients in the formulation. However, analyzing the effects of the addition of PL, (Figure 114.D and Figure 115.C) the evolution of the PSD is different for both formulations. PL reduces the ribbon strength and consequently, the resulting granules should become finer and the size distribution wider (Figure 114.D). However, in group 2 (Figure 115.C), when considering the experimental results, increasing paracetamol concentrations seem to originate larger granules with narrower distributions.

Also A200 exhibits an unexpected trend. Thus, as presented in Figure 114.A, low concentrations of A200 increase the value of both variables. A200 lessens the compact strength (Figure 112.A), however, as reported by Gray, et al. [334], it introduces electrostatic charging that causes an increase in the number of bonding bridges between particles inducing the spontaneous formation of aggregates, hence creating larger particles. Finally, the incorporation and the increment in the amount of KVA64 produced a slight increase in the value of both parameters (Figure 115.A). As a binder, KVA64 generally enhances the formation of stronger compacts and generates coarser granules. However, the unexpected low increase in ribbon strength and granule size demonstrates that KVA64 almost does not develop any remarkable binding effect on formulations with MNT.

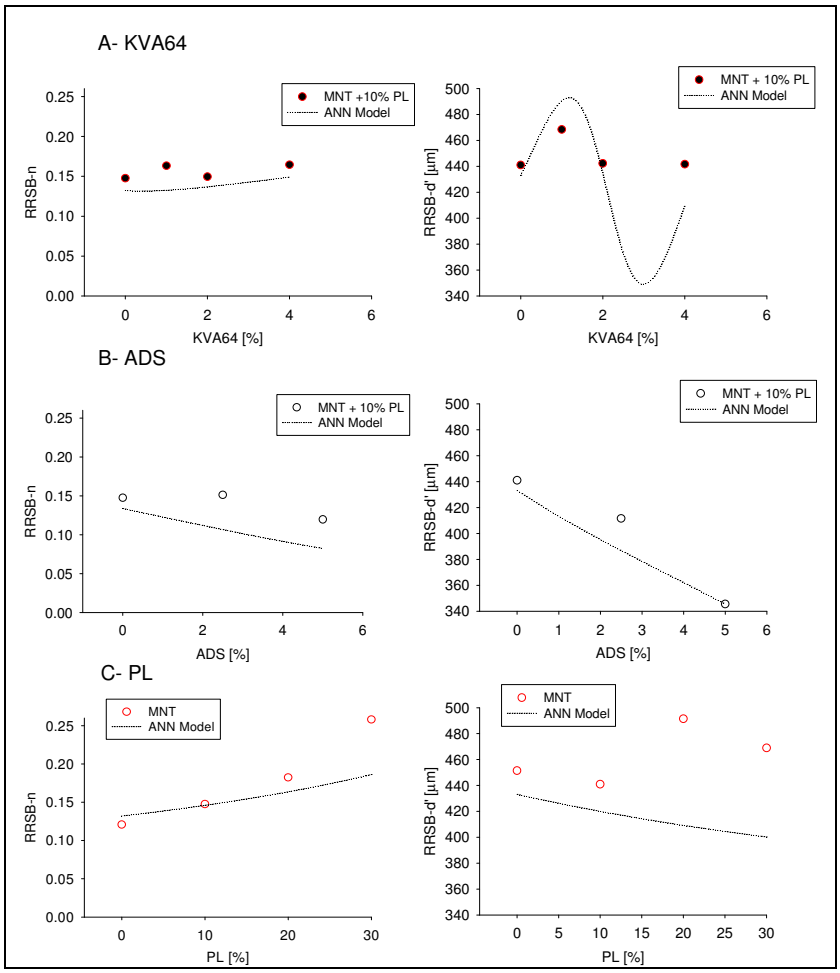

Figure 115. Group 2. Variations on the particle size induced by the changes of composition

Comparing the profiles of the response graphs of ANN models with the experimental values, it is evident that in Figure 114.B and D the predictions made by the ANN for the group 1 did not estimate satisfactorily the trends observed experimentally. This is due to the low performance neural networks obtained (r^2 = 0.678 for *n* and r^2 = 0.726 for *d'*) (Table 21). For the second group (Figure 115), the respective networks modelling the PSD-parameters presented better accuracy (r^2 = 0.924 for *n* and r^2 = 0.823 for *d'*). Consequently, the model responses for the second group are closer to the observed values, as shown by the SE values in Table 22, and as shown in Figures 114 and 115. Nevertheless,

the ANN model for the particle size, revealed the formation of finer granules when increasing the amount of PL and the response graphs drawn for the modelling of *d'* showed intricate curves, due to lack of experimental points, similarly as it was discussed in 6.1.3.3.

The second group of granule attributes studied are the granule flowability and its compressibility. The former is characterized by the value of the angle of repose of the poured bulk (4.8), whereas the latter is analyzed using the Carr index (*CI)* (4.9). These variables are two critical bulk properties in the tableting on which the interparticle interaction plays a basic role. Poor compressibility and low flowability have adverse consequences for the production of tablets. Interparticle adhesion is undesirable for the powder flow, but on the contrary, is required to ensure acceptable cohesiveness during the volume reduction [335]. Subsequently, if particles are prone to establish strong contacts between them, it will lead to poor flow properties (i.e. higher repose angle values) and hinder the particle rearrangement in the die. However, strong interactions will allow the formation of strong cohesive compacts.

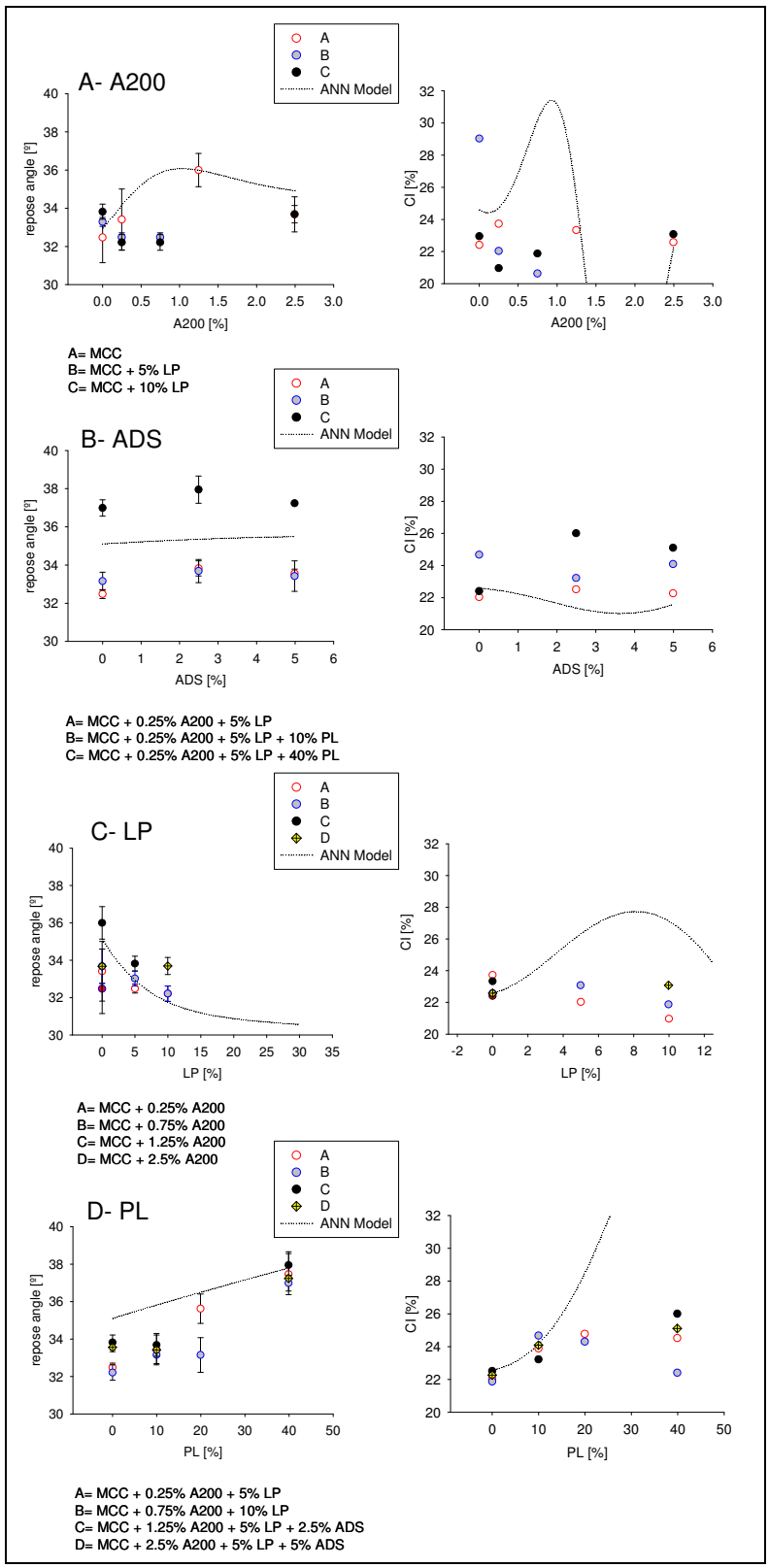

Figure 116. Group 1. Progress of the bulk flowability and compressibility due to changes in the formulation

As shown in Figures 116 and 117, angle of repose and *CI* are closely related. The enhancement of the bulk flow (lower values of angle of repose), which is caused mainly by a reduction of the interparticle interaction, produced an increase in the bulk compressibility (lower *CI* values). A200 increases the flow at low concentrations,

whereas larger amounts have a negative effect (Figure 116.A). This was already discussed in the previous experimental section (6.1.3.2) for the extragranular addition of this excipient and agrees with the findings of other authors [336]. As shown in Figure 116.B, ADS seems to reduce the particle mobility inducing a poorer flow and a reduced capacity of volume reduction (presumably by proliferation of the number of particle interactions), and consequently, the values of repose angle and CI increase. LP, in turn, causes a slight fluidization of the bulk, as shown in Figure 116.C. LP produced denser ribbons (Figure 111.B), and consequently, the granules present smoother surfaces. This enhances the bulk flow and its compressibility. As for PL, though it seems to generate denser ribbons like LP, its addition impedes the bulk flow (Figure 116.D). Paracetamol was reported to reduce the blend flowability [324, 335] due to large adhesion forces established between this substance and other components of the formulation, basically through Van der Waals forces. Therefore, the particle mobility is hindered, reducing the bulk flow and the material packing ability.

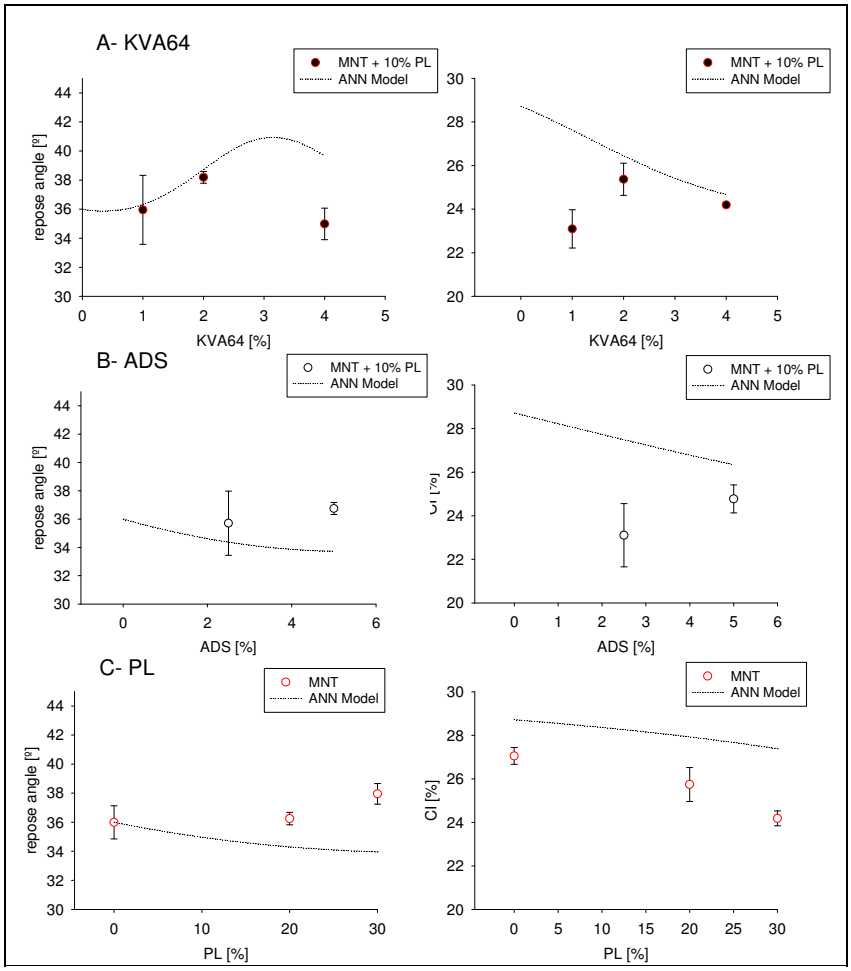

Figure 117. Group 2. Changes introduced in the bulk flowability and compressibility by the modification of the formulation

For granules from the group 2, similarly as for the formulations of the group 1, reduced flow involves generally less particle rearrangement. For instance, the effects observed after the addition of KVA64 (Figure 117.A) and ADS (Figure 117.B). KVA64 reduces the flow (and also the bulk compressibility) at low concentrations, due to its binding effect. Nevertheless, larger amounts of this substance have a positive effect. The addition of KVA64 in the formulation produces granules with more regular shape and less surface discontinuities, improving the bulk flow and increasing the compressibility. However, like it has been observed in the group 1, the addition of ADS (Figure 117. B) reduces the granule flowability. The granules generated after the addition of ADS show increased porosity, which enhances the particle interaction and reduces its mobility. In addition, this has again a negative effect on the bulk compressibility. As for PL, its addition in the formulation results in granules with worse flowability (Figure 117.C), which is attributed again to its proneness to generate inter-particle adhesion. However, the compressibility does not seem to be

affected by this. Thus, the value of the *CI* decreases, instead. As we have seen, the addition of PL makes the particle size distribution narrower, while the particle size decreases (Figure 115.C). Small sized granules can slip more easily to fill up voids generated between coarser particles, enhancing the compressibility of the granule.

The granule repose angle and the *CI* value were also modelled by means of ANNs. The model residuals to the observed values do not exceed a relative deviation of 3% for any case (Table 22), and the ANN approaches were linearly correlated with the observed values (the correlation values for both groups were ≥ 0.9) (Table 22), which proves the good performance of the models. In spite of this, the complexity of the calculation of the node weights and the generation of a response in a *black box*-like manner are evidenced in Figure 116.A for A200. The approaches of response graph for the *CI* manages to draw a curve that converges with the experimental data. However it shows an extremely intricate pattern.

6.2.3.3 Tablet properties

The change in the tablet properties with changing formulations is presented here. Only the results for one tableting pressure (100 MPa) have been considered. Again tensile strength (represented as σ) and disintegration time (represented as t_{dis}) are the tablet properties studied.

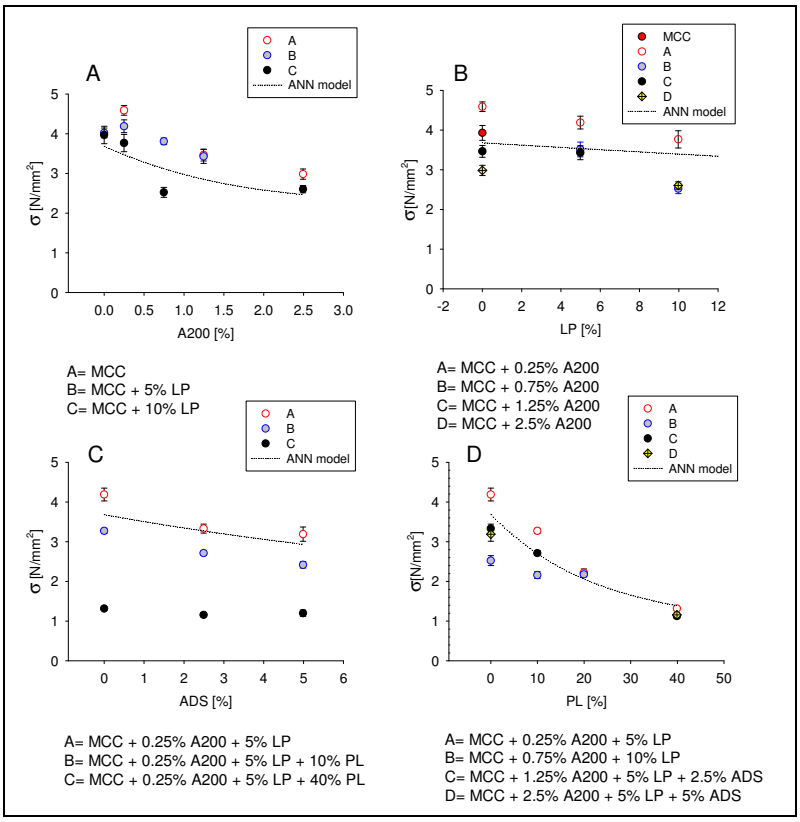

Figure 118. Group 1. Tablet tensile strength variations after the modification of the formulation (compression at 100 MPa)

In sections 2.1.4 and 5.3.3 the tabletability of a material was described to be defined by material elasto-plastic behaviour, the morphologic particle attributes and the strength of the bondings generated between them. Generally it is accepted that a material with good tabletability exhibits good powder consolidation (compressibility), a high bonding capacity, a small stress relaxation and a low lubricant sensitivity [313]. For a given compression pressure, the tensile strength provides hints about the material cohesiveness achieved by the tableting, the degree of elastic recovery of the material and the sensitivity of the blend towards the addition of lubricants. The t_{dis}, in turn, characterizes the general behaviour of the tablet when entering in contact with a watery medium and is directly related to the release rate of API. The time needed by the tablet to disintegrate is on one hand

dependent on the physical tablet properties, basically the porosity, but also on the hygroscopic behaviour of the formulation components.

As shown in Figure 118.A, with increasing amounts of A200 the granules originated tablets of lower tensile strength values. Though A200 improves the tablet strength already in small quantity when added extragranularly, this effect is not exhibited by the granules with intragranular A200, which presented reduced tablet cohesiveness. This has been already discussed in 6.1.3.4. Increasing the amount of LP in the formulation (Figure 118.B) also produces weaker tablets. As commented in previous sections (5.3.3.4), LP is a strongly plastic material and this kind of materials reduce considerably their compactibility after roller-compaction granulation, producing less deformable granules, and consequently, extending the energy necessary to overcome the elastic recovery. ADS reduced the material plasticity, losing its capacity to deform and generate new bonding points. As a consequence and, as seen in Figure 118.C, the tablet σ drops at increasing ADS concentrations. Finally, also PL has a negative effect on the tablet strength [337, 338]. PL is a low compactable material [324] as seen before for the ribbons. The elastic recovery suffered by the material [339], its brittle and fragmenting characteristics [331], and the low binding capacity [335] confer lower tensile strength to tablets.

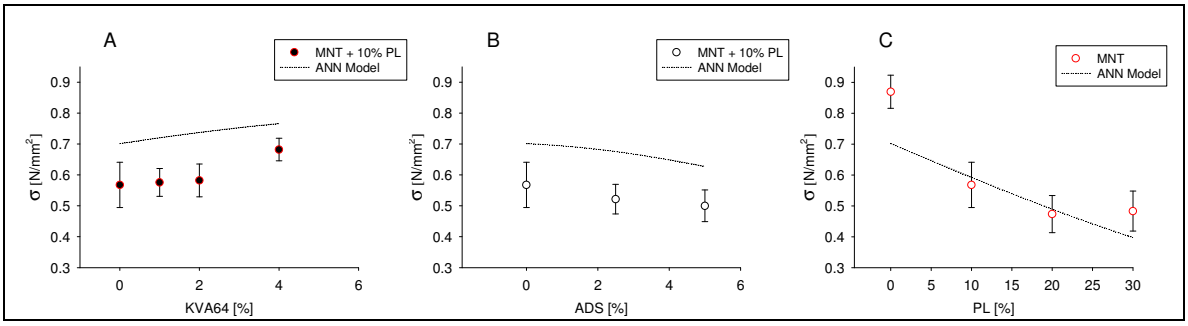

Figure 119. Group 2. Tablet tensile strength variations after the modification of the formulation. (compression at 100 MPa)

Figure 119 shows the effect introduced by the addition of components in the tensile strength of tablets from the formulations of the second group. Interestingly, the strength values are lower than for the group 1, as it has been observed for the roller compacted ribbons. The MNT used here is a β-crystalline form which presents very poor tabletability properties [340]. MNT deforms basically by fragmentation [332] and presents low bonding indexes. The low plastic yielding of MNT particles makes the re-processing of the material into tablets more difficult and reduces even more the capacity to generate cohesive structures. As a consequence, during the performance of our experiments, we were not able to produce any consistent tablet at compression pressures below 100 MPa for some of the formulations. Analyzing the addition of further components to MNT, ADS (Figure 119.B), and PL (Figure 119.C) cause similar changes in the σ as in group 1. Nevertheless, the addition of KVA64 (Figure 119.A) shows positive effects on the tablet densification. Tough the effect is unusually low, considering the overall brittleness and the poor compactability of MNT, the tablet weakness is due to the failure of the tablet structure mainly at the contact points between MNT particles, cancelling any improvement of the tablet strength by the binding effect of KVA64.

The low SE values of the ANN models of Table 22 are consistent with the proximity between the ANN response graphs and the empirical values observed in Figures 118 and 119. However, the ANN models generated for the prediction of tablet σ were more accurate for the group 1 ($r^2 = 0.9360$) than for the group 2 ($r^2 = 0.8542$).

After having analyzed the t_{dis} for the different compositions, any clear relationship between tablet strength and disintegration time could not be found. This is attributed to the fact that although harder tablets of the same material correspond generally to denser and less water permeable tablets, in some cases the affinity of the formulation components to water becomes of stronger influence over the disintegration than the tablet permeability. As we have already seen in section 6.1.3.4, the distribution of the corresponding components has considerable weight on the modulation of the tablet disintegration. Accordingly, A200 added to the blend prior to dry-granulation (also in combination with other substances), does not accelerate the tablet disintegration like added extragranularly (Figure 120.A). As depicted in this diagram, the enhancement of the tablet disintegration by A200 becomes less noticeable and the disintegration time can be even extended. Though tablets become more porous with increasing amount of A200, the complexity of the distribution of A200 within the granule reduces the A200 free on the granule surface. Consequently, the water distributes throughout the tablet mass slowlier. The different behaviour of LP extra- or intragranularly was also analyzed in section 6.1.3.4. Generally, low quantity of LP within the granule extends the time of disintegration, whereas higher amounts reduce it (see Figure 120.B). The extension of the disintegration is attributed to the fact that LP is a plastic material (i.e. reduction of the tablet porosity) which mechanism of disintegration is passive and slow. Higher concentrations of LP, on the other hand, reduce the compactness of the tablet, which needs shorter time to fragment in contact with water. In Figure 120.C ADS reduces the time of disintegration, which is inherent to the substance. As a so called *super-disintegrant*, the polymer changes its structure in contact with water, inducing the swelling of the material. The penetration of water is accelerated, reducing thus, the disintegration time [8, 323, 341-343]. Contrariwise, PL lengthens the tablet

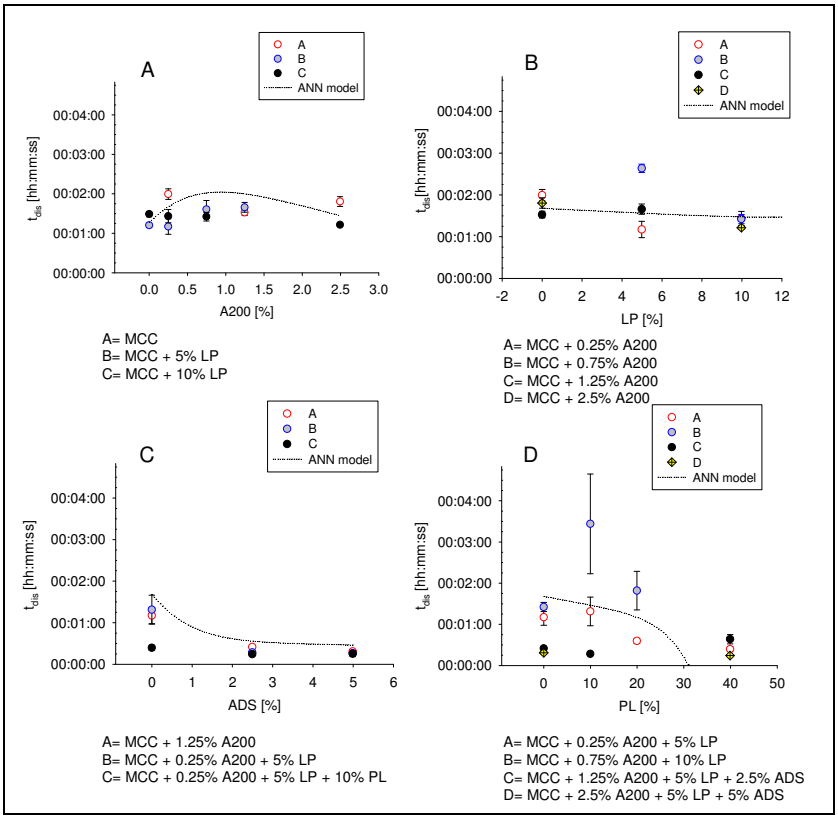

Figure 120. Group 1. Disintegration time variations after the modification of the formulation. (compression at 100 MPa)

disintegration (Figure 120.D). According to Martinello, et al. [337] one explanation for this is the rearrangement of the fragmented PL particles throughout the voids, reducing substantially the tablet porosity [338]. Moreover, the disintegration mechanism, like lactose, is the breakage of particle solid connections by dissolution, which is a slow process. As a consequence, the disintegration of tablets and granules containing PL is extended. Large quantities of PL, on the contrary, reduced the disintegration time, since particle adhesion lessens abruptly (see the progress of the tablet σ in Figure 118.D) and the disintegration of the tablets is complete after shorter time.

Though MNT is considered one of the saccharide-like fillers with the shortest disintegration time [344], the tablets containing MNT disintegrate slowly. Accordingly, MNT tablets in this study show very low tablet σ but relative long disintegration times. In Figure 121A to C the effects of the components added to MNT in the formulations of the group 2 are presented. None of the components in common with the group 1 (i.e. ADS and PL) showed the same behaviour. Moreover KVA64 exhibited again a completely unexpected profile. In Figure 121.A, the addition of KVA64 reduced the disintegration times, what contradicts the reported by others [116]. ADS also showed an anomalous profile (Figure 121.B), in which the disintegration time did not keep on decreasing for larger quantity of superdisintegrant. In turn, PL (Figure 121.C) extended the disintegration time almost linearly proportional to its concentration. The unexpected effects observed for the three components are related

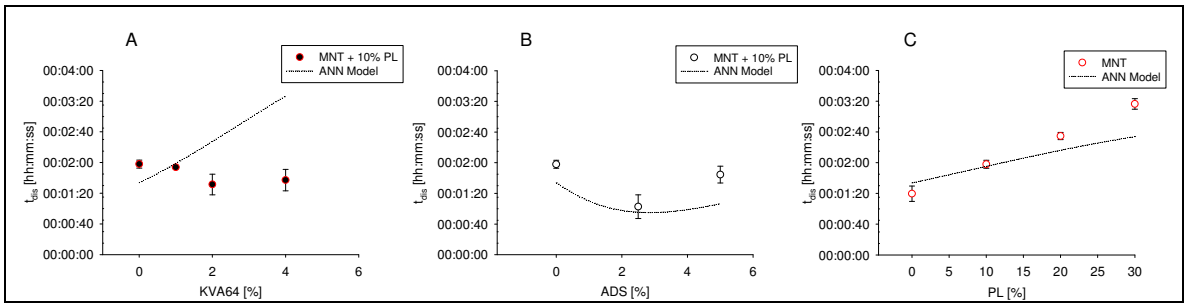

Figure 121. Group 2. Disintegration time variations after the modification of the formulation (compression at 100 MPa)

to the mechanism of disintegration of MNT and the morphology of the tablets. MNT leads to denser and slow disintegrating tablets. Dense tablets slow down the permeation of water into the tablet, which explains the low disintegrating action of ADS. Water does not reach so easily the regions in which ADS is present, so that ADS can contact the medium only after MNT dissolves. In a similar way, if there is a second substance such as PL, which dissolution takes even longer than the one of MNT, the overall disintegration is subsequently extended. However, the only logical explanation for the positive effect of the dry binder on the tablet disintegration is that KVA64 is hygroscopic [345] though it is considered to be less hygroscopic than other povidones [346]. MNT is a well known low hygroscopic substance [308] and, therefore, the stronger water affinity of KVA64 for water causes the faster disintegration of the tablet.

ANN models showed here accuracy in the calculation of estimates. Acceptable correlation and a very low SE values of few seconds (see Table 22), point out that the models have reached a satisfactory performance. This is moreover reflected in the proximity of the curves generated with ANN and the experimental points.

6.2.3.4 Drug release

The value of t_{80} was considered as the reference for the release rates. However, the data set available for the group 1 is not sufficient for the graphical representation of the effects of all components individually. In Figure 122 the effect on the dissolution time due to the addition of ADS is presented. As expected, the addition of a *super-disintegrant* in the formulation increases the release rate of the dosage form. . The addition of disintegrant was necessary in the formulations of the group 1, since the initial formulations (i.e. without ADS) did not fulfil the requirements established by the USP 31 [3] regarding the release time ("*not less than 80% has to be dissolved within 30 min*"). In addition, the deviation between t_{80} values of the tablets tested was considerable (SD above 7 min). A small addition of super-disintegrant was already enough to achieve the USP specifications and reduce the span of release times between specimens. Nonetheless, it is worth commenting that there is a strong enhancement with small quantities of ADS, while this effect is moderate after further addition. There seems to be a critical concentration of ADS up to which its activity does not increase. Thus, once this amount is exceeded, the dissolution time becomes exclusively a function of the own time of dissolution of the crystalline form of paracetamol

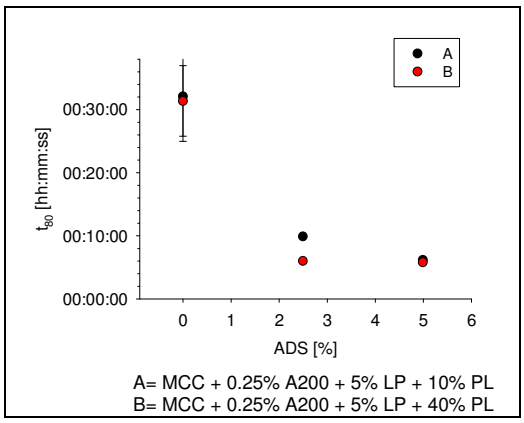

Figure 122. Group 1. Effect of ADS on the t_{80} values for the PL release times

Concerning the API release of tablets from the second group, the evolution of the rates after addition of the other components responded as expected. Accordingly, the addition of the dry binder KVA64 (Figure 123.A) increased the release time, whereas the addition of disintegrant (Figure 123.B) improved the tablet release ratio. PL shows also here a retarding effect on the dissolution (Figure 123.C), which is in line with the results reported by Martinello, et al. [337]. Again, the weak improvement of the drug release by ADS in formulations with MNT is due to the low tablet permeability and to the fact that the release time becomes a function of the dissolution of the own API crystals.

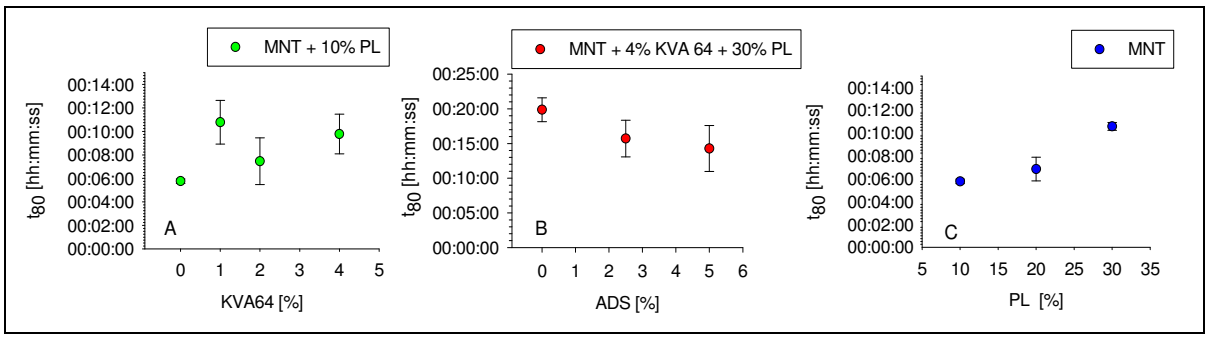

Figure 123. Group 2. Changes in the API release rates induced by the addition of the components to the formulation

6.2.4 Conclusions

Any modification in the initial formulation induces changes in the processability of the initial blend. This might produce variations in the material behaviour during roller compaction, changing the

properties of the resulting ribbons, which, in turn, affect the properties of the granules. As a result, the granules produced exhibit different tabletability and tend to establish different inter-particle interactions that also affect the main attributes of the resulting tablets.

Since the response of the component depends largely on its interaction with the rest of substances of the formulation, the addition of a same substance can show different effects depending on the formulation it has been added in.

To explain the progress on the tablet critical attributes (σ, t_{dis}), not only the tablet morphology (e.g. porosity), but also the inherent physical-chemical properties of the formulation components (e.g. bonding index and water uptake) need to be considered.

It has been shown that ANNs are useful and trustworthy tools suitable to identify, evaluate and quantify the patterns of changes experienced by the properties of intermediary and end products. The reliability of the models created needs to be quantified by means of model performance parameters. This evaluation yields enough evidences to ascertain whether the approaches made by the model are close to the real values or not.

6.3 Predictive models with GRM and ANN

In sections 6.1 and 6.2, we discussed the influence of the formulation composition on the properties of ribbons, granules and tablets. These experimental data provide the input for the experimental knowledge that is going to be included in the expert system described in section 7. However, these data can be pertinently processed to create models that aim to establish relationships between variables and response values. Moreover, these models can become valuable tools for drawing particular and general trends of variability underlying intricate interactions within the formulation components and between them and the processing variables.

In this section, we carried out an extensive study on the modelling of compact, granules and tablet attributes based on the results of previous sections. We examined the viability to use ANNs and general regression method (GRM) models for predicting product properties from the initial formulation and the processing parameters. The experimental data used to create, train and validate the models was originated following a classical systematic formulation (sections 6.1 and 6.2), i.e. only a single parameter was varied at a time. In the modelling, the composition was considered as an independent (predictor) variable, whereas the intermediary and end product properties were the dependent (response) variables. For modelling tablet characteristics, the compression pressure was also considered as independent variables. The accuracy and the predictability of all models were tested. For the former, the corresponding fit and deviation parameters were calculated. As for the latter, the predicted values for the intermediary and the end product properties of new formulations were compared to the data obtained experimentally. The developed ANNs and GRM models were finally implemented in the knowledge-base of the expert system, as described in section 2.3.2.1.

An additional group of experiments has also been included in this section. They deal with the use of ANNs as tools for implementing historical data to complete missing values from the pool of experimental candidates demanded by *design of experiments* (DOE) applications. Three different models calculated by the DOE program were compared. For the first one, the incomplete pool of experimental data was directly used for the model generation. The second one, however, was the result of processing the pool completed by using the combination of experimental values and ANN predictions. Finally, the third one was obtained exclusively by introducing the response values obtained by ANN predictions for all cases in the DOE. Furthermore, again all models were validated.

6.3.1 Introduction

6.3.1.1 ANN models

The principles of ANNs, the parameters that have to be taken in consideration for the creation of new networks, and the applications in the pharmaceutical formulation found in scientific works are described in detail section 2.3.3.2. ANNs are considered *deciphering tools*. However, it is impossible to do any interpretation or to extract clear information about the interaction established by the network

between the modelled variables. For this reason, it is commonly said that ANNs models possess *black box* characteristics.

The modelling through ANN comprises the generation of a network for the number of variables and cases it is being worked with. Once the PEs are weighed (i.e. the network is trained), the ANN has learned and has found the relationship between dependent and independent variables. This ANN is then able to generate a response value for unknown cases (i.e., is able to generalize) and, as already shown in previous sections, it also can provide response diagrams based on two variables, or even multivariable response surfaces. The goodness of prognosis depends on the network properties such as the architecture and the activation function. However, the quality and the biased character of the data set used during the development of the network also determine whether the responses generated by the ANN model are valid or not.

6.3.1.2 Mathematical models

Mathematical expressions have been traditionally used for the establishment of relationships between variables [41, 347]. Concretely in tablet formulation, different strategies for creating mathematical expressions have been followed in order to describe and model the tablet properties. One of them is the prediction of the end-product properties based on the composition and the processing variables using linear and power law mixing rules [53-55]. These assume that the variation of a property induced by a component is directly related to the amount of the component in the formulation. For the linear mixing rules, the volume fraction of each component in the end formulation becomes the multiplying factor of the effect produced by the component individually, whereas for the power law rule, the effect of the components is modulated by exponential parameters whose value vary from substance to substance.

The other methodology is the fitting of mathematical expressions that approach the response generated from the values for the independent variables considering that the response does not vary proportionally as a function neither of the volume fraction of the component nor of the linear interaction between components and processing parameters. The idea of the regression models is to find a mathematical function that generates a response close to that observed experimentally considering the values of the independent (predictor) variables and the equation parameters. In Table 23 a list of the most common regression analysing designs for continuous variables is given. The selection of the regression design will be a function of the number of variables and the potential interactions between them. For instance, multiple regressions are multiple variable analyses for which the main components (i.e. the individual variables) are considered to be independent from each other. Polynomial regressions also contemplate the individual variables and set *n*-order effects for the continuous

Table 23. Principal types of general regression analysis

Regression design	Exemplified equation
Polynomial	$Y = b_0 + b_1A + b_2A^2 + b_3C + b_4C^2$ $(Y = b_0 + b_1A)$
Multiple	$Y = b_0 + b_1A + b_2B + b_3C + b_4D$
Factorial	$Y = b_0 + b_1A + b_2B + b_3AB + b_4C + b_5D + b_6CD$
Fractional factorial	$Y = b_0 + b_1A + b_2B + b_3C + b_4AB + b_5BC$
Response surface	$Y = b_0 + b_1A + b_2A^2 + b_3C + b_4C^2 + b_5AC$
Mixture surface	$Y = b_1A + b_2B + b_3AB + b_4C + b_5D + b_6CD$

predictor variables. Factorial regressions, however, consider the effect of single variables on the response but also establish interactions between them. Mixture surfaces, on the other hand, are similar to factorial regressions only without intercept. Finally, response surfaces are multiple variable regressions in which not only n-order effects of the individual variables but also inter-variable effects are included. The selection of one regression design or the other is, therefore, based on the previous knowledge and the assumption of the network of interactions established between variables that generate the response.

As a result, the predictors and the dependent variables are fitted into an equation (i.e. the regression model is generated). The fitting (regression) equation is formed by an estimated intercept (b_0), if applicable, and by multiplying parameters (b_1-b_n). The latter correspond to the magnitude of the effect(s) on the end response introduced by a variable, the *n*-order effect(s) of the variable, or the interaction of multiple variables. Moreover, the expressions can be represented as a diagram to depict, in a visual way, the evolution of the response. However, the validity of the mathematical expression has to be tested in order to be accepted as the equation that fits the best the observed response. If the equation does not fulfil the requirements that the experimenter imposes on a good model, the next step is to redefine the regression and to evaluate the new models again.

A very recommendable practice to be followed when generating mathematical models is to try to generate as short and simple expressions as possible. This is not only for aesthetic reasons, but also because models based on simple mathematical expressions present obvious advantages over complicate long equations. They are easier to test and to understand, so that the interactions between variables and their effects are more evident and easier to be identified. Moreover, they are more manageable for their integration and implementation into the expert system reducing at the same time possible mistakes during the transference of regression parameters into the knowledge base.

Mathematical models were applied in formulation before ANNs became popular in the early nineties. Already in the eighties [11, 348] the mathematical modelling found acceptability between formulation researchers [48, 205, 206, 347]. Also known as response surface methodology (RSM) when adopting large degrees of complexity, the mathematical modelling has found applications not only in the optimization of formulations [13, 349, 350] and process parameters [351], but also in the characterisation of the behaviour of excipients during the compression [38, 350].

After the first application of ANNs in formulation appeared (see Table 7 in 2.3.3.2), in the mid and late nineties some publications were released in which ANNs and mathematic models were compared in formulation studies [134, 176, 177, 181, 182, 184, 337, 352, 353]. Although there are differences between both methods (they will be mentioned later on this section), all studies agreed that one can accommodate experimental data with regressions and even create predictive models by means of both modelling strategies.

6.3.1.3 Modelling with DOE

The other tool introduced in this section is the statistical design of experiments (DOE) applications. DOE refers to the process of planning, designing and analysing the experiment through computing programs, so that valid and objective conclusions can be drawn effectively and efficiently from experimental data [354]. The design also aims to reduce and remove possible experimental bias that could mask statistically significant factors by selecting and randomizing the experiments in order to extract the largest amount of information from the results. The outcome of the design is a structured and optimized planning of the experimentals [355] in which the number of runs is defined so as to reduce the amount of work necessary to originate an adequate model without compromising the significance and the accuracy. DOE is hence a powerful support for the development and the modelling of formulations. When thinking of the traditional approach by trial and error, it presupposes to change just one variable at a time. This requires firstly a large effort invested, and secondly, it does not guarantee that the steps followed during the development have achieved the true optimal results. Thanks to the introduction of DOE to plan the work, the number of experiments needed is significantly reduced. DOE helps in distinguishing the important factors from the multitude of possibly influencing factors. For this purpose, DOE processes more than one variable simultaneously [355].

DOE are created and evaluated by computational tools that form part of software packages of statistic processing of experimental data. The statistical design of experiments sorts out those runs from the whole pool of experiments to identify the critical factors, to reveal their interactions -either synergistic or antagonistic- and to find the experimental candidates necessary to accomplish the generation of a powerful model. As a result, the analysis of the experimental data is significantly simplified and the generation of mathematical expressions (regressions, models) and the mapping of the response over the experimental domain to determine the optimum formulations are enhanced [356].

There is a large variety of experiment designs [357]. Depending on the kind (continuous, discrete or categorical), the number, and the nature of the variable (e.g. mixture composition, processing variables), certain types of design might be more appropriate than others. The full factorial design is presumably the simplest design. It follows a normal structure of n^m number of runs, where n is the number of levels and m the number of interaction combinations between them. However, to reduce the number of runs one could make use of fractional factorial designs. In these designs, element interactions or a group of element interactions are associated to one factor, reducing the number of m, and subsequently, the number of experiments demanded by the design to build the model. Nevertheless, among other designs presented in [357], the D-optimal design is highlighted to have vast importance in the design of experiments due to its big versatility. In fact, in formulation experiment designs, the employment of the D-optimal design is extensive in the literature [24, 231, 358-360]. D-optimal design of experiments offers the option of selecting those experimental points that will extract the maximum amount of information from the experimental region of a reduced number of experiments. Basically it focuses the choice of experiments for the optimization of the determinant of a matrix [X'X] where X is the matrix of the experimental points and X' the corresponding transposed

matrix. To know more about the criteria of generating the list of experimental points and the mathematical principles of the D-optimal design, read the section 9.5 of the Appendix. Through the optimization of the value of the determinant D, only those experiments that are maximally independent from each other are selected from the bulk of all possible experimental candidates. The number of runs in an optimized design will be dependent on the number of variables, the bounds (i.e. maxima and minima values) of each variable, and the type of regression of the model. In Figure 124, the experimental space for an eight variable experiment of unknown nature and unknown bounds is represented. The situation of the points within the space and the quantity of points selected by the D-optimal design are a function of the complexity of the regression selected and, as depicted by the figure, they vary in number and quality in case of a linear and a quadratic model. The end *candidate set* of experiments corresponds to the pool of data from which the application conducts all modelling calculations. The performance of a D-optimal design depends on the condition numbers, the selected model, the number of runs, and the factors of randomness [355].

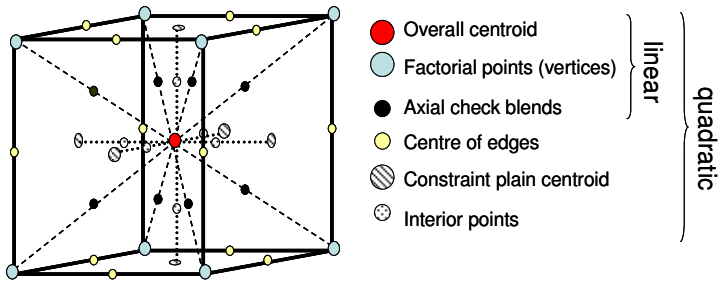

Figure 124. Experimental points selected by a D-optimal design in case of an eight variable system

When the pool of experimental data is completed, the application initiates the calculations for fitting models that generate the desired response by changing parameter values, reducing the number of element interactions, etc. The outcome of the process will be (generally) a mathematical model and the corresponding statistic analysis such as F-values, lack of fit, and r^2 values that evaluate the performance of the calculated model. Nevertheless, though DOE in formulation modelling and optimization has gained importance and is currently a common tool, less effort has been made at checking the potential utility of DOE combined with ANNs. In [134], Hussain showed the applicability of statistical principles to design experiments for the building of ANN with optimized capacity of generalization (i.e. with improved predictability). Also in [361] the authors developed ANNs for modelling film coating formulations. They concluded that designs that mapped thoroughly the experimental space delivered ANNs which were both accurate and predictive. However, none has studied the possibility of making use of the predictions generated with ANN models to increase or complete the list of data from which the models are processed.

6.3.2 Materials and Methods

For the first group of experiments presented in this section, the experimental raw data gathered in sections 6.1 and 6.2 was structured in order to become training data for the ANNs and to create data sheets for the modelling with mathematical general regression methods (GRM).

The ANNs were created with the *ANNe* software developed by Dr. Bultmann. This application creates ANNs that can be easily inserted in the expert system. For the generation of ANNs, the corresponding

data sheets containing the input and the outputs were copied into the clipboard of the operating system. The program creates the network and extracts the values required for the network training from the data available in the clipboard. All networks generated by ANNe are MLPs (see section 2.3.3) with one hidden layer. The number of PEs of each layer was variable. Though the program gives advice on the number of hidden neurons that presumably generate optimum networks, the criterion used for the selection of the number of neurons at this layer was to set the smallest number of hidden neurons that led to the best correlation values. Also the number of outputs (generally 1 or 2) was accepted or changed according to the quality of the ANN regression coefficients. A list of the architecture of the ANNs generated for the modelled variables of all formulation groups are provided in tables 38, 39 and 40 of section 9.6 in the Appendix. On the tables the variables that were considered input and output of the ANN are also listed. Program-default training parameters were used and kept invariable for all networks. Each learning process involved 105 epochs (iterations) at a learning rate of 1 and a momentum of 0.5. The networks were trained until the correlation of predicted vs. observed values reached its optimum value (i.e. previous to overtraining). This correlation coefficient was taken as indicator of the accuracy of the network calculations. The accuracy of all developed ANNs was examined by means of plots of predicted vs. target values generated by the ANNe software.

The mathematical modelling was developed using the *Statistica 7.0* software (StatSoft Inc., USA). The tools for the general linear - nonlinear modelling, referred here to as *general regression methods* (GRM) available in this program makes possible the analysis of complex multi-variable systems to generate mathematical models that establish the relationship between independent and dependent variables. However, as usual in mathematical regressions, each dependent variable (i.e. intermediary product and/or end product properties) had to be modelled individually. The same strategy for the creation of mathematical models was followed. Thus, the independent and the dependent variables were first selected. The composition was always the independent, except for the tablet properties, for which also the compression pressure became a predictor. The individual product properties were the dependent variables. Then, a first approach was generated using a full factorial design of regression (i.e. taking in consideration all variables and all possible interaction between them). The program generated the model and performed simultaneously a statistical analysis from which one could not only know the goodness of fit of the model but also the weight and the significance of each variable and each interaction on the final response. Besides the tabular summary of the parameter estimation, the program offers the possibility of representing graphically the significance values of the effects by means of *Pareto* charts which consist of bars which lengths are proportional to the absolute value of the estimated effects divided by the

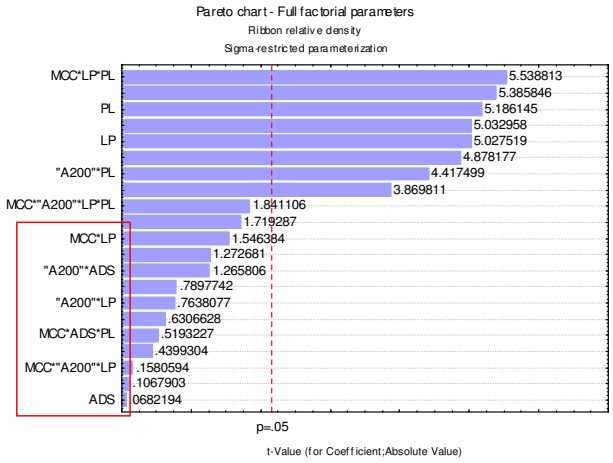

Figure 125. Pareto chart of a full factorial regression from the modelling of the tablet relative density. The factors of low significance are framed

standard error (see Figure 125). If an effect exceeds the vertical line (corresponding to the significance level p = 0.05), it is considered to have significant influence on the model response. After the evaluation of the parameter estimations, a new regression analysis was started, this time excluding those with low significance (in the example of Figure 125, those highlighted). The evaluation of the significance of the effects and the interactions on the response, and their exclusion from the fitting, was repeated until the regression coefficient reached a good correlation value and only few effects with low significance, which omission reduced the goodness of fit, remained part of the regression. As a result, we achieved a much more simplified equation of variable order. The correlation values given by the statistic analysis made by the program, and the contrast of model responses and experimental values were used for the estimation of the model quality. Furthermore, the examination of the elements from the mathematical model was used to create diagrams of the *β- coefficient* (see Appendix 9.7) for the elements. These diagrams are useful for the assessment of the relative contribution of each variable in generating the response.

Moreover, the predictability of the ANNs and the GRM models for the multicomponent formulations and the formulations of MCC granules with external components were examined. For that purpose, the response values generated by the models for the product properties of new experiments (new formulations) were compared with the observed values. The list of formulations used for the model validation can be found in 9.8.1 in Appendix. They correspond to experiments from the formulations of MCC granules with external components, and multicomponent formulations of the first group (MCC as main component). The MSE (mean squared errors) of predicted vs. observed values were calculated for each variable in order to quantify the goodness of predictability of both model strategies for each one of the response variables.

For the study carried out on DOE, the software *Design Expert v.7.0.0* (Stat-Ease, USA) was used to build a design of experiment for the multicomponent again from the group 1 of multicomponent formulations. For reasons presented previously (6.3.1.3), the design chosen was a D-optimal with combined experiments of mixture variables and process parameters for the modelling of the tablet tensile strength and the tablet dissolution time. The mixture variables were the components of the formulation (except MgSt), and the process parameter considered was the compression pressure. The order of the regression polynomial was then set to be cubic, which would ensure the generation of a data pool wide enough to be applicable also to quadratic and linear regressions in case that they could fit better. The program created a table with the record of experiments that would be needed to generate the regression model. The design requested a total of 150 runs. DOE are tools that generally are not conceived as applications for the processing of historic data. For that purpose, in order to make use of as many of our (historic) data as possible, some of the input cases (i.e. composition or tableting pressure) of the experiment design list were adapted to our experiments. Thus, the response values for 68 runs could be completed with our (historic) experimental data.

The rest of candidates remained empty or were predicted with ANNs. The corresponding predictive ANNs were modelled with the *Statistica* neural network software (sections 6.1 and 6.2). The composition (i.e. the components and their percentages) as well as the compression pressure were the

input variables whereas tablet tensile strength and disintegration time were placed in the output layer. The resulting architecture of the network is represented in Figure 126. The signal between PE was originated with a linear activation function. The training strategy was the standard δ-rule back propagation. The number of iterations for each learning process was varied between 103 and 104 epochs depending on the evolution of the training progress. The learning ratio was kept at 0.1 and the momentum at 0.3. Two types of network were achieved. The first was trained until the network reached the best correlation value for both outputs while the second network was not fully trained. Thus, a network with good predictive abilities and another of poor performance were developed.

Back to the DOE models, the regression by quadratic polynomials was observed to fit the best. A total of three DOE models were created: one based on experimental values only, and two built from the combination of experimental values and ANN predictions. Nevertheless, the ANN predictions were made by the two networks of different levels of accuracy, so that the quality of the predictions was also different. The performance of the three models was tested. Besides the goodness of fitting, the predictability of each model was validated by comparing their response values with the real observed values of new experimental cases, the list of which is in Appendix 9.8.2.

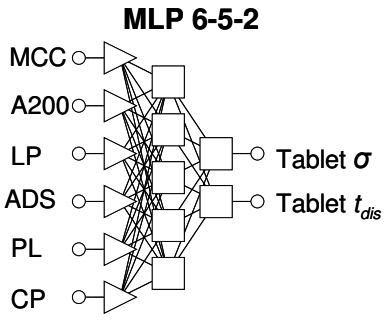

Figure 126. ANN architecture of the network created for the modelling of tablet properties from multicomponent formulations (group 1) using the Statistica software

A last experiment in this section deal with the study of the ability of DOE to decipher the *black box*-like ANN predictions. Using the same DOE as previously, all experimental records requested by the DOE were predicted by the ANN of good performance. Thereafter, a DOE based mathematical model was obtained, which predictions were compared with the responses generated directly by the ANN from the batches 1 to 9 of the validation experiments listed in 9.8.2 in the Appendix.

6.3.3 Results and discussions

6.3.3.1 Predictions with ANN Models

The architectures of the ANNs created by the ANNe software are recorded in Appendix (section 9.6). The ANNs obtained after training were saved as **.ann* files that could be recalled by the expert system in order to perform estimations. Figure 127 is a diagram generated by the ANNe software after the creation and the training of the network that modelled the disintegration time and the tensile strength of tablets made of MCC granules with external components. The program provides the user with the correlation coefficient of

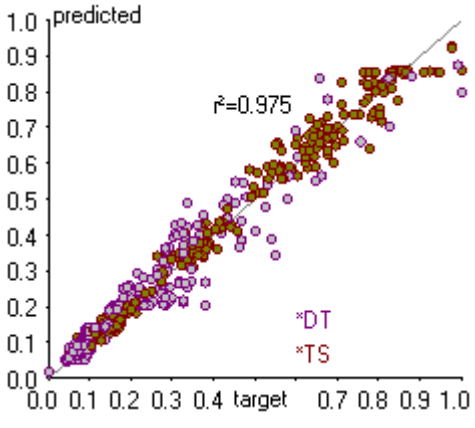

Figure 127. Graphic representation of the correlation of predicted and target values produced in ANNe

predicted and actual values. The r^2-values for all ANNs are listed in Table 24. All ANNs present fair to very good fitting coefficients. Low values of performance are due to the weakness of the models, and intricacy of the relationship between variables. As the number of networks tested for each case prior to the selection of the best performing system was large, low correlation values rather indicate that no clear relationship between the independent factors and the response variable could be established.

Table 24. Correlation coefficients of the ANNs generated for the variables analysed

	Ribbon		Blend / Granule				Tablet		
	ρ_{rel}	σ	n	d'	Rep. angle	CI	σ	t_{dis}	t_{80}
MCC-granule external component	--	--	0.9061		0.9627		0.9750		--
Multicompo. group 1	0.9944		0.9612	0.9717	0.9906	0.9864	0.9838		0.9918
Multicompo. group2	0.9942		0.9902		0.9921		0.9901	0.9562	0.9913

The value of the standard correlation coefficient R is a good indicator of the performance of the neural network. It gives valuable information about the deviation of the response produced by the ANN from the actual values. However, a good correlation does not necessarily indicate good predictability. This has to be additionally evaluated to determine how suitable are the final ANNs for making predictions from records which have not been used during the development of the ANN.

6.3.3.2 Predictions with GRM Models

An initial evaluation of the performance achieved by the GRM models was made by evaluating the correlation coefficient of the regression. In case of GRM models, finding a compromise between the value of performance and the number of parameters and elements was required. Simple models are in any case preferable, since they are easier to handle, the processing time is short, the number of mistakes when being transferred into other systems (e.g., into the expert system data-base) is reduced, and they present information about the interaction between variables in a much clearer manner. The correlation coefficients for the GRM models are listed in Table 25.

Table 25. Correlation coefficients of the GRMs models generated for the variables analysed

	Ribbon		Blend / Granule				Tablet		
	ρ_{rel}	σ	n	d'	Rep. angle	CI	σ	t_{dis}	t_{80}
MCC-granule external component	--	--	0.5062	0.5191	0.5276	0.2640	0.9353	0.8597	--
Multicompo. group 1	0.9586	0.9227	0.9568	0.8609	0.8602	0.3102	0.9638	0.7742	0.9329
Multicompo. group2	0.9803	0.8475	0.9239	0.9416	0.6340	0.7890	0.9805	0.6496	0.8917

The fitting achieved by the mathematical regressions in many cases does not reach desirable values. Thus, in general, ribbon and tablet properties were modelled satisfactorily whereas blend/granule attributes were not. When analyzing the GRM modelling parameters, it has to be considered that an optimum value for a given factor may only look optimal but be far from the truth. During the adaptation of the model to improve the fitting, the elimination or the introduction of a new interaction t influence the values of the rest of factors. Moreover, a large number of bias escapes from the GRM analysis, resulting, in some cases, in the poor performance of the model.

However, even if models do not achieve good fitting values, through the analysis of the mathematical expressions, the formulator can extract valuable information of which factors affect the dependent variable significantly and which not. The representations of the *β-coefficient* (see Appendix 9.7) reveal certain details about the influence of the substances of the formulation (and the process variable in case of the tablets) on the response. Moreover, unlike the descriptions made in sections 6.1 and 6.2 about the influence of the formulation on the tablet properties, GRM models do not only reveal the influence of the components individually, but also take into account the interactions between them, describing more accurately the mechanisms of interaction occurring between substances.

In order to compare the information extracted directly from the experimental observations in sections 6.1 and 6.2, with that delivered by the analysis of the mathematical equations, we have created Tables 49, 50 and 51, in Appendix section 9.7.4. In these tables there is a brief summary of the effects induced by the different components on the considered variables, which were gathered from the analysis of diagrams of the experimental results from sections 6.1 and 6.2 and contrasted to the information that interpreted from the representations of the GRM *β-coefficients* of the variables. From the table it is clear that though in some cases the informations provided by both sources do not match, generally there are coincidences on the identification of the dominant components. The information taken from the GRM models, moreover, reveal important clues about the possible mechanistic of interaction between variables, proved a good description of the real phenomena taking place within the system.

Having a brief look at Table 49 (9.7.4), it is clear that the changes observed after adding large amounts of external components correspond to the effects detected for the individual components by the GRM whereas the variations induced by adding low amounts match up fairly with the GRM effects for the interaction between components. This is explainable by the mechanism of interaction between components for the variable. Hence, to give an example, the flowability of the MCC granule seems to be enhanced when small quantity of A200 or LP are added, whereas large amounts have the opposite effect. This was justified in section 6.1.3.1 by the fact that, though A200 has extremely bad flowability, it formes a fine layer around MCC granules and reduces particle friction. On the other hand, the excess of LP and MCC (externally added) reduces the flow due to modifications in the particle size distribution. The *β-coefficients* calculated from the GRM model prove that even if the individual components have negative effect on the mobility, the interaction of A200 and LP with the MCC granules (occuring already when added in small amouts) improve the bulk flow.

From the information provided in Tables 50 and 51, we can read, firstly, that the complexity of interactions increases proportionally to the number of variables. Secondly, the trends observed experimentally do not correspond in all cases with the information given by the GRM parameters. This is partially due to:

1) Intricacy of interactions between components and other variables. An example of this is the RRSB-*d'* value for multicomponent formulations from the group 2. In section 6.2 we described that adding KVA64 to the formulation resulted into granules of larger size, while adding ADS

and PL lead to the opposite effect. From the GRM coefficients one can see that not only KVA64 but the interaction of KVA64 and ADS, and the binding effect of KVA64 between MNT and PL, induced larger granules. The synergic effect of ADS and PL, together with the interaction with other components, caused negative effects on the particle size. Hence, when looking at the GRM information, it seems that the interaction between components, rather than their individual effect, is responsible for the final properties.

2) Poor accuracy of the developed GRM models, which parameters might not correspond to the real effects involved in the response. For instance, the GRM model for the CI of multicomponent granules based on MCC (group 1) has a particularly low performance ($r^2 = 0.3102$). After having contrasted the observations made in section 6.2 and the information extracted from the GRM *β-coefficients*, there is poor agreement between them. In first place, ADS was not detected by the GRM models to have any significant role. Furthermore, experimental observations showed that LP has a positive effect on the blend compressibility (i.e. reduced the CI value), while according to the GRM model, the effect of LP is to reduce the blend compressibility (i.e. increase the CI value).

Thus, it has been proved that through GRM the mathematic models created contain information about the mechanistic and the interaction existing between variables that lead to the response. However, the interpretation of this information becomes complicated and even contradictory to the patterns observed if the model performance is poor or the number of variables involved is too large.

6.3.3.3 Comparing ANN with GRM

Comparing the correlation coefficient of Table 24 and Table 25, obviously, ANN performance of approaching estimations to target values was better than GRM models'. However, there are patterns on the resulting values of correlation common for both modelling methods. Thus, product attributes for which ANNs created the lowest performance networks, coincide also with the GRM models of lowest correlation values, as compared in Table 26.

Table 26. List of properties that led to weak ANN and GRM models

Formulation		*ANN*	*GRM*
MCC-granule external component	RRSB-n	0.9061	0.5062
	RRSB-d'	0.9061	0.5191
	Rep. angle	0.9627	0.5276
	CI	0.9627	0.2640
Multicompo. group 1	CI	0.9864	0.3102
Multicompo. group2	t_{dis}	0.9562	0.6496

This observation would elucidate, firstly, which of the variables studied present a stronger biased nature, and secondly, it also proves the supremacy of ANN over GRM in modelling non-linear, intricate systems. Considering those attributes with low correlation coefficients it can be concluded that variations on the PSD, the flowability and the compressibility behaviour of MCC granules with extragranular additives, are hardly explained solely by the substances in the final composition, but rather by a large number of interactions that could not be approached by the regression methods. Similar arguments can explain the low correlation for the CI and the t_{dis} of multicomponent

formulations. Thus, for these variables, the models generated by GRM and ANN show simply a rough trend, but the sources of variation in the process are not clarified.

Table 27. Analysis of the deviation (MSE-values) of the estimations made by the different models

	MSEs	MCC-granule - external components		Multicomponent granule - group 1		Multicomponent granule -group 2	
		GRM	ANN	GRM	ANN	GRM	ANN
Ribbon	ρ_{rel}	--	--	0.3595	1.29	0.06773	2.66
	Σ	--	--	0.0148	0.0054	0.0061	0.0015
Granule	RRSB-n	0.0014	0.0031	8.82E-05	7.62E-05	0.0001	5.13E-05
	RRSB-d'	957.71	1356.53	1849.08	546.43	124.00	226.43
	angle of respose	8.62	5.24	17.40	1.98	0.6420	0.8692
	CI	18.54	2.74	3.39	0.5085	0.3817	0.6995
Tablet	Σ	0.9279	0.6637	0.6547	0.1712	0.0230	0.0044
	t_{dis}	0.8823	0.7055	4.83	1.00	1.22	1.68
	t_{80}	--	--	29.66	6.02	1.43	0.1949

In Table 27, the deviation of ANNs' and GRMs' responses to the actual value for all three formulation groups and all studied variables are compared. The mean square error (MSE) of the calculated responses listed in the table shows how good are the approaches made by the models. The quality of the approaches varies from formulation group to formulation group. For the formulations of external components added to MCC granules, the GRM models showed to be more accurate on the blend characteristics, while ANNs are slightly more accurate in fitting the tablet attributes. In case of multicomponent formulations, ANNs' predictions showed better fitting in the observed values for most of the variables. Thus, in the first group of multicomponent granule formulations, the GRM models delivered better approaches only for the calculation of the ribbon solid fraction. As for the second group of multicomponent granule formulations, the accuracy of GRM models was better again for the ribbon solid fraction and also for the granule attributes.

From the results presented above, it can be concluded that the ability of ANNs to model complex systems is by much better than the one of GRM models. This is in broad agreement with the obsevations of many others [85, 174, 176, 179-182, 184, 187]. In all, the authors studied the possibility of using ANNs to predict tablet properties in order to optimize the formulation until desired requirements were met. All agreed that ANN's predictions were more accurate than the calculations made by approaching mathematic response surfaces. Our observations also have demonstrated that the divergence between ANNs and GRMs becomes even more accentuated as the degree of intricacy of the system increases. This is demonstrated by two main evidences observed here. In the first place, considering the multicomponent formulation of group 1, which contains up to five substances, almost all predictions made by GRM are less accurate than ANN estimations. Secondly, focusing on the tablet attributes (for the same group of experiments), in which the compression pressure was also included as a predictor, increased the intricacy of the system and consequently mathematical approaches, provided less accurate estimations (i.e., larger MSE-values).

However, a model that demonstrates to have good capacity of approaching accurately its estimation to the observed values does not always possess good predictive capability. In Table 28 we present the error in MSEs from the predictions made with new experimental cases of GRM and ANN models for the characteristics of products from the blends of granulated MCC with external components and the first group of multicomponent formulations (a table with the calculated values are recorded in Appendix 9.8.1). Analyzing the values of MSE listed in Table 28 one can see that the vast majority of variables from both formulation groups are predicted more accurately by ANNs models. Especially the GRM predictions for the ribbon tensile strength and the t_{80} values of multicomponent granules present great deviations. Though the GRM model correlation coefficient for these variables are fairly good (0.9586 and 0.9329, respectively), the ability to predict from new experiments is, as shown here, poor when the modelled systems present a high level of complexity. The same conclusions were reported in [176, 181, 182]. In these works, the predictions of mathematic models (response surfaces) and ANN for tablet attributes were compared. All studies demonstrated that ANNs' predictions were more accurate. ANNs were considered to be more suitable, not only for estimating values, but also for predicting accurately new experimental data. In particular Bourquin [176, 352] highlighted the better ability of ANNs to *generalize*, i.e. to find the weight of the elements and their non-linear interactions on generating a given response. This was observed to be much more useful when handling new experimental records than the limited and rather *memorized* responses of the GRM models.

Table 28. Deviation (MSE-values) of model predictions from observed values

	MSEs	MCC-granule - external components		Multicomponent granule - group 1	
		GRM	ANN	GRM	ANN
Ribbon	ρ_{rel}	--	--	1273.27	3.80
	σ	--	--	0.0455	0.0394
Granule	RRSB-n	0.0001	1.61E-05	0.0056	0.0002
	RRSB-d'	3240.66	1497.08	727.84	474.29
	angle repose	0.3576	1.89	37.68	1.22
	CI	4.57	0.7979	7.84	14.20
Tablet	σ	0.3009	0.4621	0.3906	2.93
	t_{dis}	0.5329	0.5015	3.76	1.80
	t_{80}	--	--	14066.42	38.19

However, the characteristics of ANN predictions become its main limitation when contrasted to GRM. Though in some ANN software the graphic representation of response surfaces is possible, this do not present the weight of each variable on the response value in a clear manner. This is due to the *black box* nature of the modelling with ANNs. They deliver estimations but it is not easy to follow the pathway that leads to them. In this way, mathematical models still have an important role in the understanding of the processes being modelled. Through the analysis of the mathematical expressions gathered, the formulator is provided with valuable information of which factors affects the dependent variable significantly and which do not. Accordingly, the representations of the *β-coefficient* (see Appendix 9.7) give important information about the influence of the components (and the process variable in case of the tablets) on the modelled product property. However, this information has been shown to become complex to interpret if the number of variables involved in the response is large and it can be even contradictory to the observed patterns if the model performance is too poor.

Finally, Table 29 compares briefly the pros and cons of both types of modelling according to the results presented in this section.

Table 29. Comparison of the modelling with mathematical regressions and ANN

	Mathematical regression	*ANN*
+	• Important contribution to the understanding of interaction between variables • Possibility of statistical analysis of the influence factors. • Prediction following scientific-based justifications	• Ability to detect complex non-linear associations • Better predictability • Update with new data possible • Fast processing • Effective models with incomplete data sets
-	• Functional form has to be chosen a priori • One model for one variable • Extensive non-linearity requires special effort and usually results in bad model correlations • Models are not adaptable to new data	• Prediction without mechanistic understanding *(black-box* nature) and inexistent scientific based criteria. • Extrapolation leads to aberrant predictions • Training is casuistic and in some cases irreproducible • Phenomena like "overtraining" or "memorization" are frequent

6.3.3.4 Application of ANN in DOE modelling

As described in the methods, an ANN of good and one of poor performance were created for the prediction of missing experimental values on the record tables of the DOE. The regression coefficients of their estimates for both variables are listed in Table 30. Depending on the origin of the response values three different groups of DOE-models were created for both variables. The regression coefficients are listed in Table 30.

Table 30. Regression coefficients for the ANNs used for predicting the DOE response values

r^2	ANN 1 -good performance	ANN2 -poor performance
Tablet σ	0.9912	0.9557
Tablet t_{dis}	0.9627	0.8523

All models fit a quadratic polynomial equation and are statistically significant (ANOVA, $p < 0.001$). Depending on the origin of the response values, the goodness of fit for the models was different (see Table 31). Surprisingly, the fitting values are good by making use of the reduced number of cases that were completed with *historic* experimental data. For the two variables modelled, it appears to be enough to use a reduced number of experimental responses in order to create models with good fitting. However, the insertion of combinations of experimental (real) responses and ANN predicted values in the experimental pool of the DOE have opposite effects depending on the quality of the ANN predictions. Thus, in case of making predictions with low performance ANNs, it results in models of larger lack of fit, whereas the combination with predicted values of good performance ANNs generates good to very good regression coefficients and predictions that are more robust than those of models calculated exclusively with experimental responses.

Table 31. Regression coefficients of the corresponding models generated

	Origin of data		
Variable	Experimental	Exp.+ ANN poor performance	Exp.+ ANN good performance
Tablet σ	0.9819	0.9779	0.9929
Tablet t_{dis}	0.8564	0.8432	0.9543

The predictability of the models was examined by comparing the predictions and the observed values for the new experimental records of Table 56 in Appendix, section 9.8.2. A list of the values calculated by the models and the real values has been also included in the same section. The MSE values of the models' estimations for the two dependent modelled variables are listed in Table 32.

Table 32. MSE values for the predictions made by each model from new experimental records

Tablet σ			Tablet t_{dis}		
Exp.	Exp.+ ANN good performance	Exp.+ ANN poor performance	Exp.	Exp.+ ANN good performance	Exp.+ ANN poor performance
0.088	0.037	0.144	0.002	0.002	0.004

The models based on DOE present different prediction performance depending on the quality of the predictions made by the ANNs. Complementing experimental data with ANN improves the models calculated from the experiment list of the DOE only if the ANN performance is good. Robust ANNs generate good predictions that increase the model ability to generalize, i.e. to predict the response of new cases. The error of the prediction, in turn, is larger when the experimental data has been combined with ANN estimations from a network of poor performance. With this experiment we prove that the capability of generalizing (even from historical data) of powerful ANNs would be useful in complementing data in DOE based modelling. The applicability of this in the development and the optimization of formulations for which DOE has been implemented are of high interest. Thus, ANN could be useful in the following situations:

- A (large) amount of randomized and disordered historical data is available and we need to build models from it
- We have access to historical data and we are interested in carrying out a new formulation or we need to optimize the old one
- The DOE model of best fit is a high order regression polynomial and the number of runs requested is excessively large
- Some runs have to be discarded owing to aberrant values

In all cases presented above, ANN can be used to reduce the number of new experiments or repetitions to be carried out in order to complete the experiment list of a DOE, reducing time and effort. Nevertheless, the ANN used for such a purpose has to be sufficiently robust.

Finally, the use of DOE was also implemented for interpreting the ANN modelling. The tablet tensile strength was chosen as modelled example. All responses required by the DOE were predicted using the ANN. The table with the comparison of values delivered directly by the ANN and by the DOE model, for validation experiments, are listed in Table 59 (section 9.8.3 in Appendix). Figure 128 shows the linear relationship between responses. The resulting linear equation

$$y = 0.985 \cdot x + 0.2933 \qquad (36),$$

has good linearity (r^2 = 0.9915), meaning that through the DOE modelling, we have found a mathematical expression (Table 58 in section 9.8.3 of the Appendix) that fits to the *black box*-like

responses generated by the ANN from the weighed signal transmitted from neuron layer to neuron layer. Thus, we have approached mathematically the modelling strategy followed by the ANN. The next step would be to study whether the ANNs based mathematical expressions of the DOE model have any similarities to corresponding GRM models for the same variable.

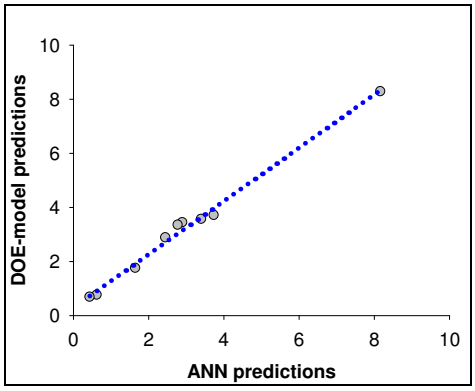

Figure 128. Correlation between ANN estimations and DOE predictions for the same experimental cases

6.3.4 Conclusions

The modelling of product properties from formulation and processing variables with general regression methods (GRM) and artificial networks (ANN) is feasible. The models generated in this section will, therefore, be used for their insertion in the expert system described in chapter 7.

The robustness of the models depends partially on the modelling strategy (i.e. the number of parameters and the order of the polynomials in case of the GRM, and the architecture and the training rules, in case of ANN). However, the biased nature and the randomized character of the dependent variables compromise the accuracy of the models.

Although the intermediary and the end-product properties of all formulation groups have been successfully modelled by either modelling methods, the quality of the models' estimations and the predictability for new experiments, are usually better with ANN models.

ANNs' requirements for creating a powerful model are less than GRM models. The number of training data required for the modelling of complex clusters of dependent-independent variables is smaller than GRM. The creation of mathematical models by GRM, in turn, demands longer time to select and evaluate the significant parameters and the model quality. It has been proved that capacity of estimating response values with ANNs is in general better than with GRM models. But ANNs show even better capacity for predicting. ANNs' ability to generalize the relationships between variables turns them into tools that are able to generate accurate predictions from new experiments. However, in some cases extrapolations in the predictions made by GRM models generated less accurate and even aberrant responses.

GRM models deliver valuable structured information about the variables involved in a response, the effect of the individual variables and the interaction between components. The obviousness of the information about all effects involved in the generation of the response depends basically on the model complexity while the reliability of the information is determined by the model robustness.

DOE reduces the number of experiments required for creating a model without compromising the accuracy of its estimations. DOE applications calculate the number of dependent variables that can be altered simultaneously following statistic criteria. Accordingly, they generate a reduced list with the

collection of experiments needed for the calculation of a powerful model. In this work, ANNs have demonstrated to be useful tools for completing the list of experiments generated by a DOE application with no need of carrying out all experiments. It has been shown that the combination of experimental values from historic data and predictions of powerful ANNs results in DOE based models of good predictability. Finally, it has been attempted to solve the *black box* nature of the ANN predictions by finding mathematical approaches. DOE models created directly from responses predicted exclusively using ANNs are able to make predictions for new experimental data which value is very close to the calculated directly by ANN. However, a comparison of predictions for larger data sets would be necessary in order to accept the mathematic model as a valid approach.

7 DEVELOPMENT OF EXPERT SYSTEMS

In the introduction (section 2.3.2) we have described extensively the background of the expert systems (ESs): the concept, the working principles, the main components and structure, the origin of expertise integrated in the system, and even the applications of ESs in the pharmaceutical formulation found in the literature.

In this section we analyze the development of an ES with applicability in the design of tablet formulations. We describe how it has been created, what are the different components, the main features that it presents, and, finally, we evaluate not only the usefulness of the resulting ES, but also the limitations.

7.1 MAX in silico

The ES presented in this section is based on a framework already used in previous PhD theses [98, 163, 164]. The rules of decision, the structure, the commands at the inference part, and the interface are exactly the same as for the ES reported in these theses. The system used for developing the ES is the MAX *in silico* expert system editor software, developed by Dr. Bultmann. From the point of view of the construction of the ES, MAX already contains the bare bones indispensable for the structure of the whole system. The algorithmic rules (tree-like), as well as the layout of the interface, are already available. Accordingly, the design and the structuring of algorithms and decisions takes place mostly in the graphic interface (the *Edit* interface) represented in Figure 129. In this interface the ES developer introduces the questions and the corresponding list of options that has to enhance the interaction between the system and the user and guide the process to find the final answer that matches the user's inquiries. As it can be seen in the figure, the algorithms are structured in a tree-like layout. A question addressed to the user is followed by an answer that will open a new dialog window with another question, a statement, information, or the solution to the problem. However, if the answer or the next step for a given question requires the recall of information outside the dialog user-interface, it is necessary to insert the appropriate commands. These are programming instructions that order the loading, selection, processing, and organization of information from files where it is stored. As a result, the ES selects and makes use of the information that presumably is helpful for the user.

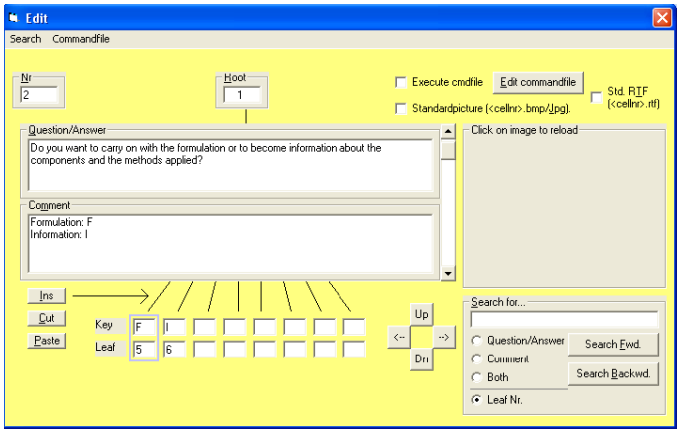

Figure 129. MAX *in silico* ES editing interface

Once the ES has been designed and all information has been incorporated into the knowledge base, the user will interact with the system through the interface window (the *Go-Interrogate the knowledge-*

base window). Figure 130 is a snapshot of the user interface in operation. The user does not need to be aware of the hidden tree-like structure of the algorithm and does not know exactly what are the commands and the decision criteria followed by the system. The dialog ES-user takes place at the text boxes, menu boxes, document windows, etc. in which the questions and the choices are presented. Following the user selections, the ES will open a new window. This can be a new dialog window similar to the previous one (i.e. as in the figure above), but it can also be the selection of information through an emerging box, the introduction of values or information by the user, or the display of informative documents (e.g. a report with the problem solution).

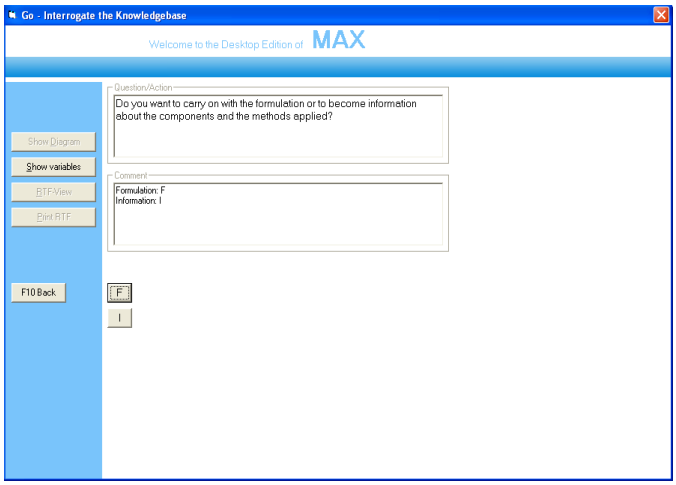

Figure 130. Interface of the dialog window in MAX *in silico*

In the next sections we describe the background of the generated ES, the development of the ES components and their organisation. Finally, we illustrate the abilities of the designed ES and evaluate its potentials and limitations.

7.2 The context

One of the aims of the experimental sections corresponding to the systematic formulation (6.1 and 6.2) was the generation of data and expertise that would be part of the knowledge-base of an ES. The idea was to create a tool able to:

- Predict the intermediary and the end-product attributes out of a random formulation presented by the user
- Analyze the results so as to deliver guidelines that might be helpful for the improvement of the formulation
- Make the expertise acquired during the performance of experiments easily accessible.

The arrangement of the information and the design of the ES components performed for the creation of a system that meets the criteria presented here is described next.

7.3 Main components of the ES

There are three main parts of any ES, as already described in section 2.3.2: data base, inference program and interface. Here we point out those features that are specific to our system. Therefore, the interface is excluded, since there is no modification from the original interface available in MAX, described above.

7.3.1 The knowledge base

This is the collection of information that constitutes the expertise stored into the ES. The knowledge base is formed by data, rules and heuristic information that define the robustness of the ES. The origin of the expertise that forms a part of this ES can be classified into three main groups:

A- *The experimental knowledge.* The material and the methods were included in the data base of the ES. This is meant to offer the possibility to have access and to learn the techniques applied for the generation of data. This has to be considered since the use of different techniques for the product manufacture and characterisation lead to variability on the results. Moreover, in the experimental data we have included the observed effects of the addition of each component to the formulation on the product properties for all three formulation groups described in sections 6.1and 6.2. With this information, the user might have an overview of what direction to take when changing the composition of the formulation. Finally, we also collected general information of each one of the components used in the modelled formulations. This complements the information provided by the experimental results and is a source of criteria for the choice of the component and the amount present in the formulation.

All this information was partially gathered and recorded in several text files (Rich Text Format or *rtf*), that can be easily recalled by the ES through the corresponding commands at the inference part. A list of the files containing the experimental expertise is presented in Tables 60, 61 and 62 in the Appendix (section 9.9.1). Furthermore, part of the experimental knowledge gathered was used for the creation of rules and conditions for the analysis of the response values generated by the ES (section 9.9.3).

B- *Mathematical regressions.* The GRM models created in section 6.3 were inserted in the ES. For that purpose, the fitting parameters estimated for every main component and every interaction were listed in a file named *data.txt* out of which the ES can recognize the value that applies to each regression parameter following the corresponding command. The mathematical equations without the parameter values have been included into the list of commands. Accordingly, to generate the prediction of a value, the ES combines the value of the independent variables (i.e. composition or process parameters) introduced by the user and the list of fitting parameters of the mathematical expression. The result of the calculation becomes a numerical variable of the ES.

C- *ANN models.* The neural networks created with the *ANNe* software in section 6.3, were also included in the ES. The networks generated for each property (or group of properties) are stored as **.ann* files which, again through the corresponding commands, can be loaded directly in the ES inference part. They make use of the input data introduced by the user to perform calculations and predict the output values, which become also a numerical variable of the ES. In Appendix (9.9.2) there is a list of the ANNs files and their location in the folder in which the whole data base is stored.

7.3.2 The inference part

As already mentioned, the inference part was designed with the editing tools of MAX. This part resulted in a combination of interlocked algorithms that lead the flow of information and interconnected the cells on the one hand, and the command files linked to certain cells that load, process and organize the information on the other. The inference part is formed by the algorithms of decision and the list of commands embedded in the corresponding levels.

The inference rules and the algorithms are followed in all three formulation groups basically the same way. Nevertheless, due to its extension, the list of commands for the generated inference part has not been reported in this thesis. A fragment is recorded in section 9.9.4 of the Appendix. The complete knowledge base with the developed inference part will be uptdated on http://www.jmbnet.de/thesis.

7.4 The completed ES

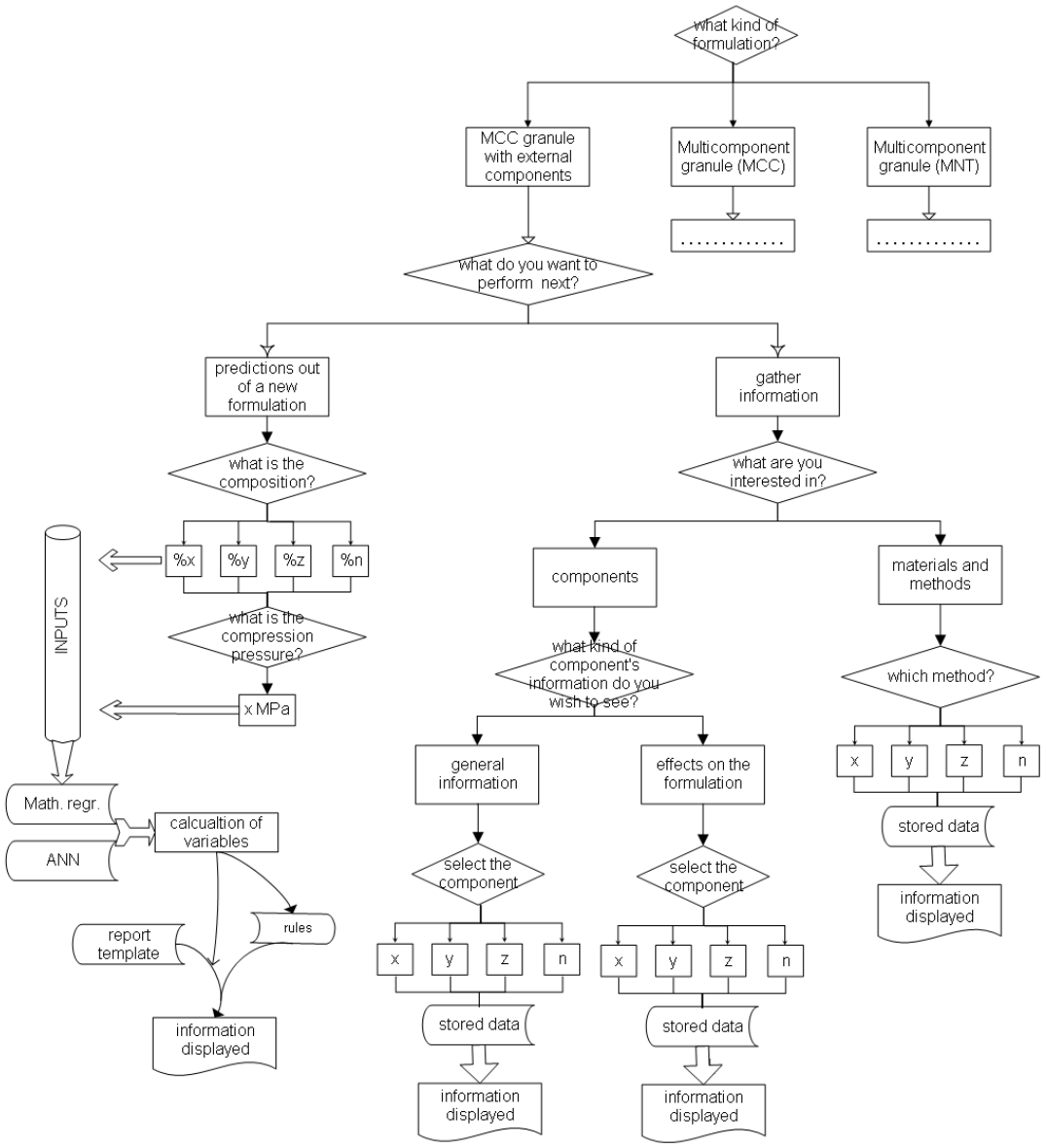

Figure 131. Flow diagram representing roughly the end structure of the ES created

In Figure 131, the flow diagram represents roughly the structure of the created ES. Some details of the system have been omitted, such as the possibility of decision of whether the user will add one, two or three components externally to the MCC granule, or the information windows that appear at the beginning of each section.

As sketched in the flow diagram, the first question of the ES leads to the selection of one out of three main branches, which are related to the selection of one of the three different formulation groups (i.e. the MCC granule with external additives, the multicomponent granules with MCC as main component -group 1-, and the multicomponent granules with MNT as main component -group 2-). The main branch split into two main tasks: the predictions of the product properties of a new formulation, and the acquisition of information. For the former, the ES use the models created in section 6.3 and the composition and process parameters introduced by the user to make predictions and to generate a response that is then accessible to the user. From the variables calculated, a group of condition rules (*if-then* clauses) are selected to generate statements and advices (e.g. for the troubleshooting during the process) as a function of the prediction values made by the system. These rules are listed in Appendix, section 9.9.3. Finally, the values of the variables are inserted in a template that produces a report including the predictions and the statements generated. The design of that template is almost the same for all three formulation groups. As shown in Appendix, Figure 135, section 9.9.5, the layout of the report has been freely designed and the ES variables (both numerical or strings) corresponding to each one of the prediction values or condition rules, has been organized in a coherent way of presentation. The name of the ES variables is written between angle brackets for the purpose of being recognised by the system and replaced by the corresponding values following the appropriate commands.

As for the second task (the retrieval of information), the user is interrogated through the dialog window in order to select the information from the knowledge-base that he is interested in. The user can access to two groups of data: one concerning the formulation components, and the other about the methods used to generate the set of experimental data for the creation of the models. According to the first one, the user can choose whether he wants to know general information about a particular component, or he prefers to see the effects on the product properties induced by the addition of the component to the formulation. The second group of information, however, comprehends all materials and methods. The in formation is presented to the user as he selects it from a list. The information is displayed to the user in a text window generated with the *rtf* file recalled by the corresponding command files.

To sum up, the ES will provide information in two ways:

1- As a written document corresponding to the information asked by the user. The documents are part of the ES knowledge-base and are inalterable neither by the ES nor by the user. These documents are the recorded recompilation of experimental observations, descriptions of the experimental methods, or technical information about the components gathered from the literature available.

2- As a document containing all predictions made on the product properties starting from a composition and compression parameters (pressure) given by the user. This document varies depending on the starting inputs and it contains the response values of predictions divided in two groups, corresponding to the values resulting from the response of GRM models and from ANN models, listed separately in the document. Moreover, in the *rtf* document they are also described the methods to be followed for the manufacture of the granules and tablets, at the same time that it reports observations, guidelines and other issues generated from the conditioning rules included in the ES that are activated for certain values of the calculated variables. Thus, although the layout of this document will be the same, the information listed in it changes as a function of the initial inputs and the predictions generated.

Two examples of the output information are presented in Figure 132.A and 132.B. Figure 132A corresponds to a window with the contents of the *rtf* file with information gathered in 6.1 and 6.2 for the effects of A200 addition in the formulation. Figure 132.B, however, is a snapshot of the form with the predicted values for a given formulation, which template is also part of the system (see 9.9.5). The variables listed in the form have been replaced by the predicted values calculated by the models integrated in the ES knowledge-base. Also the observations, the comments, and the advices that have been generated according to the predicted values, are integrated in the document displayed. The user can copy the contents of these windows to the system clipboard or can print the documents directly in order to make use of them.

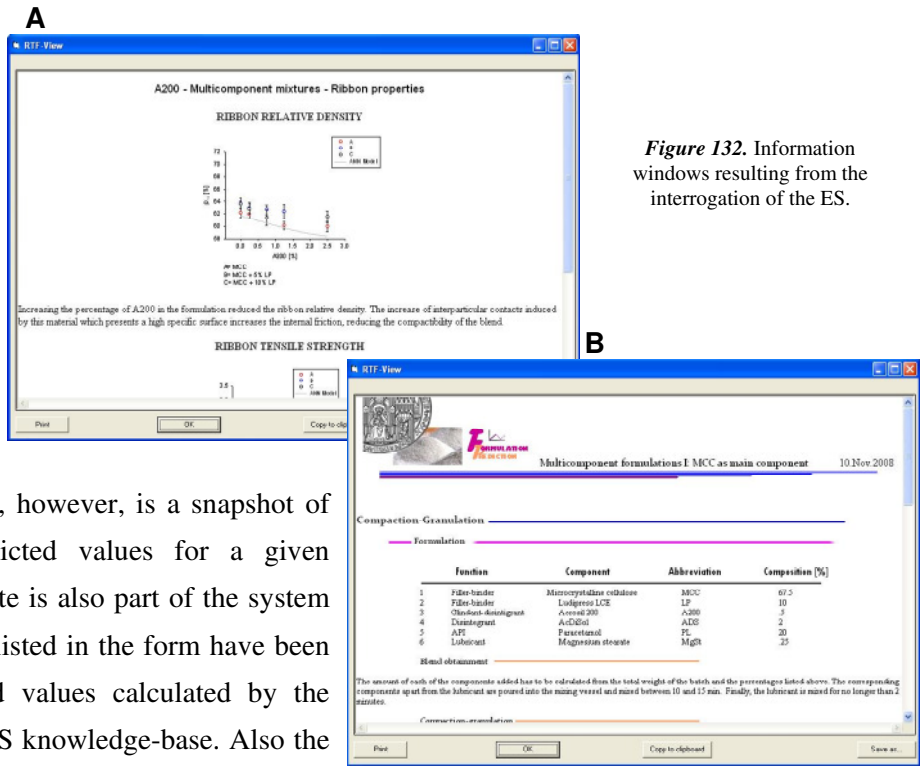

Figure 132. Information windows resulting from the interrogation of the ES.

7.4.1 ES predictability

The same models created in section 6.3 were included into the knowledge-base of the ES and, therefore, the accuracy of the predictions made was already evaluated in section 6.3.3. Thus, estimations made by both GRM and ANN can approach satisfactorily the real values when the composition lays within the modelling area covered by the data set used for the modelling. However, the predictions made by GRM for new formulations present large deviations. GRM demonstrate, hence, poor flexibility on calculations outlying the regression boundaries

.

7.4.2 ES features

In 2.3.2.2 we have presented a list of all desired qualities of a powerful ES. However, there is no ES that meets all requirements. For the ES created here, we describe next the features of the system considering also what aspects are necessary to improve in order to create an enhanced tool.

The resulting ES has proved to be able to display well-organized information that summarizes the predictions made for intermediary and end-product properties which can be used to draw a diagnosis of whether the prognosticated values are within rates of suitability for the product or not. It also supplies the user with advice of what steps to follow in order to manufacture the product with the wanted attributes. The user can furthermore retrieve information that may help him to learn more about the substances, about their role within the formulation and about the methods used in the acquisition of data for the modelling.

From the point of view of the user, the ES meets the basic requirements of any knowledge based system. Thus, the expertise can be recalled by simple interrogation. Following the rules and commands integrated in the inference, the acquisition of information occurs in a very dynamic and interactive way. Thus, the ES response is achievable easily and fast. Moreover, the ES has the ability of making predictions using two modelling methods. Finally, the information is delivered in form of an intelligible draft or text file that can be then straightforwardly used in the report of the formulation tasks.

However, the ES has certain limitations. One of them is the lack of adaptation and learning from new data introduced by the user. Since the predictive models have been created after processing historic data and then inserted in the knowledge-base, the ES is not able to use new data to adapt the ANNs and the mathematic models with new presented results. As a consequence, the user cannot update the system. Nevertheless, this is in some cases desired, for instance if the reproducibility of the predictions has to be warranted, for which purpose, the exclusive access of the ES developer into the system avoids unexpected inaccuracies due to misleading updates. A second restrained feature of the ES is the reduced versatility on changing some processing parameters and composition, as the influence of the roller compaction-granulation parameters has not been included in the ES models. Also the constrained values for the minimum and maximum amount of each component in the formulation, reduces the modelling space out of which the predictions might be inaccurate.

From the ES developer's point of view, and as applicable to the vast majority of the ESs, the elaboration of the knowledge data base is, by far, the most laborious part of the development of the ES. A large number of experiments have been carried out with the purpose of creating the corresponding predictive models for product and tablet properties, which, in turn, resulted to present different accuracy according to the modelling strategy. Nevertheless, once the knowledge was created, to handle with it in MAX becomes intuitive. The design of the algorithms of decision through the editing tool is visual and plain. The number of commands required for the performance of most actions is reduced, so that no skills in computer programming are necessary to write the inference

procedures. However, the simplicity of MAX also reduces the possibility of performing intricate operations by the system. That is the reason why the update of the system with data originated by the user is not possible. In case that the user wanted to add new data into the models, the developer would need to create new models after increasing the pool of training data available prior to replace the old existing models.

Though the limitations of MAX reported here, the main issue of this ES is the elaboration of knowledge-base of the system. The systematic development of the formulation following classic criteria (i.e. modifying only one variable at a time), required a large number of experiments to cover only a reduced modelling space. That is basically due to the reduced new information that could be extracted from each new formulation. The insufficient design of experiments restricted the range of compositions, processing parameters, and components that could be modelled simultaneously. The use of tools such as the DOE software presented in 6.3.1.3, facilitates the selection of runs that deliver valuable information and reduce the number of runs to be performed.

7.5 Conclusions

An ES was created using the MAX *in silico* ES software developed by Dr. Bultmann. Two main sources of information were introduced in the knowledge-base of the system. From one side, practical expertise, bibliographic information and experimental observations were documented and organized so as to make it accessible to the user. Moreover, the predictive models created in 6.3 for the estimation of intermediary and end-product properties starting from an initial formulation were included. Through the incorporation of command files to the algorithmic rules, the ES selected, analyzed, organized and displayed the information of the knowledge-base.

Both elements developed in this work, the knowledge-base, and the inference element, show to have a key role on the definition of the ES skills. The former determines not only the quantity of information that can be accessed by the user and the complexity of the knowledge structures, but also the goodness of predictability of the models. The latter, however, defines the level of intricacy of the ES design. The simple inference part of MAX reduced extremely the effort at editing a new ES but, in turn, reduced the capability of the system to adopt new data and adapt the estimations of the models.

8 GENERAL CONCLUSIONS

The conclusions drawn from the work carried out in this thesis can be again grouped into three main parts:

I- Roller compaction

• The roller compaction of pharmaceutical ingredients is a complex process in which the dominating factors over the obtained products depend upon the type of device, the substance(s), and the ambient conditions. The compaction between the rotating rollers is a process of material densification during which the material experiences a sequence of deformation mechanisms as a response to the volume reduction, similarly as it occurs during the tablet compression. In roller compaction, however, the bulk transport at the compaction area, its distribution across the compaction gap, and the densification of the material itself, are induced by the interaction of the material with the surface of the rotating rollers.

• The ribbon solid fraction and its distribution across the ribbon width is a critical property of the produced compact, which, in turn, serves as an indicator of the pressure level exerted on the material. In addition, it gives information about the uniformity of the process, as its value and distribution is extremely sensitive to any fluctuation in the material feeding (e.g. due to the interaction with the cheek side sealing plate) and the regularity of the material distribution across the roller surfaces. This ribbon property is therefore suitable for monitoring the compaction process. For its characterization, there is a number of techniques that demonstrate to deliver accurate values of the sample densification with different resolution. The selection of the most suitable determination method depends on the details and the purposes sought.

• The process conditions (e.g. roller speed, roller gap, and lubrication of the sealing plates) and the modification of the bulk properties (e.g. addition of a lubricant or moisture to the blend) have a strong impact on the material compaction at three main levels:

i) The material response at early stages of the compaction, which vary the bulk cohesion, the air permeation, etc.
ii) The interaction of the material with the roller surface (and the seal assembly), which changes the shear forces induced at the roller interface and the friction components, hence modifying the amount of material and the uniformity of its distribution across the roller gap.
iii) The material compaction behaviour, which is partially affected by the amount and the distribution of material in the roller gap, but also depends on the deformational response of the material to the pressure exerted by the rollers.

• The *re-workability* of a roller compacted-granulated product into tablets depends on the resulting morphology and the deformation characteristics of the particles and granules. The implications of the *work hardening* in the tabletability of the granule might be different as a function of the material

deformation behaviour. Thus, for lactose monohydrate, the loss of *re-workability* is due to a reduction of the range of pressures at which the material deformed plastically and the accentuation of the material elasticity.

II- Tablet formulation and predictive models

• For tablets produced after dry-granulation of powder blends, any modification in the formulation induces changes in the intermediary and the end product attributes. Although a single substance might present characteristic processing features, within a formulation, not only the content of the components, but also the sequence of addition (e.g. extra-granularly blended), and the interaction with the other substances forming part of the blend determine the effect of the addition, the removal, or the variation in the amount of the component on the product properties.

• The effects of the modifications in the formulation and the processing parameters on the product properties can be successfully modelled using ANNs and GRMs. ANNs are more versatile than GRM models but their *black box* nature does not permit to retrieve as much information about the variables involved in the response as mathematic models. Nevertheless, it has been observed that both methods perform differently as a function of the number of variables contemplated, and the size and the nature of the data set provided for the creation of the model. DOE applications are powerful tools for the improvement of the quality of the data. Contrariwise as for the classic systematic formulation development, a designed experiment allows the extraction of more information, as it increases the number of variables that can be changed simultaneously.

III- Expert system

• The development of an ES has been implemented successfully in the formulation of tablets produced with dry-granulated pharmaceutical substances. For that purpose, the ES contains models to draw prognoses of the product attributes and it provides guide-lines and comments that are useful to solve issues that might arise during the manufacturing process. The ES can store up (almost) unlimited amount of extra information (e.g. main component characteristics, methods and materials used during the model's development) in a well-organized manner, which can be easily retrieved by the user. ES are extremely useful tools, especially for the pharmaceutical industry, as they ease the development increasing the consistency, the quality and the efficiency of the formulation tasks. In addition they ensure the permanency and the accessibility of the knowledge and assist formulators in their work.

9 APPENDIX

9.1 Pharmaceutical ingredients

9.1.1 Microcrystalline cellulose (MCC)

Developed during the 1960s [363], MCC is originated from the hydrolysis of α-cellulose with acid. Cellulose fibres are suspended in water and are washed with an acid solution (2.5 N HCl) at high temperature (95-105ºC) at different times. The acid hydrolysis removes the amorphous cellulose linking the structures generating a suspension of microcrystallines of hydrocellulose that is next stirred and filtered. The purified hydrocellulose particles are spray-dried to form porous particles of broad-size distributions (Pharmaceutical Excipients v2.0 2001 [308]). By varying hydrolytic, shearing and drying conditions, the particle size, the morphology and the moisture content may be changed, originating different MCC grades.

MCC is a white, non toxic and non irritant material used as a pharmaceutical grade excipient It is the most frequently used filler-binder in the manufacture of solid dosage forms with the best bonding properties and the best compactibility [364]. It is used both for direct compression and for dry and wet granulation. Beside its main function as filler and dry binder, its swelling behaviour in contact with water makes it suitable as a disintegrant. MCC is high ductile [322], [50] and has a low elasticity (grade variable). Is highly hygroscopic, and the increase of water increases its plasticity. Two types of MCC were use in this work: PH101 and PH102.

i. Type PH101**:** the brand used was Vivapur PH101 (JRS, Holzmuelle, Germany). It has a degree of polymerization (DP) of 160 [365]. It is the MCC grade with the smallest mean particle size (ca. 50 μm) [366] and the best compactability #287. It has a poor flowability due to the small particle sizes what makes it unsuitable as a DC grade.

ii. Type PH102**:** Avicel PH102 (FMC Corporation, Philadelphia, USA) was used. This Type of MCC has a higher DP (180) [365] and a nominal particle size of ca. 100 μm [308]. Is also highly plastic and presents better flowability, is widely used as a DC-grade (FMC web [367]).

9.1.2 Mannitol (MNT)

Is a polyol isomer of sorbitol. Present naturally in the exudates of *Fraxinus ornus* (Manna Ash) [368], it is currently prepared mainly through two methods: by catalytic reduction of different sugars (sucrose, D-glucose, D-Mannose, D-Fructose) originating sorbitol and MNT that is then isolated [369], and by fermentation [368]. MNT is commercialized as a white fine powder. It is mainly used as a tablet and capsule filler. It has a low hygroscopicity what turns it into a very useful excipient in formulations of moisture-sensitive API [308]. Its rather moderate solubility in water (18% (w/v)) and its sweet and refreshing taste, make it the first choice in formulations for lozenges and chewable tablets. It is rarely used as native powder due to its poor flowability. It has a low compactibility that

can be improved through granulation. Formulations with MNT require larger amounts of lubricant (over 1%) and a binder to increase the tablet hardness.

9.1.3 Ludipress LCE (LP)

Ludipress LCE is a product based on lactose monohydrate (LMH) (96.5%) and pollyvinylpyrrolidone (PVP) (Kollidon 30) (3.5%) produced through co-processed agglomeration of both components [316]. It is commercialized as a white-yellowish free flowing and water soluble granule considered a multipurpose excipient [370]. The relative coarse mean particle size (260-275 μm) makes the substance free flowing. It has shown to have an excellent mixing efficiency with small drug quantities attributed to the particle surface roughness. This also reduces the sensitivity of the material towards the addition of lubricants into the blend. The co-processed PVP provides LP with higher plasticity than LMH crystalline ingredients, resulting into harder tablets with lower friability [319]. The main application of LP-LCE is as a filler-binder in DC, and in the production of chewable tablets and lozenges.

9.1.4 Colloidal silicon dioxide (Aerosil 200 -A200-)

Aerosil 200, commercialized by Degussa/Evonik, is a highly disperse silicon dioxide. It is often referred to as "fumed silica" owing to its production process, which was patented by Degussa in the early 1940's [371]. It is manufactured by the hydrolysis of chlorosilicanes ($SiCl_4$) in a high-temperature hydrogen-oxygen flame burner where an aerosol of SiO_2 with primary particles of 15 nm size is generated. The floating sub-microscopic particles are separated and tend to form spontaneously almost stable agglomerates. The colloidal silicon dioxide properties can be specifically controlled by using appropriate reaction conditions and surface modifications [321]. A200 is a fine, white-bluish, extremely light, amorphous, loose powder with a small particle size and a huge specific surface area (200 m^2/g) [372]. It belongs to the group of hydrophilic "aerosils", i.e. with silanol (-Si-OH) groups on the surface. Thus, in water A200 forms colloidal suspensions, which are used to stabilize emulsions. In solid dosage forms A200 is mainly used as a glindant. Thanks to its enormous specific surface, A200 forms a film around the particles, reducing considerably the number of interactions and consequently reducing the friction [315]. The formation of that film around has also been attached to a decrease of the sensitivity towards the lubricant addition [307]. The hydrophilic character of A200 also has been observed by Chang, et al. [318] to have a positive effect on the tablet disintegration. A200 works as a moisture scavenger increasing the wicking effect of some disintegrants. The use of A200 in solid dosage forms should not exceed a 2% due to its negative effect on the particle interaction and the compact cohesiveness and the dramatic decrease of the compact hardness.

9.1.5 Magnesium stearate (MgSt)

The magnesium stearate used in this work was supplied by Baerloch AG and Saville Whittle. MgSt is a mixture of magnesium salts of different fatty acids consisting mainly of stearic acid and palmitic acid. Other fatty acids can also be present in minor proportions. MgSt is manufactured by the reaction of magnesium chloride and sodium stearate in water or by interaction of magnesium oxide,

magnesium hydroxide or magnesium bicarbonate with stearates at elevated temperatures [308]. As a result of the process an extremely fine, white, loose powder with low bulk density, faint odour and greasy touch is obtained. MgSt is completely insoluble in water and almost all polar solvents (except ethanol) [373, 189] classified MgSt as a lubricant with strong anti-adherent character with only little glidant action and proposed its combination with talc to achieve fluent blends with low sticking tendency. The lubrication effect of MgSt is attributed to the local formation of layers of MgSt on the surface that reduce the particle-particle and particle-surface interactions. Vromans and Lerk [374] explained that for that same reason, MgSt has a negative effect on the compact cohesiveness, since at the covered areas the particles cannot interact with each other and the bonding is hindered. This is specially critic in materials with smooth surfaces which deform plastically and interact basically by increasing the particle contact surfaces [304].

9.1.6 Kollidon VA 64 (KVA64)

KVA64 was supplied by BASF SE. It is a co-polymer of vinylpyrrolidone and vinylacetate. It is manufactured by free-radical polymerization of 6 parts of vinylpyrrolidone and 4 parts of vinylacetate in isopropanol [346] and the medium is thereafter spray-dried to obtain a finely agglomerated (40 μm) [375], white-yellowish granule with good flowability, soluble in water and alcohols [345]. KVA64 presents affinity to hydrophilic and hydrophobic surfaces what turns it into a good binder regardless of its use in wet, dry granulation or in DC processes [364]. The irregular structure of the particles increases the contact surface and thus the capacity of interaction with other components. Its high plasticity confers the blend good tabletability properties resulting into less brittle tablets with lower tendency to cap. Compared to other binders [375], blends containing KVA64 are less prone to stick to the punches and are harder. Other applications of KVA64 in solid dosage forms are the addition in retard forms and the use as a coating agent for immediate release forms.

9.1.7 Croscarmellose sodium (AcDiSol -ADS-)

AcDiSol is the FMC Biopolymers brand name of internally cross-linked carboxymethylcellulose sodium. It is manufactured by steeping cellulose from wood pulp or cotton fibres in sodium hydroxide solutions. The alkali cellulose is reacted with sodium monochloracetate in excess to obtain carboxymethylcellulose sodium. When all sodium hydroxide is exhorted, the sodium monochloracetate catalyzes the formation of cross-links that result in croscarmellose sodium. The product is extracted from the medium with alcohol. Thereafter it is dried and milled. The product is commercialized as an odourless, relative free flowing, white powder. Its cross-linked structure ensures insolubility but preserves the hydrophilic character (FMC technical information [376]). ADS is used exclusively as a disintegrant in solid dosage forms. Its strong affinity to water and its rapid swelling [377] confer the substance an efficient active disintegration mechanism. Added at low concentrations, ADS speeds up the water uptake into the core of the tablet through capillarity. In contact with water ADS swells and induces the tablet fracture, resulting into short tablet disintegration times. The efficiency of the ADS as a disintegrant at different concentrations was studied by Ferrero, et al. [328]. They observed that there is a maximal concentration (over a 5%) above which the disintegrant-

efficiency of ADS decreases. This was attributed to the isolation of certain tablet areas after the water uptake in closed channelled structures at high ADS concentrations.

9.1.8 α Lactose monohydrate (LMH)

Granulac 140 by Meggle is the α Lactose monohydrate crystalline pharmaceutical grade used in this work. Lactose is a natural disaccharide of D-galactose and D-glucose. Commercially, lactose is produced from the residuals after the manufacture of lactic products such as cheese or casein. α Lactose is the crystalline form prepared by crystallization of supersaturated lactose solutions below 93.5 ºC, and is available primarily as the monohydrate conformation. The crystals are then milled to the desired particle size. Granulac 140 is a fine (mean size 40 μm) white powder with poor flowability and moderately soluble in water (20%, w/v). LMH is less hygroscopic than the anhydrous forms [308]. Its main application is as filler in capsules and tablets. Crystalline LMH has poor compressibility and needs normally the addition of binders to achieve sufficient tablet hardness ([7] pp.74-78). Lerk [305] compared the properties of different crystalline forms and described LMH as a poor compactable excipient. He discouraged the use of LMH in DC and advised the use of amorphous forms for that purpose. Riepma, et al [26] also studied the tablet hardness of different lactoses and observed that it was closely related to the crystalline structure and the crystal size. Thus smaller crystals originated porous loose tablets.

9.1.9 Paracetamol

N-acetyl-p-aminophenol

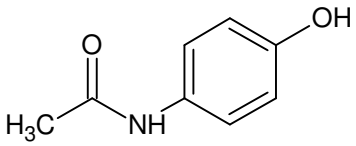

Paracetamol, also known as acetaminophen, is a non-opioide analgesic. It is the only member from the aniline-derivates currently in use in therapy. It is an antipyretic with a very low anti-inflammatory effect. The low affinity to the cyclooxigenase and the specificity of paracetamol to the inhibition of prostaglandin synthetase at the CNS found by Flower and Vane [378] explains the low antiinflamatory pharmacological effect. The most common way of administration is orally in dosages variable between 325 and 650 mg in adults and of 60-120 mg upon age and weight in children every 4 hours (Goodman Gilman, et al. [379]). Its absorption takes place entirely in the TGI by passive transport. The peak of maximal concentration in blood appears after 30 min where the union to plasma proteins is insignificant. The half time of paracetamol is between 1.5-2 hours and is excreted through the urine as a sulphate or glucoronide conjugates (Prescott [380]).

The paracetamol used in this work was supplied by Bayer. It is a white moderate coarse crystalline bulk. As ingredient for solid dosage forms, paracetamol, as many other API, has been described as a poor compactable ingredient. Rasenack, et al. [329] and Patel, et al. [333] described paracetamol as a substance with bad compressibility due to its evident elastic character that lead to loose compacts. Paracetamol dissolves slowly in water [337] extending the time of dissolution. However, this can be improved by modifying the crystalline form and the particle size [324]. Due to its poor tabletability

paracetamol has to be formulated generally together with plastic excipients (filler-binders) and binders to achieve sufficient tablet hardness.

9.1.10 True density values

The values of the density determined by pycnometry are recorded in the following table. .

Table 33. True density values of the pharmaceutical ingredients

	Density [g/cm^3]
MCC PH101	1.568
MCC PH102	1.585
MgSt	1.024
LMH	1.547
LP	1.556
ADS	1.616
MNT	1.517
KVA64	1.244
PL	1.297

9.2 Wiegel's and Kawakita's equation

Several models have tried to describe the densification process during tableting. The same Kawakita together with Ludde [40] listed, compared and criticized compressibility equations developed by several authors. Also Çelik [42] compared them and stated that each equation can deliver information for a different stage of the compression (i.e. from very low to very high compression pressures). In section 2.1.5 the Heckel equations has been introduced as a noteworthy model to characterize the compressibility of the material. It approaches the relationship between volume reduction (i.e. the densification) and compression pressure. However, the Kawakita and the Wiegel equations have been also mentioned, and are the focus of this section.

Kawakita observed empirically that the reduction of volume of material during the compression approaches this equation:

$$\frac{P}{C} = \frac{1}{ab} + \frac{P}{a} \tag{37}$$

where C is the degree of volume reduction, P is the compression pressure, and a and b are material constants. Thus, as represented in Figure 133. The densification can be fitted in a linear plot. However, as it also happens in the Heckel plot, the Kawakita equation also provides information about the deformation characteristics of the material. Accordingly, a is closely related to the initial powder bed porosity and b is a constant correlated to the cohesive forces between powder particles [40].

As for Wiegel's equation, the author [51] adapted an equation developed by Carstensen, et al. [325] considering that the "out of die" densification level of the compressed material does not achieve in any case the value of true density (i.e. absolute absence of porosity). With this equation, he was able to

describe all stages of the material compression. According to his work, the solid fraction of a compressed form at a compression pressure *P* can be calculated from the following equation:

$$\rho_{rel} = \rho_0 + (\rho_{\max} - \rho_0) \cdot (1 - e^{(-kD \cdot P)}) \qquad (38)$$

where $\rho 0$, $\rho \max$ and ρrel are the solid fraction of the bulk at a compression pressure of 0 MPa, the maximal solid fraction achievable by the material and the solid fraction of the compressed material for a given compression pressure *P,* respectively. *kD* is a coefficient which value depends directly on the material compressibility.

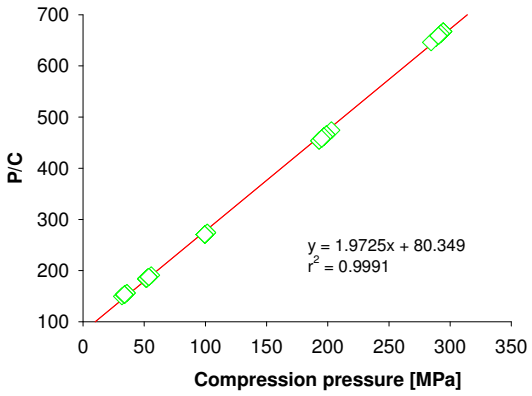

Figure 133. Kawakita plot for the compression of MCC

In Figure 134 we present the diagrams of the Wiegel's equation for the compression of two dry granulated materials: LMH and MCC. The values for the equation parameters are listed in Table 34. As shown in the figure, the value of $\rho 0$ and $\rho \max$ correspond to the intercept and the maximum value of the profile, respectively. *kD*, in turn, determines the evolution of the density values for the different pressure values. Higher values of *kD* are normally seen in compressible substances that experience large changes in densification for small variations in the pressure value.

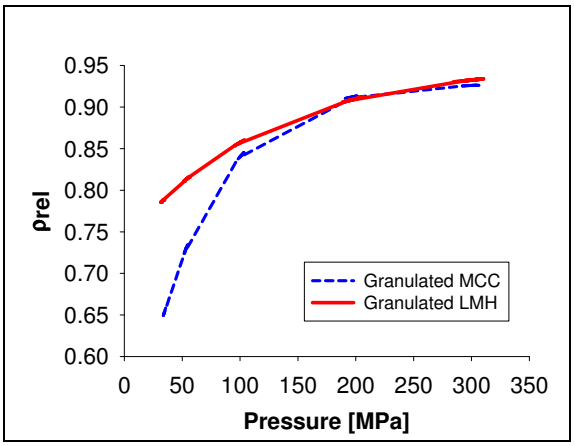

Figure 134. Representation of Wiegel plots for two tableting materials

Table 34. Wiegel parameters calculated for two granulated materials

MCC	
ρ_0 [g/cm^3]	0.4263
ρ_{max} [g/cm^3]	0.9311
kD	0.0174
LMH	
ρ_0 [g/cm^3]	0.7352
ρ_{max} [g/cm^3]	0.9504
kD	0.0084

The calculation of the three variables that are characteristic for the substance (or the blend), i.e. $\rho 0$, $\rho \max$ and *kD* is done straightforwardly by iteration and adaption of initial values, so as to to achieve the smallest SSE (summed square errors) between predicted and experimental values. With this intention, a certain number of tablets are produced at different compression pressures. Thereafter, the density of the tablets is determined geometrically and is listed in a worksheet where by means of a solver tool, the calculation of $\rho 0$, $\rho \max$ and *kD,* is possible.

9.3 MCC granule with external additives - List of blends

Table 35. MCC-granule with external additives. Record of blends and their composition

No.	Intern Phase	External Phase			
	MCC	***A200***	***LP***	***MCCext***	***MgSt***
1	99.50	0.00	0.00	0.00	0.50
2	94.28	0.24	0.00	5.00	0.49
3	96.76	0.24	0.00	2.50	0.49
4	99.25	0.25	0.00	0.00	0.50
5	96.76	0.24	2.50	0.00	0.49
6	94.28	0.24	5.00	0.00	0.49
7	93.80	0.71	0.00	5.00	0.49
8	96.28	0.73	0.00	2.50	0.49
9	98.75	0.75	0.00	0.00	0.50
10	96.28	0.73	2.50	0.00	0.49
11	93.80	0.71	5.00	0.00	0.49
12	93.33	1.18	0.00	5.00	0.48
13	95.79	1.22	0.00	2.50	0.49
14	98.57	1.25	0.00	0.00	0.18
15	93.33	1.18	5.00	0.00	0.48
16	92.15	2.37	0.00	5.00	0.48
17	94.58	2.43	0.00	2.50	0.49
18	97.01	2.49	0.00	0.00	0.49
19	94.58	2.43	2.50	0.00	0.49
20	92.15	2.37	5.00	0.00	0.48
21	92.15	0.00	2.37	5.00	0.48
22	94.58	0.00	2.43	2.50	0.49
23	97.01	0.00	2.49	0.00	0.49
24	96.77	0.25	2.49	0.00	0.49
25	96.28	0.75	2.48	0.00	0.49
26	95.80	1.25	2.46	0.00	0.49
27	89.79	0.00	4.74	5.00	0.48
28	89.79	0.00	4.74	5.00	0.48
29	92.16	0.00	4.86	2.50	0.48
30	94.53	0.00	4.99	0.00	0.49
31	94.29	0.25	4.98	0.00	0.49
32	93.34	1.25	4.93	0.00	0.48
33	85.06	0.00	9.48	5.00	0.46
34	87.31	0.00	9.73	2.50	0.47
35	89.55	0.00	9.98	0.00	0.47
36	89.33	0.25	9.95	0.00	0.47
37	88.88	0.75	9.90	0.00	0.47
38	88.43	1.25	9.85	0.00	0.47
39	92.15	0.00	5.00	2.37	0.48
40	94.58	0.00	2.50	2.43	0.49
41	97.01	0.00	0.00	2.49	0.49
42	96.77	0.25	0.00	2.49	0.49
43	96.28	0.75	0.00	2.48	0.49
44	95.80	1.25	0.00	2.46	0.49
45	89.79	0.00	5.00	4.74	0.48
46	94.53	0.00	0.00	4.99	0.49
47	94.29	0.25	0.00	4.98	0.49
48	93.81	0.75	0.00	4.95	0.49
49	93.34	1.25	0.00	4.93	0.48
50	85.06	0.00	5.00	9.48	0.46
51	87.31	0.00	2.50	9.73	0.47
52	89.55	0.00	0.00	9.98	0.47
53	89.33	0.25	0.00	9.95	0.47
54	88.88	0.75	0.00	9.90	0.47
55	88.43	1.25	0.00	9.85	0.47
56	69.58	0.00	29.93	0.00	0.50
57	69.40	0.25	29.85	0.00	0.50
58	69.05	1.25	29.70	0.00	0.50
59	66.09	0.00	28.43	5.00	0.49
60	69.58	0.00	0.00	29.93	0.50
61	69.40	0.25	0.00	29.85	0.50
62	69.05	0.75	0.00	29.70	0.50
63	66.09	0.00	5.00	28.43	0.49

9.4 Multicomponent batch composition - List of blends

Table 36. Multicomponent batch composition - Group 1

No.	***MCC***	***A200***	***LP***	***ADS***	***PL***	***MgSt***
1	99.50	0	0	0	0	0.499
2	89.52	0	0	0	9.97	0.499
3	59.60	0	0	0	39.9	0.499
4	99.25	0.249	0	0	0	0.499
5	98.25	1.246	0	0	0	0.499
6	97.00	2.493	0	0	0	0.499
7	94.51	0	4.98	0	0	0.499
8	89.52	0	9.97	0	0	0.499
9	69.57	0	29.92	0	0	0.499
10	94.26	0.249	4.98	0	0	0.499

11	89.27	0.249	9.97	0	0	0.499
12	93.76	0.748	4.98	0	0	0.499
13	88.77	0.748	9.97	0	0	0.499
14	93.26	1.246	4.98	0	0	0.499
15	87.03	2.493	9.97	0	0	0.499
16	68.82	0.748	29.92	0	0	0.499
17	93.76	0.748	4.98	0	0	0.499
18	89.27	0.249	9.97	0	0	0.499
19	84.28	0.249	4.98	0	9.97	0.499
20	74.31	0.249	4.98	0	19.95	0.499
21	54.36	0.249	4.98	0	39.9	0.499
22	78.80	0.748	9.97	0	9.97	0.499
23	68.82	0.748	9.97	0	19.95	0.499
24	48.87	0.748	9.97	0	39.9	0.499
25	91.77	0.249	4.98	2.49	0	0.499
26	89.27	0.249	4.98	4.98	0	0.499
27	81.79	0.249	4.98	2.49	9.97	0.499
28	51.87	0.249	4.98	2.49	39.9	0.499
29	79.30	0.249	4.98	2.49	9.97	0.499
30	49.37	0.249	4.98	4.98	39.9	0.499

Table 37. Multicomponent batch composition - Group 2

No.	***MMNT***	***KVA64***	***ADS***	***LP***	***MgSt***
1	99.45	0	0	0	0.55
2	90.45	0	0	10	0.55
3	79.45	0	0	20	0.55
4	69.45	0	0	30	0.55
5	88.45	1	0	10	0.55
6	78.45	1	0	20	0.55
7	87.45	2	0	10	0.55
8	57.45	2	0	40	0.55
9	85.45	4	0	10	0.55
10	55.45	4	0	40	0.55
11	86.95	0	2.5	10	0.55
12	84.45	0	5	10	0.55
13	82.95	4	2.5	10	0.55
14	62.95	4	2.5	30	0.55
15	60.45	4	5	30	0.55

9.5 D-optimal design of experiments

The D-optimal design is a genetic DoE at which there is a selection and an optimization of the number of runs necessary to extract the maximum amount of information by generating a wide experimental region with the minimum number of experiments.

The principles of the algorithm when choosing the experimental candidates forming part of the models follow the theories presented at [381] and [382]. Briefly summarized, if a matrix with all factors of the experimental candidates X, the *D-optimization* tries to find the maximum value of the determinant of the matrix resulting after multiplying the transposed matrix of *X, X'* times the matrix *X*, mentioned in the literature [355, 381] as the optimization of the value |X'X|. The calculation of the matrix determinant is carried out as follows, and is in detail described in [383].

Given a matrix *a* expressed mathematically as:

$$a_{\mu\nu} = \begin{bmatrix} a_{11} & a_{12}.... & a_{1n} \\ a_{21} & ..... & a_{2n} \\ a_{n1} & ..... & a_{nn} \end{bmatrix} \tag{39}$$

the determinant $|a_{\mu\nu}|$ will be calculated

$$\det A = \sum_{\mu=1}^{n} a_{\mu\nu} A_{\mu\nu} \tag{40}$$

Being $A_{\mu\nu}$ the determinant of immediate lower order for the matrix $a_{\mu\nu}$ times the factor $(-1)^{\mu\nu}$.
Thus, for example, a matrix the determinant of a matrix $a_{3,3}$ the determinant would be calculated as:

$$|a| = \begin{vmatrix} a & b & c \\ d & e & f \\ g & h & i \end{vmatrix} = -afh + aei - bdi + bfg - ceg + edh \tag{41}$$

Thus, recalling the matrix X and its transposed X' of our design of experiments, the D-optimization (i.e., the determinant optimization) will calculate from all possible experimental candidates that could be included into X, which of them would generate a determinant of the matrix [X'X] with a maximized value. Thus, if the vectors of X and X' are redundant, the value of the determinant D will be close to 0, whereas the more independent the factors are, the larger will be the D-value. This will generate an end matrix of experiments for which the factor effects are maximally independent from each other [381].

9.6 Neural network architecture for the product variables created with the ANNe software

Table 38. Architecture of the ANNs created for modelling the attributes of products from MCC-granules with external component

Variables		Architecture (No. PEs)		
Inputs	***Outputs***	***Input layer***	***Hidden layer***	***Output***
Composition (components and [%])	Granule RRSB-n and RRSB-d'	4	6	2
Composition (components and [%])	Granule angle of repose and CI	4	6	2
Composition (components and [%]) and compression pressure	Tablet σ and t_{dis}	5	6	2

Table 39. Architecture of the ANNs created for modelling the attributes of products from multicomponent formulations (Group 1)

Variables		Architecture (No. PEs)		
Inputs	***Outputs***	***Input layer***	***Hidden layer***	***Output***
Composition (components and [%])	Ribbon ρ_{rel} and σ	5	7	2
Composition (components and [%])	Granule RRSB-n	5	6	1
Composition (components and [%])	Granule RRSB-d'	5	6	1
Composition (components and [%])	Granule angle of repose	5	6	1
Composition (components and [%])	Granule CI	5	6	1
Composition (components and [%]) and Compression pressure	Tablet σ and t_{dis}	6	9	2
Composition (components and [%]) and Compression pressure	Tablet t_{80}	6	7	1

Table 40. Architecture of the ANNs created for modelling the attributes of products from multicomponent formulations (Group 2)

Variables		Architecture (No. PEs)		
Inputs	***Outputs***	***Input layer***	***Hidden layer***	***Output***
Composition (components and [%])	Ribbon ρ_{rel} and σ	4	5	2
Composition (components and [%])	Granule RRSB-n and RRSB-d'	4	5	2
Composition (components and [%])	Granule angle of repose and CI	4	5	2
Composition (components and [%]) and Compression pressure	Tablet σ	5	6	1
Composition (components and [%]) and Compression pressure	Tablet t_{dis}	5	6	1
Composition (components and [%]) and Compression pressure	Tablet t_{80}	5	6	1

9.7 GRM models. β-coefficients

The *β-coefficients* are the regression coefficients for the independent variables after their standardization to a mean of 0 and a standard deviation of 1. Thus, the magnitude of these *β-coefficients* allows you to compare the relative contribution of each independent variable in the prediction of the dependent variable [381].

9.7.1 MCC-granule with external components

Table 41. Pareto charts for the β-coefficients of the GRM parameters involved in the modelling of blend properties. MCC-granules with external components

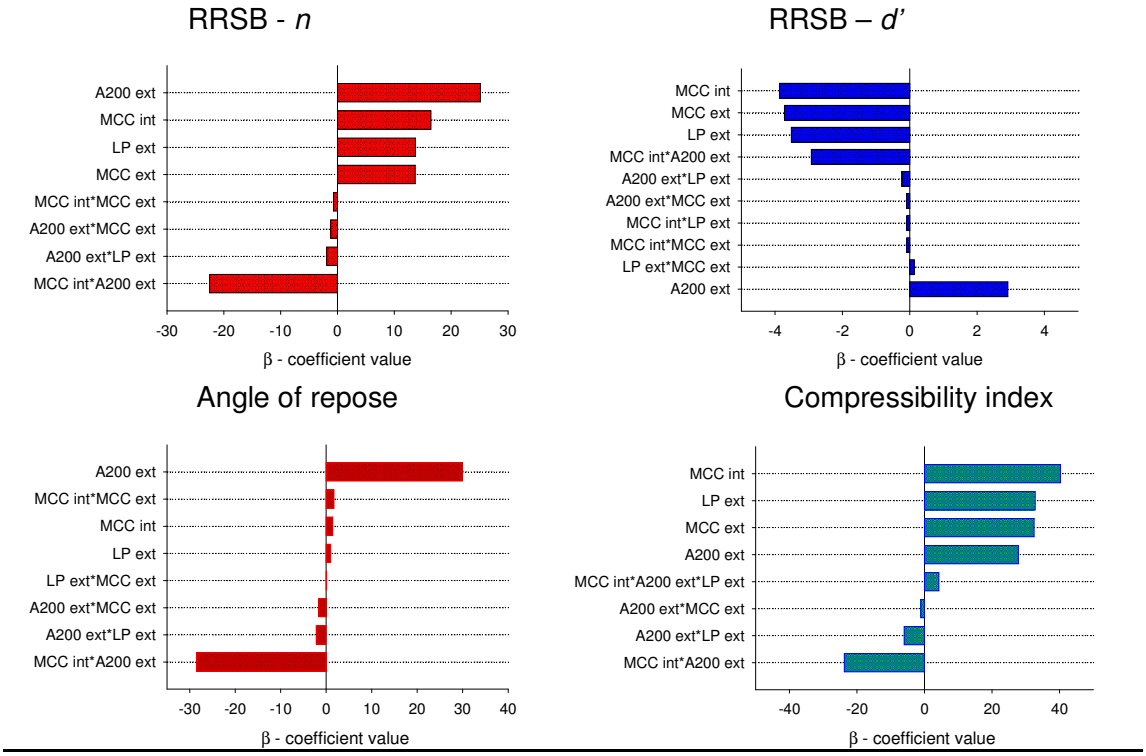

Table 42. Pareto charts for the β-coefficients of the GRM parameters involved in the modelling of tablet properties. MCC-granules with external components

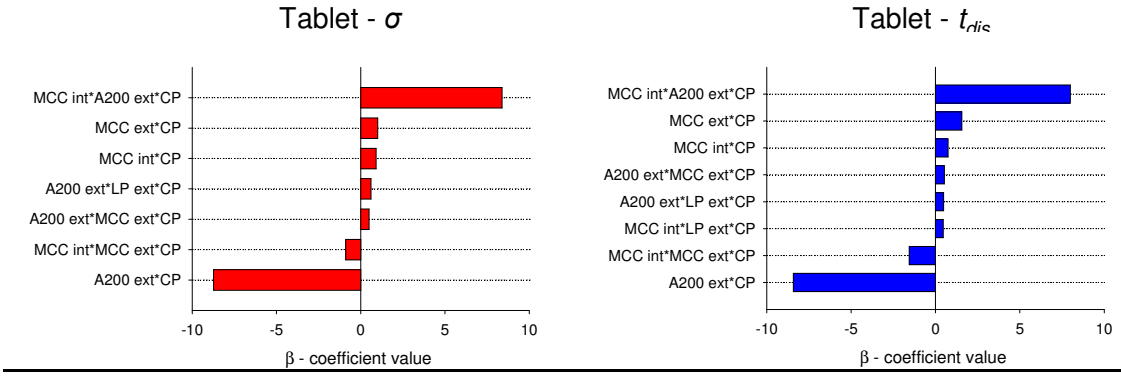

9.7.2 Multicomponent formulations - group 1 -

Table 43. Pareto charts for the β-coefficients of the GRM parameters involved in the modelling of ribbon properties. Multicomponent formulations - group 1

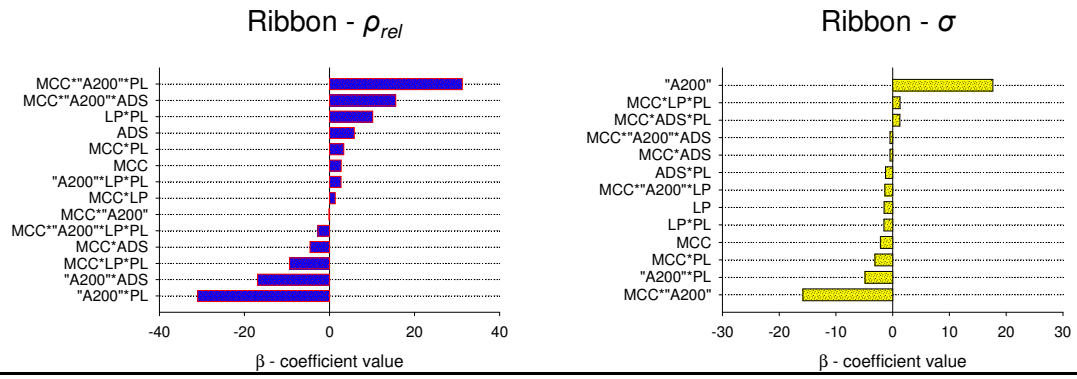

Table 44. Pareto charts for the β-coefficients of the GRM parameters involved in the modelling of blend properties. Multicomponent formulations - group 1

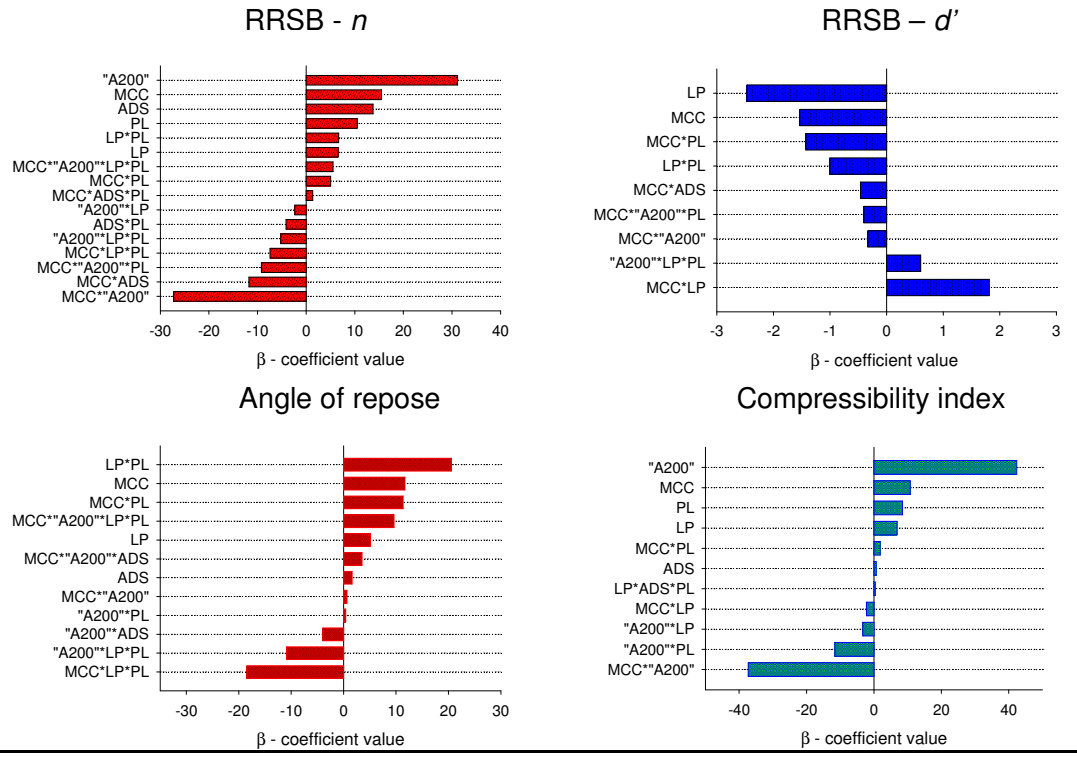

Table 45. Pareto charts for the β-coefficients of the GRM parameters involved in the modelling of tablet properties. Multicomponent formulations - group 1

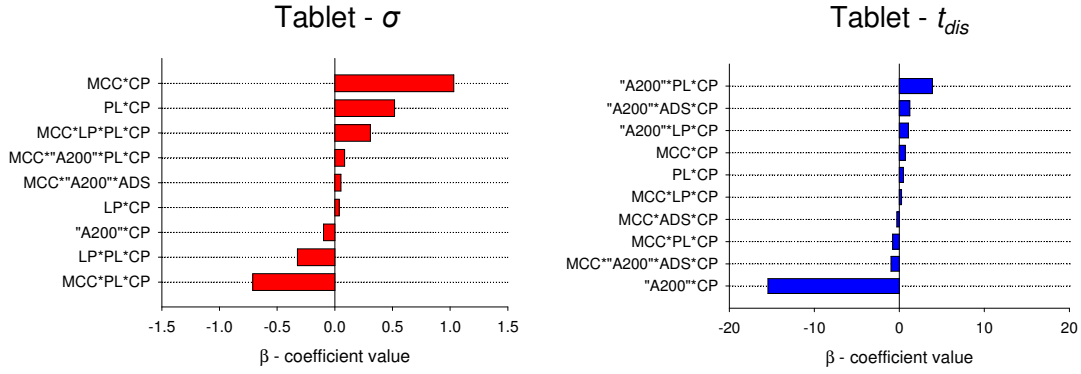

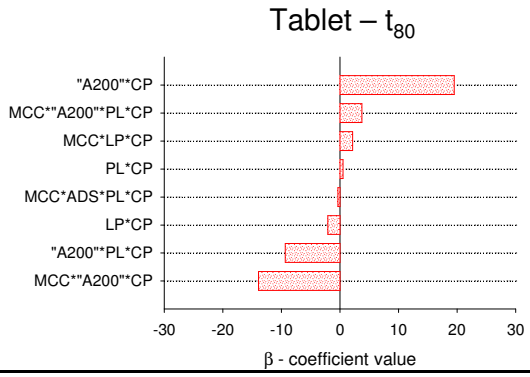

9.7.3 Multicomponent formulations - group 2 -

Table 46. Pareto charts for the β-coefficients of the GRM parameters involved in the modelling of ribbon properties. Multicomponent formulations - group 2

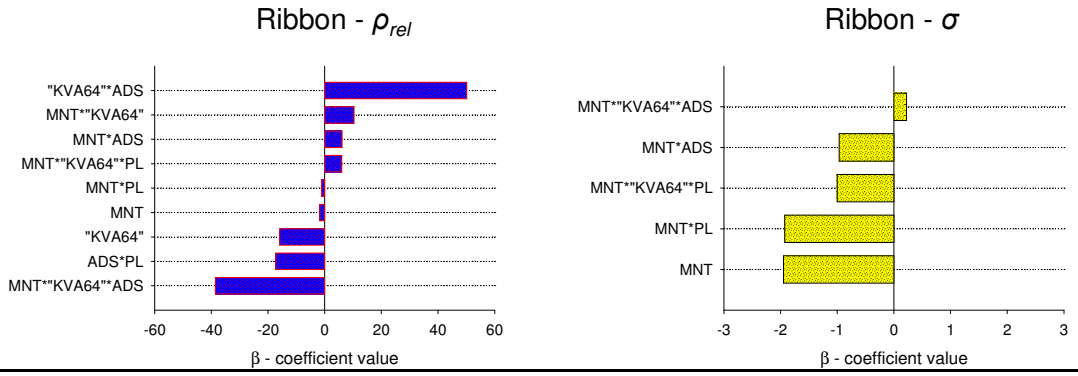

Table 47. Pareto charts for the β-coefficients of the GRM parameters involved in the modelling of blend properties. Multicomponent formulations - group 2

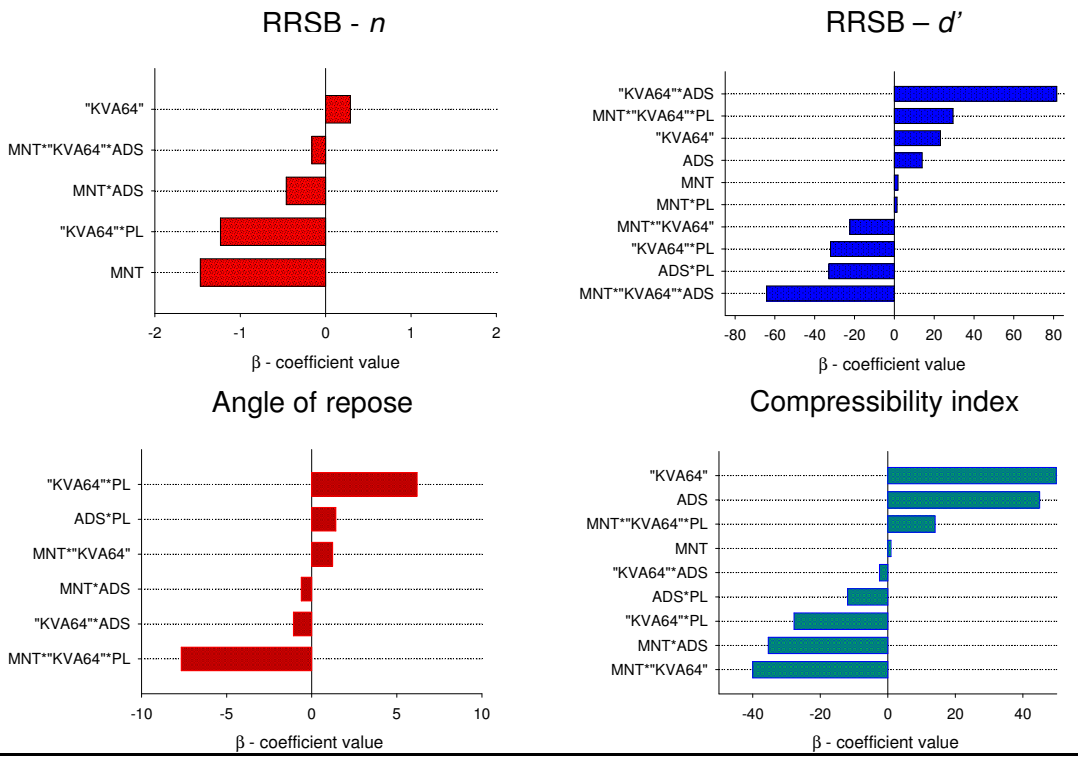

Table 48. Pareto charts for the β-coefficients of the GRM parameters involved in the modelling of tablet properties. Multicomponent formulations - group 2

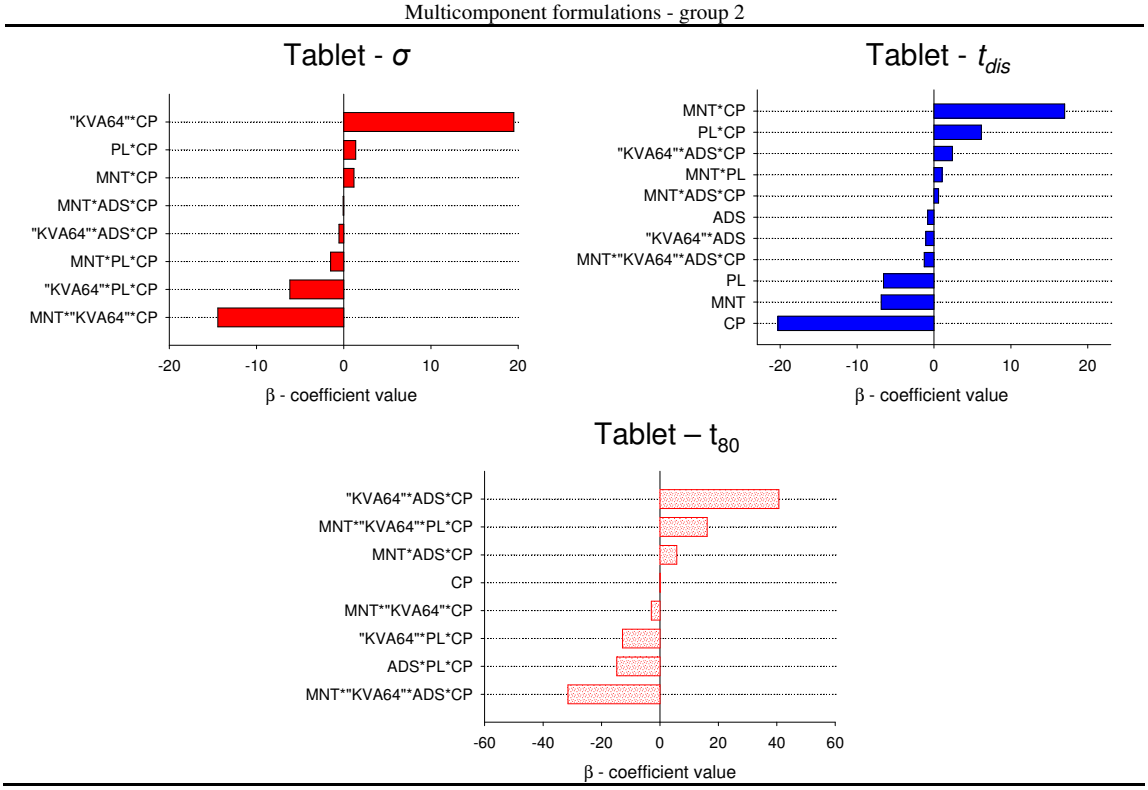

9.7.4 Interpretation of the information

The information that can be extracted from the representation of the *β-coefficient* of all effects was compared next with the observations made in sections 6.5.1 and 6.5.2 of the effect of each component on the studied properties. This is summarized in the following tables.

Table 49. Comparison of the information about the effect of the formulation on the studied attributes extracted from the GRM *β-coefficient* diagrams and from the direct observation of experimental results for the formulations of external components added to MCC-granules.

		MCC-granule with external components	
	Response	Experimental observations	GRM *β-coefficient* (Appendix 8.7.1)
Angle of repose	↑	• A200 and LP in large amounts • MCCext	• A200 • LP • MCCext
	↓	• A200 and LP in small amount	• A200 - LP, MCCint-A200 interaction • MCCint-LP interaction
CI	↑	• Large amount of MCCint, MCCext, LP and A200	• A200 • LP • MCCint • MCCext
	↓	• A200 in small quantity	• MCCint-A200 interaction
Tablet σ	↑	• SmallA200 amount • Large amounts of MCC (MCCext and MCCint)	• MCCint-A200-CP interaction • MCC (both MCCext and MCCint) -CP interaction
	↓	• Large amounts of A200	• A200-CP interaction
Tablet t_{dis}	↑	• SmallA200 amount • Large amounts of MCC (MCCext and MCCint)	• MCCint-A200-CP interaction • MCC (both MCCext and MCCint) - CP interaction
	↓	• Large amounts of A200	• A200-CP interaction

Table 50. Comparison of the information about the effect of the formulation on the studied attributes extracted from the GRM *β-coefficient* diagrams and from the direct observation of experimental results for the multicomponent formulation (group1)

		Multicomponent granules - group 1	
	Response	Experimental observations	GRM *β-coefficient* (Appendix 8.7.2)
Ribbon ρ_{rel}	↑	• Small amounts of A200 • LP • ADS • PL	• Interaction MCC-A200-PL • Interaction MCC-A200-ADS • Ineraction LP-PL • ADS
	↓	• Large amounts of A200	• Interaction MCC-A200-LP-PL • Interaction MCC-ADS • Interaction MCC-LP-PL • Interaction A200-ADS
Ribbon σ	↑	• ADS • A200 in large quantity	• A200 • ADS • Interaction MCC-LP-PL • Interaction MCC-A200-PLt
	↓	• A200 in small quantity • LP addition • PL addition	• MCC-A200 interaction • A200-PL interaction • MCC-PL interaction
RRSB- *n*	↑	• Large amount of A200 • Large amount of LP • Large amount of ADS	• A200 • ADS • PL • LP-PL interaction
	↓	• Small amounts of A200 • Small amount of LP • Small amount of ADS	• MCC-A200 interaction • MCC-ADS interaction • MCC-A200-PL interaction • MCC-LP-PL interaction
RRSB- *d'*	↑	• Small quantity of A200 • Small quantity of LP	• MCC-LP interaction • A200-LP-PL interaction
	↓	• Large amounts of LP • PL	• LP • MCC • MCC-PL interaction • LP-PL interaction
Angle of repose	↑	• PL	• LP-PL interaction • MCC • MCC-PL interaction • MCC-A200-LP-PL interaction
	↓	• Large quantities of A200 • Large quantity of A200 • LP	• MCC-LP-PL interaction • A200-LP-PL interaction • A200-ADS interaction • A200-PL interaction

CI	↑	• ADS • PL	• A200 • MCC • PL • LP
	↓	• A200 • LP	• MCC-A200 interaction • A200-PL interaction • A200-LP interaction
Tablet σ	↑		• MCC-LP interaction • PL-CP interaction • MCC-LP-PL-CP interaction
	↓	• A200 • LP • ADS • PL	• MCC-PL-CP interaction • LP-PL-CP interaction • A200-CP interaction
Tablet t_{dis}	↑	• Low A200 proportion	• A200-PL-CP interaction • A200-ADS-CP interaction
	↓	• Large amount of A200 • LP • ADS • PL	• A200-CP interaction • MCC-A200-ADS-CP interaction • MCC-PL-CP interaction • MCC-ADS-CP interaction
Tablet t_{80}	↑		• A200-CP interaction • MCC-A200-PL-CP interaction
	↓	• ADS	• MCC-A200-CP • A200-PL-CP

Table 51. Comparison of the information about the effect of the formulation on the studied attributes extracted from the GRM *β-coefficient* diagrams and from the direct observation of experimental results for the multicomponent formulation (group1)

		Multicomponent granules - group 2	
	Response	Experimental observations	GRM *β-coefficient* (Appendix 8.7.3)
Ribbon ρ_{rel}	↑	• Low quantity of KVA64 • PL	• KVA64-ADS interaction • MNT-KVA64 interaction • MNT-ADS interaction
	↓	• Large amount of KVA64 • ADS • Small quantity of PL	• MNT-KVA64-ADS interaction • ADS-PL interaction • KVA64
Ribbon σ	↑	• KVA64	• MNT-KVA64-ADS interaction
	↓	• ADS • PL	• MNT • MNT-PL interaction • MNT-KVA64-PL interaction
RRSB- n	↑	• KVA64 • PL	• KVA64
	↓	• ADS	• MNT • KVA64-PL interaction • MNT-ADS interaction

RRSB- *d'*	↑	• KVA64	• KVA64-ADS interaction • MNT-KVA64-PL interaction • KVA64
	↓	•ADS •PL	• MNT-KVA64-ADS interaction • ADS-PL interaction • KVA64-PL interaction
Angle of repose	↑	• Low quantity of KVA64 • ADS • PL	• KVA64-PL interaction • ADS-PL interaction
	↓	• KVA64 in larger quantity	• MNT-KVA64-ADS • ADS-PL • KVA64-PL
CI	↑	• KVA64	• KVA64 • ADS • MNT-KVA64-PL interaction
	↓	• ADS • PL	• MNT-KVA64 interaction • MNT-ADS interaction • KVA64-PL interaction
Tablet σ	↑	• KVA64	• KVA64-CP interaction
	↓	• ADS • PL	• MNT-KVA64-CP interaction • KVA64-PL-CP interaction
Tablet t_{dis}	↑	• PL	• MNT-CP • PL-CP
	↓	• KVA64 • ADS	• MNT • PL
Tablet t_{80}	↑	• KVA64 • PL	• KVA64-ADS-CP interaction • MNT-KVA64-PL-CP interaction
	↓	• ADS	• MNT-KVA64-ADS-CP interaction • ADS-PL-CP interaction • KVA64-PL-CP interaction

9.8 List of formulations used in the model validation

9.8.1 GRM and ANN models' validation

Table 52. MCC-granule with external additives

	Internal Phase	External phase				
No.	***MCC [%]***	***A200 [%]***	***LP [%]***	***MCCext [%]***	***MgSt [%]***	***CP [MPa]***
1	95.79	1.22	2.50	0.00	0.49	35.34
2	95.79	1.22	2.50	0.00	0.49	52.92
3	95.79	1.22	2.50	0.00	0.49	99.57
4	95.79	1.22	2.50	0.00	0.49	201.71
5	95.79	1.22	2.50	0.00	0.49	298.22
6	93.81	0.75	4.95	0.00	0.49	34.97
7	93.81	0.75	4.95	0.00	0.49	53.62
8	93.81	0.75	4.95	0.00	0.49	100.83
9	93.81	0.75	4.95	0.00	0.49	197.55
10	93.81	0.75	4.95	0.00	0.49	294.44
11	92.16	0.00	2.50	4.86	0.48	34.82
12	92.16	0.00	2.50	4.86	0.48	53.19
13	92.16	0.00	2.50	4.86	0.48	101.10
14	92.16	0.00	2.50	4.86	0.48	195.56
15	92.16	0.00	2.50	4.86	0.48	301.63

Table 53. Multicomponent formulations - Group 1

No.	***MCC [%]***	***A200 [%]***	***LP [%]***	***ADS [%]***	***PL [%]***	***MgSt [%]***	***CP [MPa]***
1	87.032	2.4938	0	0	9.975	0.499	101.34
2	87.032	2.4938	0	0	9.975	0.499	294.79
3	88.279	1.2469	0	0	9.975	0.499	101.26
4	88.279	1.2469	0	0	9.975	0.499	295.33
5	75.81	1.2469	0	2.4938	19.95	0.499	93.713
6	75.81	1.2469	0	2.4938	19.95	0.499	295.17

In the table there are listed the compression pressures (CP) settings for the manufacture of tablets.

Table 54. Comparison of observed values and estimations made by different models. MCC- granules with extragranular additives

Mixture	Variable	Obs.	ANN	GRM	CP [MPa]	Tablet σ Obs.	Tablet σ ANN	Tablet σ GRM	Tablet t_{dis} Obs.	Tablet t_{dis} ANN	Tablet t_{dis} GRM
1-5	RRSB-n	0.1338	0.1537	0.1388	34	0.73	1.31	0.99	0.73	0.51	0.71
	RRSB-d' [µm]	453.77	525.70	489.22	54	1.29	1.79	1.56	1.00	0.84	0.88
	CI [%]	21.42	22.10	20.58	100	2.98	3.01	3.22	1.39	1.66	1.40
	Rep Angle [º]	30.54	32.16	31.52	200	5.78	5.74	5.46	2.26	3.50	2.58
					300	7.49	8.32	5.94	3.73	5.25	5.99
6-10	RRSB-n	0.1415	0.1459	0.1430	34	0.8297	1.28	0.9664	0.7638	0.5999	0.7394
	RRSB-d' [µm]	448.66	505.12	485.83	54	1.47	1.74	1.53	0.7888	0.9696	0.9212
	CI [%]	22.85	22.89	21.40	100	3.42	2.99	3.30	1.38	1.95	1.47
	Rep Angle [º]	30.32	31.89	31.50	200	6.12	5.51	5.41	3.73	3.94	2.57
					300	7.92	8.00	6.06	7.40	5.91	6.70
11-15	RRSB-n	0.1240	0.1249	0.1286	34	0.7186	1.1586	0.8740	0.8066	0.4017	0.6477
	RRSB-d' [µm]	436.18	473.08	479.23	54	1.30	1.56	1.39	0.9666	0.6725	0.8070
	CI [%]	20.31	19.53	18.62	100	3.02	2.63	3.05	1.26	1.38	1.30
	Rep Angle [º]	33.95	31.01	34.02	200	4.87	4.75	5.25	2.18	2.79	2.41
					300	5.69	7.10	5.95	3.48	4.34	4.05

Table 55. Comparison of observed values and estimations made by different models. Multicomponent granules - group 1

Mixture	Variable	Exp.	ANN	GRM	CP [MPa]		Exp	ANN	GRM
1-2	Ribbon σ	68.28	63.33	123.69		Tablet σ [N/mm2]	2.93	1.85	2.27
	Ribbon t_{dis}	1.19	1.17	1.24	100	Tablet t_{dis} [min]	1.2	1.20	1.60E+00
	RRSB-n	0.0938	0.0960	-3.30E-02		Tablet t_{80} [min]	14.54	19.16	-56.14
	RRSB-d' [µm]	291.96	310.59	253.01		Tablet σ [N/mm2]	5.83	4.28	6.66
	Rep. angle [º]	35.48	34.61	39.00	300	Tablet t_{dis} [min]	4.31	5.71	6.70E+00
	CI [%]	19.19	19.99	23.91		Tablet t_{80} [min]	78.35	91.04	-162.42
3-4	Ribbon σ	63.99	64.04	93.45		Tablet σ [N/mm2]	3.43	2.62	2.44
	Ribbon t_{dis}	1.65	1.33	1.32	100	Tablet t_{dis} [min]	1.35	1.51	2.09E+00
	RRSB-n	0.0927	1.16E-01	7.09E-02		Tablet t_{80} [min]	2.73	2.83	-32.44
	RRSB-d' [µm]	306.35	291.88	331.69		Tablet σ [N/mm2]	7.35	4.16	7.17
	Rep. angle [º]	35.36	35.94	41.02	300	Tablet t_{dis} [min]	4.72	1.75	8.16E+00
	CI [%]	23.41	28.10	22.84		Tablet t_{80} [min]	47.51	54.36	-92.50
5-6	Ribbon σ	68.20	65.71	89.28		Tablet σ [N/mm2]	2.55	1.32	2.17
	Ribbon t_{dis}	1.23	1.14	1.12E+00	100	Tablet t_{dis} [min]	0.2416	0.3891	0.3413
	RRSB-n	0.0894	9.85E-02	7.39E-02		Tablet t_{80} [min]	2.29	2.28	-4.26
	RRSB-d' [µm]	268.97	269.36	273.90		Tablet σ [N/mm2]	6.17	4.88	5.89
	Rep. angle [º]	37.22	37.78	45.50	300	Tablet t_{dis} [min]	0.9222	0.9606	2.99
	CI [%]	24.91	25.87	25.87		Tablet t_{80} [min]	13.82	13.82	-9.36

9.8.2 DOE models' validation

Table 56. Multicomponent formulations - Group 1

No.	***MCC***	***A200***	***LP***	***PL***	***ADS***	***MgSt***	***CP***
1	99.25	0.25	0.00	0.00	0.00	0.50	54.34
2	98.25	1.25	0.00	0.00	0.00	0.50	100.17
3	94.50	0.00	5.00	0.00	0.00	0.50	101.56
4	89.5	0.00	10.00	0.00	0.00	0.50	290.94
5	94.25	0.25	5.00	0.00	0.00	0.50	99.47
6	89.25	0.25	10.00	0.00	0.00	0.50	34.34
7	88.75	0.75	10.00	0.00	0.00	0.50	33.51
8	93.25	1.25	5.00	0.00	0.00	0.50	100.96
9	87.00	2.50	10.00	0.00	0.00	0.50	100.67
10	68.75	0.75	30.00	0.00	0.00	0.50	299.78
11	90.25	0.25	10.00	0.00	0.00	0.50	34.03
12	84.25	0.25	5.00	10.00	0.00	0.50	53.81
13	54.25	0.25	5.00	40.00	0.00	0.50	100.16
14	78.75	0.75	10.00	10.00	0.00	0.50	54.61
15	68.75	0.75	10.00	20.00	0.00	0.50	54.91
16	48.75	0.75	10.00	40.00	0.00	0.50	99.77
17	91.75	0.25	5.00	0.00	2.50	0.50	101.56
18	89.25	0.25	5.00	0.00	5.00	0.50	198.73
19	81.75	0.25	5.00	10.00	2.50	0.50	292.00
20	51.75	0.25	5.00	40.00	2.50	0.50	34.97
21	79.25	0.25	5.00	10.00	5.00	0.50	101.78
22	49.25	0.25	5.00	40.00	5.00	0.50	200.34

Table 57. Table with values of MSE for the predictions made by each model

No.	***Tensile strength***				***Disintegration time***			
	True value	Experimental	Exp.+ANN good performance	Exp. + ANN bad performance	True value	Experimental	Exp.+ANN good performance	Exp. + ANN good performance
1	2.143	1.844	2.108	2.214	00:01:38	00:01:00	00:01:06	00:01:17
2	3.465	3.460	3.603	3.429	00:01:32	00:01:44	00:01:44	00:02:03
3	4.023	3.761	4.142	3.828	00:01:12	00:01:50	00:02:40	00:02:15
4	8.261	7.530	7.932	8.441	00:14:03	00:07:43	00:07:53	00:07:35
5	4.189	3.597	3.887	3.648	00:01:10	00:01:45	00:02:28	00:02:08
6	0.926	0.759	0.728	1.171	00:00:47	00:00:36	00:00:29	00:00:31
7	0.562	0.660	0.534	1.009	00:00:38	00:00:46	00:00:42	00:00:25
8	3.429	3.303	3.370	3.256	00:01:39	00:01:35	00:01:55	00:01:55
9	2.605	2.671	2.678	2.497	00:01:13	00:01:11	00:01:07	00:01:26
10	7.543	7.571	7.547	7.953	00:17:33	00:15:49	00:15:26	00:08:54
11	0.860	0.745	0.712	1.159	00:01:05	00:00:36	00:00:29	00:00:31
12	1.448	1.433	1.394	1.613	00:01:02	00:00:48	00:01:02	00:00:54
13	1.318	1.431	1.431	1.302	00:00:24	00:00:59	00:01:00	00:00:37
14	0.866	1.257	1.103	1.319	00:01:03	00:00:48	00:00:59	00:00:38
15	0.849	0.974	0.824	0.897	00:00:35	00:00:42	00:00:49	00:00:25
16	1.124	1.067	1.326	0.877	00:00:38	00:00:44	00:00:36	00:00:20
17	3.331	3.427	3.623	3.401	00:00:25	00:01:07	00:00:56	00:01:19
18	6.819	6.097	6.307	5.564	00:02:17	00:01:42	00:01:09	00:02:38
19	6.737	6.696	6.613	7.135	00:02:09	00:04:02	00:02:01	00:05:11
20	0.260	0.099	0.276	-0.124	00:00:14	00:00:09	00:00:13	
21	2.417	2.632	2.536	2.493	00:00:16	00:00:14	00:00:05	00:00:04
22	2.484	2.337	2.387	2.225	00:00:25		00:00:35	
	MSE	0.088	0.037	0.144	**MSE**	0.002	0.002	0.004

The MSE of the disintegration time was calculated by introducing the time in minutes.

9.8.3 Decipherment of ANN prediction by DOE models

All values required by the DOE program to build the model were estimated by the ANN. The resulting parameters and elements of the equation corresponding to the data modelling by the DOE application after processing the values estimated is given next.

Table 58. Parameters and factors of the resulting model based on DOE and ANN predictions

Parameter	Elements
-0.96942	* MCCint
3.938163	* A200int
-0.18007	* LPint
1.128003	* PL
7.848158	* ADS
0.054768	* MCCint * CP
-0.35039	* A200int * CP
0.015857	* LPint * CP
-0.01929	* PL * CP
-0.15531	* ADS * CP
-7.4E-05	* MCCint * CP^2
0.000798	* A200int * CP^2
1.42E-07	* LPint * CP^2
1.08E-05	* PL * CP^2
0.000465	* ADS * CP^2

The estimations of cases 1 to 9 on Table 56 in 9.8.2 by the ANN and the corresponding DOE model are listed in the next table.

Table 59. Comparison of estimations made by the ANN and the DOE model derived from ANN predictions

ANN	ANN-DOE
1.652434	1.7523
2.902732	3.438087
3.740228	3.710748
8.168083	8.284595
3.404706	3.5628
0.628582	0.758337
0.438084	0.681691
2.781687	3.348014
2.451608	2.879326

9.9 List of data introduced in the Expert System

9.9.1 Experimental information

The experimental information was gathered and summarized in *rtf* files. A record of files is listed in the following tables:

Table 60. List of RTF files for the general methods used to carry out the experiments

Method	….\locationfolder\filename.rtf
Mixing (Planetary mixer)	….\ExpertSystem\rtf\planetary..rtf
Mixing (Turbula mixer)	….\ExpertSystem\rtf\turbula..rtf
Roller compaction-granulation	….\ExpertSystem\rtf\RC.rtf
Ribbon sampling	….\ExpertSystem\rtf\ribbonsampling.rtf
Granule sampling	….\ExpertSystem\rtf\granulesampling.rtf

Ribbon ρ_{rel} determination	….\ExpertSystem\rtf\ribbonRD.rtf
Ribbon σ determination	….\ExpertSystem\rtf\TS.rtf
Granule size characterisation	….\ExpertSystem\rtf\PSD.rtf
Granule Flowability	….\ExpertSystem\rtf\Gflow..rtf
Granule compressibility	….\ExpertSystem\rtf\CI..rtf
Tableting	….\ExpertSystem\rtf\\tableting..rtf
Tablet σ determination	….\ExpertSystem\rtf\TS..rtf
Tablet t_{dis}	….\ExpertSystem\rtf\.DT.rtf
Tablet t_{80}	….\ExpertSystem\rtf\\t80..rtf

Table 61. List of RTF files for the general characteristics of the formulation components

Component	….\locationfolder\filename.rtf
MCC	….\ExpertSystem\rtf\MCC.rtf
A200	….\ExpertSystem\rtf\A200.rtf
LP	….\ExpertSystem\rtf\LP.rtf
ADS	….\ExpertSystem\rtf\ADS.rtf
PL	….\ExpertSystem\rtf\PL.rtf
MNT	….\ExpertSystem\rtf\MNT.rtf
KVA64	….\ExpertSystem\rtf\KVA64.rtf

Table 62. List of RTF files with the information about the effects of the components on the intermediary and end product properties

		MCC granule with external additives	Multicomponent granules MCC main component
MCC	Processability	….\ExpertSystem\rtf\MCCprocess.rtf	
	Tablet t_{dis}	….\ExpertSystem\rtf\MCCDT.rtf	
	Tablet σ	….\ExpertSystem\rtf\TS.rtf	
A200	Ribbon properties		….\ExpertSystem\rtf\M1A200_ribbons.rtf
	Processability	….\ExpertSystem\rtf\A200process.rtf	….\ExpertSystem\rtf\M1A200_processability.rtf
	PSD		….\ExpertSystem\rtf\M1A200_PSD.rtf
	Tablet t_{dis}	….\ExpertSystem\rtf\A200DT.rtf	….\ExpertSystem\rtf\M1A200_Tablet properties.rtf
	Tablet σ	….\ExpertSystem\rtf\A200TS.rtf	….\ExpertSystem\rtf\M1A200_Tablet properties.rtf
LP	Ribbon properties		….\ExpertSystem\rtf\M1LP_rib.rtf
	Processability	….\ExpertSystem\rtf\LPprocess.rtf	….\ExpertSystem\rtf\M1LP_processability.rtf
	PSD		….\ExpertSystem\rtf\M1LP_PSD.rtf
	Tablet t_{dis}	….\ExpertSystem\rtf\LPDT.rtf	….\ExpertSystem\rtf\M1LP_Tablet properties.rtf
	Tablet σ	….\ExpertSystem\rtf\A200TS.rtf	….\ExpertSystem\rtf\M1LP_Tablet properties.rtf
		Multicomponent granules (group 1)	Multicomponent granules (group 2)
ADS	Ribbon properties	….\ExpertSystem\rtf\M1ADS_ribbons.rtf	….\ExpertSystem\rtf\M2ADS_Ribbon properties.rtf
	Processability	….\ExpertSystem\rtf\M1ADS_Processability.rtf	….\ExpertSystem\rtf\M2ADS_Processability.rtf
	PSD	….\ExpertSystem\rtf\M1ADS_PSD.rtf	….\ExpertSystem\rtf\M2ADS_PSD.rtf
	Tablet properties	….\ExpertSystem\rtf\M1ADS_Tablet properties.rtf	….\ExpertSystem\rtf\M2ADS_Tablet properties.rtf
PL	Ribbon properties	….\ExpertSystem\rtf\M1PL_ribbons.rtf	….\ExpertSystem\rtf\M2PL_Ribbon properties.rtf
	Processability	….\ExpertSystem\rtf\M1PL_Processability.rtf	….\ExpertSystem\rtf\M2PL_Processability.rtf
	PSD	….\ExpertSystem\rtf\M1PL_PSD.rtf	….\ExpertSystem\rtf\M2PL_PSD.rtf
	Tablet	….\ExpertSystem\rtf\M1PL_Tablet	….\ExpertSystem\rtf\M2PL_Tablet

	properties	properties.rtf	properties.rtf
MNT	Ribbon properties		….\ExpertSystem\rtf\M2MNT_Ribbon properties.rtf
	Processability		….\ExpertSystem\rtf\M2MNT_Processability.rtf
	PSD		….\ExpertSystem\rtf\M2MNT_PSD.rtf
	Tablet properties		….\ExpertSystem\rtf\M2MNT_Tablet properties.rtf
KVA64	Ribbon properties		….\ExpertSystem\rtf\M2KVA64_Ribbon properties.rtf
	Processability		….\ExpertSystem\rtf\M2KVA64_Processability.rtf
	PSD		….\ExpertSystem\rtf\M2 KVA64_PSD.rtf
	Tablet properties		….\ExpertSystem\rtf\M2 KVA64_Tablet properties.rtf

9.9.2 ANN files

Table 63. List of ANN files available for the ES calculations

Formulation block	Variable	Location
MCC-granule external additives	Processability	….\ExpertSystem\Block1_repangle_CI.ann
	PSD	….\ExpertSystem\Block1_n_d.anntf
	Tablet properties	….\ExpertSystem\Block1_CP_TS_DT.ann
Multicomponent granules group 1	Ribbon properties	….\ExpertSystem\ann_block2\Block2_ribbon_TS_RD.ann
	Processability	….\ExpertSystem\ann_block2\Block2_granule_CI.ann ….\ExpertSystem\ann_block2\Block2_granule_flow.ann
	PSD	….\ExpertSystem\ann_block2\Block2_granule_RRSB_N.ann ….\ExpertSystem\ann_block2\Block2_granule_RRSB_d'.ann
	Tablet properties	….\ExpertSystem\ann_block2\Block2_tablet_DT_TS.ann ….\ExpertSystem\ann_block2\Block2_tablet_t80.ann
Multicomponent granules group 2	Ribbon properties	….\ExpertSystem\ann_block3\Block3_ribbon_ts_rd.ann
	Processability	….\ExpertSystem\ann_block3\Block3_granule_repangle_CI.ann
	PSD	….\ExpertSystem\ann_block3\Block3_granule_RRSB_n_d.ann
	Tablet properties	….\ExpertSystem\ann_block3\Block3_tablet_TS.ann ….\ExpertSystem\ann_block3\Block3_tablet_DT.ann ….\ExpertSystem\ann_block3\Block3_tablet_t80.ann

9.9.3 Condition rules formulation

The next table lists the condition rules from which the expert system introduces the following advices into the formulation prediction report.

Table 64. Condition rules introduced in the command list for the generation of advises and guide-lines included in the report of the predictions made by the ES

FORMULATION	
IF	THEN
A200 [%] > 1.25	"It is recommendable to blend all components together for two minutes and sieve the material through a 0.4 mm mesh sieve to break possible agglomerates" "During roller compaction, the PDI might no respond properly due to irregular powder conveyance. Start the compaction at lower speed until and set the rate tamp - horizontal auger manually. Once the gap remains invariable, activate the PID and set the desired roller rotation speed" "The addition of A200 causes that the blend has a low bulk density. The die depth has to be set accordingly. The flow of the bulk is hindered, it is preferable to compress at slow tableting speed"
PL [%] > 0	"If sticking occurs, try changing the knurled roller by a smooth one" "The addition of PL increases the bulk density. The die depth has to be reset"
PRODUCT PROPERTIES	
IF	THEN
Ribbon properties	
Ribbon ρ_{rel} [%] > 70	"Dense ribbons result in granules with low internal porosity. This is linked normally to bad tabletability properties. Reduce the compaction specific

	force."
Ribbon ρ_{rel} [%] > 100	"Attention: Ignore the predictions if the relative density values are aberrant (> 100%)
Ribbon σ [N/mm^2] > 2.5	"Ribbons may be too hard. PSD and flowability are enhanced. However, compactibility can be compromised. If granules result to be poorly tabletable, reduce the compaction specific force"
Ribbon σ [N/mm^2] < 1	"Ribbons may be loose. PSD can be affected by production of large amount of fines. Increase the compaction specific force."
Granule properties	
RRSB-d' [µm] > 500	"The proportion of coarses might be good."
RRSB-d' [µm] < 400	"The amount of fines may be large. If the predicted ribbon relative density laid within values of low to fair density (50-65%), increase the specific compaction pressure"
CI [%] < 18	"The tableting material presents good compressibility."
CI [%] > 25	"The tableting material can present bad compressibility characteristics. The use of higher compression pressures may be considered."
Angle of repose [º] > 40	"The tableting mixture might present bad flowability. Tablet mass fluctuations and air entrapment can occur. Compression process should be set at low speed"
Angle of repose [º] 30 - 40	"The tableting mixture might have fair flowability properties. However, irregularities on the die filling may occur. Use intermediate tableting speeds."
Angle of repose [º] < 30	"The tableting mixture might present good flowability properties. The die filing will be regular and, therefore, the compression speed can be set to large values."
Tablet properties	
Tablet σ [N/mm^2] < 1	"Tablets will be too weak. If possible, increase the compression pressure"
Tablet σ [N/mm^2] < 2	"The tablets could not have enough endurance. If possible, increase the compression pressure"
Tablet σ [N/mm^2] > 8	"The tablets might be too hard. Capping, friability problems or too long disintegration times can appear. Reduce the compression pressure."
Tablet t_{dis} [min] > 10	"The tablet disintegration is too slow. If tablet tensile strength values are as desired, the addition of a disintegrant is advisable."
Tablet t_{dis} [min] > 5	"The tablet disintegration lasts quite long. If tablet tensile strength values are not large (i.e. 5 -8 N / mm^2) , the addition of a disintegrant is advisable."
Tablet t_{dis} [min] < 1	"The tablet disintegration is fast. Please, make sure that the corresponding tensile strengths lay within desired values."
Tablet t_{80} [min] > 30	"The API release rate could not meet the USP 31 requirements. Check that the tablet disintegration times are not too long. The addition of disintegrants could be necessary"
Tablet t_{80} [min] < 30	"The API release rate meets the USP 31 requirements"
Tablet t_{80} [min] < 0	"Ignore GRM/ANN predictions with aberrant t_{80} values."

9.9.4 Inference part

A fragment of the final inference part of the expert system developed is included here.

No: **1**
Root:
Question:
What kind of formulation are you interested in?

Comment:
Microcrystalline cellulose granulate with excipients as external components (G)
Multicomponent mixtures with microcrystalline cellulose as main component (M)
Multicomponent mixtures with mannitol as main component (T)

Branches:
Key: **G** branch to cell nr. **2**
Key: **M** branch to cell nr. **3**
Key: **T** branch to cell nr. **4**

No: **2**
Root: 1

Question:
Do you want to carry on with the formulation or to become information about the components and the methods applied?

Comment:
Formulation: F
Information: I

Branches:
Key: **F** branch to cell nr. **5**
Key: **I** branch to cell nr. **6**

No: **3**
Root: 1

Question:
Do you want to carry on with the formulation or to become information about the components and the methods applied?

Comment:
Formulation: F
Information: I

Branches:
Key: **F** branch to cell nr. **26**
Key: **I** branch to cell nr. **27**

No: **4**
Root: 1

Question:
Do you want to carry on with the formulation or to become information about the components and the methods applied?

Comment:

Formulation: F
Information: I

Branches:
Key: **F** branch to cell nr. **30**
Key: **I** branch to cell nr. **31**

No: **5**
Root: 2

Question:
How many external components do you want to add to your granule?

Comment:
Choose the number underneath this box

Branches:
Key: **1** branch to cell nr. **7**
Key: **2** branch to cell nr. **8**
Key: **3** branch to cell nr. **9**

Commandfile:
```
minimize
rtfload "rtf1.rtf"
rtfview
maximize
```

No: **6**
Root: 2

Question:
What kind of information do you want to be displayed?

Comment:
Information about the formulation components (E)
Information about the methods used for the obtained models (M)

Branches:
Key: **E** branch to cell nr. **13**
Key: **M** branch to cell nr. **14**

No: **7**
Root: 5

Question:
Do you agree with your selection?

Comment:
Yes (Y)
No (N)

Branches:
Key: **Y** branch to cell nr. **10**
Key: **N** branch to cell nr. **7**

Commandfile:
```
'select the excipients added externally to the MCC granule
'first external excipient
Tablechoosefrom "First external excipient", "choices.txt",
"excipients", longE1$, shortE1$, s

If shortE1$ = "MCC" then
askfor "proportion of MCC", "Type value in % between 0 and 30%",
x.mccext
If x.mccext > 30
then
message "Value out of range", "Please, type a valid value"
askfor "proportion of MCC", "Type value in % between 0 and 30%",
x.mccext
If x.mccext > 30
then
message "Value out of range", "The values might not be trustworth"
else
endif
endif
endif

If shortE1$ = "LP" then
askfor "Proportion of Ludipress", "Type value in % between 0 and
30%", x.lp
If x.lp > 30
message "Value out of range", "Please, type a valid value"
askfor "Proportion of Ludipress", "Type value in % between 0 and
30%", x.lp
If x.lp > 30
message "Value out of range", "The values might not be trustworth"
else
endif
endif
endif

If shortE1$ = "A200" then
askfor "Proportion of A200", "Type value in % between 0 and
2.5%", x.a200
If x.a200 > 2.5
message "Value out of range", "Please, type a valid value"
askfor "Proportion of A200", "Type value in % between 0 and
2.5%", x.a200
If x.a200 > 2.5
message "Value out of range", "The values might not be trustworth"
else
endif
endif
endif

formulation.comment$ = ""
compression.comment$ = ""
If x.a200 > 0.75
concat formulation.comment$, formulation.comment$, "By an A200
percentage of [x.a200] would be recommendable to mix intensively
( e.g. increasing the mixer speed ) ."
concat compression.comment$, compression.comment$, "Since
A200 concentration is pretty large, the bulk flow is hindered. As a
consequence, more attention has to be payed on the die filling."
endif
```

No: **8**
Root: 5

Question:
Do you agree with your selection?

Comment:
Yes (Y)
No (N)

Branches:
Key: **Y** branch to cell nr. **11**
Key: **N** branch to cell nr. **8**

Commandfile:
```
'select the excipients added externally to the MCC granule
'first external excipient
Tablechoosefrom "First external excipient", "choices.txt",
"excipients", longE1$, shortE1$, s

If shortE1$ = "MCC" then
askfor "proportion of MCC", "Type value in % between 0 and 30%",
x.mccext
If x.mccext > 30
then
message "Value out of range", "Please, type a valid value"
askfor "proportion of MCC", "Type value in % between 0 and 30%",
x.mccext
If x.mccext > 30
then
message "Value out of range", "The values might not be trustworth"
else
endif
endif
endif

If shortE1$ = "LP" then
askfor "Proportion of Ludipress", "Type value in % between 0 and
30%", x.lp
If x.lp > 30
message "Value out of range", "Please, type a valid value"
askfor "Proportion of Ludipress", "Type value in % between 0 and
30%", x.lp
If x.lp > 30
message "Value out of range", "The values might not be trustworth"
else
endif
endif
endif

If shortE1$ = "A200" then
askfor "Proportion of A200", "Type value in % between 0 and
2.5%", x.a200
If x.a200 > 2.5
message "Value out of range", "Please, type a valid value"
askfor "Proportion of A200", "Type value in % between 0 and
2.5%", x.a200
If x.a200 > 2.5
message "Value out of range", "The values might not be trustworth"
else
endif
endif
endif


'second external excipient

Tablechoosefrom "Second external excipient", "choices.txt",
"excipients", longE2$, shortE2$, s

If shortE2$ = shortE1$
message "Invalid formulation", "Choose a second external excipient
different from the first one"
Tablechoosefrom "Second external excipient", "choices.txt",
"excipients", longE2$, shortE2$, s
else

endif [....]
```

9.9.5 Template of the ES prediction report

Figure 135. Layout of the template for the report generated by the ES

Multicomponent formulations I: MCC as main component[date$]

Compaction-Granulation

Formulation

	Function	Component	Abbreviation	Composition [%]
1	Filler-binder	Microcrystalline cellulose	MCC	[x.mcc,round2]
2	Filler-binder	Ludipress LCE	LP	[x.lp,round2]
3	Glindant-disintigrant	Aerosil 200	A200	[x.a200,round2]
4	Disintegrant	AcDiSol	ADS	[x.ads,round2]
5	API	Paracetamol	PL	[x.pl,round2]
6	Lubricant	Magnesium stearate	MgSt	[x.mgst,round2]

Blend obtainment

The amount of each of the components added has to be calculated from the total weight of the batch and the percentages listed above. The correspondin components apart from the lubricant are poured into the mixing vessel and mixed between 10 and 15 min. [formulation.comment$] Finally, the lubricant is mixed for no longer than 2 minutes.

Compaction-granulation

The roller compaction is executed in a Gerteis MiniPactor. A knurled roller as slave roller and a smooth one as master are mounted. The seal of the compaction are cheek side plates. The specific compaction pressure is 5 kN/cm. The rotation speed is set at 2 rpm and the gap between roller at 3 mm. The PID control of the feeding parameters is activated and the ratio tamp-horizontal auger is set at 150%. [compaction.comment$] The granulator unit is equipped with the 1 mm mesh rasp sieve and the rotator is anticlockwise rotating at a speed of 50 rpm. The end granule is collected for the elaboration o the subsequent formulations.

Compact properties

Compact property	Parameter	Prediction A - MRM	Prediction B - ANN
Ribbon densification [ANN.RSF,round2]	Relative density [%]	[RSM.RIBBONDENSITY,round2]	
Ribbon strength [ANN.RTS,round2]	Tensile strength [N/mm^2]	[RSM.RIBBONTS,round2]	

MRM : [ribboncommentRD1$] [ribboncommentTS1$]
ANN : [ribboncommentRD2$] [ribboncommentTS2$]

Tableting

Formulation

	Addition [%]	Quantity [mg]
Granule	[x.mccg,round2]	[m.mccg,round2]
Magnesium stearate	[x.mgst,round2]	[m.mgst,round2]
	Total tablet mass	200.0

Mixing

[x.mgst]% of the lubricant is added to the granule and is mixed for no longer than 2 min.

Tableting blend properties

Blend property	Parameter	Prediction A - MRM	Prediction B - ANN
Particle size [ANN.RRSBD,round2]	RRSB-d' [µm]	[RSM.RRSBD,round2]	
Particle distribution [ANN.RRSBN,round4]	RRSB-n	[RSM.RRSBN,round4]	
Flowability [ANN.REPANGLE,round2]	Angle of repose [°]	[RSM.REPANGLE,round2]	
Compressibility [ANN.COMPINDEX,round2]	CI [%]	[RSM.COMPINDEX,round2]	

MRM : [rrsbd.comment1$] [granCI.comment1$] [granrepangle.comment1$]
ANN : [rrsbd.comment2$] [granCI.comment2$] [granrepangle.comment2$]

Compression

The tablet press is adjusted correspondingly in order to achieve tablets of 200 mg at a compression pressure of [x1.cp] MPa. [compression.comment$]

Tablet properties

Tablet property	Parameter	Prediction A - MRM	Prediction B - ANN
Tablet strength [ANN.TTS,round2]	Tensile strength [N/mm^2]	[RSM.TABLETTS,round2]	
Tablet disintegration [ANN.TDT,round2]	Disintegration time [min]	[RSM.TDT,round2]	
API release [ANN.T80,round2]	t 80 [min]	[RSM.T80,round 2]	

MRM: [tabletts.comment1$] [tabletdt.comment1$] [tablet80.comment1$] [tablet80wrong.comment1$]
ANN: [tabletts.comment2$] [tabletdt.comment2$] [tablet80.comment2$] [tablet80wrong.comment2$]

References

[1] Random House Unabridged Dictionary, Random House, Inc. 2006
[2] European Direction for the Quality of Medicine and Health Care, European Pharmacopoeia 6.2 online, http://online6.edqm.eu, 2008
[3] United States Pharmacopoeia Convention, US Pharmacopoeia - 31 online, http://www.uspnf.com, 2008
[4] M. Çelik, *The past, present, and future of tableting technology*, Drug. Dev. Ind. Pharm. 22, 1996, 1, 1-10
[5] P. Basu, G. Joglekar, S. Rai, P. Suresh, J. Vernon, *Analysis of manufacturing costs in pharmaceutical companies*, J. Pharm. Innov. 3, 2008, 30-40
[6] G.E. Peck, G.J. Baley, V.E. McCurdy, G.S. Banker, Tablet formulation and design, Pharmaceutical dosage forms: Tablets (volume 1), Marcel Dekker New York, 1989, 75-130
[7] W.A. Ritschel, A. Bauer-Brandl, Die Tablette, Editio Cantor Verlag, Aulendorf, Germany, 2002
[8] C. Caramella, P. Colombo, U. Conte, F. Ferrari, A. La Manna, H.V. Van Kamp, G.K. Bolhuis, *Water uptake and disintegrating force measurements: towards a general understanding of disintegration mechanisms*, Drug. Dev. Ind. Pharm. 12, 1986, 11-13, 1749-1766
[9] J.T. Carstensen, *Pharmaceutical principles of solid dosage forms*, Informa Health Care, 1993, 47-62
[10] C.D. Melia and S.S. Davis, *Review article: mechanisms of drug release from tablets and capsules. I: Disintegration*, Alim. Pharmacol. Ther. 31, 1989, 3, 223-232
[11] N.-O. Lindberg, C. Joensson and B. Holmquist, *Optimization of disintegration time and crushing strength of a tablet formulation*, Drug. Dev. Ind. Pharm. 11, 1985, 4, 931-943
[12] I.C. Sinka, J.C. Cunningham, A. Zavaliangos, *The effect of wall friction in the compaction of pharmaceutical tablets with curved faces: a validation study of the Drucker-Prager Cap*, Powder Tech., 2003, 133, 33-43
[13] H. Sunada, Y. Bi, *Preparation, evaluation and optimization of rapidly disintegrating tablets*, Powder Tech. 122, 2002, 188-198
[14] G.K. Bolhuis, A.J. Smallenbroek, C.F. Lerk, *Interaction of Tablet disintegrants and magnesium stearate during mixing I: Effect on tablet disintegration*, J. Pharm. Sci. 70, 1981, 12, 1328-1330
[15] J.-I. Kikuta and N. Kitamori, Effect of mixing time on the lubricating properties of magnesium stearate and the final characteristics of the compressed tablets, Drug. Dev. Ind. Pharm. 20, 1994, 3, 343-355
[16] R. Loebenberg, G.L. Amidon*, Modern bioavailability, bioequivalence and biopharmaceutics classification system. New scientific approaches to international regulatory standards*, Eur. J. Pharm. Biopharm. 5, 2000, 3-12
[17] N. Rasenack and B.W. Mueller, *Ibuprofen crystals with optimized properties*, Int. J. Pharm. 245, 2002, 9-24
[18] C.-Y. Wu, L. Dihoru, A.C.F. Cocks, *The flow of powder into simple and stepped dies*, Powder Tech. 134, 2003, 24-39
[19] C.-Y. Wu*, Flow behaviour of powders during die filling*, Powder Metallurgy 47, 2004, 2, 127-136
[20] C.-Y. Wu and A.C.F. Cocks, *Numerical and experimental investigations of the flow of powder into a confined space*, Mech. Mater. 38, 2006, 4, 304-324
[21] O.Coube, A.C.F. Cocks, and C.-Y. Wu, *Experimental and numerical study of die filling, powder transfer and die compaction*, Powder Metall. 48, 2005, 1, 68-76
[22] H. Leuenberger, B.D. Rohera*, Fundamentals of powder compression. I. The compactibility and compressibility of pharmaceutical powders*, Pharm. Res. 3, 1986, 1, 12-22
[23] P.E. Wray, *The Physics of tablet compaction revised*, Drug. Dev. Ind. Pharm. 18, 1992, 6&7, 627-658
[24] M.G. Herting, P. Kleinebudde, *Roll compaction/dry granulation: Effect of raw material particle size on granule and tablet properties*, Int. J. Pharm. 338, 2007, 110-118
[25] M.G. Herting, K. Klose, and P. Kleinebudde*, Comparison of different dry binders for roll compaction/ dry granulation*, Pharm. Dev. Technol. 12, 2007, 525-532
[26] K.A. Riepma, H. Vromans, K. Zuurman, C.F. Lerk, *The effect of dry granulation on the consolidation and compaction of crystalline lactose*, Int. J. Pharm. Technol. Biopharm. 1-3, 1993, 29-38
[27] N. A. Armstrong, T.-M. Cham, *Changes in the particle size and size distribution during compaction of two pharmaceutical powders with dissimilar consolidation mechanisms*, Drug. Dev. Ind. Pharm. 12 (II), 1986, 11-13, 2043-2059
[28] M. Eriksson and G. Alderborn, *The Effect of particle fragmentation and deformation on the interparticualte bond formation process during powder compaction*, Pharm. Res. 12, 1995, 7, 1031-1039
[29] S. Inghelbrecht, J.P. Remon*, Roller compaction and tableting of microcrystalline cellulose / drug mixtures*, Int. J. Pharm. 161, 1998, 215-224
[30] M. Wikberg and G. Alderborn, *Compression characteristics of granulated materials. IV. The effect of granule porosity on the fragmentation propensity and the compactibility of some granulations*, Int. J. Pharm. 69, 1991, 239-253
[31] M. Wikberg and G. Alderborn, *Compression characteristics of granulated materials. VII. The effect of intragranular binder distribution on the compactibility of some lactose granulations*, Pharm. Res. 10, 1993, 1, 88-94
[32] B. Johansson, G. Alderborn, *The effect of shape and porosity on the compression behaviour and tablet forming ability of granular materials formed from microcrystalline cellulose*, Eur. J. Pharm. Biopharm. 52, 2001, 347-357
[33] P.G. Karehill, M. Glazer and C. Nystrom, Studies on direct compression of tablets. XXIII. *The importance of surface roughness for the compactability of some directly compressible materials with different bonding and volume reduction properties*, Int. J. Pharm. 64, 1990, 35-43
[34] F. Freitag, K. Reincke, J. Runge, W. Grellmann, P. Kleinebudde*, How do roll compaction/dry granulation affect the tableting behaviour of inorganic materials? Microhardness of ribbons and mercury porosimetry measurements of tablets*, European J. Pharm. Sci. 2, 2004, 325-333
[35] E. Horisawa, K. Danjo, and H. Sunada*, Influence of granulating method on physical and mechanical properties, compression behavior, and compactibility of lactose and microcrystalline cellulose Granules*, Drug. Dev. Ind. Pharm. 26, 2000, 6, 583-593
[36] L.W. Wong and N. Pilpel, *The effect of particle shape on the mechanical properties of powders*, Int. J. Pharm. 59, 1990, 145-154

[37] K.A. Riepma, K. Zuurman, G.K. Bolhuis, A.H. De Boer, C.F. Lerk, *Consolidation and compaction of powder mixtures: III. Binary mixtures of different particle size fractions of different types of crystalline lactose*, Int. J. Pharm. 85, 1992, 121-128
[38] K.M. Picker, *The relevance of glass transition temperature for the process of tablet formation*, J. Therm. Anal. Calorim. 73, 2003, 597-605
[39] C. Nystrom, G.O.R. Alderborn, M. Duberg, and P.G. Karehill, *Bonding surface area and bonding mechanism-Two important factors for the understanding of powder compactability*, Drug. Dev. Ind. Pharm. 19, 1993, 17&18, 2143-2196
[40] K. Kawakita and K.-H. Luedde*, Some considerations on powder compression equations*, Powder Tech. 4, 1970/71, 61-68
[41] J.M. Sonnergaard, *A critical evaluation of the Heckel equation*, Int. J. Pharm. 193, 1999, 63-71
[42] M. Celik*, Overview of compaction data analysis techniques*, Drug. Dev. Ind. Pharm. 18, 1992, 6, 767-810
[43] V. Busignies, P. Tchoreloff, B. Leclerc, M. Besnard, and G. Couarraze, *Compaction of crystallographic forms of pharmaceutical granular lactoses. I. Compressibility*, Eur. J. Pharm. Biopharm. 58, 2004, 569-576
[44] J. Ilkka and P. Paronen, *Prediction of the compression behaviour of powder mixtures by the Heckel equation*, Int. J. Pharm. 94, 1993, 181-187
[45] G. Sun and D.J.W. Grant, *Influence of elastic deformation of particles on Heckel analysis*, Pharm. Dev. Technol. 6, 2001, 2, 193-200
[46] M.C. Monedero-Perales, A. Munoz-Ruiz, M.V. Velasco-Antequerea, M.R. Jimenez-Castellanos-Ballesteros, *Study of the compaction mechanisms of lactose-based direct compression excipients using Indentation hardness and Heckel Plots*, J. Pharm. Pharmacol. 46, 1994, 46, 177-181
[47] A. Michrafy, D. Ringenbacher, and P. Tchoreloff*, Modelling the compaction behaviour of powders: application to pharmaceutical powders*, Powder Tech. 127, 2002, 257-266
[48] B. van Veen, K. van der Voort Maarschalk, G.K. Bolhuis, and H.W. Frijilink, *Predicting mechanical properties of compacts containing two components*, Powder Tech. 139, 2004, 154-164
[49] G. Alebiowu and O.A. Itiola, *Compressional characteristics of native and pregelatinized forms of sorghum, planain, and corn starches and the mechanical properties of their tablets*, Drug. Dev. Ind. Pharm. 6, 2002, 28, 663-672
[50] Y. Zhang, Y. Law, and S. Chakrabarti, *Physical properties and compact analysis of commonly used direct compression binders*, AAPS Pharm. Sci. Tech. 4, 2003, 4, Article 62
[51] S. Wiegel, *Systematik der Entwicklung direktverpresster Tabletten*, Ph Thesis University of Heidelberg, 1996
[52] M. Whiteman and R.J. Yarwood*, The evaluation of six lactose-based materials as direct compression tablet excipients*, Drug. Dev. Ind. Pharm. 14, 1988, 8, 1023-1040
[53] M. Kuentz, H. Leuenberger, *A new theoretical approach to tablet strength of a binary mixture consisting of a well and a poorly compactable substance*, Eur. J. Pharm. Biopharm.49, 2000, 151-159
[54] N. Ramirez, L.M. Melgoza, M. Kuentz, H. Sandoval and I. Caraballo, *Comparison of different mathematical models for the tensile strength-relative density profiles of binary tablets*, European J. Pharm. Sci. 22, 2004, 1, 19-23
[55] A. Michrafy, M. Michrafy, M.S. Kadiri and J.A. Dodds, *Predictions of tensile strength of binary tablets using linear and power law mixing rules*, Int. J. Pharm. 333, 2007, 118-126
[56] H. Larhrib. J.I. Wells, M.H. Rubinstein, *Compressing polyethylene glycols: the effect of compression pressure and speed*, Int. J. Pharm. 147, 1997, 199-205
[57] S. Dawoodbhai and C.T. Rhodes, *The effect of moisture on powder flow and on compaction and physical stability of tablets*, Drug. Dev. Ind. Pharm. 15, 1989, 10, 1577-1600
[58] H. Ando, M. Ishii, M. Kayano and H. Ozawa, *Effect of moisture on crystallization of theophylline in tablets*, Drug. Dev. Ind. Pharm. 18, 1992, 4, 453-467
[59] T. Sebhatu, C. Ahlneck, G. Alderborn, *The effect of moisture content on the compression and bond-formation properties of amorphous lactose particles*, Int. J. Pharm. 146, 1997, 101-114
[60] A. Michrafy, J.A. Dodds, M.S. Kadiri, *Wall friction in the compaction of pharmaceutical powders: measurement and effect on the density distribution*, Powder Tech. 148, 2004, 53-55
[61] C.-Y.Wu, C. Thornton, L.Y. Li, *Coefficients of restitution for elastoplastic oblique impacts*, Adv. Powder Tech. 14, 2003, 4, 435-448
[62] C.-Y. Yang, X.-Y. Fu, *Development and validation of a material-labelling method for powder process characterization using X-ray computed tomography*, Powder Tech. 146, 2004, 10-19
[63] I.C. Sinka, J.C. Cunningham, A. Zavaliangos, *Analysis of tablet compaction. II. Finite Element Analysis of density distributions in convex tablets*, J. Pharm. Sci. 93, 2004, 8, 2040-2053
[64] C.Y. Wu, O.M. Ruddy, A.C. Bentham, B.C. Hancock, S.M. Best, J.A. Elliott, *Modelling the mechanical behaviour of pharmaceutical powders during compaction*, Powder Tech. 152, 2005, 107-117
[65] F. R. Dehont, P. M. Hervieu, E. Jerome, A. Delacourte, J.C. Guyot, *Briquetting and granulation by compaction new granulator-compactor for the Pharmaceutical Industry*, Drug. Dev. Ind. Pharm. 15, 1989, 14, 2245-2263
[66] S. Wenerstrum, *Ten things you need to consider when choosing and installing a roller press system*, Powder Bulk Eng. February, 2000.
[67] W. Pietsch, *Agglomeration in industry. Occurrence and applications*, Wiley-VCH, 2005, 85-147
[68] J. Swarbrick, J.C. Boylan (R. Miller, P. Sheskey), *Encyclopaedia of Pharmaceutical Technology*, Informa Health Care, London UK, 2004, 397-415
[69] C. Vervaet, J.P. Remon, *Continuous granulation in the Pharm. Ind.*, Chem. Eng. Sci. 60, 2005, 3949-3957
[70] M. Hariharan, C. Wowchuk, P. Nkansah, V. K. Gupta, *Effect of formulation composition on the properties of controlled release tablets prepared by roller compaction*, Drug Dev. Ind. Pharm. 30, 2004, 6, 565-572
[71] T. Abberger, *Neuere entwicklungen in der granulierung*, PZ Prisma 8. Jahrgang 1, 2001, 14-17
[72] A. Gupta, G.E. Peck, R.W. Miller, K.R. Morris, *Near infrared monitoring of roller compaction*, Proceedings: Biennial conference of the Institute for Briquetting and agglomeration 28, 2004, 65-78
[73] P. Sheskey, K. Pacholke, G. Sackett, L. Maher, and J. Polli, *Roll compaction granulation of a controlled-release matrix Tablet formulation containing HPMC. Effect of process scale-up on robustness of tablets, tablet stability, and predicted in vivo performance*, Pharm. Tech., 2000, 11, 30-52

[74] J.C. Cunningham, *Experimental studies and modelling of the roller compaction of pharmaceutical powders*, PhD Thesis - Drexel University, 2005
[75] P. Guigon, O. Simon, K. Saleh, G. Bindumadhavan, M.J. Adams and J.P.K. Seville, Handbook of Powder Tech.: Vol. 11. Granulation, Elsevier, UK, 2007, 256-286
[76] E. Jerome, A. Delacourte, P. Leterme, J.C. Guyot, *The measurement of resulting forces on a roller compactor*, Drug. Dev. Ind. Pharm. 12, 1991, 17, 1571-1591
[77] Y. Funakoshi, T. Asogawa, E. Satake, *Use of a novel roller compactor with a concavo-convex roller pair to obtain uniform compacting pressure*, Drug. Dev. Ind. Pharm. 6, 1977, 3, 555-573
[78] E.L. Parrott, *Densification of powders by concavo-convex roller compactor*, J. Pharm. Sci. 70, 1981, 3, 288-291
[79] G. Shlieout, R.F. Lammens, P. Kleinebudde, *Dry granulation with a roller compactor. Part I: The functional units and operation modes*, Pharm. Tech. Europe, 2000, November, 25-35
[80] J.K. Prescott and R.G. Barnum, *On powder flowability*, Pharm. Tech. October, 2000, 60-85
[81] P.A. Moysey, M.R. Thompson, *Modelling the solids inflow and solids conveying of single-screw extruders using the discrete element method*, Powder Tech. 153, 2005, 95-107
[82] S.Peter, R.F. Lammens and K.J. Steffens, *Roller compaction: invention of an uncomplex prediction model on the basis of tabletting experiments*, International Congress of Pharmaceutical Scientists, Barcelona, 2008
[83] R.T. Dec, R.K. Komarek, K.R. Komarek, *Optimization of roll press screw feeder design using experimental simulation*, Proceedings of the technical program powder and bulk solids conference and exhibition - USA, 1994, 145-156
[84] U. Sander and K. Schoenert, *Operational conditions of a screw-feeder-equipped high-pressure roller mill*, Powder Tech. 105, 1999, 282-287
[85] S. Inghelbrecht, J-P. Remon, P. Fernandes de Aguiar, B. Walczak, D.L. Massart, F. Van de Velde, P. De Baets, H. Vermeersch, and P. De Backer, *Instrumentation of a roll compactor and the evaluation of the parameter settings by neural networks*, Int. J. Pharm. 148, 1997, 103-115
[86] A.M. Falzone, G.E. Peck, G.P. McCabe, *Effects of changes in roller compactor parameters on granulations produced by compaction*, Drug. Dev. Ind. Pharm. 18 (I), 1992, 4, 469-489
[87] O. Simon, P. Guigon, *Correlation between powder-packing properties and roll press compact heterogeneity*, Powder Tech. 130, 2003, 1, 257-254
[88] P. Guigon, O. Simon, *Roll press design - influence of force feed systems on compaction*, Powder Tech. 130, 2003, 1, 41-48
[89] O. Simon and P. Guigon, *Interaction between feeding and compaction during lactose compaction in a laboratory roll press*, KONA Powder Part. 18, 2000, 131-138
[90] J.H. Thundermann and A.R.E. Singer, *The flow of iron powder during roll compaction*, Powder Metall. 11, 1968, 2, 261-294
[91] P. Hervieu, F. Dehont, E. Jerome, A. Delacourte, J.C. Guyot, *Granulation of pharmaceutical powders by compaction. An experimental study*, Drug. Dev. Ind. Pharm. 20, 1994, 1, 65-74
[92] R.F. Lammens, *Roll compactor Instrumentation: key to -rationalistic Formulation Development, - reproducible manufacturing, - adequate trouble shooting*, Proc. 4th World Meeting ADRITELF/APGI/APV, Florence 8/11 April 2002
[93] R.W. Miller, *Handbook of Pharmaceutical Granulation Technology*, Marcel Dekker Inc., New York - Basel, 1997, 102-104
[94] C. Nystroem and P.-G. Karehill, *The importance of intermolecular bonding forces and the concept of bonding surface area*, Pharmaceutical Powder Compaction Technology, Marcel Dekker, New York, 1996, 17-53
[95] J.R. Johanson, *A rolling theory for granular solids*, J. Appl. Mech., 1965, 842-848
[96] K. Schonert, *The characteristics of comminution with high pressure roller mills*, KONA 9, 1991, 149-158
[97] P.D. Daugherity and J.H. Chu, *Investigation of serrated roll surface differences on ribbon thickness during roller compaction*, Pharm. Dev. Technol. 12, 2007, 603-608
[98] J.A. Brudy, *Systematische Rezepturentwicklung fuer die Walzenkompaktierung. Anhand binaerer und ternaerer Mischungen ausgewaehlter Komponenten*, PhD Thesis - University of Heidelberg, 2007
[99] A.P. Chekmarev, P.A. Klimenko, and G.A. Vinogradov, *Investigation of specific pressure, specific friction, and the coefficient of friction during metal powder rolling*, Translated from Poroshkovaya Metallurgiya 2, 1963, 14, 26-30
[100] G. Bindhumadhavan, J.P.K. Seville, M.J.Adams, R.W. Greenwood, S. Fitzpatrick, *Roll compaction of a pharmaceutical excipient: Experimental validation of rolling theory for granular solids*, Chem. Eng. Sci. 60, 2005, 3891-3897
[101] R.T. Dec and K.R. Komarek, *Problems with processing of fine powders in roll press*, Briquetting and Agglomeration 24, 1995, 199-210
[102] K. Sommer and G. Hauser, *Flow and compression properties of feed solids for roll-type presses and extrusion presses*, Powder Tech. 130, 2003, 272-276
[103] Y.A. Yusof, A.C. Smith and B.J. Briscoe, *Roll compaction of maize powder*, Chem. Eng. Sci. 60, 2005, 3919-3931
[104] J.J.A.M. Verheezen, K. van der Voort Maarschalk, F. Faassen, H. Vromans, *Milling of agglomerates in an impact mill*, Int. J. Pharm. 278, 2004, 165-172
[105] E.L. Parrot, *The theory and practice of industrial pharmacy*, Lea & Febiger, Philadelphia, USA 3rd, 1986, 21-46
[106] J.S. Rudolph and R.J. Sepelyak, *Pharmaceutical process validation: an international third edition, revised and expanded*, Marcel Dekker, Inc. Basel, Switzerland 3rd, 2003, 177-178
[107] J.M. Bultmann, *Influence of sieve size and rotor-sieve distance in the roller compaction process on granule size distribution*, Proc. 4th World Meeting ADRITELF/APGI/APV, Florence 8/11 April 2002
[108] A.J. Hlinak, K. Kuriyan, K.R. Morris, G.V. Reklaitis and P.K.Basu, *Understanding critical material properties for solid dosage form design*, J. Pharm. Innov., Sept-Oct, 2006, 12-17
[109] S. Inghelbrecht, J.P. Remon, *The roller compaction of different types of lactose*, Int. J. Pharm. 166, 1998, 135-144
[110] S. Inghelbrecht, Jean Paul Remon, *Reducing dust and improving granule and tablet quality in the roller compaction process*, Int. J. Pharm. 171, 1998, 195-206

[111] B. Rambali, L. Baert, E. Jans, D.L. Massart, *Influence of the roll compactor parameter settings and the compression pressure on the buccal bio-adhesive tablet properties*, Int. J. Pharm. 220, 2001, 129-140
[112] F. Wöll, P. Kleinebudde, *Influence of roll compaction force on the disintegrating activity of crospovidone, croscarmellose sodium, sodium starch glycolate and L-HPC*, Proc. 4th World Meeting ADRITELF/APGI/APV, Florence 8/11 April 2002
[113] R. Grulke, P. Kleinebudde, *Roll compaction/dry granulation for modified release granules with lipophilic matrix formers*, Proc. 4th World Meeting ADRITELF/APGI/APV, Florence 8/11 April 2002
[114] J. M. Bultmann, *Multiple compaction of microcrystalline cellulose in a roller compactor*, Eur. J. Pharm. Biopharm.54, 2002, 59-64
[115] F. Freitag, P. Kleinebudde, *Walzenkompaktieren / Trockengranulieren von Magnesiumarbonat: Einfluss zweier Bindemittel*, Proc. 4th World Meeting ADRITELF/APGI/APV, Florence 8/11 April 2002
[116] P.W.S. Heng, L.W. Chan, C.V. Liew, S.N. Chee, J.L.P. Soh and S.M. Ooi, *Roller compaction of crude plant material: influence of process variables, polyvinylpyrrolidone, and co-milling*, Pharm. Dev. Technol. 9, 2004, 2, 135-144
[117] W. Weyenberg, A. Vermeire, J. Vandervoort, J.P. Remon, A. Ludwig, *Effects of roller compaction settings on the preparation of bioadhesive granules on ocular minitablets*, Eur. J. Pharm. Biopharm.59 (2005) 527-536 59, 2005, 527-536
[118] A. Gupta, G.E. Peck, R.W. Miller, K.R. Morris, *Influence of ambient moisture on the compaction behavior of microcrystalline cellulose powder undergoing uni-axial compression and roller-compaction: a comparative study using near-infrared spectroscopy*, J. Pharm. Sci.94, 2005, 10, 2301-2313
[119] A. Gupta, G. E. Peck, R.W.Miller, K.R. Morris, *Effect of the variation in the ambient moisture on the compaction behavior of powder undergoing roller-compaction and on the characteristics of tablets produced from the post-milled granules*, J. Pharm. Sci.94, 2005, 10, 2314-2326
[120] M.T. am Ende, Sara K. Moses, A.J. Carella, R.A. Gadkari, T.W. Graul, A.L. Otano, R.J. Timpano, *Improving the content uniformity of a low-dose tablet formulation through roller compaction optimization*, Pharm. Dev. Technol. 12, 2007, 391-404
[121] Peter Kleinebudde, *Roll compaction/dry granulation: pharmaceutical applications*, Eur. J. Pharm. Biopharm. 58, 2004, 317-326
[122] P.J. Sheskey, T.D. Cabelka, R.T. Robb, B.M. Boyce, *Use of roller compaction in the preparation of controlled-release hydrophilic matrix tablets containing methylcellulose and hydroxypropyl methylcellulose polymers*, Pharm. Tech., 1994, 18, 132-150
[123] P.J. Sheskey, T.P. Dasbach, *Evaluation of various polymers as dry binders in the preparation of an immediate-release tablet formulation by roller compaction*, Pharm. Tech. 19, 1995, 10, 98-112
[124] M.Murray, A. Laohavichien, W. Habib, A. Sakr, *Effect of process variables on roller-compacted ibuprofen tablets*, Pharm. Ind. 60, 1998, 3, 257-262
[125] S.G. von Eggelkraut-Gottanka, S.A. Abed, W. Mueller, and P.C. Schmidt, *Roller compaction and tabletting of St. John's wort plant dry extract using a gap width and force controlled roller compactor. I. Granulation and tabletting of eight different extract batches*, Pharm. Dev. Technol. 7, 2002, 4, 433-445
[126] S.G. von Eggelkaut-Gottanka, S.A. Abed, W. Mueller, and P.C. Schmidt, *Roller compaction and tabletting of St. John's wort plant dry extract using a gap width and force controlled roller compactor. II. Study of roller compaction variables on granule and tablet properties by a 3^3 factorial design*, Pharm. Dev. Technol. 7, 2002, 4, 447-455
[127] L.A. Lira Soares, G. Gonzalez Ortega, P.R. Petrovick, and P.C. Schmidt, *Dry granulation and compression of spray-dried plant extracts*, AAPS Pharm. Sci. Tech. 6, 2005, 3, 359-366
[128] D.Z. Bozic, R. Dreu, F. Vrecer, *Influence of dry granulation on compactibility and capping tendency of macrolide antibiotic formulation*, Int. J. Pharm. 357, 2008, 44-54
[129] Ph. Arnaud, D. Brossrad, and J.C. Chaumeil, *Effect of the granulation process on nitrofurantoin granule characteristics*, Drug. Dev. Ind. Pharm. 24, 1998, 1, 57-67
[130] H.-J. Chang, H.N. Han, S.-H. Joo, K.-H. Lee and K.H. Oh, *Prediction model for surface temperature of roller and densification of iron powder during hot roll pressing*, Int. J. Mach. Tools Manuf. 47, 2007, 1573-1582
[131] A. Zavaliangos, R.T. Dec, R.K. Komarek, *Analysis of powder processing in the roller press using Finite Element Modelling*, XXII International Mineral Processing Congress, 28 September - 3 October, 2003
[132] R.T. Dec, A. Zavaliangos, J.C. Cunningham, *Comparison of various modelling methods for analysis of powder compaction in roller press*, Powder Tech., 2003, 103, 265-271
[133] D. Rhind, *Computer-aided cartography*, Transactions of the Institute of British Geographers, New Series 2, 1977, 1, 71-97
[134] A. S. Hussain, P. Shivanand and R.D. Johnson, *Application of neural computing in pharmaceutical product development: computer aided formulation design*, Drug. Dev. Ind. Pharm. 20, 1994, 10, 1739-1752
[135] B. Hoffman and D. Ritchie, *Using multimedia to overcome problems with problem based learning*, Instr. Sci. 25, 1997, 97-115
[136] W.J. Barnes, A. Johnson, G. Horseman, M. Macauley, *Computer-aided studies of vision in crabs*, Mar. Fresh. Behav. Physiol. 35, 2001, 1-2, 37-56
[137] F. Adam, D.S. Hammer, D.Pape, D. Kohn, *Femoral anatomy, computed tomography and computer-aided design of prosthetic implants*, Arch. Orthop. Trauma Surg. 122, 2002, 262-268
[138] L. Constantinou, K. Bagherpour, R. Gani, J.A. Klein and D.T. Wu, *Computer aided product design: problem formulations, methodology and applications*, Comp. Chem. Eng. 20, 1996, 6-7, 685-702
[139] A. Wren and J.M Rousseau, *Bus driver scheduling - An overview,* 6th Int. Workshop on Computer Aided Scheduling of Public Transport, Lisboa, Portugal 6-9th July, 1993
[140] Susan Craw, Nirmalie Wiratunga and Ray Rowe, *Case-based design for tablet formulations*, European Conference/Workshop on Case-Based Reasoning, 1998, 358-369
[141] Stephen I. Gallant, *Neural Network learning and Expert Systems*, MIT Press, MA, USA, 1993, 255-263
[142] R.C. Rowe and R.J. Roberts, *Artificial intelligence in pharmaceutical product formulation: knowledge-based and expert systems*, Pharm. Sci. & Tech. Today (PSTT) 1, 1998, 4, 153-159
[143] F. Podczeck, *The development and optimization of tablet formulations using mathematical methods*, *Pharmaceutical powder compaction technology* Marcel Dekker, 1996, NY-US, 586-594

[144] J.M. Bultmann, S. Schmitt, F.-C. Lintz, *Use of the self-learning Expert System "AXS" in roller compaction troubleshooting*, Proc. 4th World Meeting ADRITELF/APGI/APV, Florence 8/11 April 2002
[145] C.A. Jain, L. Hailemariam, P. Suresh, P. Akisetty, G. Joglekar, V. Venkatasubramanian, G.V. Reklaitis, K. Morris, and P. Basu, *Toward intelligent decision support for pharmaceutical product development*, J. Pharm. Innov. Sept-Oct, 2006, 23-35
[146] J. Frank, B. Rupprecht and V. Schmelmer, *Knowledge-based assistance for the development of drugs*, IEEE Jan-Feb, 1997, 40-48
[147] J. Watine*, Are expert systems "more intelligent" than laboratory doctors?,* Clin. Biochem. 32, 1999, 485-486
[148] A. Kusiak and S.S. Heragu, *Expert System and Optimization*, IEEE Trans. Softw. Eng. 15, 1989, 8, 1017-1020
[149] M. Çelik, *Catching up with expert systems*, Pharm. Tech. July, 2001, 122-124
[150] H. Stricker, R. Haux, T. Wetter, G. Mann, *Das "Galenische Entwicklungs-System Heidelberg"*, Pharm. Ind. 53, 1991, 6, 571-578
[151] H. Stricker, S. Fuchs, R. Haux, R. Roessler, B. Rupprecht, V. Schmelmer and S. Wiegel, Das *Galenische Entwicklungs-System Heidelberg. Systematische Rezepturentwicklung*, Pharm. Ind. 56, 1994, 7, 641-647
[152] T.C. Rock, *Wissensbasierte Entwicklung von parenteralen Peptidloesungen und Lyophilisaten*, PhD Thesis - University of Heidelberg, 1999
[153] M. Bultmann, *Wissensbasierte Entwicklung von Tabletten aus Granulaten*, PhD Thesis - University of Heidelberg, 1998
[154] F.-C. Lintz*, Systematik der Rezepturentwicklung von ueberzogenen Tabletten und Pellets als Grundlage fuer ein wissensbasiertes System*, PhD Thesis - University of Heidelberg, 1999
[155] K.U. Ramani, M.R. Patel, and S.K. Patel*, An expert system for drug preformulation in a pharmaceutical company*, Interfaces 22, 1992, 101-108
[156] R.C. Rowe, *Expert system in solid dosage development*, Pharm. Ind. 55, 1993, 11, 1993
[157] R.C. Rowe and R.J. Roberts, *Expert systems in pharmaceutical product development*, *Encyclopaedia of Pharmaceutical Technology* 1, Informa Healthcare UK, 2002, 1188-1210
[158] S.M. Ha Lai, F. Podczeck, J. M. Newton, and R. Daumesnil, *An expert system for the development of powder filled hard gelatine capsule formulations*, AAPS Annual Meeting, 1995, S-150
[159] S.D. Bateman, J. Verlin, M. Russo, M. Guillot and S.M. Laughlin, *The development and validation of a capsule formulation knowledge-based system*, Pharm. Tech. March, 1996, 174-184
[160] M. Guo, G. Kalra, W. Wilson, Y. Peng and L.L. Augsburger, *A prototype intelligent hybrid system for hard gelatin capsule formulation development*, Pharm. Tech. Sept., 2002, 44-60
[161] W.I. Wilson, Y. Peng and L.L. Augsburger, *Generalization of a prototype intelligent hybrid system for hard gelatine capsule formulation development*, AAPS Pharm. Sci. Tech. 6, 2005, 3, 449-457
[162] F.-C. Lintz , J.M. Bultmann*, Use of the self-learning expert system "AXS" for the optimisation of nebuliser formulation*, Proc. 4th World Meeting ADRITELF/APGI/APV , Florence 8/11 April 2002
[163] S. Schmitt, *Systematische Rezepturentwicklung von Tabletten aus Lyophilisaten*, PhD Thesis - University of Heidelberg, 2005
[164] A. Raposo, *Systematic development of formulations suitable for pulmonary applications by nebulisation*, PhD Thesis - University of Heidelberg, 2006
[165] P. Perez, J.M. Sune-Negre, M. Minarro, M. Roig, R. Fuster, E. Garcia-Montoya, C. Hernandez, R. Ruhi, and J.R. Tico, *A new expert systems (SeDeM Diagram) for control batch powder formulation and preformulation drug products*, Eur. J. Pharm. Biopharm. 64, 2006, 351-359
[166] J.M. Suné-Negre, P. Perez-Lozano, M. Minarro, M. Roig, R. Fuster, C. Hernandez, R. Ruhi, E. Garcia-Monotya, J.R. Tico, *Application of the SeDeM Diagram and a new mathematical equation in the design of direct compression tablet formulation*, Eur. J. Pharm. Biopharm., 2008, In press
[167] *Introduction to artificial neural networks,* Electronic Technology Directions to the Year 2000, 1995. Proceedings. 32-62
[168] L. Fausett*, Fundamentals of neural networks. Architectures, algorithms, and applications*, Prentice-Hall, US, 1994, 289-333
[169] R.L. King, *Artificial neural networks and computational intelligence*, IEEE Com. Appl. Power, 1998, October, 14-25
[170] R. Aggarwal and Y. Song*, Artificial neural networks in power systems*, Power Eng. J., 1998, February, 41-47
[171] R.C. Rowe and R.J. Roberts, *Artificial intelligence in pharmaceutical product formulation: neural computing and emerging technologies*, PSTT 1, 1998, 5, 200-205
[172] S. Wiriyacoonkasem and A.C. Esterline, *Adaptive learning expert system*, IEEE Trans. Softw. Eng., 2000, 445-446
[173] S. Agatonovic-Kustrin, R. Beresford, *Basic concepts of artificial neural network (ANN) modelling and its application in Pharm. Res.*, J. Pharm. Biom. Anal. 22, 2000, 717-727
[174] A.S. Hussain, X.Yu, R.D. Johnson, *Application of neural computing in pharmaceutical product development*, Pharm. Res. 8, 1991, 10, 1248-1252
[175] J.G. Kesavan and G.E. Peck, *Pharmaceutical granulation and tablet formulation using neural networks*, Pharm. Dev. Technol. 1, 1996, 4, 1391-404
[176] J. Bourquin, H. Schmidli, P. van Hoogevest, and H. Leuenberger, *Application of artificial neural networks (ANN) in the development of solid dosage forms*, Pharm. Dev. Technol. 2, 1997, 2, 111-121
[177] J. Bourquin, H. Schmidli, P. van Hoogevest and H. Leuenberger, *Advantages of artificial neural networks (ANNs) as alternative modelling technique for data sets showing non-linear relationships using data from a galenical study on a solid dosage form*, European J. Pharm. Sci.7, 1998, 5-16
[178] C.J. Richardson and D.J. Barlow, *Neural network computer simulation of medical aerosols*, J. Pharm. Pharmacol. 48, 1996, 581-591
[179] D. Zupancic Bozic, F. Vrecer, F. Kozjek, *Optimization of diclofenac sodium dissolution from sustained release formulations using an artificial neural network*, European J. Pharm. Sci. 5, 1997, 163-169
[180] J. Takahara, K. Takaoyama, T. Nagai, *Multi-objective simultaneous optimization technique based on an artificial neural network in sustained release formulations*, J. Controlled Release 49, 1997, 11-20
[181] K. Takaoyama, M. Fujiyama, T. Nagai, *Artificial neural network as a novel method to optimize pharmaceutical formulations*, Pharma. Res. 16, 1999, 1, 1-6

[182] K. Takayama, A. Morva, M. Fujikawa, Y. Hattori, Y. Obata, T. Nagai, *Formula optimization of theophylline controlled-release tablet based on artificial neural networks*, J. Controlled Release 68, 2000, 175-186
[183] M. Turkoglu, I. Aydin, M. Murray, A. Sakr, *Research paper Modelling of a roller-compaction process using neural networks and genetic algorithms*, Eur. J. Pharm. Biopharm.48, 1999, 239-245
[184] K. Rocksloh, F.-R. Rapp, S. Abu Abed, W. Mueller, M. Reher, G. Gauglitz, and P.C. Schmidt, *Optimization of crushing strength and disintegration time of a high-dose plant extract tablet by neural networks*, Drug. Dev. Ind. Pharm. 25, 1999, 9, 1015-1025
[185] T. Wu, W. Pan, J. Chen, R. Zhang, *Formulation optimization technique based on artificial neural network in salbutamol sulphate osmotic pump tablets*, Drug. Dev. Ind. Pharm. 26, 2000, 2, 211-215
[186] Y. Chen, S.S. Thosar, R.A. Forbess, M.S. Kemper, R.L. Rubinovitz, A.J. Shukla, *Prediction of drug content and hardness of intact tablets using artificial neural network and near-infrared spectroscopy*, Drug. Dev. Ind. Pharm. 27, 2001, 7, 623-631
[187] Y. Sun, Y. Peng, Y. Chen, A.J. Shukla, *Application of artificial neural networks in the design of controlled release drug delivery systems*, Adv. Drug Delivery Rev. 55, 2003, 1201-1215
[188] R.F. Mansa, R.H. Bridson, R.W. Greenwood, H. Barker, J.P.K. Seville, *Using intelligent software to predict the effects of formulation and processing parameters on roller compaction*, Powder Tech. 181, 2008, 217-225
[189] P.C. Lerk and H. Sucker, *Interaction of magnesium stearate and talc upon tabletting mixtures, II: Effect on wettability of powder blends*, Acta Pharm. Technol. 34, 1988, 2, 72-76
[190] M. Sheikh-Salem, J.T. Fell, *The tensile strength of tablets of binary mixtures lubricated with magnesium stearate*, Drug. Dev. Ind. Pharm. 14, 1988, 7, 895-903
[191] G. Shlieout, R.F. Lammens, P. Kleinebudde, M. Bultmann, *Dry granulation with a Gerteis 3-W-Polygran roll compactor. Evaluation of different operation modes*, Proc. 4th World Meeting ADRITELF/APGI/APV, Florence 8/11 April 2002, 51-52
[192] B. Michel, *Contribution a l'etude de l'agglomeration des poudres en presse a rouleaux lisses*, PhD Thesis - Universite de Technologie de Compiegne, 1994
[193] G. Bindhumadhavan, *Roll compaction of pharmaceutical powders*, PhD Thesis - University of Birmingham, 2004
[194] R. Freeman, J. Cooke, *Understanding powder behaviour by measuring bulk, flow and shear properties*, Pharm. Tech. Europe Nov 1, 2006
[195] Y. S.L. Lee, R. Poynter, F. Podcezck, J.M. Newton, *Development of a dual approach to assess powder flow from avalanching behaviour*, AAPS Pharm. Sci. Tech. 1, 2000, 3, art. 21
[196] N.-O. Lindberg, M. Palsson, A.-C. Pihl, R. Freeman, T. Freeman, H. Zetzener and G. Enstad, *Flowability measurements of pharmaceutical powder mixtures with poor flow using five different techniques*, Drug. Dev. Ind. Pharm. 30, 2004, 7, 785-791
[197] A.R. Fassihi and I. Kanfer, *Effect of compressibility and powder flow properties on tablet weight variation,* Drug. Dev. Ind. Pharm. 12, 1986, 11-13, 1947-1966
[198] A.H. Sorensen, J.M. Sonnergaard and L. Hovgaard, *Bulk characterization of pharmaceutical powders by low-pressure compression*, Pharm. Dev. Technol. 10, 2005, 197-209
[199] R. Carr, *Evaluating flow properties of solids*, Chem. Eng., 1965, January, 163-168
[200] V. Kumar, M.L. Reus-Medina, D. Yang, Preparation*, characterization, and tabletting properties of a new cellulose-based pharmaceutical aid*, Int. J. Pharm. 235, 2002, 129-140
[201] M.K. Tylor, J. Ginsburg, A.J. Hickey, F. Gheyas, *Composite method to quantify powder flow as a screening method in early tablet or capsule formulation development*, AAPS Pharm. Sci. Tech. 1, 2000, 3, article 18
[202] K. Leschoneki, W. Alex und B. Koglin, *Teilchengroesseanalyse. 1. Darstellung und Auswertung von Teilchengroessenverteilungen (Fortsetzung)*, Chemie Ingenieur Technik 46, 1974, 3, 101-106
[203] J.T. Fell and J.M. Newton, *Determination of tablet strength by the diametral-compression test*, J. Pharm. Sci. 59, 1970, 5, 688-691
[204] P. Porion, N. Sommier and P. Evesque*, Dynamics of mixing and segregation processes of grains in 3d blender by NMR imaging investigation*, Europhysics letters 50, 2000, 3, 319-325
[205] C.-Y. Wu, S.M. Best, A.C. Bentham, B.C. Hancock, and W. Bonfield, *A simple predictive model for the tensile strength of binary tablets*, European J. Pharm. Sci.25, 2005, 331-336
[206] C.-Y. Wu, S.M. Best, A.C. Bentham, B.C. Hancock, and W. Bonfield, *Predicting the tensile strength of compacted multi-component mixtures of pharmaceutical powders*, Pharm. Res. 23, 2006, 8, 1898-1905
[207] P.J. Sheskey and J. Hendrey, *The effects of roll compaction equipment variables, granulation technique, and HPMC polymer level on a controlled-release matrix model drug formulation*, Pharm. Tech. 23, 1999, March, 90-106
[208] T. Hirohata, S. Masaki and S. Shima, *Experiment on metal powder compaction by differential speed rolling*, J. Mat. Process. Technol. 111, 2001, 113-117
[209] R. Mansa, *Roller compaction of pharmaceutical excipients and prediction using intelligent software*, PhD Thesis - University of Birmingham, 2006
[210] R.W. Miller, Handbook of pharmaceutical granulation technology, Marcel Dekker Inc. New York - Basel, 1997, 106-108
[211] A.V. Zinchuk, M.P. Mullarney, B.C. Hancock*, Simulation of roller compaction using a laboratory scale compaction simulator*, Int. J. Pharm. 269, 2004, 403-415
[212] V.P. Katashinskii, G.A. Vinogradov, and G.Ya. Kalutskii, *Non-uniformity of strain and stress distribution over the width of rolled powder strip*, Translated from Poroshkovaya Metallurgiya 12, 1975, 156, 28-32
[213] U. Lubjuhn, U. Sander, K. Schonert, *Pressure profile in the compression zone of the high-pressure roller mil*l, ZKG Int. 6, 1994, E157-E163
[214] H. Busies, *Dichteverteilung in Shülpen*, Verlag Dr. Hut, München, 2006
[215] L.N.F.J. Perera, *Roll compaction of pharmaceutical excipients / by Luke Neluka Faustinus Julius Perera*, PhD Thesis - University of Birmingham, 2005
[216] B.C. Hancock, J.T. Colvin, M.P. Mullarney, A.V. Zinchuk, *The relative densities of pharmaceutical powders, blends, dry granulations, and immediate-release tablets*, Pharm. Tech., 2003, April, 64-80
[217] M.S. Kadiri, A. Michrafy, J.A. Dodds, *Pharmaceutical powders compaction: Experimental and numerical analysis of the density distribution*, Powder Tech., 2005, 157, 176-182

[218] P. Nkansah, S.-J. Wu, S. Sobotka, K. Yamamoto, Z.-J. Shao, *A novel method for estimating solid fraction of roller-compacted ribbons*, Drug. Dev. Ind. Pharm. 34, 2008, 2, 142-148
[219] V. Busignies, P. Tchoreloff, B. Leclerc, C. Hersen, G. Keller, and G. Couarraze, *Compaction of crystallographic forms of pharmaceutical granular lactoses. II. Compacts mechanical properties*, Eur. J. Pharm. Biopharm. 58, 2004, 577-586
[220] Y. Gonnissen, J.P. Remon and C. Vervaet, *Development of directly compressible powders via co-spray drying*, Eur. J. Pharm. Biopharm. 67, 2007, 1, 220-226
[221] F. Wöll, *Entwicklung von Methoden zur charakterisiterung von Schülpen*, PhD Thesis - ULB Sachsen-Anhalt, 2003
[222] J.L.P. Soh, N. Boersen, M.T. Carvajal, K.R. Morris, G.E. Peck, R. Pinal, *Importance of raw material attributes for modeling ribbon and granule properties in roller compaction: multivariate analysis on roll gap and NIR spectral slope as process critical control parameters*, J. Pharm. Innov. 2, 2007, 106-124
[223] G.W. Gereg and M.L. Cappola, *Roller compaction feasibility for new drug candidates. Laboratory to production scale*, Pharm. Tech. 2002, Tableting, 14-23
[224] F. Sanchez, A. Bolarin, J. Coreño, A. Martinez, J.A. Bas, *Effect of compaction process sequence on axial density distribution of green compacts*, Powder Metall. 44, 2001, 4, 351-355
[225] Y. Taniguchi, K. Dohda, Z. Wang, *Lubricating effect on density distribution in uniaxial powder compaction*, Material Forum 29, 2005, 356-362
[226] N. Trivic, *Cyclic compaction of soft-hard powder mixtures*, Drexel University Print - Doctoral Thesis, 2003
[227] US- Department of Health and Human Service, FDA, CDER, CVM, ORA, *Guidance for industry. PAT- A framework for innovative pharmaceutical development, manufacturing and quality assurance*, http://www.fda.gov/cvm/guidance/published.html, 2004
[228] D.C. Hinz, *Process analytical technologies in the Pharmaceutical Industry: the FDA's PAT initiative*, Anal. Bional. Chem. 384, 2006, 1036-1042
[229] K.M. Morisseau and C.T. Rhodes, *Pharmaceutical uses of near-infrared spectroscopy*, Drug. Dev. Ind. Pharm. 21, 1995, 9, 1071-1090
[230] G. Reich, *Near-infrared spectroscopy and imaging: Basic principles and pharmaceutical applications*, Adv. Drug Delivery Rev. 57, 2005, 1109-1143
[231] A.S. El-Hagrasy, F. d'Amico, J.K. Drennen, *A process analytical technology approach to near-infrared process control of pharmaceutical powder blending. Part I: D-optimal design for characterization of powder mixing and preliminary spectral data evaluation*, J. Pharm. Sci. 95, 2006, 2, 392-406
[232] P. Frake, D. Greenhalgh, S.M. Grierson, J.M. Hemenstall, D.R. Rudd, *Process control and end-point determination of a fluid bed granulation by application of near infra-red spectroscopy*, Int. J. Pharm. 151, 1997, 75-80
[233] P. Corti, G. Ceramelli, E. Dreassi and S. Mattii, *Near infrared transmittance analysis for the assay of solid pharmaceutical dosage forms*, The Analyst 124, 1999, 755-758
[234] M. Blanco and M. Alcala, *Content uniformity and tablet hardness testing of intact pharmaceutical tablets by near infrared spectroscopy. A contribution to process analytical technologies*, Anal. Chimica Acta 557, 2006, 353-359
[235] J.D. Kirsch, J.K. Drennen, *Nondestructive tablet hardness testing by near-infrared spectroscopy: a new and robust spectral best-fit algorithm*, J. Pharm. Biomed. Anal. 19, 1999, 351-362
[236] V.J. Bijlani, M. Delgado-Lopez, C.M. Adeyeye and J.K. Drennen III, *Near infrared spectroscopy for monitoring the hardness of roller compacted ribbons*, NIR news: the newsletter of the International committee for Near Infrared Spectroscopy 13, 2002, 5, 8-14
[237] Ronald W. Miller, *The use of near infra red technology to map roller compaction processing applications*, Proceedings: Biennial conference of the Institute for Briquetting and Agglomeration 26, 1999, 17-26
[238] A. Gupta, G.E. Peck, R.W. Miller, and K.R. Morris, *Nondestructive measurements of the compact strength and the particle-size distribution after milling of roller compacted powders by near-infrared spectroscopy*, J. Pharm. Sci.93, 2004, 4, 1047-1053
[239] A. Gupta, G.E. Peck, R.W. Miller, K.R. Morris, *Real-time near-infrared monitoring of content uniformity, moisture content, compact density, tensile strength, and Young's modulus of roller compacted powder blends*, J. Pharm. Sci. 94, 2005, 1589-1597
[240] F. Wang, R. Pinal, Garnet E. Peck, M.T. Carvajal, *Monitoring the effects of the roller compaction process variables on ribbon properties using non-destructive near-infrared reflectance spectroscopy*, Conference proceedings, AIChE spring national meeting, Orlando, FL, 2006
[241] B.D. Rohera and N.H. Parikh, *Influence of plasticizer type and coat level on surelease film properties*, Pharm. Dev. Technol. 7, 2002, 4, 407-420
[242] V. Busignies, P. Tchoreloff, B. Leclerc, C. Hersen, G. Kller, G. Couarraze, *Compaction of crystallographic forms of pharmaceutical granular lactoses. II. Compacts mechanical properties*, Eur. J. Pharm. Biopharm.58, 2004, 577-586
[243] J. Lee, *Structural heterogeneity of pharmaceutical compacts probed by micro-indentation*, J. Mat. Sci.: Mat. Med. 19, 2007, 1981-1990
[244] B.C. Hancock, P. Mullarney, *X-ray microtomagrapy of solid dosage forms*, Pharm. Tech., 2005, April, 92-100
[245] L. Farber, G. Tardos, James N. Michaels, *Use of X-ray tomography to study the porosity and morphology of granules*, Powder Tech. 132, 2003, 57-63
[246] D.H. Phillips, J.J. Lannutti, *Measuring physical density with X-ray computed tomography*, NDT&E International 30, 1997, 6, 339-350
[247] S. Burch, *Measurement of density variations in compacted parts using X-ray computerised tomography*, MPR February, 2002, 24-28
[248] I.C. Sinka, S.F. Burch, J.H. Tweed and J.C. Cunningham, *Measurement of density variations in tablets using X-ray computed tomography*, Int. J. Pharm. 271, 2004, 215-224
[249] V. Busignies, B. Leclerc, P. Porion, P. Evesque, G. Couarraze, P. Tchoreloff, *Quantitative measurements of localized density variations in cylindrical tablets using X-ray microtomography*, Eur. J. Pharm. Biopharm. 64, 2006, 38-50

[250] V. Busignies, B. Leclerc, P. Porion, P. Eveque, G. Couarraze, P. Tchoreloff, *Investigation and modelling approach of the mechanical properties of compacts made with binary mixtures of pharmaceutical excipients*, Eur. J. Pharm. Biopharm. 64, 2006, 51-65
[251] C.Y. Wu, B.C. Hancock, A. Mills, A.C. Bentham, S.M. Best, J.A. Elliott, *Numerical and experimental investigation of capping mechanisms during pharmaceutical tablet compaction*, Powder Tech. 181, 2008, 121-129
[252] S.E. Harms, T.J. Morgan, W.S. Yamansashi, T.S. Harle, G.D. Dodd, *Principles of nuclear magnetic resonance imaging*, Radio-Graphs 4, 1984
[253] G. Nebgen, D. Gross, V. Lehmann, and F. Muller, *H-NMR microscopy of tablets*, J. Pharm. Sci. 283, 1995, 3, 283-291
[254] A. Djemai, I.C. Sinka, *NMR imaging of density distributions in tablets*, Int. J. Pharm. 319, 2006, 55-62
[255] C.D. Melia, A.R. Rajabi-Siahboomi and R.W. Bowtell, *Magnetic resonance imaging of controlled release pharmaceutical dosage forms*, PSTT 1, 1998, 32-39
[256] A. Djemai, I.C. Sinka*, NMR imaging of density distributions in tablets*, Int. J. Pharm. 319, 2006, 55-62
[257] R.C. Lyon, D.S. Lester, E.N. Lewis, E. Lee, L.X. Yu, E.H. Jefferson and A.S. Hussain, *Near-infrared spectral imaging for quality assurance of pharmaceutical products: analysis of tablets to assess powder blend homogeneity*, AAPS Pharm. Sci. Tech. 3, 2002, 3, Article 17
[258] T. Lecompte, P. Doremus, G. Thomas, L. Perier-Camby, J-C. Le Thiesse, J-C. Masteau, L. Debove, *Dry granulation of organic powders -dependence of pressure 2D-distribution on different process parameters*, Chem. Eng. Sci. 60, 2005, 3933-3940
[259] K. Zuurman, K. Van der Voort Maarschalk, G.K. Bolhuis, *Effects of magnesium stearate on bonding and porosity expansion of tablets produced from materials with different consolidation properties*, Int. J. Pharm. 179, 1999, 107-115
[260] Peter Stanley, *Mechanical strength testing of compacted powders*, Int. J. Pharm. 227, 2001, 27-38
[261] C.K. Tye, C. Sun, G.E. Amidon, *Evaluation of the effects of tableting speed on the relationships between compaction pressure, tablet tensile strength, and tablet solid fraction*, J. Pharm. Sci. 94, 2005, 3, 465-472
[262] T. Schmitz and D. Kupper, *Einfluss rheologischer Parameter auf den Prozess der Gutbett-beanspruchung in der Walzenmuehle*, Teil 1, ZKG Int. Edition B 2, 1992, 79-85
[263] O.A. Katrus, *Friction in powder rolling*, Poroshkavaya Metallurgiya 3, 1982, 231, 5-13
[264] I.E. Kuleshov, *Kinematics and stress-strain state of metal powder issuing from a hopper device. Part II*, Poroshkavaya Metallurgiya 10, 1986, 286, 22-26
[265] G.A. Vinogradov and V.P. Katashinskii, *Investigation of the kinematics of powder motion in hoppers during rolling*, Translated from Poroshkavaya Metallurgiya 1, 1964, 19, 81-90
[266] R. Komarek, *Selecting a roll-press briquetter to improve material handling*, Powder Bulk Eng. February, 1994
[267] K. Hutter, K.R. Rajagopal, *On flows of granular materials*, Continuum Mech. Thermodyn. 6, 1994, 81-139
[268] V.P. Katashinskii, *Effects of the shape of the densification zone on the distribution of density in rolled powder strip,* Translated from Poroshkovaya Metallurgiya 2, 1977, 182, 7-10
[269] Ali Nokhodchi, *Effect of Moisture on compaction and compression*, Pharm. Tech. 6, 2005, 46-66
[270] Ali Nokhodchi, Yousef Javadzadeh, *The effect of storage conditions on the physical stability of tablets*, Pharm. Tech. Europe January, 2007, 20-26
[271] L.H. Christensen, H.E. Johansen, T. Schaefer, *Moisture-activated dry granulation in a high shear mixer*, Drug. Dev. Ind. Pharm. 20, 1994, 14, 2195-2213
[272] C.-M. Chen, D. Alli, M.R. Igga, and J.L. Czeisler, *Comparison of moisture-activated dry granulation process with conventional granulation methods for sematilide hydrochloride tablets*, Drug. Dev. Ind. Pharm. 16, 1990, 3, 379-394
[273] K.A. Khan, P. Musikabhumma, J.P. Warr, *The effects of moisture content of microcrystalline cellulose on the compressional properties of some formulations*, Drug. Dev. Ind. Pharm. 7, 1981, 5, 525-538
[274] F.R.G. Bourseul, *Investigations on roll pressing as a forming operation*, PhD Thesis - University of Birmingham, 2001
[275] O.A. Katrus, *Critical speeds in powder rolling*, Translated from Poroshkovaya Metallurgiya 1, 1978, 181, 34-40
[276] V.A. Spinov, G.A. Vinogradov and G.Ya. Kalutskii, *Influence of air on the rolling of powders*, Translated from Poroshkavaya Metallurgiya 8, 1967, 56, 97-99
[277] R.T. Dec, R.K. Komarek, *Experimental investigations of roll press compaction*, Powder Handling & Processing 4, 1992, 1
[278] G.A. Vinogradov, Application of the method of reference points for calculating the density of strips rolled from powders, Translated from Poroshkavaya Metallurgiya 4, 1962, 10, 63-71
[279] V.P. Katashinskii, *Length of the densification zone in metal powder rolling*, Translated from Poroshkovaya Metallurgiya 7, 1968, 67, 19-21
[280] V.P. Katshinskii and G.A. Vinogradov, *Investigation into the compactability of metal powders during rolling*, Poroshkavaya Metalluriya 5, 1965, 29, 9-16
[281] G.A. Vinogradov and V.P. Katashinskii, *The angle parameters of the metal-powder rolling process*, Translated from Poroshkovaya Metallurgiya 9, 1965, 33, 722-726
[282] V.P. Katashinskii, G.A. Vinogradov, *Theory and technology of component formation processes*, Translated from Poroshkovaya Metallurgiya 3, 1966, 39, 21-26
[283] Y.I. Kovalenko and G.A. Vinogradov, *Mechanism of the deformation of metal powders during rolling in the lower part of the feeding region*, Translated from Poroshkovaya Metallurgiya 12, 1974, 144, 18-21
[284] F. Khan, N. Pilpel, and S. Ingham, *The effect of moisture on the density, compaction and tensile strength of microcrystalline cellulose*, Powder Tech. 54, 1988, 161-164
[285] G.E. Amidon, M.E. Houghton, *The effect of moisture on the mechanical and powder flow properties of microcrystalline cellulose*, Pharm. Res. 12, 1995, 6, 923-929
[286] V. Nicolas, O. Chambin, C. Andres, M.-H. Rochat-Gonthier, and Y. Pourcelot, *Preformulation: Effect of moisture content on microcrystalline cellulose (Avicel PH-302) and its consequences on packing performances*, Drug. Dev. Ind. Pharm. 25, 1999, 10, 1137-1142
[287] C.C. Sun, *Mechanism of moisture induced variations in true density and compaction properties of microcrystalline cellulose*, Int. J. Pharm. 346, 2008, 93-101

[288] M. Duberg and C. Nystrom, *Studies on direct compression of tablets XVII. Porosity-pressure curves for the characterization of volume reduction mechanisms in powder compression*, Powder Tech. 46, 1986, 67-75
[289] S. Malkowska and K.A. Khan, *Effect of re-compression on the properties of tablets prepared by dry granulation*, Drug. Dev. Ind. Pharm. 3, 1983, 9, 331-347
[290] D.B. Beten, N. Yuksel, T. Baykara, *The changes in the mechanic properties of a direct tableting agent microcrystalline cellulose by pre-compression*, Drug. Dev. Ind. Pharm. 20, 1994, 14, 2323-2331
[291] J.M. Bultmann, *Influence of magnesium-stearate addition during the roller compaction process: Effect on process and granule properties*, Proc. 4th World Meeting ADRITELF/APGI/APV, Florence 8/11 April 2002
[292] S.K. Kochhar, M.H. Rubinstein, D. Barnes, *The effects of slugging and recompression on pharmaceutical excipients*, Int. J. Pharm. 115, 1995, 35-43
[293] X. He, P.J. Secreast, G.E. Amidon, *Mechanistic study of the effect of roller compaction and lubricant on tablet mechanical strength*, J. Pharm. Sci. 96, 2007, 5, 1342-1355
[294] C. Sun, M. W. Himmelspach, *Reduced tabletability of roller compacted granules as a result of granule size enlargement*, J. Pharm. Sci. 1, 2006, 1, 200-206
[295] L. Farber, K.P. Hapgood, J.N. Michaels, X-Y. Fu, R. Meyer, M.-A. Johnson, F. Li, *Unified compaction curve model for tensile strength of tablets made by roller compaction and direct compression*, Int. J. Pharm. 246, 2008, 17-24
[296] C.C.Sun, *On the mechanism of reduced tabletability of granules prepared by roller compaction*, Int. J. Pharm. 374, 2008, 22, 171-172
[297] M.G. Herting, P. Kleinebudde, *Reply to the letter to the editor*, Int. J. Pharm. 347, 2008, 1-2, 173-174
[298] U.F. Kocks, H. Mecking, *Physics and phenomenology of strain hardening: the FCC case*, Prog. Mat. Sci. 48, 2003, 171-273
[299] R.J. Roberts and R.C. Rowe, *The compaction of pharmaceutical and other model materials - A pragmatic approach*, Chem. Eng. Sci. 42, 1987, 4, 903-911
[300] F. Freitag, P. Kleinebudde, *Effect of dry granulation on the tabletting behaviour of inorganic materials: magnesium carbonate*, Proc. 4th World Meeting ADRITELF/APGI/APV, Florence 8/11 April 2002
[301] S. Hein, K.M. Picker-Freyer, J. Langridge, *Simulation of roller compaction with subsequent tableting and characterization of lactose and microcrystalline cellulose*, Pharm. Dev. Technol. 13, 2008, 523-532
[302] N.G. Lordi, H. Cocolas, and H. Yamasaki, *Analytical interpretation of powder compaction during the loading phase*, Powder Tech., 1997, 90, 173-178
[303] S.J. Wu, C.C. Sun, *Insensitivity of compaction properties of brittle granules to size enlargement by roller compaction*, J. Pharm. Sci. 96, 2007, 5, 1445-1450
[304] A.M. Juppo, L. Kervinen, J. Yliruusi and E. Kristoffersson, *Compression of lactose, glucose and mannitol granules*, J. Pharm. Pharmacol. 47, 1995, 543-549
[305] C. F. Lerk, *Consolidation and Compaction of Lactose*, Drug. Dev. Ind. Pharm. 19, 1993, 17&18, 2359-2398
[306] T. Sebhatu, G. Alderborn, *Relationships between the effective interparticulate contact area and the tensile strength of tablets of amorphous and crystalline lactose of varying particle size*, Eur. J. Pharm. Sci. 8, 1999, 235-242
[307] S. Jonat, S. Hasanzahl, A. Gray and P.C. Schmidt, *Influence of compacted hydrophobic and hydrophilic colloidal silicon dioxide on tableting properties of pharmaceutical excipients*, Drug. Dev. Ind. Pharm. 31, 2005, 687-696
[308] R.C. Rowe, P. J. Sheskey, P.J. Weller, *Pharmaceutical Excipients*, Pharmaceutical Press, London, 2001
[309] G. Pifferi, P. Santoro, M. Pedrani, *Quality and functionality of excipients*, Il Farmaco 54, 1999, 1-14
[310] B. Perissutti, F. Rubessa, M. Moneghini, D. Voinovich, *Formulation design of carbamazepine fast-release tablets prepared by melt granulation technique,* Int. J. Pharm. 256, 2003, 53-63
[311] J.Z. Li, G.S. Rekhi, L.L. Augsburger, and R.F. Shangraw, *The role of intra- and extragranular microcrystalline cellulose in tablet dissolution*, Pharm. Dev. Technol. 1, 1996, 4, 343-355
[312] D.S. Hausman, *Comparison of low shear, high shear, and fluid bed granulation during low dose tablet process development*, Drug. Dev. Ind. Pharm. 30, 2004, 3, 259-266
[313] Van der Voort Maarschalk and G.K. Bolhuis, *Improving properties of materials for direct compaction*, Pharm. Tech., 1999, May, 34-45
[314] F. Podczeck, Y. Miah, *The influence of particle size and shape on the angle of internal friction and the flow factor of unlubricated and lubricated powders*, Int. J. Pharm. 144, 1996, 187-194
[315] B. van Veen, G.K. Bolhuis, Y.S. Wu, K. Zuurman, H.W. Frijlink, *Compaction mechanism and tablet strength of unlubricated and lubricated (silicified) microcrystalline cellulose*, Eur. Jour. Phar. Biopharm. 59, 2005, 133-138
[316] Ludipress LCE, BASF Technical Information Register 9 May, 1999
[317] P. Paronen and M. Juslin, *Compressional characteristics of four starches*, J. Pharm. Pharmacol. 35, 1983, 627-635
[318] R.-K. Chang, M. Leonzio, M.A. Hussain, *Effect of colloidal silicon dioxide on flowing and tableting properties of an experimental, crosslinked polyalkylammonium polyme*r, Pharm. Dev. Technol. 4, 1999, 2, 285-289
[319] K. Kolter, R. Heinz, B. Fussnegger, *Ludipress LCE. A new direct compression excipient*, ExAct - Technical product information May, 2003, 10, 2-3
[320] S. Edge, D.F. Steele, A. Chen, M.J. Tobyn, J.N. Staniforth, *The mechanical properties of compacts of microcrystalline cellulose and silicified microcrystalline cellulose*, Int. J. Pharm., 2000, 200, 67-72
[321] S. Jonat, *The mechanism of hydrophilic and hydrophobic colloidal silicon dioxide types as glidants*, PhD Thesis - University of Tuebingen, 2005,
[322] F. Ferrari, M. Bertoni, M.C. Benferoni, S. Rossi, C. Caramella, and C. Nystrom, *Investigation on bonding and disintegration properties of pharmaceutical materials*, Int. J. Pharm., 1996, 136, 71-79
[323] Y.X. Bi, H. Sunada, Y. Yonezawa, and K. Danjo, *Evaluation of rapidly disintegrating tablets prepared by a direct compression method*, Drug. Dev. Ind. Pharm. 25, 1999, 5, 571-581
[324] J.S. Kaerger, S. Edge, R. Price, *Influence of particle size and shape on flowability and compactibility of binary mixtures of paracetamol and microcrystalline cellulose*, Eur. J. Pharm. Sci.22, 2004, 173-179
[325] J.T. Carstensen, J.-M. Geoffroy and C. Dellamonica, *Compression characteristics of binary mixtures*, Powder Tech. 62, 1990, 119-124

[326] A.T.M. Serajuddin, A.B. Thakur, R.N. Ghoshal, M.G. Fakes, S.A. Ranadive, K.R. Morris and S.A. Varia, *Selection of solid dosage form composition thorugh drug-excipient compatibility testing*, J. Pharm. Sci.88, 1999, 7, 696-704
[327] P. Mura, P. Gratteri and M.T. Faucci, *Compatibility studies of multicomponent tablet formulations. DSC and experimental mixture design*, Jour. of Therm Anal. Calorim. 68, 2002, 541-551
[328] C. Ferrero, N. Munoz, M.V. Velasco, A. Munoz-Ruiz, R. Jimenez-Castellanos, *Disintegrating efficiency of croscarmellose sodium in a direct compression formulation*, Int. J. Pharm. 147, 1997, 11-21
[329] N. Rasenack, B.W. Mueller, *Crystal habit and tableting behaviour*, Int. J. Pharm. 244, 2002, 45-57
[330] G. Alderborn, K. Pasanen, C. Nystroem, *Studies on direct compression of tablets. XI. Characterization of particle fragmentation during compaction by permeametry measurements of tablets*, Int. J. Pharm. 23, 1985, 79-86
[331] C. Nystrom and M Glazer, *Studies on direct compression of tablets. XIII. The effect of some dry binders on the tablet strength of compounds with different fragmentation propensity*, Int. J. Pharm. 23, 1985, 255-263
[332] S. Majuru, D.E. Wurster, *The effect of composition on the tableting indices of binary powder mixtures*, Pharm. Dev. Technol. 2, 1997, 4, 313-321
[333] S. Patel, A.M. Kaushal, and A.K. Bansal, *Effect of particle size and compression force on compaction behaviour and derived mathematical parameters of compressibility*, Pharm. Res. 24, 2007, 1, 111-124
[334] A. Gray, M. Sler, R. Hofmann, *Use of roll compacted pyrogenically produced silicon dioxide in pharmaceutical compositions*, World Intellectual Property Organization WO 2007/128349 A1, 2007
[335] Q. LI, V. Rudolph, B. Weigl, A. Earl, *Interparticle van der Waals force in powder flowability and compactibility*, Int. J. Pharm. 280, 2004, 77-93
[336] K.M. Nagel, G.E. Peck*, Investigating the effects of excipients on the powder flow characteristics of theophylline anhydrous powder formulations*, Drug. Dev. Ind. Pharm. 29, 2003, 3, 277-287
[337] T. Martinello, T.M. Kaneko, M.V. Robles-Velasco, M.E. Santos-Taqueda, and V.O. Consiglieri, Optimization of poorly compactable drug tablets manufactured by direct compression using the mixture experimental design, Int. J. Pharm., 322, 2006, 87-95
[338] H.C.M Yu, M.H. Rubinstein, I.M. Jackson and H.M. Elsabbagh, *Compaction characterisation of paracetamol and Avicel mixtures*, Drug. Dev. Ind. Pharm. 15, 1989, 5, 801-823
[339] H.A. Arekani, J.L. Ford, M.H. Rubinstein, and A.R. Rabaji-Siahboomi*, Effect of compression force, compression speed, and particle size on the compression properties of paracetamol*, Drug. Dev. Ind. Pharm. 27, 2001, 9, 935-942
[340] T. Yoshinari, R.T. Forbes, P. York, Y. Kawashima, *The improved compaction properties of mannitol after a moisture-induced polymorphic transition*, Int. J. Pharm. 38, 2003, 121-131
[341] D. Faroongsarng, G.E. Peck, *The swelling of core tablets during aqueous coating II: An application of the model describing extent of swelling and water penetration for insoluble tablets*, Drug. Dev. Ind. Pharm. 18, 1527-1534, 14, 1992
[342] D. Faroonsarng, G.E. Peck, T*he swelling of core tablets during aqueous coating I: a simple model describing extent of swelling and water penetration for insoluble tablets containing a superdisintegrant*, Drug. Dev. Ind. Pharm. 17, 1991, 18, 2439-2455
[343] D. Faroongsarng, G.E. Peck, *The swelling & water uptake of tablets III: Moisture sorption behavior of tablet disintegrants*, Drug. Dev. Ind. Pharm. 20, 779-798, 5, 1994
[344] T. Mizumoto, Y. Masuda, T. Yamamoto, E. Yonemochi, K. Terada, *Formulation design of a novel fast-disintegrating tablet*, Int. J. Pharm. 306, 2005, 83-90
[345] Kollidon VA 64, BASF Technical information
[346] Volker Buehler, *Kollidon. Polyvinylpyrrolidone for the Pharmaceutical Industry*, BASF Book, 1996, 190-229
[347] J.C. Masteau, G. Thomas, *Modelling to understand porosity and specific surface area changes during tabletting*, Powder Tech. 101, 1999, 240-248
[348] A. Devay, P. Fekete and I. Racz, *Application of factorial design in the examination of tofizopam microcapsules*, J. Microencapsulation 1, 1984, 4, 299-305
[349] B. Iskandarani, J.H. Clair, P. Patel, P.K. Shiromani and R.E. Dempski, *Simultaneous optimization of capsule and tablet formulation using response surface methodology*, Drug. Dev. Ind. Pharm. 19, 1993, 16, 2089-2101
[350] K.M. Picker, *A new theoretical model to characterize the densification behavior of tableting materials*, Eur. J. Pharm. Biopharm.49, 2000, 267-273
[351] N.O. Lindeberg, E. Hansson and B. Holmquist, *The granulation of a tablet formulation in a high-speed mixer, Diosna P25. Influence on intragranular porosity and liquid saturation*, Drug. Dev. Ind. Pharm. 13, 1987, 6, 1069-1079
[352] J. Bourquin, H. Schmidli, P. van Hoogevest, H. Leuenberger, *Comparison of artificial neural networks (ANN) with classical modelling techniques using different experimental designs and data from a galenical study on a solid dosage form*, European J. Pharm. Sci. 6, 1998, 287-300
[353] R. Linden, G.G. Ortega, P.R. Petrovick, V.L. Bassani*, Response surface analysis applied to the preparation of tablets containing a high concentration of vegetable spray-dried extract*, Drug Dev. Ind. Phar. 26, 2000, 4, 441-446
[354] J. Antony, *Design of experiments for engineers and scientists*, Butterworth-Heinemann, 2003
[355] L. Eriksson, E. Johansson, C. Wikstrom, *Mixture design-design generation*, *PLS analysis, and model usage*, Chemom. Intell. Lab. Syst. 43, 1998, 1-24
[356] B. Singh, S.K. Chakkal, and N. Ahuja, *Formulation and optimization of controlled release mucoadhesive tablets of atenolol using response surface methodology*, AAPS Pharm. Sci. Tech. 7, 2006, 1, Article 3
[357] A.C. Atkinson, *Developments in the design of experiments*, Int. Stat. Rev. 50, 1982, 161-177
[358] A. Bodea, S.E. Leucuta, *Optimization of hydrophilic matrix tablets using a D-optimal design*, Int. J. Pharm. 153, 1997, 247-255
[359] B. Rambali, G. Verreck, L. Baert, and D.L. Massart, *Itraconazole formulation studies of the melt-extrusion process with mixture design*, Drug. Dev. Ind. Pharm. 29, 2003, 6, 641-652
[360] P. Mura, S. Furlanetto, M. Cirri, F. Maestrelli, A.M. Marras, S. Pinzauti, *Optimization of glibenclamide tablet composition through the combined use of differential scanning calorimetry and D-optimal mixture experimental design*, J. Pharm. Biomed. Anal. 37, 2005, 65-71

[361] A.P. Plumb, R.C. Rowe, P. York, C. Doherty, *The effect of experimental design on the modelling of a tablet coating formulation using artificial neural networks*, European J. Pharm. Sci. 16, 2002, 281-288
[362] O.A. Battista, P.A. Smith, *Microcrystalline cellulose. The oldest polymer finds new industrial uses*, Ind. Eng. Chem. 54, 1962, 9, 20
[363] O.A. Battista, D. Hill, *Cellulosic fibers and fibrous articles and method of making same*, US Patent No. 3,052,593
[364] G.K. Bolhuis, N.A. Armstrong, *Excipients for direct compaction - an update*, Pharm. Dev. Technol. 11, 2006, 111-124
[365] E. Doelker, *Comparative compaction properties of various microcrystalline cellulose types and generic products*, Drug. Dev. Ind. Pharm. 19, 1993, 17, 2399-2471
[366] E. Doelker, D. Massuelle, F. Veuillez, P. Humbert-Droz, *Morphological, packing, flow and tableting properties of new Avicel types*, Drug. Dev. Ind. Pharm. 21, 1995, 6, 643-661
[367] FMC BioPolymer, Avicel for solid dosage forms, http://www.fmcbiopolymer.com/Products/Avicelforsuspensions/tabid/2920/Default.aspx, Jan. 2009
[368] W. Soetaert, P.T. Vanhooren, E.J. Vandamme, *The production of mannitol by fermentation*, Carbohydrate Biotechnology Protocols, 1999, 261-275
[369] A.J. Melaja and L. Hamalainen, *Process for the production of mannitol and sorbitol*, US Patent No. 3,864,406, 1975
[370] K. Kolter and B. Fussnegger, Ludipress LCE. *Development of tablet formulations using Ludipress LCE as a direct compression excipient*, BASF ExAct. Technical product information November, 1998, 1, 2
[371] Make fine products with fine particles. Aerosil, Degussa. Technical information, September 2001, 3-4
[372] Aerosil 200. Colloidal Silicon Dioxide, Evonik, Degussa Technical Information, 2001
[373] Peter C. Lerk, and Heinz Sucker, *Interaction of magnesium stearate and talc upon tabletting mixtures, I: Effect on ejection force after compaction*, Acta Pharm. Technol. 34, 1988, 2, 68-71
[374] H. Vromans and C. F. Lerk, Densification *properties and compactibility of mixtures of pharmaceutical excipients with and without magnesium stearate,* Int. J. Pharm. 46, 1988, 183-192
[375] K. Kolter, and D. Flick, *Structure and dry binding activity of different polymers, including Kollidon VA 64*, Drug. Dev. Ind. Pharm. 26, 200, 11, 1159-1165
[376] FMC, Ac-Di-Sol, Technical information
[377] D. Faroongsamb, G.E. Peck, *The swelling of core tablets during aqueous coating I: a simple model describing extent of swelling and water penetration for insoluble tablets containing a superdisintegrant*, Drug. Dev. Ind. Pharm. 17, 1991, 2439-2455
[378] R.J. Flower, J.R. Vane, *Inhibition of prostaglandin synthetase in brain explains the anti-pyretic activity of paracetamol (4-acetamidophenol)*, Nature 240, 1972, 410-411
[379] A. Goodman Gilman, L.S. Goodman, A. Gilman, *The pharmacological basis of therapeutics*, MacMillan Publishing Co. Inc., New York 6th, 1980, 701-705
[380] L.F. Prescott, *Kinetics and metabolism of paracetamol and phenacetin*, Br. J. Clin. Pharm. 10, 1980, 291S-298S
[381] T. Hill, P. Lewicki, *Statistics: Methods and applications. A comprehensive reference for science, industry and data mining*, Statsoft Inc., 2006, 181-229
[382] Z. Galil, J. Kiefer, *D-Optimum weighing desings*, Ann. Stat. 8, 1980, 6, 1293-1306
[383] I.N. Bronstein, K.A. Semendjajew, G. Musiol, H. Muehlig, *Taschenbuch der Mathematik*, Verlag Harri Deutsch, 1997, 244-247

Index

T

U

V

W

X

Y

B

Δ